UNIVERSITÀ DEGLI STUDI
DI MODENA E REGGIO EMILIA

Dottorato di ricerca in "Industrial and Environmental Engineering"

Ciclo XXXIV

Tribological characterization of PTFE matrix composites: most influential parameters and stability of the transfer-film

Caratterizzazione tribologica di materiali compositi a matrice PTFE: parametri più influenti e stabilità del tribofilm

Candidato: Federica Amenta

Relatore (Supervisor): Prof. Luca Lusvarghi

Correlatore (Co-Supervisor): Prof. Giovanni Bolelli

Coordinatore del Corso di Dottorato: Prof. Alberto Muscio

Contents

Summary

Tribology, i.e. the study of friction, lubrication and wear of interacting solids, has received increasing attention from the scientific, technical and practical points of view over decades. This is because the operation of many mechanical systems depends on their friction and wear performance. In addition, the annual dissipation of energy and waste of valuable raw materials resulting from high friction and wear is of great economical significance.

The wear characteristics of polymers are considered a very complex phenomenon, and may vary largely not only for different polymers but also for the same polymer under different sliding conditions. It also greatly depends upon the surrounding (environmental) factors such as the presence of contamination, oxide layer on the solid surfaces, thermal heat, in addition to the intrinsic chemical, physical and mechanical properties of the two interacting bodies and operational conditions of contact pressure and relative speed. There is another factor that may change the tribological performance of two bodies and that is the presence of loose debris materials that is ejected from either of the interacting bodies and this is known as the 'third-body'. With this background, tribology of polymers and their different modifications presents further complexity as polymers are easily influenced by the operating conditions and the prevailing environment [1].

In this Ph.D. thesis the wear mechanism of different PTFE composites, widely used for sealing components, against different counter-surfaces was studied, starting from the main significative factors that influence the tribological behaviour of the unfilled PTFE. The aim of this work is going to be the design and development of a model able to provide indicative data on the useful life of PTFE based material components, in condition of tribological sliding contact with a counter-surface. This model is based on an equation that identifies the relationship between the independent variables of the process and the desired result (dependent variable). The prediction of the useful life of fluorinated polymers and polymer matrix composites in tribological applications would be a significant improvement compared to the simple "trial and error" approach.

PTFE has self-lubricating properties providing excellent tribological properties in many applications where low friction is sought for. During a sliding wear process, in fact, a polymer transfer is carried out on the surface of the antagonist, which can be metallic or

ceramic, with the creation of a thin film (also called transfer-film) where the macromolecules stretch along the sliding direction. In the contact zone, a polymer-polymer interaction and no longer polymer-ceramic / metal one is created, resulting in a very low adhesion work that means a low coefficient of friction (normally between 0.05 and 0.15). The approach in this Ph.D. thesis has been the research and analysis of functional parameters that determine the tribological characteristics of coupling systems. These parameters must be then correlated to the transfer-film formation process and heat exchange in the tribological contact areas.

The PTFE based materials, also called PTFE compounds, were provided by ATP S.p.A, a company based in Modena (Italy) that deals with the design and production of sealing systems in polymeric material. To simulate the sliding conditions, tribological pin on disc tests were carried out. The Design of Experiment (DOE) statistical method was applied to design the experiments and investigate the influence of the tribological testing variables (speed, load, distance), as single or interacting factors, on the wear rate of the PTFE pin. Minitab was used as software to elaborate the collected data applying DOE algorithms. In the first part of the Ph.D. period, tribological tests were carried out on unreinforced PTFE samples in order to investigate the wear mechanism of the material in dynamic contact with AISI 304 stainless steel countersurfaces, either uncoated or coated with plasma sprayed Cr_2O_3. A factorial plane has been generated with load, speed, and sliding distance as factors, making them vary in a range of minimum and maximum values. In Table 1 the operating conditions of the first tribological tests are reported. Each test has been repeated 3 times.

Load (N)	5		10
Speed (m/s)	0,54		1,8
Sliding distance (m)	3000	5000	7000

Table 1

The significant factors on the trend of the wear rate and of the coefficient of friction have been subsequently evaluated with the DoE statistical method: the results showed that load and speed are the most influential factors on the wear rate of the unreinforced PTFE, unlike the sliding distance which can be considered a non-significant parameter.

In the second part of the Ph.D. period, the influence of the thermal conductivity of PTFE composites on their tribological behaviour and the stability of transfer film created in a

tribological coupling were studied. This phenomenon was investigated by performing tribological tests measuring the contact temperature with an infrared thermographic camera and by the evaluation of the heat transfer coefficient through specific conductivity measurements on the polymer samples and on the surfaces of the tribological counterparts. The thermal conductivity of PTFE composites and their tribological behaviour are also affected by the amount of fillers added to the PTFE matrix. In this work different families and shapes of filler were studied:

- Carbon fibres, as heat conductive fillers
- Glass fibres, as non-conductive fillers
- Bronze particles, as heat conductive fillers (spheroidal and lamellar shape)
- PEEK particles, as non-conductive fillers, in two different contents: 10% and 20% by weight

The first tests were carried out on the fibres to investigate the influence of the thermal conductivity of the fillers on the wear mechanisms of the PTFE matrix composite. The other fillers have been studied and analysed at a later stage to determine whether the transfer-film formation mechanism is comparable in the case of materials with filler additions with similar thermal conductivity values, knowing from the literature that carbon fibres and bronze are fillers of conductive nature, unlike glass fibres and PEEK.

The thermal diffusivity of PTFE composites, pure PTFE (as a reference), AISI 304 stainless steel and plasma sprayed Cr_2O_3 was measured by the laser flash technique. Thermal conductivity (λ [W/(m·K)]) was computed from thermal diffusivity (α [m^2/s]) according to the definition of the latter: $\lambda = \alpha \cdot c \cdot \rho$, where c [J/(kg·K)] is the specific heat and ρ [kg/m^3] is the density. For this purpose, c was measured by differential scanning calorimetry. Based on specific heat values from DSC analyses and on thermal diffusivities measured by the laser flash method, thermal conductivities were obtained as a function of temperature up to 200 °C, which covers the range of interest for the tribological applications of PTFE-based composites.

In parallel, pin on disk tests were carried out with an infrared thermographic camera to monitor the temperature in the contact area .The counterparts for the wear tests were AISI 304 stainless steel uncoated and coated with a plasma sprayed Cr_2O_3 layer.

This configuration was chosen to mimic the contact conditions of a lip seal, which is one of the most frequent configurations for rotary seal joints. A lip seal indeed produces a non-conformal (line) contact with the mating shaft surface, which progressively turns into

a conformal contact as the lip itself wears down. Likewise, the spherical tip of the pins produces an initially nonconformal contact with the disc, that turns into a conformal contact as the pin wears down.

For all pin/disc couples, four different test conditions were employed by combining normal loads of 5 N and 10 N and sliding speeds of 0.54 m/s and 1.8 m/s. The sliding distance was 3000 m in all cases and each test was repeated at least twice. The friction coefficient was calculated by measuring the tangential force acting on the pin during the test through a load cell. The diameter of the circular wear scar left on the tip of the pin after the test was measured with an optical microscope, whence the volume of the worn cap was calculated through geometrical relations. Data was converted to specific wear rate, expressed in units of $mm^3/(N•m)$, by normalizing over the sliding distance and the applied load. In pin-on-disc tests, the friction coefficient usually rises during the earliest stages and soon attains a steady-state regime. The temperature of the pin also increases during the test; indeed, the pin is subjected to steady-state heating conditions, at least as soon as the friction coefficient attains a stable value.

The characterization of pins and counter-surfaces was carried out using SEM microscopy EDS microanalysis and FT-IR analyses.

These analyses showed that a transfer-film covers the entire wear surface of the glass fibers reinforced PTFE against both surfaces. In general, the glass fibres have undergone a comminution: the tribo-layer, in the case of AISI 304 stainless steel, appears to be made up by the compaction of fine, mostly sub-micrometric debris particles originating from the matrix (C and F), the glass fibres (O, Si, Al, Ca) and the steel counter-surface (Fe, Ni, Cr). This means that debris from all the elements of the tribo-system, including the uncoated stainless-steel disc, concur to the formation of the tribo-layer.

Carbon fibre-reinforced composites cannot establish analogous tribo-layers due to the different chemical nature and fracture behaviour of the carbon fibres. The carbon fibres are fragmented: as the PTFE matrix is abraded, contact mainly takes place between protruding carbon fibres and the counter-body, resulting in higher friction coefficients. The counter-surfaces also exhibit less transfer material, compared to the tests against the glass fibers reinforced PTFE composites. This is true both for uncoated AISI 304 and for the Cr_2O_3-coated disc. In the latter case, some empty pores in the wear trace are recognisable through their bright boundaries. Detailed views confirm that some pores,

including some of the large ones, are mostly empty, though others are partly or entirely filled.

The analysis carried out on PTFE composites reinforced with bronze and PEEK show that the wear mechanism and wear rates of the materials cannot be categorized according to the thermal conductivity of the filler. It has been shown that PTFE composites reinforced with conductive fillers, having a similar value of thermal conductivity, do not have the same wear mechanism and the same transfer-film creation process.

PTFE composites reinforced with PEEK, probably due to poor chemical affinity of the filler with the discs, are not able to form a significant transfer-film layer, like CF-PTFE. Especially against the Cr_2O_3-coated disc, the particles form not continuous agglomerates on the surface, resulting in high values of the wear rate.

The transfer-film formation process requires, in general, a high amount of material. In fact, the samples with more stable transfer-film are those with the highest overall wear rates.

PTFE composites reinforced with bronze, especially the one with the lamellar shape, manage to form a more continuous and compact transfer-film layer, like GF-PTFE composites, against both counter-surfaces: this leads to a rapid decrease in the coefficient of friction, favouring a smoother sliding. The FT-IR analyses showed that the samples made with bronze-PTFE composites are characterized by the presence of -OH groups, like GF-PTFE, indicative of the moisture absorbed by the material when transfer-film formation occurs. This fact can be considered positive because it involves the formation of a more regular and homogeneous transfer-film. The presence of the -OH groups also depends on the debris released from the disc: in fact, metal particles, which oxidize, tend to bind more the -OH groups. The surfaces of the most worn discs, those against PTFE reinforced with bronze, are also the ones with the more evenly distributed transfer-film.

The temperature developed inthe pin-disc contact area does not influence the wear mechanism of the material and the stability of the transfer-film, but rather the presence of debris released by the counter-surface: it has been demonstrated that the presence of metal debris contributes to a better stability of the transfer-film and therefore to a not sever wear state.

After this experimental phase, an analytical model was developed using the DoE method: the aim of this model is to predict the tribological behavior in terms of wear rate of a real

component made with a certain material and tested under specific operating conditions of load and speed, starting from tests carried out on a small scale (pin on disc).

The results, in terms of wear rate,obtained from the tribological tests carried out on PTFE composites reinforced with spheroidal bronze and PEEK (10-20%) against the Chromia coated surface were imported on the software Minitab, to generate the factorial plane with the Design of Experiment method.

Since the test rig is the only method that allows to provide indicative data on the useful life of real components, in our case of sealing systems in polymeric material, thanks to this model it is possible to perform simple pin-on-disc tests and obtain a reasonable agreement (order of magnitude) with the test-rig experiments.

Furthermore, the validation of this model would allow to significantly reduce the response times to the needs of ATP customers.

Summary (Italian version)

La tribologia, ovvero lo studio dell'attrito, della lubrificazione e dell'usura di solidi interagenti, ha ricevuto nel corso dei decenni una crescente attenzione dal punto di vista scientifico, tecnico e pratico. Questo perché il funzionamento di molti sistemi meccanici dipende dalle loro prestazioni di attrito e usura. Inoltre, la dissipazione annuale di energia e lo spreco di materie prime preziose derivanti da un elevato attrito e usura è di grande importanza economica.

Il processo di usura dei polimeri è considerato un fenomeno molto complesso e può variare non solo per polimeri diversi ma anche per lo stesso polimero in condizioni di scorrimento diverse; tale fenomeno dipende ampiamente dai fattori circostanti (ambientali) come la presenza di contaminazione, lo strato di ossido sulle superfici solide, il calore dissipato, oltre alle proprietà chimiche, fisiche e meccaniche intrinseche dei due corpi interagenti e alle condizioni operative di pressione di contatto e velocità relativa. C'è un altro fattore che può cambiare le prestazioni tribologiche di due corpi ed è la presenza di detriti, noti anche come “terzo corpo”, che vengono espulsi da uno dei corpi interagenti [1].

In questa tesi di dottorato è stato studiato il meccanismo di usura di diversi compositi in PTFE, ampiamente utilizzati per la progettazione di sistemi di tenita, contro diverse controsuperfici, partendo dai principali fattori significativi che influenzano il comportamento tribologico del PTFE tal quale (non rinforzato). Lo scopo di questo lavoro sarà successivamente la progettazione e lo sviluppo di un modello in grado di fornire dati indicativi sulla vita utile dei componenti a base di PTFE, in condizione di scorrimento tribologico con una contro-superficie. Questo modello si basa su un'equazione che identifica la relazione tra le variabili indipendenti del processo e il risultato desiderato (variabile dipendente). La previsione della vita utile dei polimeri fluorurati e dei compositi a matrice polimerica nelle applicazioni tribologiche sarebbe un miglioramento significativo rispetto al semplice approccio "trial and error".

Il PTFE ha proprietà autolubrificanti che forniscono eccellenti proprietà tribologiche in molte applicazioni in cui è richiesto un basso attrito. Durante un processo di usura per scorrimento, infatti, viene effettuato un trasferimento di polimero sulla superficie dell'antagonista, che può essere di natura metallica o ceramica, con la creazione di un film sottile (detto anche transfer-film) in cui le macromolecole si allungano lungo la direzione

di scorrimento. Nella zona di contatto si crea un'interazione polimero-polimero e non più polimero-ceramica/metallo, risultando in un lavoro di adesione molto basso che significa un basso coefficiente di attrito (normalmente tra 0,05 e 0,15). L'approccio in questa tesi di dottorato è stato la ricerca e l'analisi dei parametri funzionali che determinano le caratteristiche tribologiche dei sistemi di accoppiamento. Questi parametri devono quindi essere correlati al processo di formazione del film di trasferimento e allo scambio termico nelle aree di contatto tribologico.

I compound a matrice PTFE, sono stati forniti da ATP S.p.A, società con sede a Modena (Italia) che si occupa della progettazione e produzione di sistemi di tenuta in materiale polimerico. Per simulare le condizioni di scorrimento, sono stati eseguiti test tribologici in configurazione "pin on disk". Il metodo statistico Design of Experiment (DOE) è stato applicato per progettare gli esperimenti e studiare l'influenza delle variabili dei test tribologici (velocità, carico, distanza), come fattori singoli o interagenti, sul tasso di usura del pin in PTFE. E' stato utilizzato Minitab come software per elaborare i dati raccolti applicando algoritmi DOE. Nella prima parte del periodo di dottorato sono stati effettuati test tribologici su campioni di PTFE non rinforzato al fine di indagare il meccanismo di usura del materiale in contatto dinamico con controsuperfici in acciaio inox AISI 304, non rivestito o rivestito con Cr_2O_3 termo-spruzzata al plasma. E' stato generato un piano fattoriale avente come fattori il carico, la velocità e la distanza di strisciamento, facendoli variare in un range di valori minimo e massimo. In tabella 1 vengono riportate le condizioni operative dei primi test tribologici. Ciasuna prova è stata ripetuta 3 volte.

Load (N)	5		10
Speed (m/s)	0,54		1,8
Sliding distance (m)	3000	5000	7000

Tabella 1

I fattori significativi sull'andamento del tasso di usura e del coefficiente di attrito sono stati quindi successivamente valutati con il metodo statistico DoE: i risultati hanno mostrato che il carico e la velocità sono i fattori più influenti sul tasso d'usura del PTFE non caricato, a differenza della distanza di strisciamento che si può considerare un parametro non significativo.

Nella seconda parte del periodo di dottorato sono state studiate l'influenza della conduttività termica dei compositi PTFE sul loro comportamento tribologico e la stabilità

del film di trasferimento creato in un accoppiamento tribologico. Questo fenomeno è stato indagato eseguendo test tribologici con l'ausilio di una termocamera a infrarossi,per misurare la temperatura sviluppata nell'area di contatto pin-disco, e valutando il coefficiente di scambio termico attraverso specifiche misure di conducibilità sui campioni polimerici e sulle superfici delle controparti tribologiche. La conducibilità termica dei compositi a matrice PTFE e il loro comportamento tribologico sono influenzati, come noto dalla letteratura, anche dalla quantità di riempitivi aggiunti alla matrice ptfe; per questo motivo in questo lavoro sono state studiati filler di divera natura e famiglia:

- Fibre di carbonio, come filler di natura conduttiva
- Fibre di vetro, come filler di natura isolante
- Bronzo, come filler di natura conduttiva (forma sferoidale e lamellare)
- PEEK, come filler di natura isolante, in due diverse percentuali di contenuto: 10% e 20% in peso.

I primi test sono stati effettuati sui compositi rinforzati con le fibre per studiare l'influenza della conducibilità termica di queste ultime sui meccanismi di usura del composito a matrice di PTFE. Gli altri riempitivi sono stati studiati e analizzati in una fase successiva per determinare se il meccanismo di formazione del tribofilm è comparabile nel caso di compositi rinforzati con filler aventi simili valori di conducibilità termica, conoscendo dalla letteratura che le fibre di carbonio e il bronzo sono riempitivi di natura conduttiva, a differenza invece delle fibre di vetro e del PEEK.

Con l'analisi LFA (Laser Flash Analysis) è stata misurata la diffusività termica di tutti i compositi a matrice PTFE, del PTFE puro (come campione di riferimento), e dei dischi in acciaio inox AISI 304 rivestito e non. La conducibilità termica (λ [W/(m·K)]) è stata calcolata dalla diffusività termica (α [m^2/s]) secondo la definizione di quest'ultima: $\lambda = \alpha \bullet c \bullet \rho$, dove c [J/(kg·K)] è il calore specifico e ρ [kg/m3] è la densità. A tale scopo, il valore di "*c"* è stato misurato mediante calorimetria differenziale a scansione. Sulla base dei valori del calore specific derivanti da analisi DSC e di diffusività termiche misurate con il metodo LFA, le conduttività termiche sono state ottenute in funzione della temperatura fino a 200 °C, range che copre la gamma di interesse per le applicazioni tribologiche dei compositi a matrice PTFE.

In parallelo, i test pin on disk sono stati effettuati con una termocamera a infrarossi per monitorare la temperatura nell'area di contatto.

Questa configurazione è stata scelta per simulare le condizioni di contatto di una guarnizione a labbro, essendo una delle configurazioni più frequenti nei sistemi di tenuta montati all'interno di giunti rotanti. Una guarnizione a labbro produce infatti un contatto non conforme con la superficie dell'albero di accoppiamento, che si trasforma progressivamente in un contatto conforme man mano che il labbro stesso si consuma. Allo stesso modo, la punta sferica dei pin produce un contatto inizialmente non conforme con il disco, che si trasforma in un contatto conforme quando il pin stesso si consuma.

Per tutte le coppie pin/disco, sono state impiegate quattro diverse condizioni di prova combinando carichi normali di 5 N e 10 N e velocità di strisciamento di 0,54 m/s e 1,8 m/s. La distanza di scorrimento è stata di 3000 m in tutti i casi e ogni prova è stata ripetuta almeno due volte. Il coefficiente di attrito è stato calcolato misurando la forza tangenziale che agisce sul pin durante la prova attraverso una cella di carico. Il diametro della superficie usurata del pin è stato misurato dopo il test con un microscopio ottico, da cui è stato successivamente calcolato, attraverso opportune relazioni geometriche, il volume del materiale asportato (ovvero della calotta sferica). I dati sono stati convertiti in un tasso di usura specifico, espresso in $mm^3/(N•m)$, normalizzando la distanza di strisciamento e il carico applicato. Nei test pin-on-disc, il coefficiente di attrito di solito aumenta durante le prime fasi e presto raggiunge un regime di stato stazionario. Anche la temperatura del pin aumenta durante il test; in regime stazionario la temperatura diventa stabile non appena anche il coefficiente di attrito raggiunge un valore stabile.

La caratterizzazione dei pin e delle contro-superfici è stata effettuata mediante il microscopio SEM, la microanalisi EDS e le analisi FT-IR.

Queste analisi hanno dimostrato che il tribofilm copre l'intera superficie di usura del GF-PTFE contro entrambe le superfici. In generale, le fibre di vetro hanno subito una comminuzione: il tribofilm, nel caso dell'acciaio inox AISI 304, sembra essere costituito dalla compattazione di particelle di detriti fini, per lo più sub-micrometrici, provenienti dalla matrice (C e F), dalle fibre di vetro (O, Si, Al, Ca) e dalla contro-superficie in acciaio (Fe, Ni, Cr). Ciò significa che i detriti di tutti gli elementi del tribo-sistema, incluso il disco in acciaio inossidabile non rivestito, concorrono alla formazione del tribofilm.

I compositi rinforzati con fibra di carbonio non stabiliscono un tribofilm analogo a causa della diversa natura chimica e del comportamento a frattura delle fibre di carbonio. Le fibre di carbonio risultano infatti frammentate: poiché la matrice di PTFE è abrasa, il contatto avviene principalmente tra le fibre di carbonio sporgenti e la contro-superficie,

con conseguenti coefficienti di attrito più elevati. Le contro-superfici presentano anche meno materiale di trasferimento, rispetto ai test contro i compositi GF-PTFE. Questo vale sia per l'AISI 304 non rivestito che per il disco rivestito in Cr_2O_3. Le immagini a maggiori ingrandimenti confermano che alcuni pori sono per lo più vuoti, anche se altri sono parzialmente o interamente riempiti.

Le analisi effettuate su compositi in PTFE rinforzati con Bronzo e PEEK mostrano che il meccanismo di usura e i tassi di usura dei materiali non possono essere classificati in base alla conduttività termica del riempitivo. È stato dimostrato che i compositi in PTFE rinforzati con riempitivi di natura conduttiva aventi un valore simile di conduttività termica, non hanno lo stesso meccanismo di usura e lo stesso processo di formazione di film di trasferimento.

I compositi in PTFE rinforzati con PEEK, probabilmente a causa della scarsa affinità chimica del riempitivo con la contro-superficie, non sono in grado di formare uno strato significativo di tribofilm, come il CF-PTFE. Soprattutto contro la Chromia, le particelle formano agglomerati non continui sulla superficie, con conseguenti valori elevati del tasso di usura.

Il processo di formazione del film di trasferimento richiede, in generale, un'elevata quantità di materiale. In effetti, i campioni con film di trasferimento più stabile sono quelli con i più alti tassi di usura complessivi.

I compositi in PTFE rinforzati con bronzo, in particolare quello a forma lamellare, riescono a formare un tribofilm più continuo e compatto, come i compositi GF-PTFE, contro entrambe le controsuperfici: questo porta ad una rapida diminuzione del coefficiente di attrito, favorendo uno scorrimento più fluido. Le analisi FT-IR hanno mostrato che i campioni realizzati con compositi bronzo-PTFE sono caratterizzati dalla presenza di gruppi -OH, indicativi dell'umidità assorbita dal materiale quando si verifica la formazione del tribofilm. Questo fatto può essere considerato positivo perché comporta la formazione di un film di trasferimento più regolare e omogeneo. La presenza dei gruppi -OH dipende anche dai detriti rilasciati dal disco: infatti, le particelle metalliche, che si ossidano, tendono a legare maggiormente i gruppi ossidrili. Le superfici più usurate dei dischi, quelle contro PTFE rinforzato con bronzo, sono anche quelle con il tribofilm più uniformemente distribuito.

La temperatura sviluppata nell'area di contatto pin-disco non influenza il meccanismo di usura del materiale e la stabilità del tribofilm, ma piuttosto la presenza di detriti rilasciati

dalla contro-superficie: è stato dimostrato che la presenza di detriti metallici contribuisce ad una migliore stabilità del tribofilm e quindi ad uno stato di usura non severo.

Dopo questa fase sperimentale, è stato elaborato un modello analitico utilizzando il metodo DoE: lo scopo di questo modello è prevedere il comportamento tribologico in termini di tasso di usura di un componente reale realizzato con un determinato materiale e testato in specifiche condizioni operative di carico e velocità, partendo da prove eseguite su piccola scala (pin-on-disc) .

I risultati, in termini di tasso di usura, ottenuti dalle prove tribologiche effettuate su compositi PTFE rinforzati con bronzo sferoidale e PEEK (10-20%) contro la superficie rivestita di Chromia sono stati importati sul software Minitab, per generare il piano fattoriale con il metodo del Design of Experiment.

Poiché il banco prova è l'unico metodo che permette di fornire dati indicativi sulla vita utile dei componenti reali, nel nostro caso di sistemi di tenuta in materiale polimerico, grazie a questo modello è possibile eseguire semplici prove pin-on-disc ed ottenere una ragionevole corrispodenza (in termini di ordine di grandezza) con i test eseguiti su banco prova.

Inoltre, la validazione di questo modello permetterebbe di ridurre sensibilmente i tempi di risposta alle esigenze dei clienti ATP.

1 Introduction

In this chapter, the general aspects and tribological properties of polymeric materials have been studied. In particular, the following topics have been briefly described:

- Generalities and historical notes on Fluoropolymers.
- Properties and production technologies of the main PTFE based composites used for the manufacturing of sealing rings and gaskets.

Furthermore, general properties of the coatings used in this Ph.D. thesis have been described.

1.1 Properties of polymeric materials

Polymeric materials are often used in tribological applications where wear is caused by sliding, especially the ones reinforced with carbon or glass fibres, ceramic particles, graphite and so on, to improve mechanical properties and confer (or improve) lubricating properties [2].

The principal properties of polymeric materials are:

- Low chemical affinity for metals.
- High chemical inertia against many aggressive agents.
- Self-lubricating capacity.
- Low density (around 1 g/cm3).
- Ability to dampen vibrations.

These characteristics make polymeric materials particularly suitable to realize:

- Bearings and gaskets.
- Gear wheels.
- Rings for pistons.
- Biomedical applications.

The main materials used in tribological applications are reported in Table 2:

Material	Density (g/cm^3)	Elastic modulus (GPa)	Maximum operating temperature (°C)	K_a (m^2/N)	Observations
HDPE	0.96	0.4–1.2	120	10^{-14} to 10^{-15}	Used for piping, toys, houshold ware
					UHMWPE is used in orthopedic implants
Polyamide (nylon 66)	1.14	3.3	180	10^{-14} to 10^{-15}	Widely used in gears, bearings, bushes
Polyamide + graphite	1.2	4	180	$\approx 10^{-15}$	Graphite reduces friction and wear
Polyacetal (POM)	1.4	2.9–3.3	140	$\approx 10^{-15}$	Excellent dimensional stability; high mechanical properties; recommended for precision parts
PTFE (teflon®)	2.1–2.2	0.48–0.76	260	$\approx 10^{-13}$	Produced by powder sintering; excellent self-lubricating properties; high chemical inertness
PTFE + glass or carbon fibers			260	$\approx 10^{-14}$	Reinforced to increase strength
Polyimide	1.42	2–3	320	$\approx 3 \times 10^{-15}$	Excellent mechanical properties (up to 250 °C). Quite expensive
Polyimide + graphite	1.5	5–14	320	$\approx 3 \times 10^{-16}$	Graphite reduces friction and wear
Phenolics	1.4	50	200	$\approx 10^{-14}$	
Phenolics + PTFE	1.4	50	200	$\approx 2 \times 10^{-16}$	

Table 2: Main characteristics of some polymers widely used in tribological applications: the specific wear rate, K_a, refers to dry sliding tests against steel antagonist [2].

1.2 Fluoropolymers

Fluoropolymers are polymers consisting of strong bonds between carbon and fluorine. This class of materials is often referred to as per-fluoropolymers to distinguish them from partially fluorinated polymers [3] . The properties of these polymers derive precisely from the atomic structure of the two elements and from the covalent bonds that are established (C-C= 607 kJ/mol and C-F= 552 kJ/mol). The fluorine atom has a high electronegativity and consequently the C-F bond is more stable than the C-H bond. Furthermore, in the linear chains - [CF2] -, the C-C bonds are completely shielded by the fluorine atoms, due to their much greater atomic radius than the hydrogen atom, greatly increasing chemical stability and reducing the reactivity of the macromolecule.

In polymers, the replacement of the C-H bond with a C-F bond therefore confers greater stability of the molecule, a low surface tension, low refractive index [4].

Fluoropolymers are considered "high tech" materials with very high performance. Their main characteristics can be summarized as follows [5]:

- Low adhesion: the surface energy is very low, so they offer excellent hydrophobic and non-stick properties.
- Environmental resistance: they are transparent to UV rays, extremely resistant to oxidation and maintain their properties even at very low temperatures; furthermore, the fluoropolymers are resistant to the attack of microorganisms and not biodegradable.
- Corrosion Resistance: they resist aggressive chemicals over a wide temperature range.
- Heat resistance: some fluoropolymers can work at temperatures of 260 ° C continuously, with higher peaks for short periods.
- Fire resistance: they have a resistance to LOI (Limited Oxygen Index) degrees above 95%, which means there must be more than 95% oxygen to support combustion (air alone contains ~ 21% oxygen), so a material with an LOI greater than 21 is very flame retardant resistant.
- Wear resistance: they are the materials with the lowest coefficient of friction and this generally leads to good wear resistance.
- Long service life: they are characterized by excellent resistance to aging, even in the presence of high temperatures and aggressive chemicals; the resistance to dynamic stresses, such as vibrations or bending, is also high.

Among all the fluoropolymers [6], the one with the best features from the tribological point of view is polytetrafluoroethylene (PTFE) whose discovery dates to 6 April 1938 by Roy J. Plunkett, employed at the DuPont laboratory in Jackson (USA).

Table 3 lists the patents relating to PTFE and its processing technologies in chronological order [7].

Invention	Inventor	Patent	
		Number	Issue Date
Discovery of PTFE	R. Plunkett	US 2,230,654	February 4, 1941
Granular PTFE	M.M. Brubaker	US 2,393,967	February 5, 1946
Dispersion PTFE	M. M. Renfew K.L. Berry Lontz and Happoldt	US 2,534,058 US 2,559,752 Paper	December 12, 1950 July 19, 1951, 1952
Paste extrusion of fine powder PTFE	J.F. Lontz	US 2,893,582	April 22, 1952
Finely ground granular PTFE	Paul E. Thomas and Curtis C. Wallace	US 2, 936,301	May 10, 1960
Free-flowing granular PTFE	(a) Robert Roberts and Ronald F. Anderson (b) Mathew B. Black, Ellsworth E. Faust, William S. Barnhart, and Raymond Netsch[b]	US 3,766,133 US 3,265,679	October 16, 1973 August 9, 1966
High strength porous PTFE sheeting	R.L. Gore[c]	US 3,953,566	April 27, 1976

PTFE, Polytetrafluoroethylene.
[a]Lontz JF, Happoldt WB. Teflon tetrafluoroethylene resin dispersion: a new aqueous colloidal dispersion of polytetrafluoroethylene. Ind Eng Chem *1952;44(8):1800–5.*
[b]Assigned to Pennsalt Corp (now Arkema).
[c]Assigned to WL Gore and Associates.
Other patents assigned to Dupont.

Table 3: Stages in the development of PTFE.

1.3 PTFE

Polytetrafluoroethylene or PTFE is a fluoropolymer resulting from the polymerization of monomers of tetrafluoroethylene in the gas phase (C_2F_4), which are subjected to radical chain polymerization according to the mechanism shown in Figure 1.

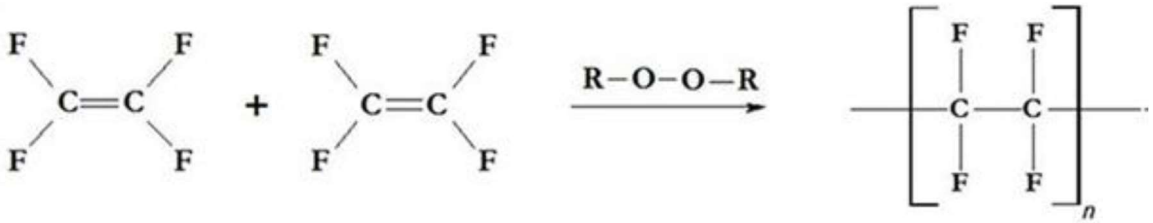

Figure 1:PTFE Synthesis mechanism starting gas phase Tetrafluoroethylene [8]

The material obtained is a crystalline polymer with a melting temperature of 327 ° C and a very stable chemical structure, due to the complete saturation of the double bonds by fluorine atoms which guarantee a high chemical inertness as an effective protective shield is formed for the chain of carbon atoms, due to their high charge density / size

ratio [5]. The strong C-F bond gives PTFE excellent thermal stability up to temperatures not exceeding 260 ° C.

Furthermore, being made up of long linear chains, PTFE has a high density compared to other polymeric materials, between 2.13 and 2.18 g / cm^3.

PTFE is inert towards all known chemical reagents, its chemical resistance comes from the very stable bond between carbon and fluorine, this being one of the strongest organic bonds. The fluorine atom forms an impermeable sheath that surrounds the carbon chain. Table 4 and Table 5 summarize the chemical resistance values of polytetrafluoroethylene exposed to the most common solvents, and to the most common basic and acidic chemical reagents. The resistance values are expressed in terms of weight loss for a given time and a given exposure temperature [9].

Solvent	Exposure Temperature, °C	Exposure Time	Weight Gain, %
Acetone	20	12 months	0.3
	50	12 months	0.4
	70	2 weeks	0
Benzene	78	96 h	0.5
	100	8 h	0.6
	200	8 h	1.0
Carbon tetrachloride	25	12 months	0.6
	50	12 months	1.6
	70	2 weeks	1.9
	100	8 h	2.5
	200	8 h	3.7
Ethanol (95%)	25	12 months	0
	50	12 months	0
	70	2 weeks	0
	100	8 h	0.1
	200	8 h	0.3
Ethyl acetate	25	12 months	0.5
	50	12 months	0.7
	70	2 weeks	0.7
Toluene	25	12 months	0.3
	50	12 months	0.6
	70	2 weeks	0.6

Table 4: PTFE chemical resistance to common solvents [9]

Reagent	Exposure Temperature, °C	Exposure Time	Weight Gain, %
Hydrochloric acid			
10%	25	12 months	0
10%	50	12 months	0
10%	70	12 months	0
20%	100	8 h	0
20%	200	8 h	0
Nitric acid			
10%	25	12 months	0
10%	70	12 months	0.1
Sulfuric acid			
30%	25	12 months	0
30%	70	12 months	0
30%	100	8 h	0
30%	200	8 h	0.1
Sodium hydroxide			
10%	25	12 months	0
10%	70	12 months	0.1
50%	100	8 h	0
50%	200	8 h	0
Ammonium Hydroxide			
10%	25	12 months	0
10%	70	12 months	0.1

Table 5: PTFE chemical resistance to the most common acids and bases [9]

PTFE has a low thermal conductivity. It is not flammable and is stable for long times at temperatures not exceeding 260 ° C.

The values of dielectric constant (representing the ability of a material to store electrostatic energy with respect to vacuum) and of the dissipation factor (index of how the electrical energy is absorbed when the dielectric material is exposed to an altering field) of PTFE are the lowest compared to all known solid materials. These characteristics are still linked to the PTFE structure, which is highly symmetrical with respect to the fluorine atoms, uniformly distributed along the main chain as shown in Figure 2.

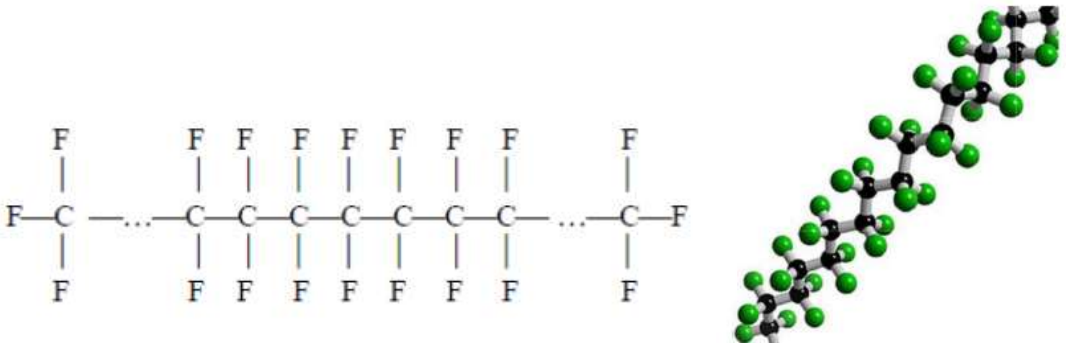

Figure 2: PTFE structure

PTFE has a transition point at temperatures between 19 ° C and 21 ° C, determined by a change in its crystalline structure which causes a volume variation of about 1%.

For the dimensional control of PTFE products, it is necessary to use suitable techniques. The existence of the transition point around 20 ° C makes it necessary to take special precautions if very narrow dimensional tolerances are required; in these cases, standard control procedures must be established.

Figure 3 shows the PTFE state diagram. The diagram highlights the solid-state phase transitions as a function of temperature and pressure. Phase 2, the one at temperatures below 19 ° C, is the most stable from a structural point of view thanks to the structure of a triclinic unit cell formed by 13 carbon atoms. Above 19 ° C the chains are able to make an angular displacement, which causes distortions in the polymer helix and changes the type of crystalline structure switching to a pseudo-hexagonal repetitive cell until reaching the melting point (327 C °) [5].

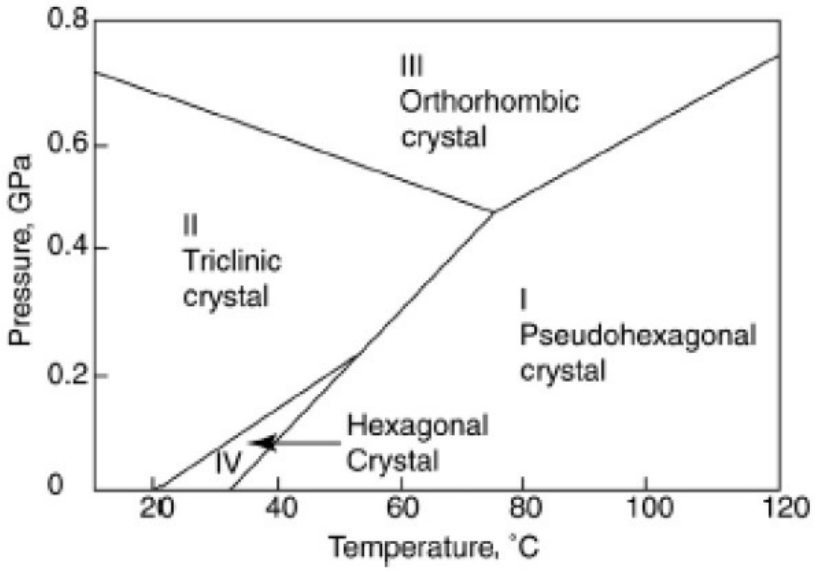

Figure 3: PTFE state diagram

1.4 Tribology: wear and friction

Tribology is defined as "the science and technology of interactions between contact surfaces in relative motion, under load", and then deals with all aspects related to the study of phenomena of friction, lubrication, and wear. Friction is a "resistant force due to the interaction between two contact surfaces"; it involves the loss of energy (10-30% of the produced energy) that is dissipated in form of heat and, therefore, a loss of performance. Wear is defined as "damage to a solid surface, which generally involves the progressive loss of material, due to the relative movement between the surface and one or more substances in contact" [10]

"Tribological system" is defined as the system consisting of two bodies in contact, in relative motion, with a possible third body interposed, placed in a defined environment.

The analysis of any tribological system, even complex, involves the identification of the elementary structure, or the so-called "tribological system" (Figure 4) consisting of:

- Two contact bodies, under load and in relative motion (triboelements 1 and 2)
- The interfacial element (triboelement 3)
- The environment in which the elements are placed

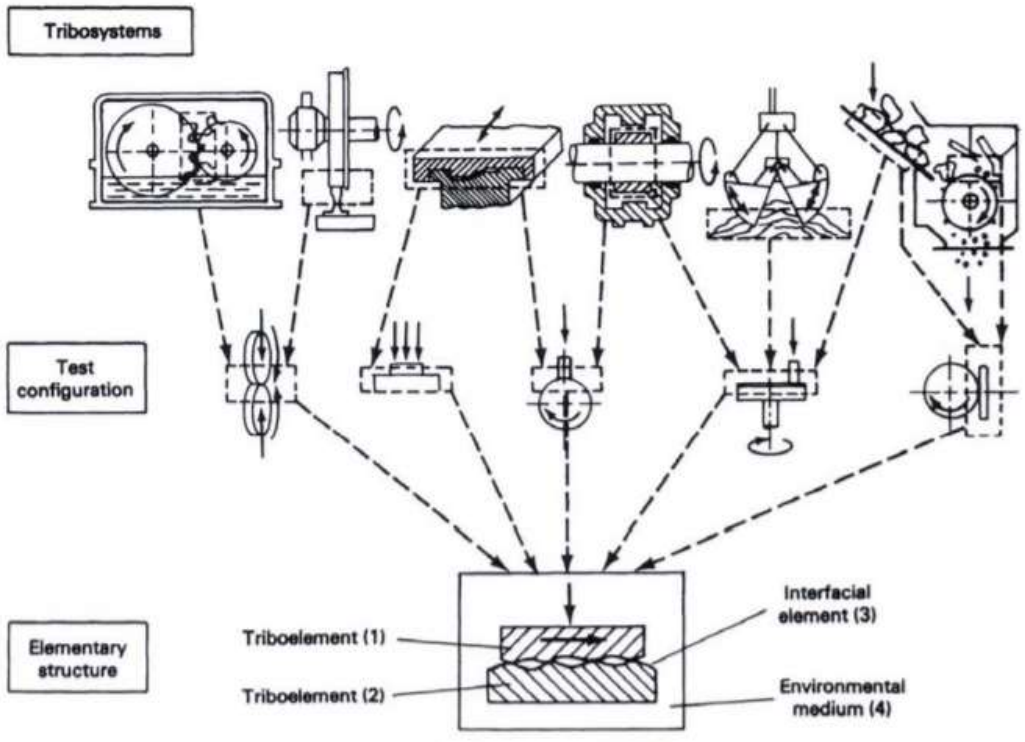

Figure 4: Simplification of a tribological system [10].

Friction and wear are not intrinsic properties of the material, but characteristics of the tribological system. The coefficient of friction therefore depends on the nature of the contact materials, on the possible lubrication regime, on the operating environment.

1.5 Wear mechanism of polymeric materials

Polymers are being used increasingly in tribological applications due to their elasticity, accommodation to shock loading, low friction and wear resistance. However, tribology of polymers is different from tribology of metals for many reasons. In contrast to metals, polymers are viscoelastic, and their properties are dependent on time. External liquid lubricants, which work well for other classes of materials, are easily absorbed by polymers. Further complexity arises as polymers are easily influenced by the operating conditions and the prevailing environment. Nevertheless, it is a fascinating area because polymers can be modified, both on the surface and in bulk, by various chemical and physical means to suit a particular application. For this reason, they became attractive candidates and very promising materials for tribologists with the ability to control their friction and wear behaviours. This has resulted in various tribosystems composed of polymers, metals and ceramic materials in sliding or rolling tribological contacts.

The adhesion between two polymers or between a polymer and another material is based on secondary bonds and is therefore generally low. However, due to the low ratio between E (elastic modulus) and H (hardness), the contact is predominantly elastic, and the deformation component may be more important than the adhesive one: moreover, the coefficient of friction is greatly affected by the load, sliding speed and temperature. As a result of the low cohesion energy, a polymer is easily worn out by a harder material and its fragments can remain trapped on the antagonist surface to form a real transfer layer [1]. Under these conditions, the initial coupling is modified, and the polymer slides against itself. The tribological behaviour of PTFE is based on this phenomenon (see Section 1.7).

The wear mechanisms that may affect polymeric materials are:

- Adhesive wear.
- Abrasive wear from hard particles.
- Tribo-chemical wear
- Fatigue wear.

1.5.1 Adhesive wear

Adhesive wear is the most common form of dry wear, which arises from the shear of adhesive bonding. This form of wear is likely to be the most significant in the wear of a polymer when it slides repeatedly over the same wear track on a smooth metal counter-surface. During repeated sliding, high local pressure is experienced between the polymer surface and the counter-surface, causing plastic deformation leading to the formation of an adhesive junction. Further motion results in continuous formation and rupture of these junctions (Figure 5) [1]. A thin film of the soft polymer is transferred onto the hard mating surface. As the transfer film builds up, the surface topography of the counterpart changes and equilibrium may be reached, in which the amount of material removed from the bulk polymer by adhesive wear is equal to the rate of subsequent detachment of wear particles from the transfer film.

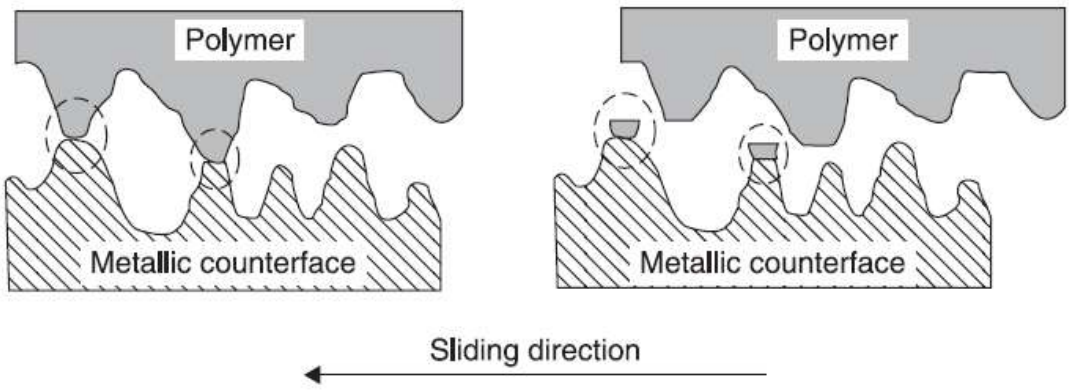

Figure 5: Schematic illustration of adhesive junction [1]

Another consequence of polymer transfer is a change in roughness of both surfaces in contact. The roughness of the polymer rubbing surface undergoes large variation during the primary stage, running- in, of wear until the steady state wear is reached, while metal surface roughness is modified due to transfer of the polymer. In many cases, adhesive wear is independent of surface roughness, often occurring on very smooth surfaces as well as rougher ones.

One of the most used relations for the adhesion wear was derived by Archard [11] and could be applied to polymer- metal pairs. Considering that the real area of contact between sliding pairs is determined by the hardness of the softer material and hemispherical wear particle removal, the total removed volume of the polymer V by adhesive wear is given by the following equation:

$$V = \frac{kLX}{H}$$

where L is the normal load, X is the sliding distance, H is the Brinell hardness of the softer material, and k is the proportionality constant. The main disadvantages of this model are that the factor k must be estimated experimentally through wear tests, and the Brinell hardness is a senseless material property for thermoplastics due to creep occurring under ambient conditions. The linear relationship between worn volume and the load is often observed experimentally, but it should be emphasised that this is true only when changes in load do not include changes in other variables, such as the type of transfer film involved, or the surface temperature, which depends not only on the load but also on the sliding configuration and its heat transfer characteristics [1].

1.5.2 Abrasive wear

Abrasive wear is caused by hard asperities on the counter-surface, which dig into the rubbing surface of the polymer and remove material, resulting in micro- machining, wear grooves, tearing, ploughing, scratching and surface cracking (Figure 6). The wear debris produced usually takes the shape of fine chips or flecks, like those produced during machining (Figure 7). The abrasive wear is dependent on the shape and apex angle of the abrasive points moving along the polymer surface

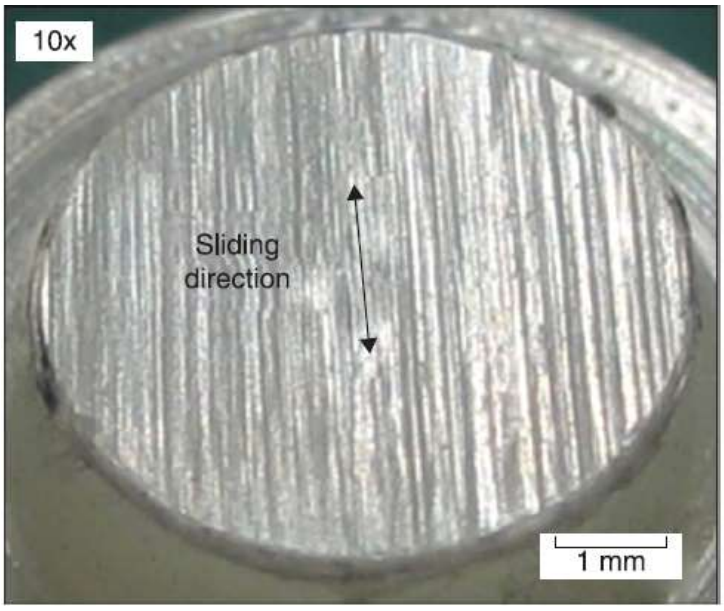

Figure 6: Rubbing surface of polyamide 66 after 80 km of sliding against dry steel counter-surface, at 90 N. Grooves run across the surface of the wear pin parallel to the sliding direction [12].

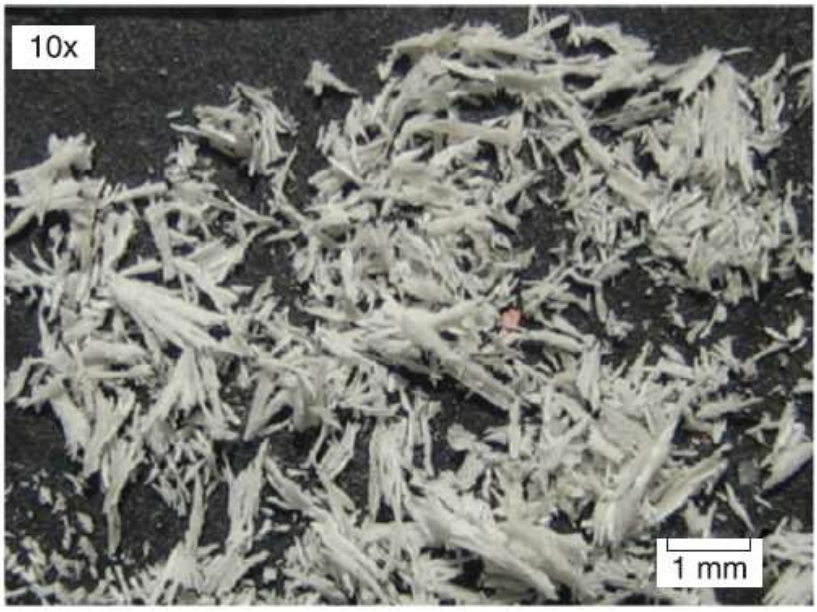

Figure 7: Wear debris of polyamide 66 after 20 km of sliding against dry steel counter-surface, at 90 N [12].

The abrasive wear of polymers is inversely proportional to the product of the nominal tensile breaking stress σ_u and the elongation at break ε_u (Figure 8).

The abrasion of polymers may also correlate with its cohesive energy, flexure modulus, yield strain or energy- to-rupture [13]. A wide range of studies on the effect of the counterpart surface on wear of polymers demonstrated that the abrasive wear process involves plastic deformation and shear, and it was found that for abrasion the dominant material property is the energy- to-fracture of the polymer [14].

Based on the above, several equations have been proposed to express the abrasive wear of polymers. Mainly there are three stages involved in the production of wear debris:

1. deformation of the surfaces to an area of contact is determined by the indentation hardness.
2. relative motion opposed by the frictional force (f), $f = \mu L$, where L is the normal load and μ represents the coefficient of sliding friction.
3. disruption of material at the contact points involving an amount of work equal to the integral of the stress- strain relationship [15].

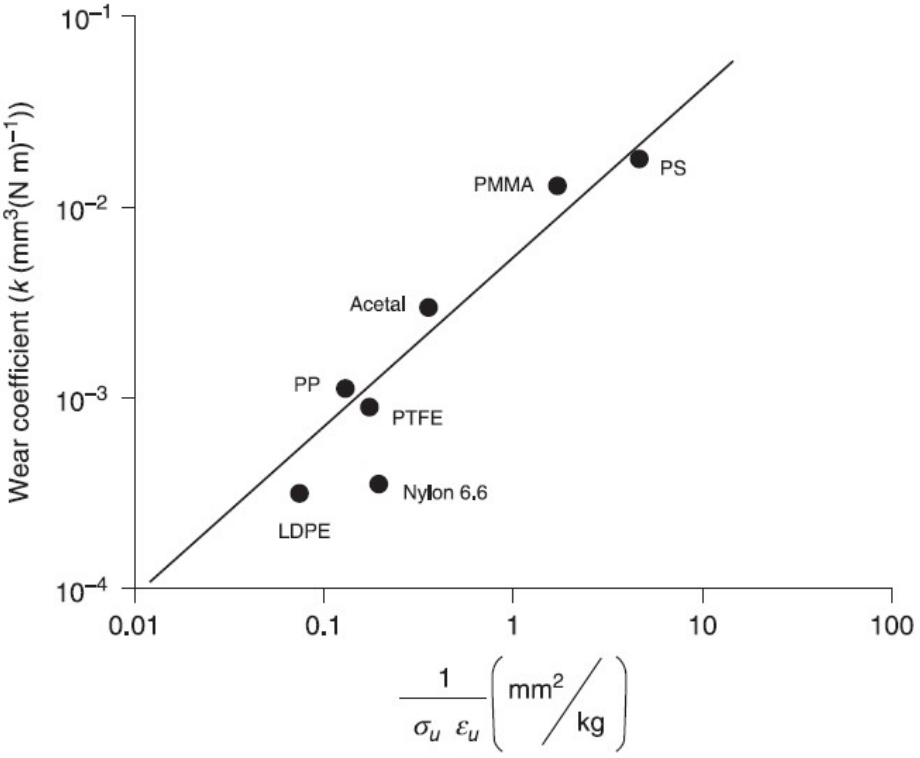

Figure 8: Ratner-Lancaster correlation for abrasion [14]

An approximate measure of the latter is the product of the breaking stress and the elongation to break. As these three processes occur sequentially, the total wear can be regarded as proportional to the probability of completion of each stage. Thus, for the sliding distance X, the worn volume V is given by the following expression [14]:

$$V = \frac{\mu L X}{H\ (\sigma_u \varepsilon_u)}$$

because the product ($\sigma_u\varepsilon_u$) is related to the area under the stress- strain curve, the toughness or impact strength of the material. Therefore, correlations have been sought between abrasive wear and impact strength, or notched impact strength. The particular importance of the parameter $\frac{1}{\sigma_u \varepsilon_u}$ is demonstrated by Lancaster [14] who obtained a linear relation between this parameter and the resulting wear during single traverses of different polymers. It should be noted that both elongation and breaking strength are sensitive to strain rate and temperature variation. Attempts have been made to relate notched impact strength to the wear of several polymers, but the correlation obtained was not convincing. As a result of these arguments, it is considered that the resistance of a polymer to abrasive wear can be increased by changing its mechanical properties. For example, both the breaking strength and elongation at break tend to increase with increasing molecular

weight, to a limiting value. In particular, with polyethylene, the impact strength increased with molecular weight to a maximum at an average molecular weight of about 1.5×10^6 [16]. The abrasion test showed that the abrasion resistance improved greatly with increasing molecular weight, reaching a maximum and constant value at the molecular weight of 1.75×10^6 and greater. Thus, abrasion resistance and impact strength show similar correlation with molecular weight.

Another form of abrasion is the three- body abrasion, which occurs when hard abrasive particles are inserted into a polymer tribo- system. The free abrasive particle readily penetrates the polymer surface, which begins to operate like an emery cloth (Figure 9). This results in direct wear of the polymer analogous to the two- body abrasion process. Otherwise, the abrasive particle may wear the counterpart and, in turn, indirectly affect the polymer as already mentioned.

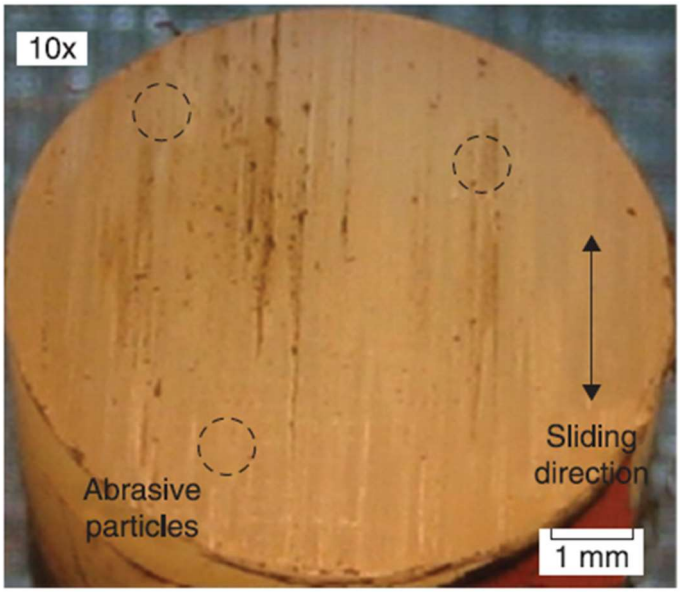

Figure 9: Polyamide 66 worn surface after 50 km of sliding against dry steel at 90 N. Abrasive particles embedded to the polymer surface [14].

1.5.3 Tribo-chemical wear

Corrosive wear occurs when both corrosion and wear mechanisms are involved during sliding of polymers in a chemical environment. This situation can result in total worn volume that is much greater than the additive effects of each process taken alone. Generally, this wear process occurs in two stages. First, corrosion takes place on the polymer surfaces due to the attack of the chemical environment. Then, the sliding process removes the corroded surface layer by abrasion. The fresh surface will again suffer from

corrosive attack, and the wear rate is accelerated by abrasive sliding action. A few examples of corrosive wear are as follows:

- Water absorption: can lead to deterioration in the mechanical properties and swelling of many thermoplastics.
- Oxidation of polymers: results in reduction in the average molecular weight and chain disengagement. Consequently, causes increases in the modulus of elasticity, density, and percentage crystallinity. Oxidation of polymeric materials can be determined by detecting the carbonyl groups that are formed [1].

1.5.4 Fatigue wear

Hertz theory shows that when a contact occurs between two bodies pressed against each other and limited by surfaces with relative not zero curvature, the maximum stress is at a certain depth which in many cases of technical interest is of the order of 0.1-0.3 mm [17]. If the load is repeatedly applied and removed, in the sub-surface area where the stress is highest, a crack may occur, which even after thousands of cycles may propagate and extend to the surface, resulting in the release of a material fragment. The diagram of this phenomenon is shown in Figure 10 [18].

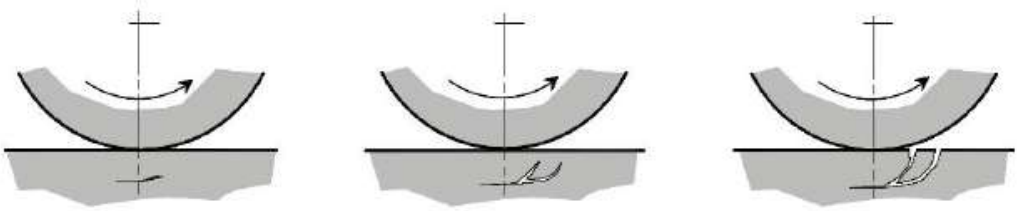

Figure 10: pattern of crack propagation during a wear fatigue mechanism [19]

This kind of wear, also called pitting, is typical of contact with rolling, with or without sliding, under high pressures. Unlike other types of wear, surface fatigue may occur even if a lubricant layer is inserted between the two solid bodies.
A periodic superficial stress can in fact damage the material, usually in the sub-superficial zones where the maximum shear effort is reached, with the nucleation and the subsequent propagation of a fatigue crack. Following the propagation of the crack, a wear debris, usually of high dimensions, may be formed.

1.6 Effect of temperature on friction and wear of polymers

When a thermoplastic polymer comes into sliding contact with a metallic counter-surface, almost all the energy dissipated by the friction appears in the form of heat, which is distributed between the two rubbing surfaces and significantly raises their temperature at the area of the sliding contact above that of the surrounding environment. The temperature produced during rubbing of polymers is a combination of three separate heat sources. These are the room temperature, the bulk temperature and the asperity flash temperature. The room temperature is the temperature of the medium in which the polymer slides and in most cases may be considered as constant. The bulk temperature refers to the temperature of the entire polymer body when run continuously, and after steady state conditions have been achieved. The flash temperature, which occurs close to the area of true contact at which the energy is dissipated, occurs in a very short period; it is caused by adhesive friction at the instantaneous (spot- to-spot) contact interface, and is often the most important one. This temperature can be several hundreds of degrees or more, higher than the bulk temperature, and can have a critical influence on the frictional and wear characteristics of the contacting surfaces because of the changes in mechanical, chemical, and thermal properties of the polymer rubbing surface. The mechanical properties of a polymer show a transition from the glassy state to the rubbery state upon heating [20]. Also for PTFE, not only the physical properties such as density, permeability and thermal characteristics [21] but also its tribological properties, are affected by the structural state of the polymer (its crystallinity), adding information to the transfer film material concept [22], investigated thoroughly by Bahadur [23].

This reduction in the properties of polymers is often exacerbated since they have low thermal conductivity and low heat resistance. Consequently, in extreme unlubricated cases, the flash temperature can lead to local melting and subsequent rapid wear (Figure 11)

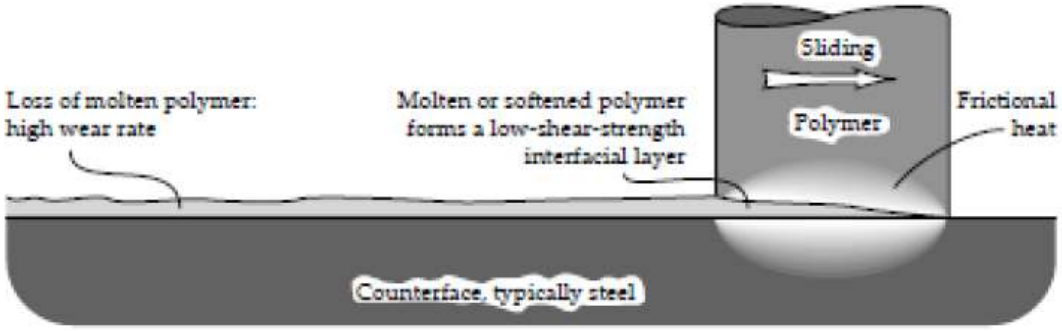

Figure 11: Melting wear of polymers caused by frictional contact temperatures [24].

The knowledge of these flash temperatures at the sliding interface is of fundamental importance for the tribological behaviour, especially of thermoplastic polymers. For example, if the polymer in sliding contact has a mechanical strength that drops off dramatically as the temperature is raised, it becomes important to calculate the maximum temperature reached during sliding to ascertain whether the material will be able to meet its structural requirements. Because of their short duration (say 10^{-3} s or less) and because they occur only over small regions (say 10^{-4} m or less), direct measurements of flash temperatures are difficult, and a theoretical estimate is usually sought. Thus, calculating the temperature is the most convenient method for determining the flash temperature [24].

The model developed by Ashby et al. [25] is accepted [2] as a simple yet effective tool to estimate the bulk and flash temperatures of mating surfaces in sliding couples, and it was accordingly employed in the present work.

Wang and Rodkiewicz [26] refined some aspects of the model, particularly regarding the calculation of junction radius and micro-scale heat diffusion lengths for the estimation of the flash temperature rise:

- The model for the calculation of the junction radius (r_j) was adjusted by introducing a lower threshold at low loads, when the real contact area (A_r) is small.
- The expressions to calculate the heat diffusion lengths in flash heating were modified, avoiding the inconvenience of having to estimate the hardly definable ratio between the lifetime of an asperity junction and the asperity transit time, as Ashby et al.' original model required.

There is experimental evidence of a critical temperature that causes rapid wear of a polymer. This temperature may not be equal to the melting point of the polymer. At high

contact pressure and at low sliding speed, the critical temperature may be below the melting or softening point of a polymer [24] .

Tribological research has focused on the effects of frictional heating or temperature on the friction and wear behaviour of polymers because most polymers undergo a change in physical, mechanical and tribological properties with increasing temperatures; however, even low ambient temperatures can affect the friction coefficient of polymers.

The combination of a rough counterpart and a high contact temperature generally leads to rapid wear of a polymer even if there is no continuous melting of the surface. The wear process involved in such cases is a severe abrasion of the softened polymeric surface.

The increase in contact temperature involves a change in wear kinetics from a linear process at constant speed to a series of discrete periods of rapid wear separated by longer periods of essentially negligible wear [24]. This phenomenon could be explained with the periodic release of molten polymer from the contact area. When the temperature is too low to sustain continuous melting, the latter proceeds by a cycle of gradual formation of molten polymer. This is followed by the sudden release of the molten material when the entire wear surface is covered. This model of polymer wear is illustrated schematically in Figure 12 [24].

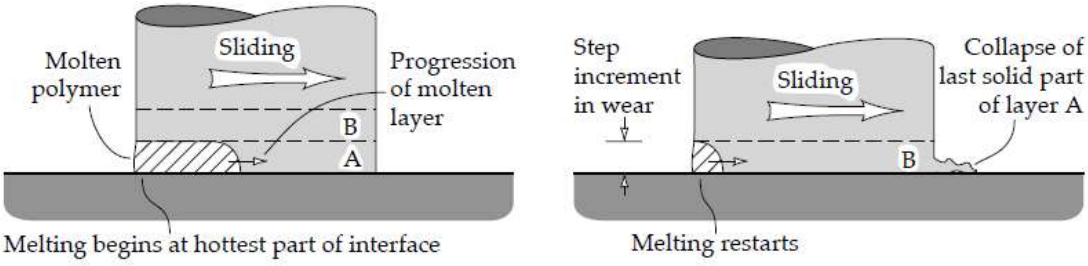

Figure 12: Mechanism of polymer wear at temperatures slightly lower than the transition to continuous melting wear [24].

1.7 PTFE tribological properties

Polymeric materials, generally reinforced, are often used in tribological contacts, especially with metal counterparts, and ceramics. The adhesion between two polymers or between a polymer and another material is based on secondary bonds and is therefore generally low. Having low cohesion energy, a polymer is easily worn out by a harder material, and the fragments can remain trapped on the antagonist surface to form a real

transfer layer. Under these conditions the initial coupling is modified, and the polymer slides against itself.

PTFE, as well as other linear chain polymers (e.g., polyamides and acetal resins), has self-lubricating properties, which means it can act as a solid lubricant. This gives it excellent properties from the tribological point of view. During a sliding wear process, in fact, a transfer of polymer particles is carried out on the antagonist (ceramic or metal, in particular in the latter case the presence of F atoms greatly facilitates the adhesion of the polymer), with the creation of a thin film (also called transfer-film) in which macromolecules stretch along the sliding direction, also facilitated by the smooth and linear structure of the chains [27]. This transfer mechanism is schematically illustrated in Figure 13.

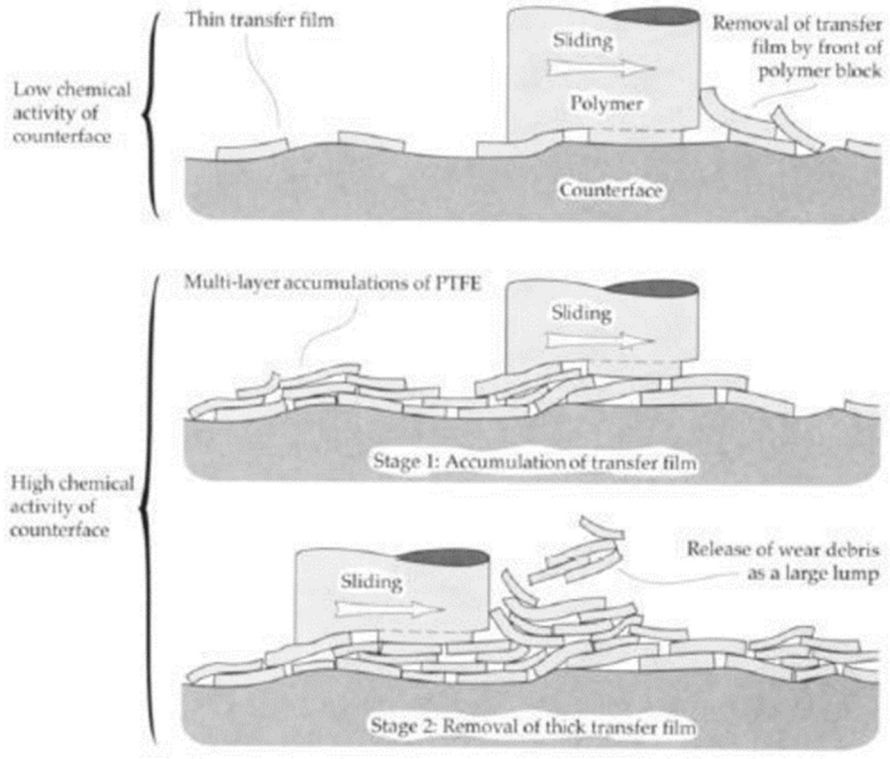

Figure 13:Adhesion mechanism of PTFE transfer-film during the sliding movement [19].

Therefore, in the contact zone, an interaction of polymer-polymer type and no longer polymer-ceramic/metal type is achieved and, due to the absence of polar groups, the adhesion work is very low, which determines low values of coefficient of friction (usually between 0,03 and 0,15). As shown in Figure 13, the transfer-film layer, during its process of continuous formation, reaches a limit thickness and there is the detachment of PTFE

"blocks", which are stretched in the direction of sliding, like those illustrated in Figure 14 [27].

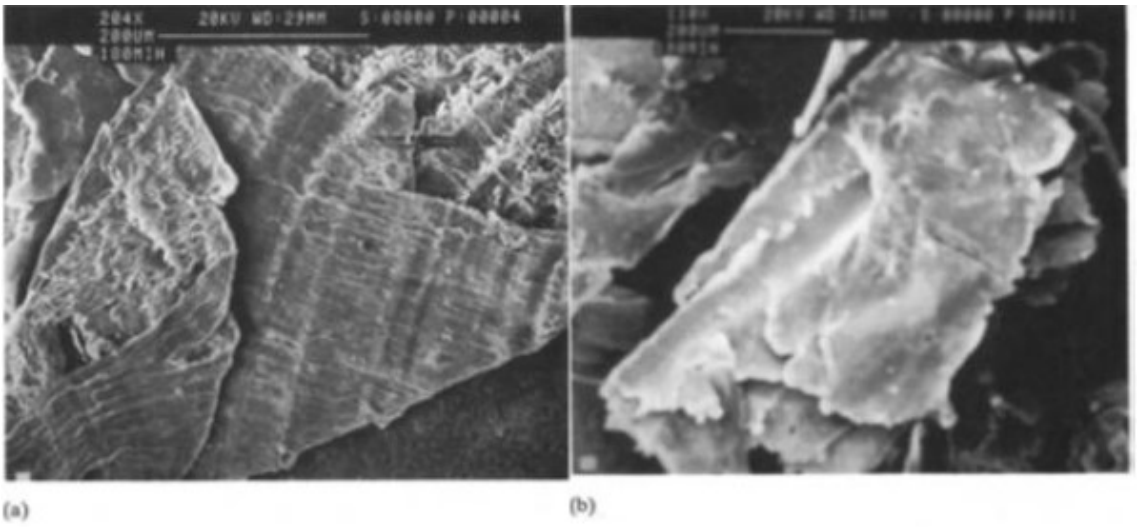

Figure 14:SEM image of wear debris from sliding of PTFE against steel En24 Ra=0,3 μm. P (contact pressure): 0,24 MPa; relative speed: 0,42 m/s. a) High crystalline debris; b) Lower crystalline debris [27].

This periodic detachment of the transfer-film and its resetting during the sliding can lead to an increase in the PTFE wear rate even in conditions of low friction coefficient.

Despite its interesting tribological properties, unreinforced PTFE is poorly used in tribological applications. This is due to its low modulus of elasticity E, between 0,4 and 0,8 GPa, which causes an excessive deformation under an applied load.

For this reason, PTFE is often used as a matrix to make composite materials reinforced with different fillers, which raise the Young's modulus to values between 2 and 4 GPa, maintaining (and in some cases improving) at the same time the tribological characteristics of the unreinforced material [2].

The transfer-film formation mechanism is linked to different conditions such as: particle's size, roughness of the counter-surface, environment, moisture, which make it very difficult to reproduce. Experimental tests have shown how, regardless of the differences between the different tribological pairs, three general stages of transfer-film formation can be distinguished during the sliding [28]:

- Run in: the sliding between the two surfaces starts; debris, with the same chemical and mechanical structure of the massive piece, are released. These will struggle to adhere to the counter-surface and will hardly be able to bind in a compact layer. If they are not ejected from the contact area they can act as a third body in the

sliding movement, this will lead to a gradual consumption of particles as cycles repeat.

- Transition: as the sliding process progresses, there are no large volumes of material removed, the debris are < 20 nm thick and begin to settle on the metal surface.
- Steady state: a continuous transfer-film layer is created, generated by the compaction of PTFE debris. In general, the smaller the size of the particles released, the more likely they will be able to compact to form a continuous layer.

In general, the formation of a continuous and compact transfer-film is facilitated by small particles released during the contact (Figure 15).

The degradation of the polymer is often due to the high local temperatures that the material reaches on the rubbing surface. In fact, temperature can be considered a very important variable in the definition of the tribological system. As it is well known polymers suffer a reduction in mechanical properties already for small temperature increases, even if PTFE is indeed one of the polymers with the highest temperature resistance, ensuring proper functioning up to 260°C. This feature, combined with a low thermal conductivity, means that in the contact point the polymer may suffer a progressive decreasing of mechanical properties. Under such conditions the wear rate of the material during tribological application could be particularly high.

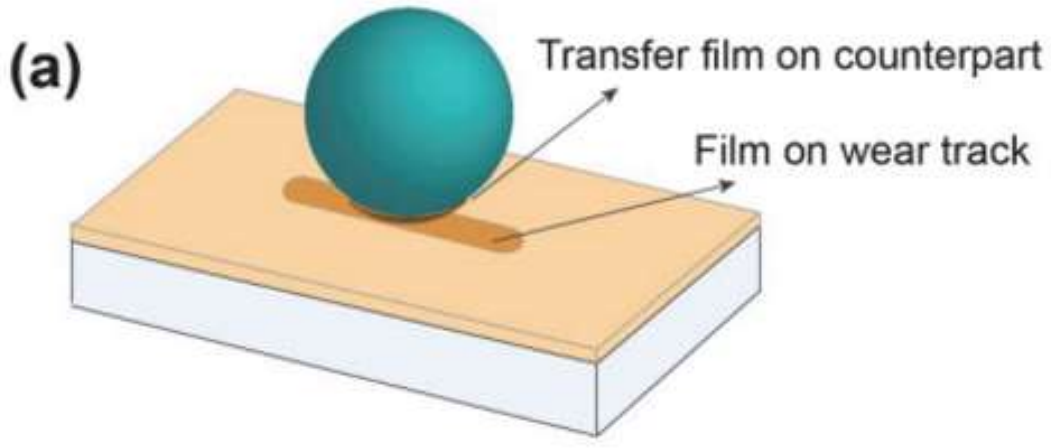

Figure 15: Transfer film formation mechanism during sliding by degradation of polymer material: a thin layer of compacted debris released from both materials covers both the polymer surface and the wear trace on the counterpart [29].

1.8 PTFE composites production processes

The properties of unreinforced PTFE make this material suitable for particular and complex applications. However, there are specific applications for which it is necessary to modify its properties by introducing charges into the polymer matrix.

The properties of the PTFE can be modified using charges of different nature, and composition. For example, carbon fibres, particles from other harder polymers (such as peek, polyimides and Ekonol) can be used, mineral-like particles, and metallic particles.

Depending on the type of charge used, the following properties can be modified:

- Wear resistance
- Coefficient of linear thermal expansion
- Thermal conductivity
- Mechanical properties
- Coefficient of friction
- Dielectric properties
- Service temperature

As noted above, PTFE is a thermoplastic material which unlike other thermoplastics does not become liquid over the melting point at 327 °C, but maintains a transparent and amorphous gel state, which occurs at ≈345 °C [6], with very high viscosity ($10^9 \div 10^{11}$ Pa×s).

Therefore, these characteristics prevent the processing of reinforced PTFE with conventional techniques normally used for other thermoplastics, such as extrusion and injection moulding.

Compression moulding is the most common production process used for PTFE powders: semi-finished or preforms, typically cylindrical in shape, are produced by applying different moulding pressures and finally sintered.

The mixing between PTFE and fillers is carried out by means of appropriate mixers [30]. This treatment allows the correct dispersion and homogenization of the components in the composite.

After mixing, the powders are loaded inside the mould and subjected to a compression moulding: the moulding pressure varies from 25 to 60 MPa, depending on the type of

powder to be pressed. Figure 16 shows in detail the pressing phases for obtaining the preform, consolidation through sintering and cooling, of the PTFE matrix composites.

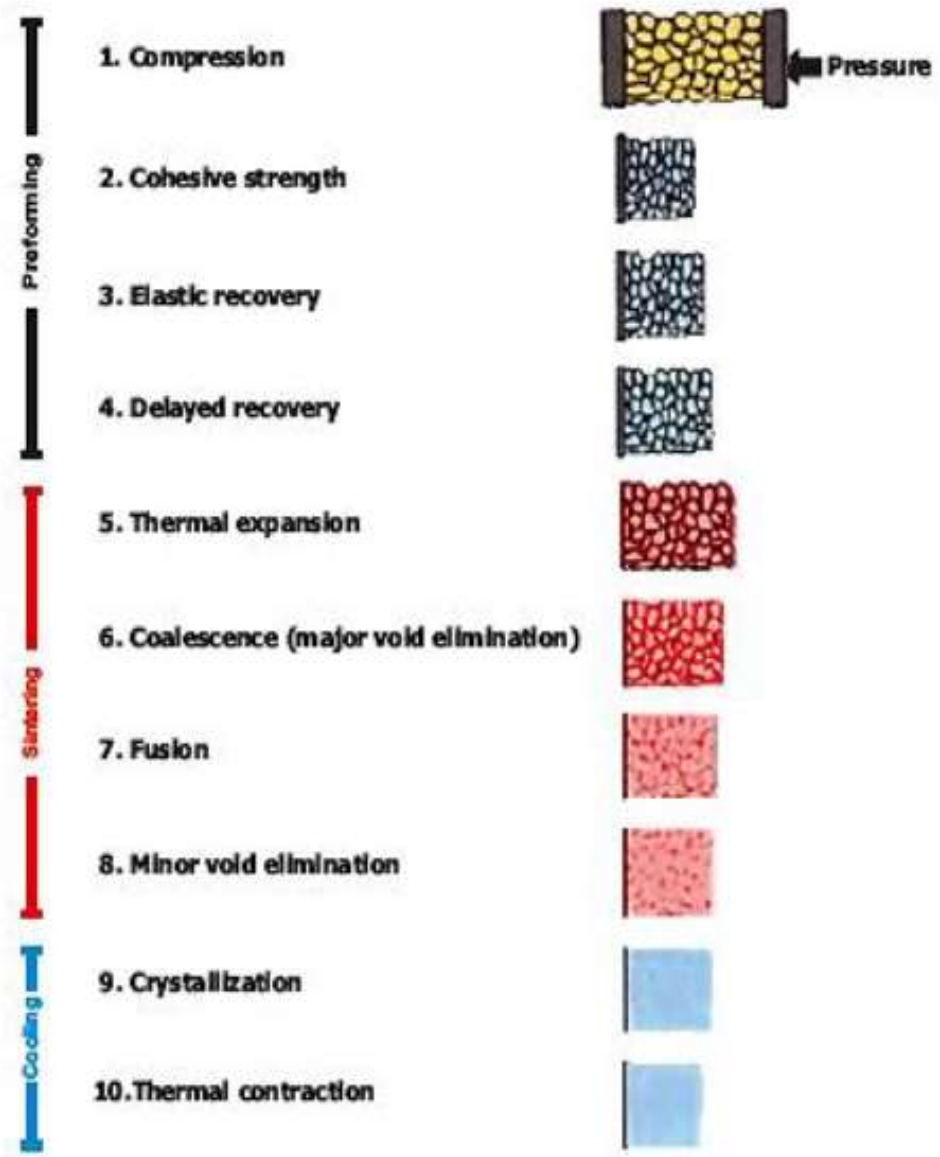

Figure 16:Preparation of the PTFE billet [5]

Pressing PTFE powders is followed by sintering, a thermal process that leads from the powders to a denser, less porous, and more resistant compact. During sintering there is an evolution of the solid phase but also of porosity: the fundamental variables are time and temperature. The most common sintering temperatures are between 360 and 380 °C; as shown in Figure 17, the sintering process is divided into 3 phases:

- Heating up
- Dwell time at sintering temperature
- Cooling down

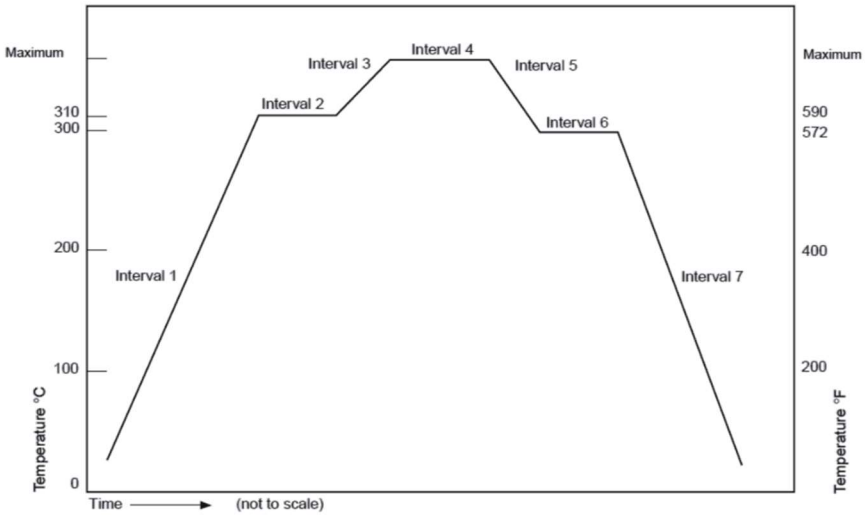

Figure 17: Sintering cycle of PTFE [31]

The speed of heating up (temperature ramp rate) and the dwell time at sintering temperature are primarily determined by the dimensions of the moulded parts to be sintered, in particular the wall thickness. The cooling rate, which must be slow to avoid stress cracks, influences the crystallinity of the finished part and so determines its end properties.

1.8.1 Effect of fillers on tribology of PTFE composites

Fillers are generally classified according to the desired properties of the final composite; they can be distinguished in reinforced and lubricants type. The reinforcement fillers, like glass fibres and carbon fibres, are characterized by a resistance and an elastic module higher than the matrix, their presence is essential as they are able to interrupt crack propagation and avoid the formation of macroscopic debris.

The aims of the filler inside the PTFE matrix are:

- Improving the mechanical strength of the material,
- Reducing the volume of material removed during the tribological contact by hindering the sub-surface propagation of cracks, which lead to the detachment of large “sheets” of material with unreinforced PTFE
- Improving internal thermal conductivity. The sliding process can lead locally to very high temperatures that favour the degradation of the material. A good heat dissipation reduces this phenomenon, leading to a more uniform consumption.

- Improving the transfer-film stability: studies [32] show that this layer plays a fundamental role in the tribological system, and once it degrades, there is a rapid increase of the friction coefficient and the wear rate.

In general, the wear rate of the material is not affected by the hardness of the selected filler but is strongly dependent on its chemical affinity with the counter-surface and its ability to form a stable transfer-film layer during the tribological contact. In fact, the function of the filler is to improve the properties of the transfer-film, making it as thin, uniform, and reproducible.

In this Ph.D. thesis different families and shapes of fillers were studied, based on their thermal conductivity:

- Glass fibres
- Carbon fibres
- PEEK (in two different weight percent)
- Bronze (spheroidal and lamellar shape)

Foremost among the inorganic reinforcements employed for PTFE-based composites are glass and carbon fibres. Various works have documented the improved sliding wear resistance of PTFE-based composites containing glass and/or carbon fibres [33, 34]

However, much fewer works have, until now, been devoted to understanding the role of the counter-surface material [35], and specifically whether composites with distinct types of reinforcements respond differently to a change in counter-surface material. The mentioned work by P. Johansson et al. [35] showed that the performance of two PTFE-based composites containing carbon fibres changes when mated with low alloy steel or ductile grey iron. Further, each composite was affected differently by a change in counter-surface material. Likewise, Wang et al. showed that nitriding or carbonitriding a steel counter-surface affects the friction and wear responses of glass fibre-containing composites [36]. The early data published by Tanaka [37] suggested that, over a wide range of sliding speeds, the tribological performance of carbon fibre-reinforced PTFE was degraded (higher friction coefficients and specific wear rates) when changing the counter-surface material from steel to glass, whilst the same did not occur (or occurred to a much lower extent) with glass fibre-reinforced PTFE.

This means there is likely much interaction between reinforcement type and counter-surface. The available information, however, is still scarce: in particular, little is known on the behaviour of PTFE-based composites when mated with coated counter-surfaces.

Coatings are often employed on metal counter-surfaces in sealing systems: the coating protects expensive mechanical parts from being scratched and abraded, either by the hard phases in the polymer composite gasket or by trapped debris [38]. The work of Surberg et al. [39], who studied the behaviour of glass fibre-reinforced PTFE composites against counter-surfaces coated with Diamond-Like Carbon (DLC), a thermally sprayed WC-based hard metal, or hard chromium, looks especially pertinent to applications in a sealing system, where coating techniques for metal counter-surfaces must be selected with a view to respecting often strict dimensional and geometrical tolerances. Some of the results reported in the cited work [39] are noteworthy. For example, DLC, which is usually known for its especially good tribological performance when coupled to metallic or ceramic counterparts [40], seems not to provide any special benefit when slid against a PTFE-based composite [36], since friction and wear are not lower than are observed with some other counter-surfaces. A thermal spray WC-based hard metal also looks quite abrasive towards PTFE-based composites, and apparently does not build a stable transfer film [36]. Apart from this work, however, there seems to be practically no other source of information for the tribological behaviour of PTFE-based composites slid against thermally sprayed ceramics and hard metals, although these are among the most widely employed coatings for seal counter-surfaces [41] [42].

Polyetheretherketone (PEEK) is a thermoplastic polymer widely used in tribological applications [43] due to its very high thermal stability, corrosion resistance and mechanical strength. However, the choice of a polymer as a filler results in a low chemical affinity with the metal counter-surface, hindering the formation of the surface transfer-film. For all the fillers studied, the "sacrificial approach" method was used: the composite is PTFE matrix, while the reinforcement generally has a higher hardness. The mechanical stress induced by the sliding therefore involves a degradation of the soft component, that is PTFE. Studies conducted by Onodera et al [44]show the principles of operation of the mixture consisting of PTFE and PEEK: it allows the achievement of wear rates and friction coefficients lower than the two materials considered separately (Figure 18).

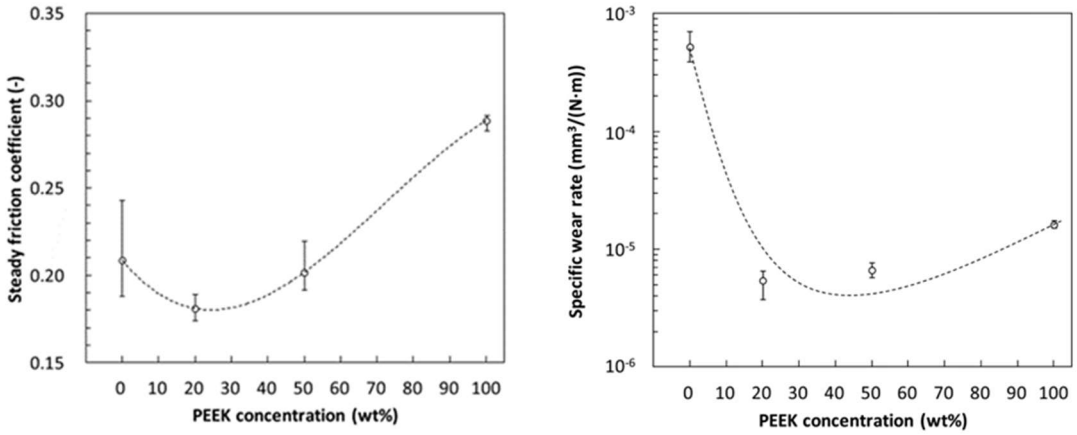

***Figure 18**: Changes in friction coefficient (a) and wear rate (b) as the percentage of PEEK within the composite changes.*

Through a MD-type simulation (Figure 19) it has been possible to trace the mechanism of formation of the transfer film when the moving counterpart is an aluminium disk. The transfer film consists of two different layers, one with a prevalence of PTFE and one richer in PEEK that manages to better bind the oxides on the surface of the disc.

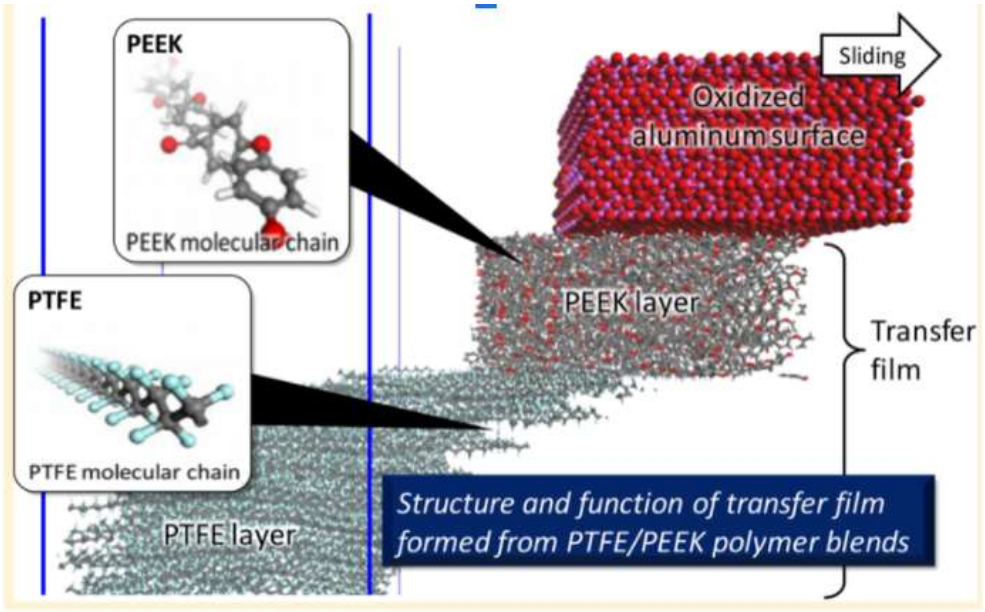

Figure 19:MD simulation in which a PTFE/PEEK composite is in contact with an aluminium disc.

The addition of bronze particles in the PTFE matrix improves its wear resistance [45] Pasha et al. [46] noted that the origin of the good interface between the PTFE matrix and the bronze particle is due to the formation of copper fluoride (CuF_2), which is caused by the degradation of PTFE and bronze.

PTFE matrix composites filled with bronze particles are widely used in different sectors, thanks to their good mechanical and especially tribological properties that depend on weight fraction [47]. Several research studies [48]have shown that the incorporation of bronze particles in a PTFE matrix is a good solution to improve its friction behavior. Under certain conditions, the addition of bronze particles in a PTFE matrix, during sliding, can lead to increase of the friction coefficient, the activation of abrasion, and the reduction of the chemical resistance of composite. Unlike PEEK, the addition of bronze particles leads to an increase in the thermal conductivity of the PTFE composite and thus promotes heat dispersion from the contact zone: standardizing the temperatures over the entire volume of the pin it is possible to reduce the phenomenon of local degradation and increase the useful life of the component. On the other hand, unlike PEEK, bronze does not have a good chemical compatibility with PTFE: for this reason, it is necessary to ensure an excellent dispersion of bronze within the matrix and avoid areas with different concentration of fillers.

1.9 Surface Engineering in tribology

Tribological stresses involve the surfaces of bodies in contact, therefore a correct choice of the nature and properties of the counterpart may result in a reduction of the friction coefficient and an improvement of the wear rate in the considered tribological system.
Surface treatment techniques can vary greatly depending on the nature of the material used, the treatment temperature and the desired properties (surface hardness and thickness of the treated surface layer).
Commercially, a large variety of processes are available; each one is characterized by a range of penetration depth in the case of integral coatings and thickness for discrete coating.
The choice of surface treatment is, mainly, related to:

- specific application.
- environment.
- substrate material.
- component dimension and geometry.
- coatings material.
- coating thickness.

For a more complete overview of the main features of surface treatments most used in tribological applications, Table 6 can be used as a reference.

Treatment	Metals treated	Processing temperature (°C)	Maximum surface hardness (kg/mm^2)	Typical thickness (mm)
Treatments for microstructural modification				
Surface rolling	Steels, Ti, and Ni alloys	Room temperature		
Shot-peening	Steels, Ti, and Ni alloys	Room temperature		
Flame hardening	Hardenable steels and cast irons	850–1100	500–600	1–6
Induction hardening	Hardenable steels and cast irons	850–1100	500–700	0.2–2
Laser hardening	Hardenable steels and cast irons	850–1100	500–700	0.1–0.6
Thermochemical diffusion treatments				
Carburizing and carbonitriding	Low carbon steels	800–1100	700–900	0.05–1.5
Nitriding	Nitriding steels Tool steels (hot working and HSS)	500–600	800–1200	0.025–0.5
Ion implantation	All	200–600	600–1100	$<10^{-3}$
Chemical conversion coatings				
Phosphate coatings	Steels, Al alloys	25–95 (drying at 200 °C)	–	Up to 0.01
Hard anodizing	Mainly Al alloys	0	>1100	0.04–0.05
Surface coatings				
Hard chromium	Most ferrous and non ferrous alloys	<70	700–1200	0.001–0.5
Electroless nickel	Most ferrous and non ferrous alloys	Room temperature (ageing between 200 and 500 °C)	Up to 1000	0.001–0.025
Physical vapour deposition (PVD) coatings	All metals	150–500	2000–2500 (TiN)	0.001–0.003
Chemical vapour deposition (CVD) coatings	All metals (with the limitation of the process temperature)	800–1000 (lower temperatures in new techniques)	2800–3000 (TiC)	0.001–0.01
Thermal spray coatings	All metals	<200	700–2000	0.5–1
Hardfacing by welding	Steels and non ferrous alloys with melting point greater than 1100 °C	1200–1600	800–2000	3–10

Table 6: Main characteristics of surface treatments most used in tribological applications [2].

1.9.1 Thick coatings

Thick coatings can be divided into two classes: welding coatings and thermal spraying coatings; the latter technology has been described in this section, which was used to deposit the Cr_2O_3 coatings used in this Ph.D. thesis.

In thermal spraying technology, the material to be deposited, fed into the plant in powder or wire shape, is melted and projected, in the form of droplets, on the substrate to be coated. The impact with the surface involves deformation of the droplets which solidify in the form of lamellae; the typical thickness of the coatings, formed by the overlapping of many layers of lamellae, varies between 0,1 mm and 1 mm.

Thermal spraying can be classified into:

- Flame spraying.
- Electric arc spraying system.
- Plasma spraying (in air or vacuum).
- By detonation (D-gun).
- High-speed combustion spraying (HVOF).

These energy sources are used to heat, melt and accelerate feedstock materials (in powder, wire, rod form or suspension/solution particles) toward the cold solid surface of the substrate (Figure 20).

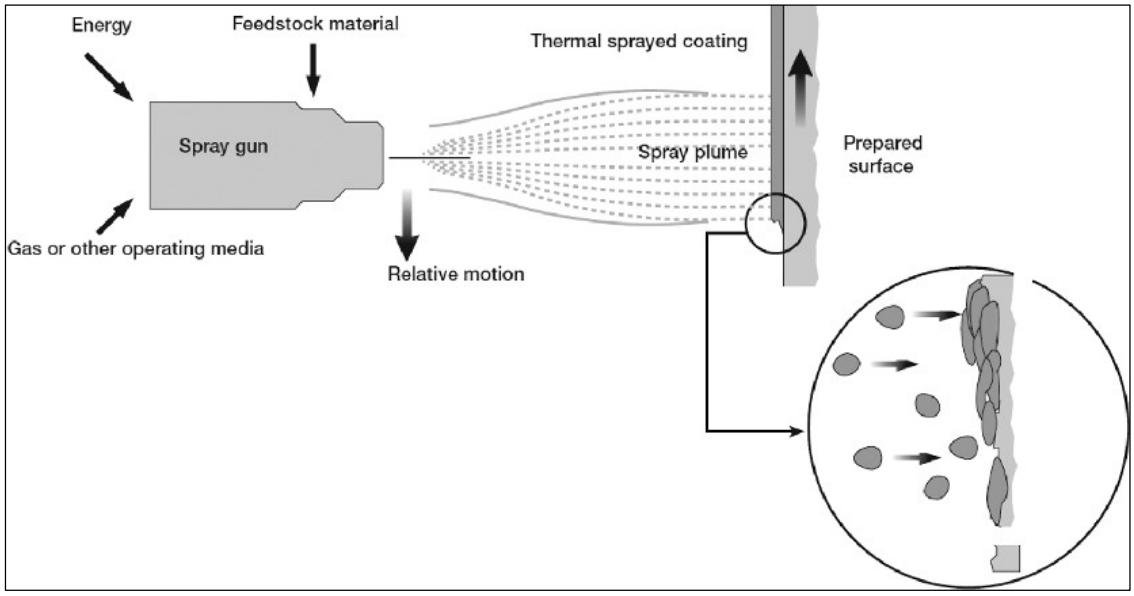

Figure 20: Diagram of a thermal spray process: a gas at elevated temperature and/or pressure, accelerate, heats and melts the feedstock powders that impact against the substrate [49].

Upon impact, the particles, molten or semi-molten in flight, solidified in a lamellar structure made of "splats", forming a bond with the surface as shown in (Figure 21) [50].

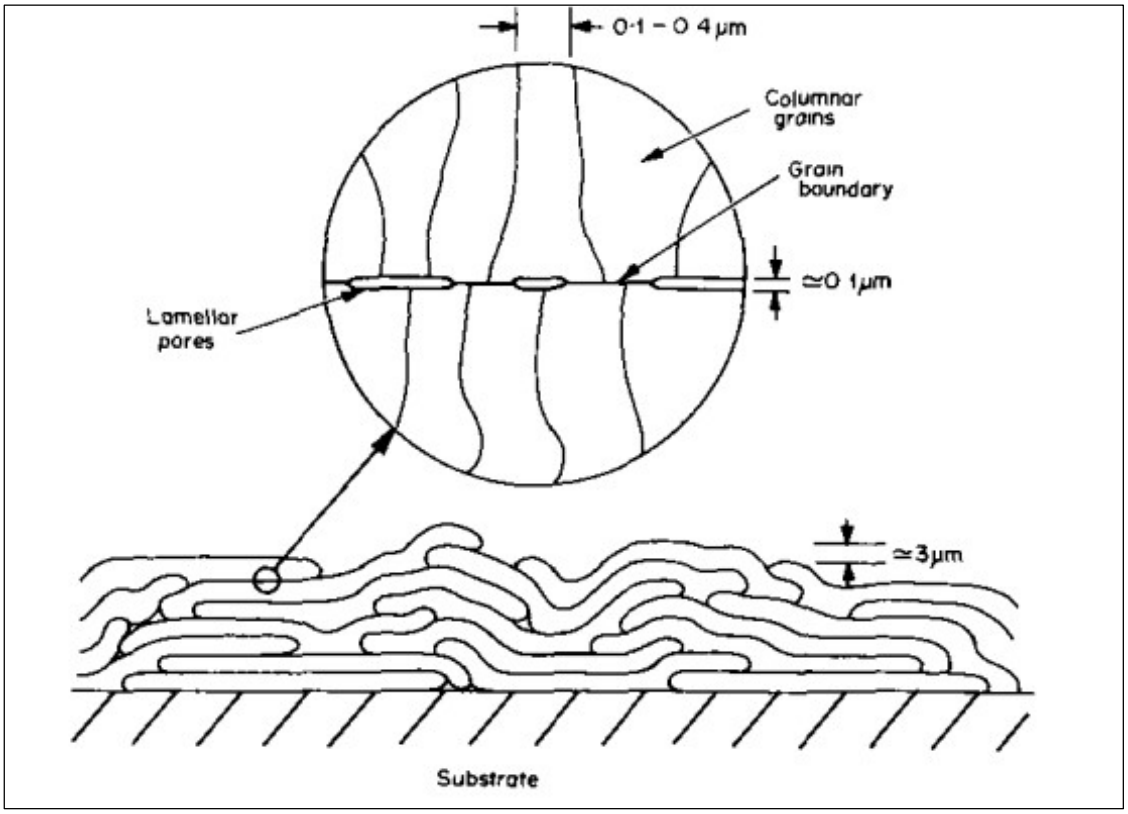

Figure 21: Lamellar structure typical of a thermal spray coating [51]

Generally, the adhesion between the coating and the substrate is lower than other techniques, such as thin coatings. The tensile release effort varies from values of 10 MPa, for flame thermal spraying processes, to values of 30 - 50 MPa for plasma thermal spraying processes, up to values of 70 MPa in the case of deposition by D-gun or HVOF. For this reason, the use of these coatings in tribological applications is not recommended in the presence of particularly severe mechanical stresses [2], although the high thickness can withstand sufficiently high contact pressures without the risk of deforming and consequently fragmenting the substrate, which characterizes thin coatings obtained by PVD/PECVD processes.

The low adhesion between the coating and the substrate is due to the low temperatures reached by the substrate during the coating phase. This condition prevents interdiffusion phenomena that would guarantee a high adhesion, but at the same time it has the advantage of avoiding problems due to distortion phenomena.

Due to the lamellar structure, this kind of coatings is often characterized by a certain residual porosity which may result in a reduction in fracture toughness. The lamellar

morphology also determines a relatively high roughness, which requires a grinding treatment to achieve the best tribological performance [52].
Thermal-spraying coatings generally show good abrasive wear resistance in conditions of low contact forces, but the lamellar nature (characterized by a certain residual porosity) damages these coatings in case of high punctual contact forces except for high-speed combustion coatings, which have the lowest porosity (often <1%).

1.9.1.1 Chromia coatings

Chromia coatings (Cr_2O_3) are obtainable mainly through plasma-spray and D-gun processes. The thickness of this kind of coatings varies from 0.1 to 0.5 μm; they have also a porosity between 1 and 5% and an arithmetic average roughness R_a of about 3 μm (before any grinding work) [53]. From a tribological point of view, this coating is very interesting as it offers high hardness (about 1500 HV), excellent resistance to corrosive agents, low wear in dry and lubricated conditions, at the expense of a very high friction coefficient in conditions of low sliding speeds, as shown in Figure 22.

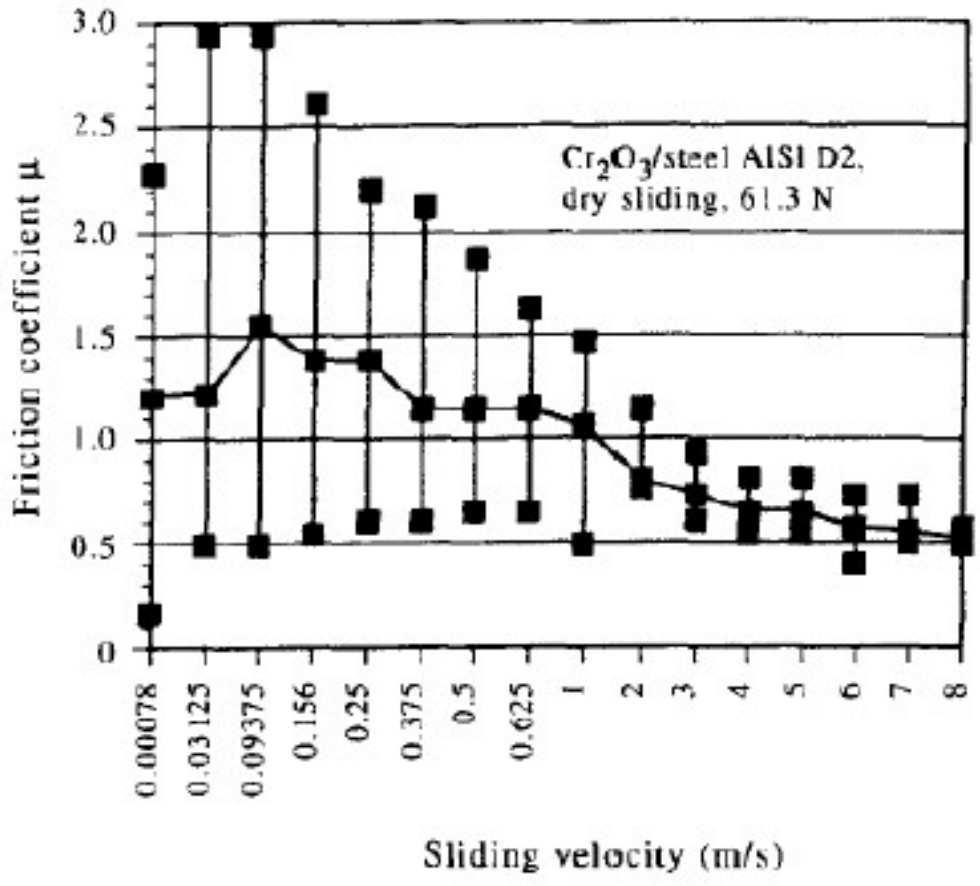

Figure 22: Variation of the friction coefficient as a function of the sliding speed for a Cr_2O_3/steel coupling. Applied load: 61.3 N [54].

The wear rate instead increases as the contact pressure increases, as shown in Figure 23.

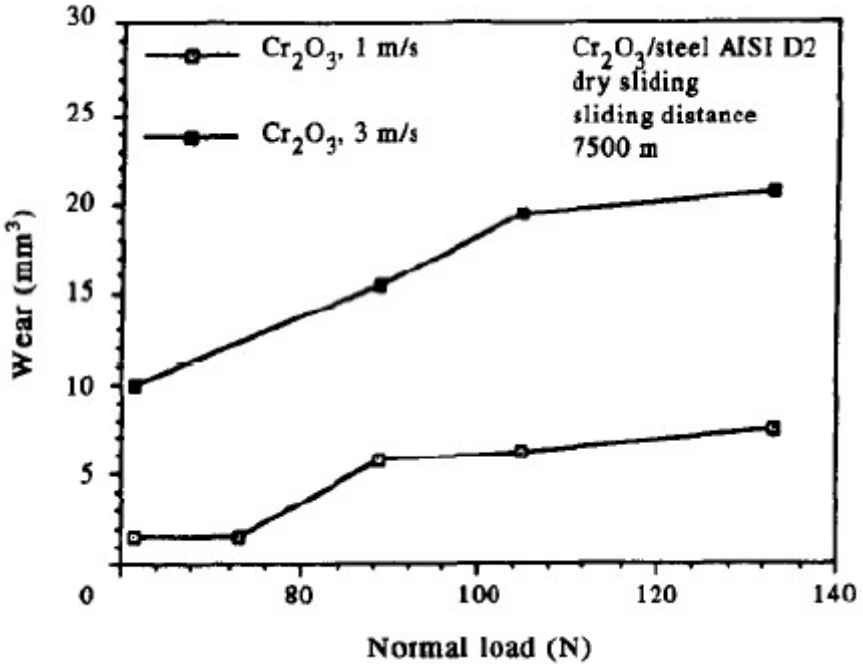

Figure 23:Change in wear rate as a function of applied pressure for Cr_2O_3/steel coupling. Sliding distance: 7500 m [54].

2 Experimental Procedure

This chapter describes the materials analysed and the tribological tests to which they have been subjected, with the aim of subsequently evaluating the main wear mechanisms triggered. The method of statistical analysis (Design of Experiment) used to evaluate the most influential parameters on the tribological behaviour of the unreinforced PTFE is also illustrated.

2.1 Materials of the tribosystem

All the PTFE matrix composite materials used in this Ph.D. thesis have been supplied by the company ATP (Modena, Italy) which, in addition to producing and designing polymer sealing systems, is also a manufacturer of customized PTFE matrix compounds and semi-finished products. The materials have been produced from the raw material powder, as is usual in the case of PTFE-based material due to the impossibility of processing them in the molten state (PTFE has too high viscosity to be processed technologically with processes such as injection moulding). The compounds consisting of PTFE powders and reinforcement, properly mixed, were then compacted by compression moulding and sintered in the oven at 360-380° C to form cylindrical sleeves which, machined by turning, allowed to obtain semi-spherical head pins as shown in Figure 24:

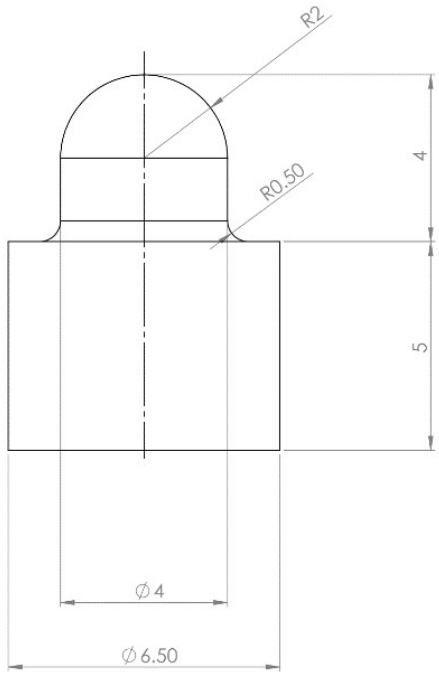

Figure 24: Schematic refiguration of the pin

The materials analysed in this thesis are listed in the Table 7:

Matrix	Filler (wt%)	Density (g/cm^3)	Name
PTFE	Glass fibres 15%	2,25	GF-PTFE
PTFE	Carbon fibres 10%	2,08	CF-PTFE
PTFE	Lamellar bronze 40%	2,94	Sintek BRL
PTFE	Spheroidal bronze 40%	3,00	Sintek BRS
PTFE	PEEK 10%	1,95	Sintek PK10
PTFE	PEEK 20%	1,89	Sintek PK20

Table 7: : Features of analysed materials

Considering the densities of PTFE (2.17 g/cm^3), carbon fibre (1,65 g/cm^3), glass fibre (2,5 g/cm^3), PEEK (1.3 g/cm^3), the weight percentages were selected to correspond to a reinforcing fraction of 15% vol. In this way, it is possible to compare the effects of the different materials with the same volumetric fraction. In the case of the PTFE composites reinforced with 20% PEEK, the volumetric fraction of PEEK was doubled to correspond to about 30 vol.%, to assess the effect of that variable. This fraction is also among the most frequently reported in the literature. In the case of PTFE composites reinforced with bronze, the concentration is 40 wt% since it is considered a standard according to ASTM D4745, corresponding to 30% vol.

As previously discussed in section 1.8.1, the wear rate is highly dependent on the chemical nature of the filler, intended as its chemical affinity with the counter-surface, even more than its mechanical properties. An important function of the filler is to improve the properties of the transfer-film, making it as thin, uniform, sticky and reproducible.

Tribological tests where the contact temperature was monitored with an infrared thermocamera were carried out to investigate the influence of the thermal conductivity of the fillers on the wear mechanisms of the PTFE matrix composite, to determine whether the transfer-film formation mechanism is comparable in the case of materials with filler additions with similar thermal conductivity values, knowing from the literature that carbon fibres and bronze are fillers of conductive nature, unlike glass fibres and PEEK.

2.2 Counter-surfaces

The tribological behaviour of the mentioned materials have been evaluated against two different counter-surface:

- Uncoated AISI 304 Stainless Steel
- AISI 304 Stainless Steel coated with Cr_2O_3 (commercial name "K702") deposited by plasma thermal spraying.

It is an industrially frequent occurrence to have these composites sliding against either austenitic stainless steel, the most prominent among the food-contact materials, or plasma sprayed Cr_2O_3 coatings. Not only is Cr_2O_3 one of the recommended coatings for sealing applications [42] but various industrial suppliers have also achieved food-contact certifications for this kind of coating [41],due to its chemical inertness and sliding wear resistance; indeed, it is one of the most common coating solutions in this field. Therefore, with rotary seals in the food & beverage industry as the target application, it is a fully sensible choice to use uncoated and Cr_2O_3-coated AISI 304 as counter-surfaces.

The counterparts for sliding wear tests were discs of 70 mm diameter × 6 mm thickness. Both uncoated discs and discs were employed. Specifically, the coated discs had a plasma sprayed Cr_2O_3 layer of ≈200 – 250 μm thickness, which is typical of plasma-sprayed protective coatings for rotary seal joints. The coatings were procured from a job shop so that the tested samples are representative of real industrial samples.

Both types of surfaces (uncoated and Cr_2O_3-coated) were ground and polished under industrial processing conditions to achieve the typical finishes used especially for food-contact parts. Their surface roughness was assessed by optical profilometry using a structured-light detector (ConfoSurf, ConfoVis GmbH, Jena, Germany) mounted onto a Nikon Eclipse LV150N microscope operated with a 50× objective. Four measurements were made on each surface, acquiring 0.6×0.6 mm^2 surface areas. Surface-related topographical parameters were extracted according to the definitions in ISO 25178-2, including the arithmetical average surface roughness (Sa), the skewness of the height distribution (Ssk), core height (Sk), and reduced peak (Spk) and valley (Svk) heights. The Sk, Spk, Svk parameters were calculated by applying a Gaussian filter with 0.08 mm cut-off. AISI 304 stainless steel plates of 30 × 30 × 2 mm^3 were also coated by plasma sprayed Cr2O3 together with the discs, and further cut into 12.5 × 12.5 × 2 mm^3 specimens using a metallographic cutting machine for measuring the thermal properties (see Section 2.3). A thicker coating was deposited on the plates (450±30 μm, which was verified by optical

microscopy on the polished sections) than on the discs, so that the coating bears a greater influence on the thermal conductivity and diffusivity of the sample. This results in a more accurate assessment of these properties after decoupling the effect of the substrate, as described in Section 2.3.

Cross-sectional specimens were also cut from the coated plates and discs, hot mounted in phenol resin, ground with SiC papers, and polished with 3 μm polycrystalline diamond slurry and colloidal silica (≈60 nm) suspension for microstructural characterization. Specifically, porosity was assessed by image analysis (FIJI – ImageJ software) on 16 optical micrographs acquired at 200× magnification on cross-sectional specimens obtained from various locations across the plates. The images were automatically thresholded using the default ImageJ routine to minimise the arbitrariness associated with manual thresholding.

Thickness was measured by image analysis on 50× optical micrographs of the same cross-sections (16 images, 5 manual thickness measurements on each image). Vickers microhardness of both the coating and AISI 304 stainless steel was measured by depth-sensing indentation testing (MHT3, Anton-Paar TriTec, Corcelles, CH). The results were averaged from 19 indentations performed at 3 N (≈300 gf) maximum load, 6 N/min loading/unloading rate, 15 s holding time at maximum load.

The microstructure of the Cr_2O_3 coating was further assessed by scanning electron microscopy (SEM: Nova NanoSEM 450, FEI Thermo Fisher Scientific, Hillsboro, USA).

2.3 Characterization of thermal properties

The thermal diffusivity of PTFE composites, pure PTFE (as a reference), AISI 304 stainless steel and plasma sprayed Cr_2O_3 was measured using the laser-flash method (LFA 447, Netzsch, Selb, Germany) in accordance with ASTM E-1461, using the 12.5 mm-diameter disc samples and the 12.5 × 12.5 × 2 mm^3 plates, respectively. (Figure 25 - Figure 26).

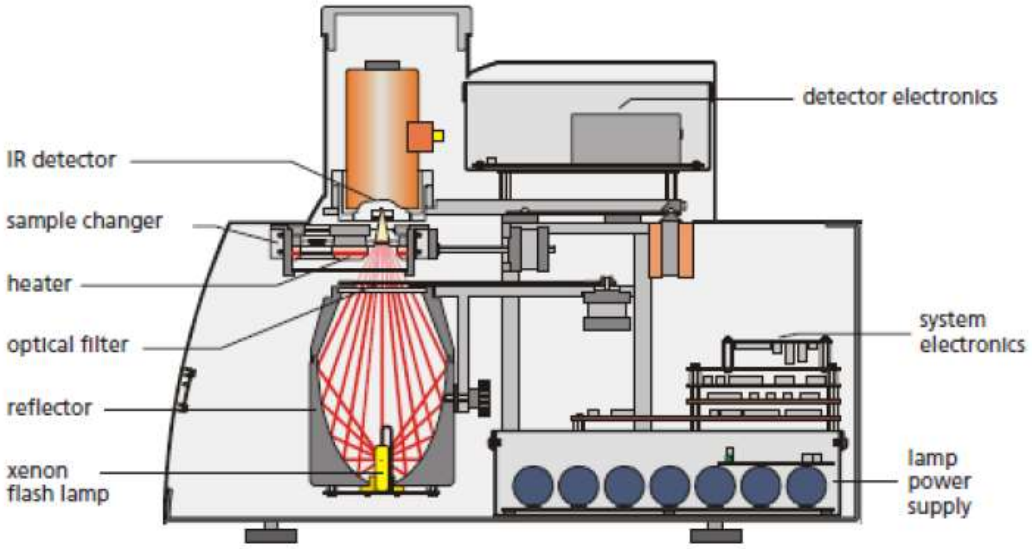

Figure 25: Schematization of the LFA apparatus, taken from Operating Istructions NETZSCH

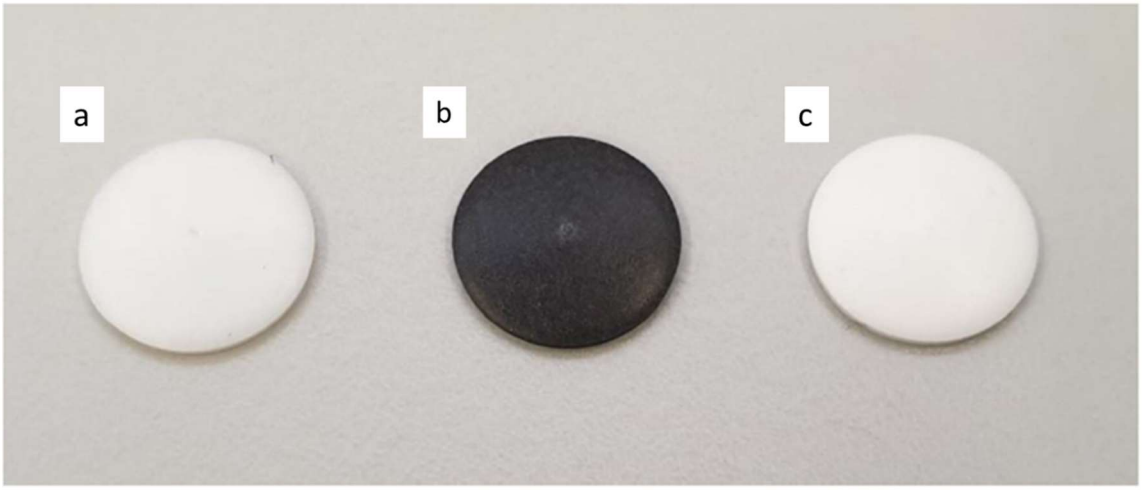

Figure 26: Example of samples used for thermal testing: unrenforced PTFE (a), CF-PTFE (b), GF-PTFE (c).

A thin layer of spray graphite (Graphit 33, CRC Industries Europe) was applied on both faces of each sample before testing to maximise emissivity and absorbance over the entire spectrum of wavelengths employed by the instrument. Diffusivity measurements were performed between 40°C and 200 °C in steps of 20°C. The graphite coated specimen was heated to the step temperature (±1°C) and equilibrated for five minutes before the flash test. At each step, five flash measurements were performed to determine any variability in the measurements. To re-equilibrate the temperature, there was a 60 s wait time between each flash. The thermal diffusivity of the coatings was calculated by decoupling the effect of the substrate from the laser flash measurement on coated samples, on the basis of the diffusivity of the substrate and the exact thickness of substrate and coating,

and neglecting the possible thermal resistivity due to micro inhomogeneities at the interface. The precise thickness of the coating on the plates is specified in Section 2.2.

Thermal conductivity (λ [W/(m·K)]) was computed from thermal diffusivity (α [m2/s]) according to the definition of the latter: $\lambda = \alpha \cdot c \cdot \rho$, where c [J/(kg·K)] is the specific heat and ρ [kg/m3] is the density.

For this purpose, c was measured by differential scanning calorimetry (DSC-214 Polyma, Netzsch) according to ISO 11357-4. Samples with a mass of 8-15 mg were cut from the plate or disc specimens and loaded into an Al crucible. An empty Al crucible was employed as reference. Measurements were performed under inert gas (N_2) flow according to the following heating program: 10 min-long isotherm at -10 °C; heating stage from -10 °C to 230 °C at a rate of 10°C/min; 10 min-long isotherm at 230 °C, and free cooling to room temperature ≈40 °C/min. To ensure that the results were not affected by the prior thermal and mechanical history of a specimen, the entire measurement procedure was repeated at least three times on each sample, and until two consecutive DSC traces were seen to overlap completely.

In accordance with ISO 11357-4, identical measurements were also performed on an empty sample crucible (to define the behaviour of a "blank" sample) and a sapphire standard specimen (disc, Ø=4 mm, thickness = 0.75 mm) with a known specific heat.

All laser-flash and DSC measures were repeated on two samples per material.

The densities of polymer composites are listed in Table 1. The density of pure PTFE is 2.2 g/cm3; and the density of AISI 304 stainless steel is 8.00 g/cm3 [55] The density of bulk Cr2O3, 5.22 g/cm3 [53] was corrected through the measured porosity of the coating (Section 2.2).

2.4 Pin on disc sliding wear test

Tests were carried out at room temperature (≈20 °C) using a pin-on-disc tribometer (TRB, Anton Paar – Tritec, Corcelles, CH), where the pins were mated to uncoated and Cr_2O_3-coated AISI 304 steel discs.

This configuration (Figure 27) was chosen to mimic the contact conditions of a lip seal, which is one of the most frequent configurations for rotary seal joints.

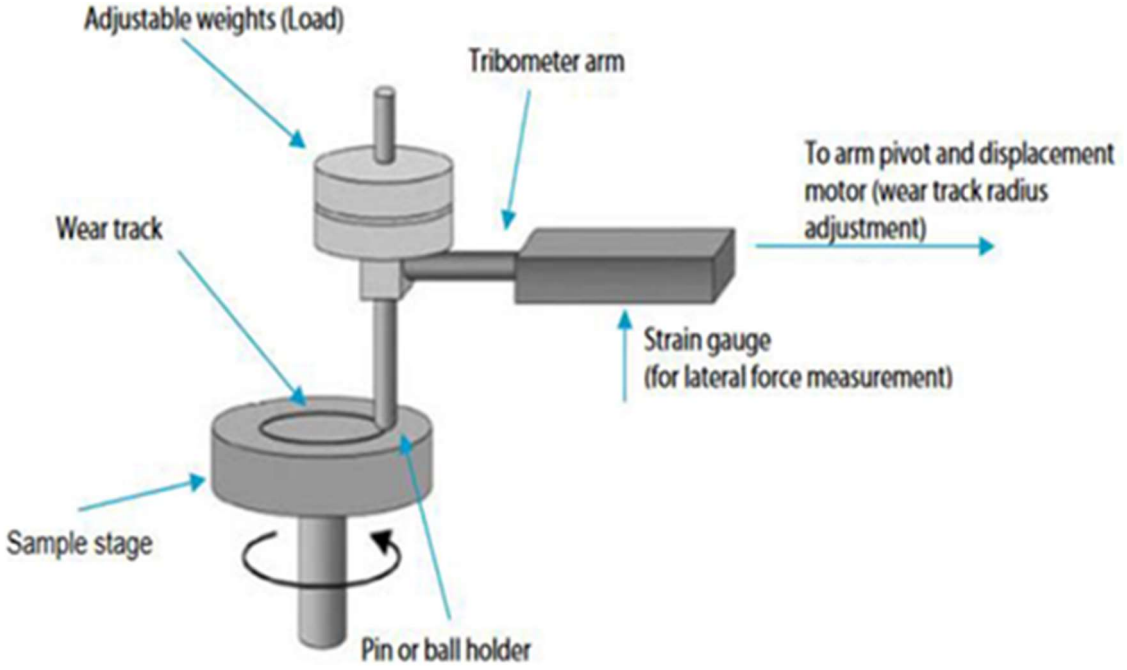

Figure 27: Tribological test in pin-on-disc configuration.

A lip seal produces a non-conformal (line) contact with the mating shaft surface, which turns into a conformal contact as the lip itself wears down. Likewise, the spherical tip of the pins (Section 2.2 and Figure 24) produces an initially non-conformal contact with the disc, which turns into a conformal contact as the pin wears down.

For all pin / disc couples four different test conditions were employed by combining normal loads of 5 N and 10 N and sliding speeds of 0.54 m/s and 1.8 m/s. The sliding distance was 3000 m in all cases. Speeds were consistent with those expected in a typical rotary seal joint for automatic food and beverage processing machinery. The loads chosen resulted in final contact pressures (after the pin and disc had conformed to each other) of the order of 4 – 10 MPa. These are comparable to the typical contact pressures computed by finite element simulations for lip seals in rotary seal joints for specific fields.

Each test was repeated at least twice. The friction coefficient (μ) was calculated by measuring as the ratio between the tangential force acting on the pin during the test, which was measured through a load cell, and the normal force applied on the pin itself following this formula:

$$\mu = \frac{F_T}{F_N}$$

Where:

F_T is the tangential force measured through a load cell.

F_N is the normal force acting on the pin.

The diameter of the circular wear scar (left on the tip of the pin after the test) was measured with an optical microscope, and the volume of the worn cap was calculated through geometrical relations. The volume of removed material depends on the height of the spherical cap, removed during the wear test. The micrographs of each pin, at 50x magnification, were processed with the ImageJ software, to determine the diameters and then their average value. The diameters of the worn surface were measured as shown in Figure 28.

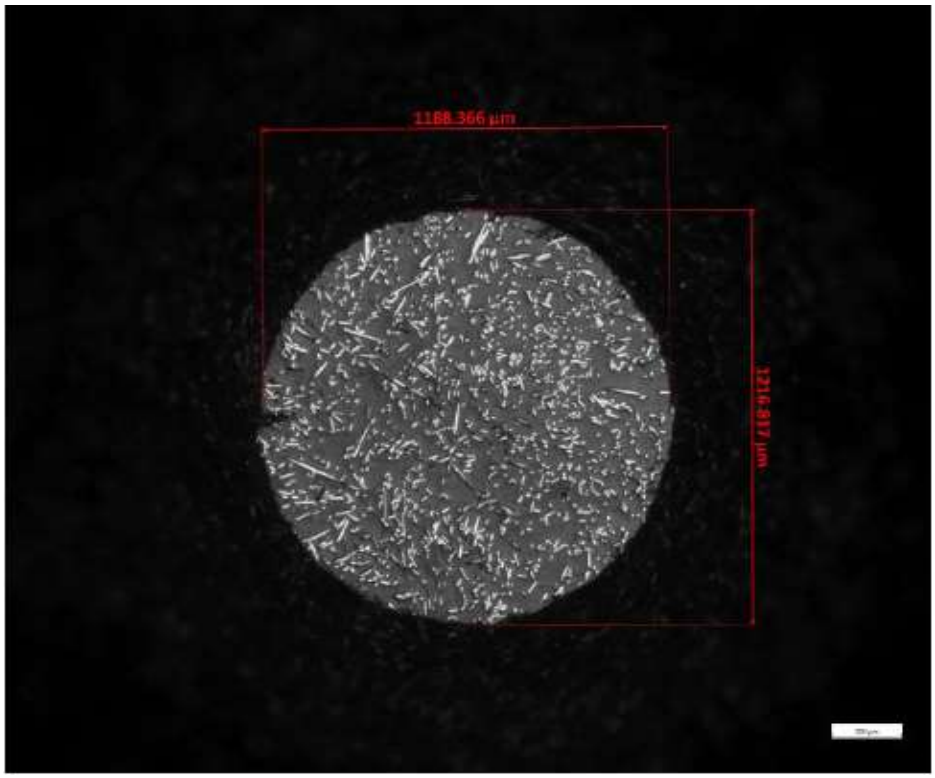

Figure 28: Diameters of the worn surface measured with ImageJ software.

The average value (Ø) of these values has been calculated in order to obtain the height of the spherical cap (h) and the specific wear rate WR through the following formula:

$$WR = \frac{V}{F * d}$$

Where:

V is the volume of removed material [mm^3]

F is the normal load applied to the pin

d is the sliding distance.

The results are reported as an average ± error range, where the error range is defined as the half-difference between the maximum and minimum values.

The volume of removed material depends on the height of the spherical cap, removed during the wear test, and it is defined as follows:

$$V = \pi * h^2 * (r - \frac{h}{3})$$

Where:

r is the radius of the spherical cap

h is the height of the removed spherical cap, $h = r - \sqrt{r^2 - \frac{Ø^2}{4}}$.

Worn surfaces and cross-sections of pins and of sliding tracks on the discs, as well as the wear debris, were characterized by scanning electron microscopy (SEM: Nova NanoSEM 450) equipped with energy dispersive X-ray (EDX) spectroscopy (Quantax-200, Bruker AXS, Billerica, USA).

The surfaces of non-conductive polymer samples (pins and debris) were observed under low vacuum conditions (water vapour atmosphere, 40 Pa pressure) using a 3 kV acceleration voltage. The conductive discs were observed under standard high-vacuum conditions at 12 kV acceleration voltage. Samples were tilted by 45° - 70° for imaging purposes to enhance the morphological contrast.

For the cross-sectional preparation, the pins were embedded in a cold-setting epoxy resin, cut with a diamond disc, ground using SiC abrasive papers (up to P2500 in size), and polished with 3 μm polycrystalline diamond slurry and colloidal Al2O3 suspension. The discs were cut using standard metallographic equipment, cold-mounted in the same type of epoxy resin, ground with SiC abrasive papers (up to P2500 size), and polished with 3 μm polycrystalline diamond slurry and colloidal SiO2 suspension. Polished cross-sectional samples were metallized with a thin layer of sputtered Au to ensure electrical conductivity and observed at either 3 kV or 12 kV acceleration voltage. On all surfaces and cross-sections, EDX analyses were acquired at a 12 kV acceleration voltage.

Worn and pristine surfaces of pins were further characterized by Fourier Transform – Infrared Spectroscopy (FT-IR: Vertex 70, Bruker), operated in attenuated total reflection (ATR) mode, and by micro-Raman spectroscopy (LabRam, Horiba Jobin-Yvon,

Longjumeau, France), operating with a 532 nm-wavelength solid-state laser as the excitation source, focused through a 100× objective.

2.5 Infrared termography during pin-on-disc experiments

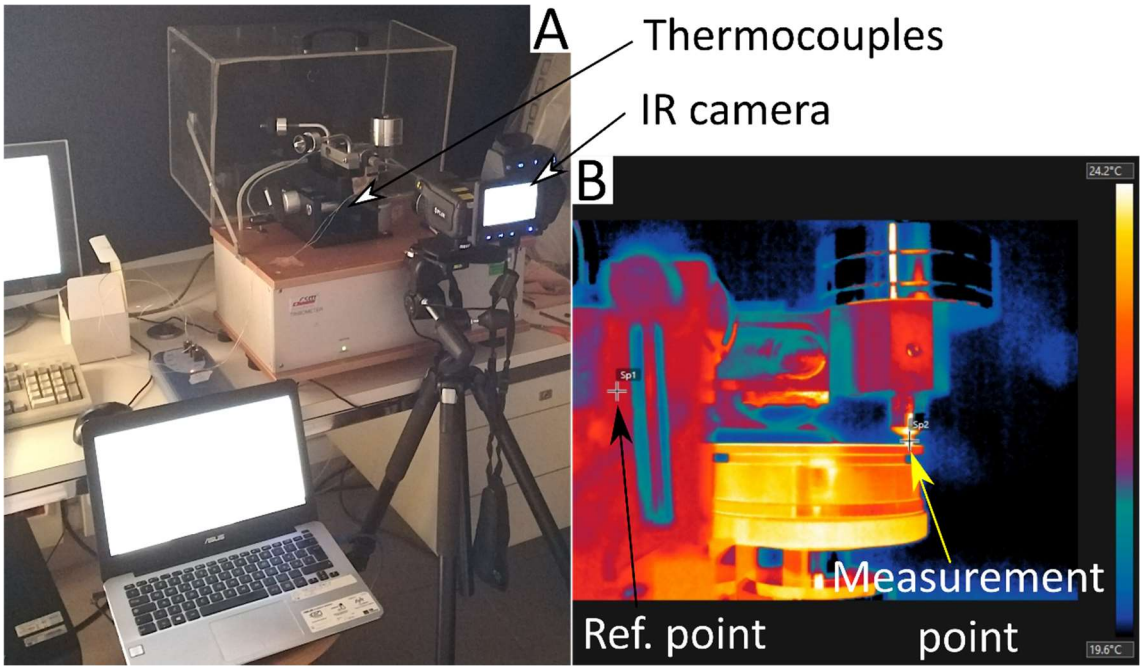

Figure 29: The experimental setup with an IR thermo-camera in front of the pin-on-disc tribometer and thermocouples for simultaneous measurement of the reference temperature on a black surface (A). An example of a thermographic frame with the measurement points on the pin, and the reference point to calibrate the temperature scale (B).

The temperature evolution of the pins during sliding wear testing was measured using an infrared (IR) thermographic camera (T640, FLIR). The camera has a 30 Hz infrared detector with 640×480 resolution, 0.035 °C thermal sensitivity, and -40 to 2000 °C temperature measurement range. Data was acquired at 10 Hz during every pin-on-disc experiment (see Figure 29A). The temperature at a representative point located approximately 1 mm from the tip of the pin was extracted from each frame (Figure 29B) connecting the camera in real-time to a PC and using FLIR Thermal Studio Suite software. The thermal camera emissivity set point was calibrated by reading the environmental temperature from a reference point on a black surface with emissivity close to 1 (Figure 29B), the temperature of which was simultaneously measured with two class I K-type thermocouples (Nickel- Chromium / Nickel-Alumel) connected to a Pico TC-08 datalogger (Figure 29A). Thermocouples were previously calibrated using a Julabo F20 thermostatic bath with a 0.01 °C resolution.

2.6 Flash and bulk temperatures measurements

As previously discussed in Section 1.6, the model developed by Ashby et al. [25] is accepted [2] as a simple yet effective tool to estimate the bulk and flash temperatures of mating surfaces in sliding couples, and it was accordingly employed in the present work. The rise in bulk temperature of the mating surfaces, i.e. the macro-scale average surface temperature, which, for continuity reasons, is assumed to be identical for both mating bodies in the contact area, is estimated by Ashby et al. [25] assuming that the pin and disc behave as a parallel between two thermal resistances. Indeed, the heat generated at the contact interface can flow either along the path entering the disc or the pin, depending on their respective thermal resistances. It follows:

$$\Delta T_{bulk} = \frac{\mu F v}{A_n}\left(\frac{k_1}{l_{b1}} + \frac{k_2}{l_{b2}}\right)^{-1}$$

Where:

μ is the friction coefficient

F [N] is the normal force

v [m/s] is the relative sliding speed

k_1 [W/(m·K)] is the thermal conductivity of the pin

k_2 [W/(m·K)] is the thermal conductivity of the disc

A_n [m^2] is the nominal contact area

l_{b1} [m] is the heat diffusion distance for bulk heating of the pin

l_{b2} [m] is the heat diffusion distance for bulk heating of the disc

The rise in flash temperature at the actual contact junctions, i.e. the transient, micro-scale temperature peaks that occur when accounting for actual (rough) surface profiles, is likewise estimated as [25]:

$$\Delta T_{flash} = \frac{\mu F v}{A_r}\left(\frac{k_1}{l_{f1}} + \frac{k_2}{l_{f2}}\right)^{-1}$$

Where:

A_r [m^2] is the real contact area

l_{f1} [m] is the heat diffusion distance in flash heating (pin)

l_{f2} [m] is the heat diffusion distance in flash heating (disc)

The nominal contact area $A_n = \pi r_0^2$ requires knowledge of the nominal contact radius r_0 in the pin-on-disc tests. In our tests (see Section 2.4), the contact radius increased more rapidly during the early stages, when the spherical tip of the pin wore down and the contact turned from a non-conformal to a conformal one. The increase in contact radius became much slower at later stages of the test, due to the spherical tip geometry itself. Because our aim was to compare the computed rise in steady-state bulk temperature to the thermographic measurements of the overall temperature rise in the pin at the end of the test, r_0 was assumed to be identical to the eventual radius of the circular wear scar on the pin itself.

Computing A_n with the wear scar radius at the end of the test introduced an approximation in the results, yet we regarded this approximation as acceptable because the model was not supposed to return perfectly accurate values but estimates.

The thermal conductivity values (k_1, k_2) of the mating bodies changed with temperature, as seen in Section 3.2. However, in a first approximation, they were considered constant for the purpose of the present computations.

The heat diffusion length in the pin was assumed to be $l_{b1} \approx 2l_1$ in accordance with [26]. This assumption accounted for the unavoidably imperfect contact between the pin and its holder, which adds to the total thermal resistance associated to the heat flow through the pin towards its holder (assumed as a heat sink of infinite capacity).

The heat diffusion length in the disc is calculated according to Ashby et al. [25]:

$$l_{b2} = \frac{r_0}{\sqrt{\pi}} \tan^{-1} \sqrt{\frac{2\pi\alpha_2}{r_0 v}}$$

The rise in flash temperature at the actual contact junctions, i.e. the transient, micro-scale temperature peaks that occur when accounting for actual (rough) surface profiles, is likewise estimated as [25]:

$$\Delta T_{flas} = \frac{\mu F v}{A_r} \left(\frac{k_1}{l_{f1}} + \frac{k_2}{l_{f2}} \right)^{-1}$$

$A_r = \frac{F}{H}\sqrt{1 + 12\mu^2}$ is the real contact area between the mating bodies. The use of this expression involves an approximation: it is strictly valid only for plasticized contacts, but the low elastic modulus (high *H/E* ratio) of polymers means this might have not been fully true in our case.

The heat diffusion length in the stationary partner, i.e. the pin, is $l_{f1} = \frac{\pi r_j}{4}$ [26].

The heat diffusion length in the rotating partner, i.e. the disc, is calculated differently depending on whether the transit time of a point across the contact region is small or large compared to the time needed to diffuse heat away from that point, which is expressed by Peclet's number [25]:

$$Pe = \frac{\pi \alpha_2}{v r_0}$$

According to Wang and Rodkiewicz [26]:

$$l_{f2} = \begin{cases} \pi r_j/4 & for\ Pe \geq 10\pi \\ (\pi r_j/4) \cdot B_L & for\ \pi/5 < Pe < 10\pi \\ 0.31\pi r_j \sqrt{\alpha_2 / v r_j} & for\ Pe \leq \pi/5 \end{cases}$$

B_L is a correction factor, whose values are tabulated in [26] as a function of Pe.

The definition of Pe made by Wang and Rodkiewicz [3] is slightly different than did Ashby et al. [25]; therefore, the definition of l_{f2} was modified compared to the version published in [26] to keep consistency with notation adopted here.

The junction radius is estimated as [26]:

$$r_j = \begin{cases} \sqrt{A_r/\pi} & for\ A_r \leq \pi r_a^2 \\ r_0 \Big/ \sqrt{1 + \left(1 - \frac{A_r}{A_n}\right)\left(\frac{r_0}{r_a}\right)^2} & for\ A_r > \pi r_a^2 \end{cases}$$

The average asperity radius is estimated as $r_a = (10^5\ N/m)/H$, where H is the hardness of the softest surface (i.e. the polymer composite pin, in this case) expressed in Pa.

2.7 Design of Experiment

Polymers and their composites have generated wide interest in various sliding applications, because of their unique inherent tribological properties, such as low friction and high wear resistance. The nature of sliding determines the mechanism by which polymers, and composites, tribo- systems will wear. One of the major tasks in the study of the wear of polymers and composites is the prediction of the wear behaviour, based on

the relationship between surface traction, temperature, operating variables, material properties and wear mechanisms.

The aim of this part of the work is the design and development of a model able to provide quantitative data on the useful life of PTFE based components, in conditions of tribological sliding contact with a counter-surface. This model is based on an equation that identifies the relationship between the independent variables of the process and the desired result (dependent variable).

To obtain such equation, the Design of Experiment (DOE) statistical method was applied to design the experiments and investigate the influence of the tribological testing variables (speed, load, distance), as single or interacting factors, on the wear rate of the unreinforced PTFE samples, measured after the wear test.

More in detail, DOE is a statistical analysis technique that allows to analyse the effects of the input variables (factors) on an output variable (response). This is achieved through a series of tests in which input variables are changed according to an experimental plan, on the completeness of which depends the ability to evaluate more or less precisely the possible interactions between input factors. The core the DoE methodology, therefore, is that it provides a criterion for planning the minimum number of tests needed to achieve the desired level of "resolution", i.e. the ability to identify qualitatively and evaluate quantitatively the effects of factors and their interactions up to a certain order. Factors are varied within a certain range, selecting minimum, maximum and (where applicable) intermediate values based on the expected service conditions in the targeted application. After the experiments have been performed, the resulting data is then subjected to a combination of established statistical and mathematical analyses including normality tests; analysis of variance (ANOVA) to identify the statistical significance of distinct factors and their interactions on the response; and linear regression to identify quantitative (albeit purely empirical) relations between factors and response.

Different types of DOE plans are usually applied either as a screening approach, when the involved experimental phenomena are poorly known, or as powerful optimizing tool, when the most influential factors, their main variability ranges and interactions are already known. In other words:

- Screening phase: identification of significant factors and their correlations
- Optimization phase: identification of a quantitative response model (regression model).

In this work, the Minitab software was used to elaborate the collected data applying DOE algorithms. A full-factorial plan was performed where 2 values for each factor are selected, and three factors are identified. The input variables in the tribological system were:

- Load
- Speed
- Sliding distance.

This model allows to build a linear regression model where all first-order effects of each factor and their interactions can be evaluated without aliasing. Because Archard's law postulates that the wear volume varies linearly with load and distance and it is independent of speed (i.e. the specific wear rate is independent of all three variable), it is assumed that a linear model, where the specific wear rate varies linearly with these factors and their interactions, is sufficiently accurate to capture even effects that would cause the response to deviate from Archard's law, whilst effects of even higher order are probably not significant, at least to a first approximation. One or more central points are usually added to provide a more complete overview of the factor interactions and an estimate of the intrinsic variability of the output response. For example, if using a full factorial design with three replicates for each condition and one centre point, then 12 combinations will be performed. The central point was chosen only for the sliding distance (5000 m) because, during the design of the tests, it was thought that it could be the most influential parameter on the trend of the wear rate.

Each test was repeated 3 times, for a total amount of 36 tests, and the factors ranges are shown in Table 8.

Load (N)	Speed (m/s)	Sliding distance (m)
5	0,54	3000
		5000
10	1,8	7000

Table 8: factor ranges in the tribological tests of unreinforced PTFE samples

The specific wear rate, expressed in units of $mm^3/(N \cdot m)$, and the friction coefficient were chosen as the output responses for this study: they were reported on Minitab and appropriate analyses of the generated factorial plan were performed.

Output evaluation was performed in several phases:

1. Processing of graphs including the "Pareto graph" and the normal probability graph to analyse the significance of the factors. The Pareto graph contains a bar chart, in which the studentized effects of every factor are represented by bars in descending order, and a reference line to indicate which effects are statistically significant according to the Bonferroni selection criterion for comparison among multiple series of data. On the Pareto graph, bars that cross the reference line can be regarded as being statistically significant.
2. Analysis of the effects of the main factors from the "factorial plots" and "interaction plots". The main effects diagram, where the mean value of the response variable for a given level of a chosen factor is plotted against the value of the factor itself, allows to evaluate the relationship between the response and the predictors in the following way:
    - When the line is horizontal (parallel to the x axis), no main effect is present. The value of the answer does not vary based on the value of the predictor.
    - When the line is not horizontal, there is a main effect. The response value is not the same for all values of the predictor. The steeper the slope of the line, the greater the magnitude of the main effect.

    If the interaction effects are statistically significant in this analysis, it is not possible to interpret the main effects without considering the interaction effects. Therefore, the interaction graphs, where the average response value is plotted against the value of one factor for different levels of a second factor (i.e. one line for each level of the second factor), are used to evaluate the lines between predictors and the response, in the following way:
    - Parallel lines: no interaction occurs.
    - Non-parallel lines: an interaction occurs.
3. Creation of a regression model, i.e. an equation that relates quantitatively the response (dependent variable) to the factors. With a 2^3 full factorial plan, the regression model is a linear model where each of the selected factors and interactions are multiplied by a coefficient.

3 Results

This chapter summarizes the overall results of the present research. In the first part, the results obtained from the statistical analysis with DoE carried out on the unreinforced PTFE samples, subjected to tribological tests with the aim of identifying the most influential parameters on the tribological behaviour of the material, are discussed.
The influence of adding fillers to the PTFE matrix is then reported, paying particular attention to the wear mechanisms triggered by different reinforcement combinations and also to the effect that the temperature, developed in the contact area during the sliding motion, can have on the wear mechanism of the material coupled to a specific counter-surface.
The analysis of these parameters is aimed at the realization of a model that is able to predict the useful life of sealing components made of fluoropolymer materials.

3.1 Surface topography of the discs

The profilometry of the discs allows to infer:

- whether the roughness (Sa, Sk) is sufficient to hold the transfer-film or even too high to induce abrasive wear of the polymer;
- whether the disc surface is characterised by a great number of valleys, which may help to retain the transfer film or, on the contrary, whether it is predominantly made of protruding peaks which may abrade the polymer surface (from the evaluation of the Ssk parameter as well as the reduced peak and valley heights Spk, Svk)

The characteristic parameters of the counter-surfaces obtained from the profilometric measurements are listed in *Table 9*.

Disc	**AISI 304**	**Cr_2O_3**
Sa [µm]	0.018±0.002	0.200±0.019
Ssk	-1.33±0.73	-4.45±0.15
Sk [µm]	0.048±0.005	0.286±0.015
Spk [µm]	0.016±0.002	0.136±0.035
Svk [µm]	0.041±0.012	0.754±0.067

Table 9: surface parameters of the used disc counter-surfaces

Analysing these parameters, it should be noted that polished, uncoated AISI 304 has an extremely smooth finish with a slightly negatively skewed height distribution, which indicates that the overall roughness profile is predominantly characterized by deeper valleys, rather than by prominent peaks. This is confirmed by the slightly larger reduced valley depth (Svk) compared to the reduced peak height (Spk). This profile can result from some grinding marks left on an otherwise very smoothly polished surface, and it can be regarded as desirable for a counter-surface working against a polymer-based material, because any protruding peak engenders an abrasion risk for the polymer.

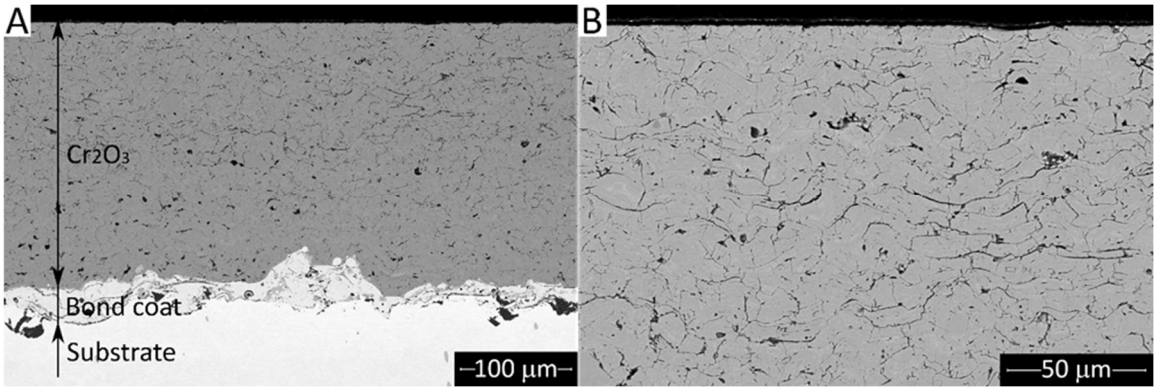

Figure 30: SEM micrographs of the cross-section of the plasma sprayed Cr_2O_3 coating after surface grinding/polishing (A: overview; B: detail near the top surface).

Plasma sprayed Cr_2O_3 exhibits greater roughness despite the polishing process, which is mainly ascribed to the presence of pores and surface defects. Accordingly, its height distribution is much more negatively skewed and the difference between Svk and Spk has grown much larger, compared to uncoated AISI 304.

Cross-sectional micrographs show pores and microcracks in the coating (*Figure 30*, A-B). A very thin bond layer made of plasma sprayed AISI 304 stainless steel is also present, its purpose being to improve the adhesion of the ceramic layer to the substrate. Due to the very low thickness of this layer, and since it is made of the same material as the substrate,

its presence was neglected during the processing of data from thermal properties testing (Section 3.2).

Overall, the microstructure of this coating is quite typical of plasma sprayed Cr_2O_3 [56]. Polishing likely opens the pores and cracks to the outer surface, explaining the observed topographical features. More details on this aspect are provided later in Section 3.4.1.2 where SEM images of the top surface of the coating are shown. The porosity of the Cr2O3 layer is estimated by image analysis to be 4.1±0.8%, whereas thickness is 230±5 µm (average ± standard deviation), also see in *Figure 30*A. The microhardness of the coating is 844±34 HV0.3, which, as expected, is much higher than the microhardness of uncoated AISI 304 stainless steel, 160±5 HV0.3. The latter value is reasonably consistent with literature data of ≈130 HV [55].

3.2 Thermal properties of reinforced polymers and counter-surface materials

Based on specific heat values from DSC analyses (*Figure 32*) and on thermal diffusivities measured by the laser flash method (*Figure 33*), thermal conductivities were obtained as a function of temperature up to 200 °C, which covers the range of interest for the tribological applications of PTFE-based composites (*Figure 33*).

Plasma sprayed Cr_2O_3 (Figure 31) has much lower thermal conductivity than AISI 304 stainless steel (λ ≈ 3.801 – 3.45 W/(m·K) from 60 °C to 200 °C).

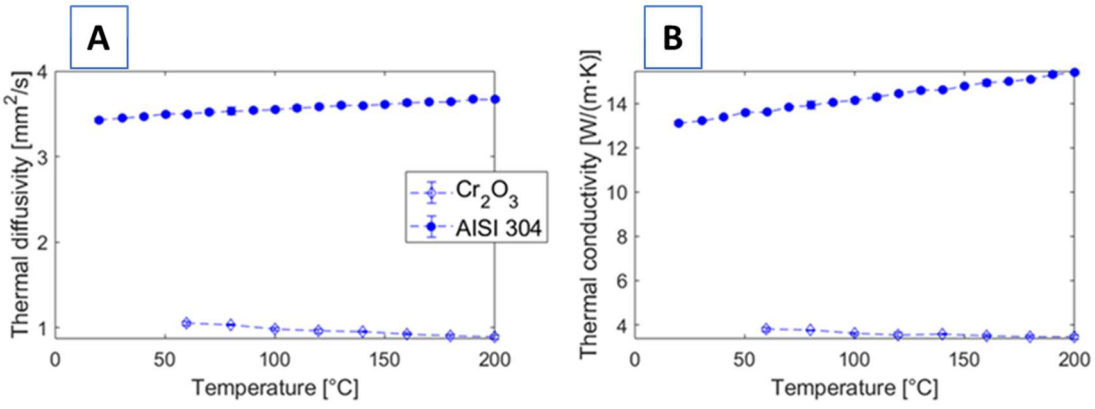

Figure 31: Thermal properties of AISI 304 stainless steel and Chromia coated surfaces: thermal diffusivity(A) and thermal conductivity (B).

The values are in excellent agreement with analogous laser flash measurements performed by Hay et al. [57], who reported c = 750 J/(kg·K) and λ = 3.55 W/(m·K) for

plasma sprayed Cr_2O_3 at 200 °C. With an average porosity of 4.1% (Section 3.1) the density of the coating, employed to calculate the thermal conductivity values from the measured diffusivity, is $\rho_{Cr_2O_3-coat.} = (1-p) * \rho_{Cr_2O_3-bulk} = 5{,}01\ g/cm^3$, which is very close to the value of 4.98 g/cm3 measured in [57] by the Archimedes' method on a free-standing coating sample.

As explained in [57] the low thermal conductivity of Cr_2O_3 is mainly due to its network of pores and microcracks, including microcracks oriented parallel to the substrate surface, which are particularly effective at blocking the heat flow. Indeed, bulk Cr_2O_3 would have almost identical thermal conductivity as AISI 304 (16 W/(m·K) according to data quoted in [57]). The Cr_2O_3 coating therefore acts as a thermally insulating layer on top of the stainless-steel substrate.

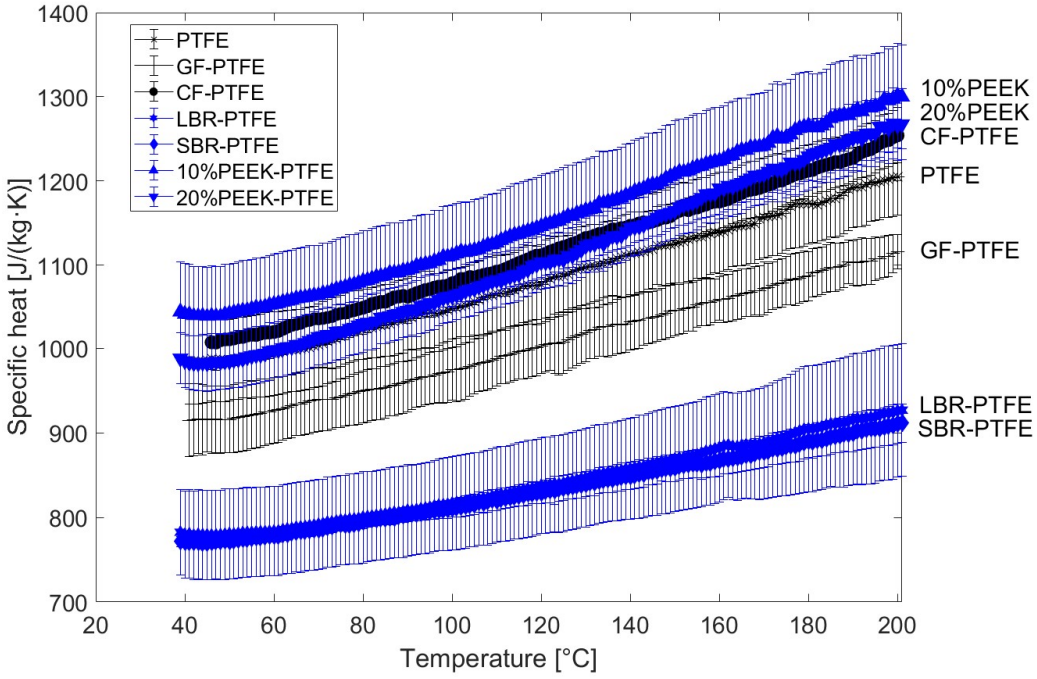

Figure 32: Specific heat of pure PTFE and all PTFE-based composites reinforced with fibres (GF = glass fibres, CF = carbon fibres) and particles (LBR = lamellar bronze, SBR = spherical bronze), and of the counter-surfaces, measured as a function of temperature up to 200 °C.

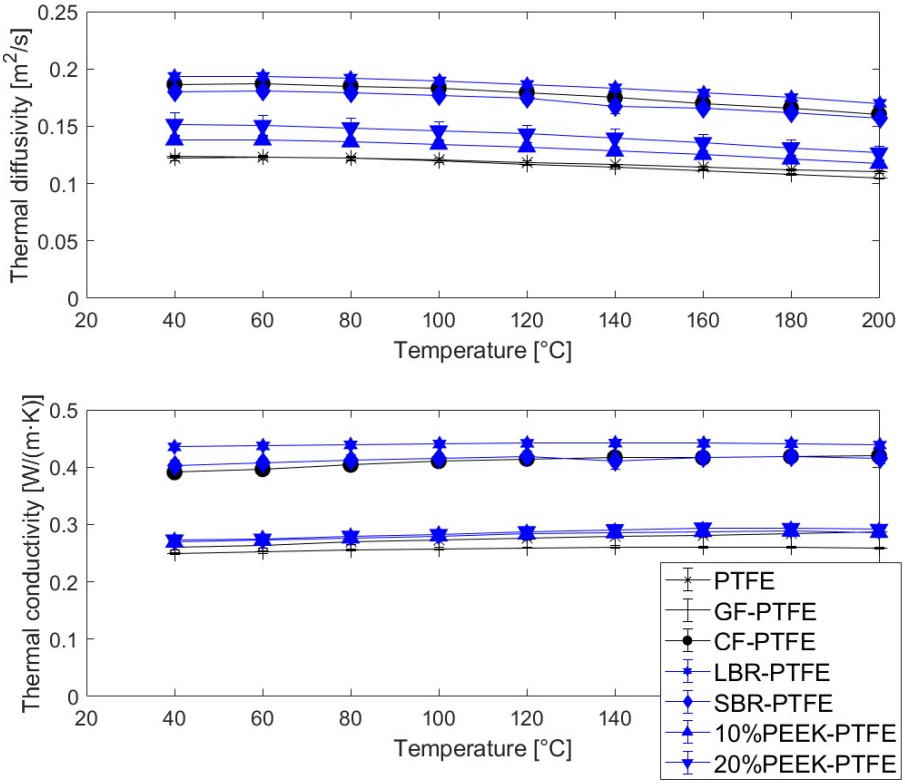

Figure 33: Thermal diffusivity and thermal conductivity of all materials (including pure PTFE as reference) as a function of temperature up to 200 °C.

The curves for PTFE-based samples and the plasma sprayed Cr_2O_3 coating do not start from 20 °C, unlike the curves for AISI 304. Both materials indeed exhibit endothermic transitions around 30 °C: PTFE has two crystalline phase changes at 19 °C and 30 °C [58, 59] (*Figure 34*), whilst Cr_2O_3 has its Néel temperature at approximately 34 °C (*Figure 35*) [60]. Therefore, anomalies in the thermal response of the materials during the tests do not allow the experimental assessment of specific heat and thermal diffusivity data in that range.

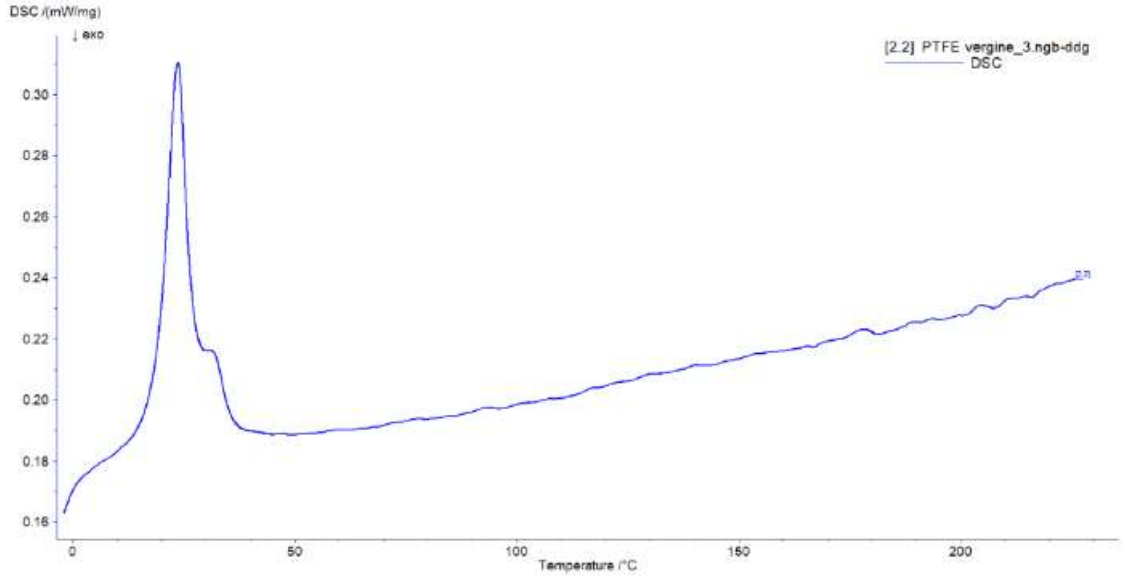

Figure 34: DSC curve of unreinforced PTFE

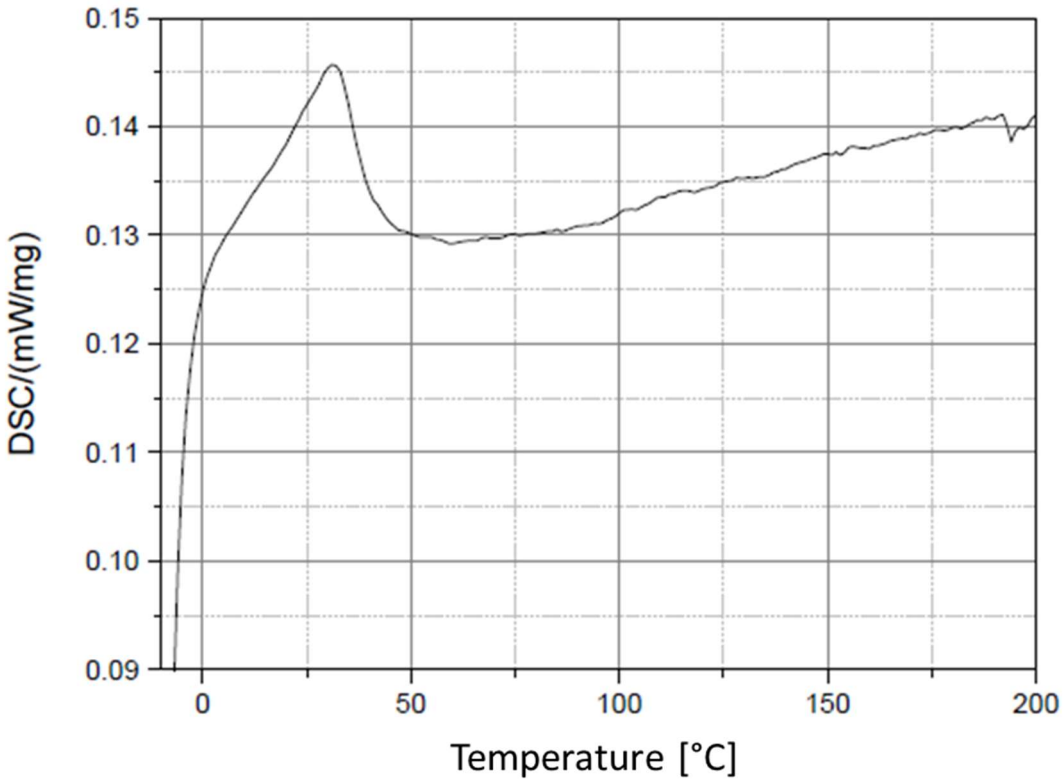

Figure 35: DSC curve of the Chromia coating

The thermal capacity of the PTFE composites reinforced with PEEK and bronze increases with increasing of the temperature; in particular, the composites reinforced with PEEK reach values of $c_=$ 1 J/(g·K) at 40°C (*Figure 32*).

The specific heat is slightly dependent on the percentage of fillers present, with SINTEK PK10 having values slightly higher than SINTEK PK20, and it is independent of the shape of the filler. Indeed, composites with spheroidal bronze and lamellar bronze paricles show overlapping values: c= 0.79 J/(g·K) (*Figure 32*).

The thermal diffusivity values (*Figure 33*) have a specular trend compared to the ones of the specific heat. Samples made with PTFE reinforced with bronze have the highest thermal diffusivity values, equal to $\alpha = 0.19\ mm^2/s$ at 40°C. Instead, among the PTFE samples reinforced with PEEK, Sintek PK20 (PTFE reinforced with 20% of PEEK) has a higher diffusivity, but also a generally higher variability of data.

The experimental results for pure PTFE ($c \approx 985 – 1204$ J/(kg·K) and $\lambda \approx 0.261 – 0.287$ W/(m·K) from 40 °C to 200 °C) are consistent with tabulated values [61] and so is data for AISI 304 stainless steel ($c \approx 485 – 532$ J/(kg·K) and $\lambda \approx 13.11 – 15.41$ W/(m·K) from 26 °C to 200 °C) [55]. This testifies to the reliability of the present measurements.

The addition of glass fibres reduces slightly the thermal conductivity of the composite compared to pure PTFE: from $\lambda \approx 0.26 – 0.29$ W/(m·K) to $\lambda \approx 0.25 – 0.26$ W/(m·K) over the 40 °C – 200 °C range (*Figure 33*). The addition of PEEK, on the other hand, seems to have a negligible effect on the thermal conductivity of the composites ($\lambda \approx 0.27 – 0.29$ W/(m·K) over the 40 °C – 200 °C for both PK10 and PK20 materials). In *Figure 33*, the thermal conductivity curves for the PEEK-containing samples, i.e. PK10 (containing 10 wt.% PEEK) and PK20 (containing 20 wt.% PEEK) are just very slightly above that of pure PTFE, although PEEK is intrinsically more insulating than the glass fibres, its thermal conductivity being barely higher than that of PTFE ($\lambda \approx 0.30$ W/(m·K) according to [61]. Glass fibres are also not good heat conductors; however, the thermal conductivity of E glass is 1.30 W/(m·K) [62], i.e. higher than that of PTFE and PEEK. It is therefore inferred that the decrease in thermal conductivity of the glass fibre-reinforced composite is an indication of limited adhesion between the fibres and the PTFE matrix, whilst PEEK particles would seem to adhere better to the matrix itself.

Carbon fibres, by contrast, increase thermal conductivity to $\lambda \approx 0.39 – 0.42$ W/(m·K) over the same range (*Figure 33*), which, in this case, can be ascribed to their much higher thermal conductivity than both PEEK and glass fibres. The same is true for bronze-based composites, with the lamellar bronze providing slightly higher thermal conductivity and diffusivity than spherical bronze, probably due to the larger specific surface area of the lamellar particles. Because of the very high thermal conductivity of carbon fibres and

bronze, it is difficult to draw any conclusion on the quality of their interface adhesion with PTFE.

Overall, from these thermal analyses it was concluded that:

- The thermal conductivity of all PTFE-based samples shows very little dependence on temperature, which is probably the result of the opposing trends of specific heat (increasing with temperature) and thermal diffusivity (decreasing with temperature).
- The sample reinforced with lamellar bronze has the highest values: $\kappa = 0.44$ W/ (m·K) at 40 °C, while the use of spheroidal bronze reduced the thermal conductivity by about 5%.
- Samples of PTFE reinforced with PEEK show completely overlapping values, ranging from 0.27 – 3 W/ (m·K), which are close to pure PTFE and higher than glass fibre-reinforced PTFE.

3.3 Design of Experiment for unreinforced PTFE

First, DoE analysis was carried out on the unreinforced PTFE samples to study the influence of the main input variables in a tribological system on the wear rate, which is the output variable. The input variables in the tribological system are:

- Load
- Speed
- Sliding distance.

Then a full factorial design has been generated, in which the factors are the input variables of the tribological system, and the levels represent the range within which the factors vary. The sliding distance of 5000 m was chosen as the central point of the factorial plane.

Each tribological test was repeated 3 times.

The values of the specific wear rate of unreinforced PTFE samples after pin-on-disc test against uncoated and Cr_2O_3-coated AISI 304 stainless steel were processed with Minitab.

3.3.1 Un-reinforced PTFE against Chromia coated surface

The picture below (Figure 36) shows the Pareto chart for unreinforced PTFE against the Chromia coated surface.

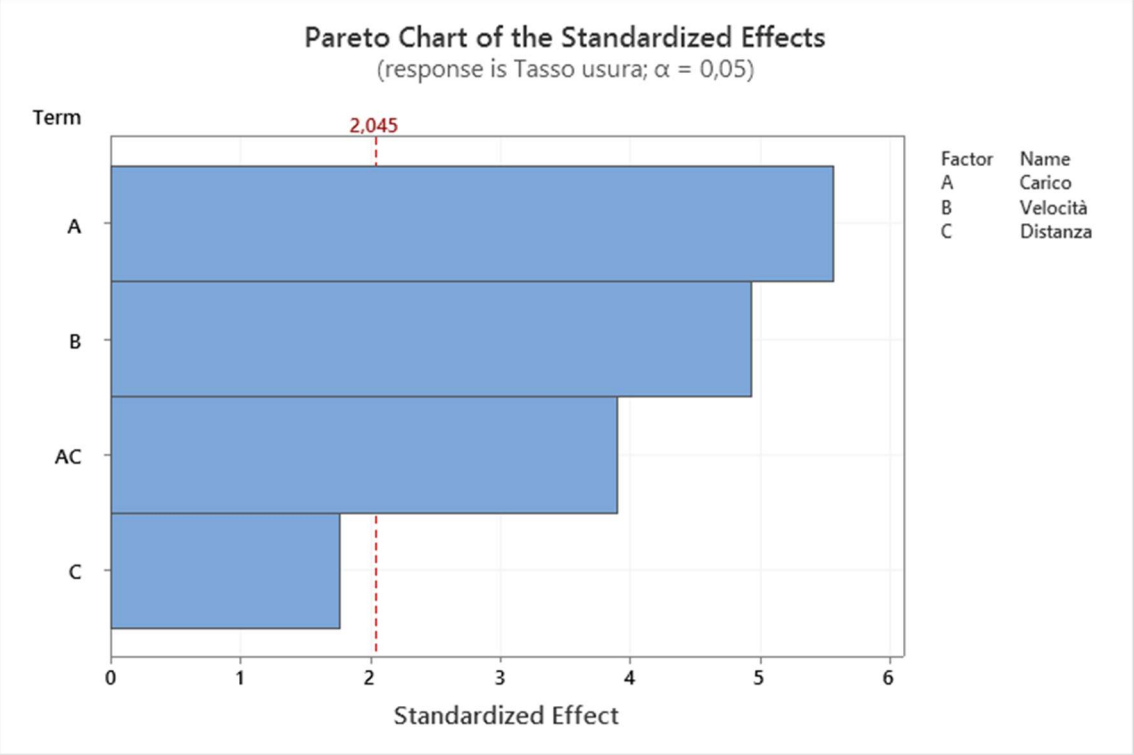

Figure 36: Pareto graph of the statistically significant effects on the specific wear rate of unreinforced PTFE against Chromia coated surface. The light blue bars are the analysed factors according to the Bonferroni criterion. Legend: A = load, B= speed, C = distance.

From this graph it can be deduced that the load and the speed are the most influential parameters on the determination of the wear rate, because, as explained in Section2.7, they exceeded the reference line, while the influence of the sliding distance is negligible. The interaction between load and distance (AC) is also significant because the wear rate is extremely different at various sliding distances as the load increases: in particular at 3000 m the wear rate does not change as the load increases, while at 5000 m and 7000 m the wear rate curves are similar to each other. (Figure 37-D), probably because an increase of the load alters the run-in phase, which affects the volume of removed material and consequently the wear rate.

The interaction graphs of the factors selected for the analysis of the wear rate of un-reinforced PTFE in contact with Chromia are showed in Figure 37.

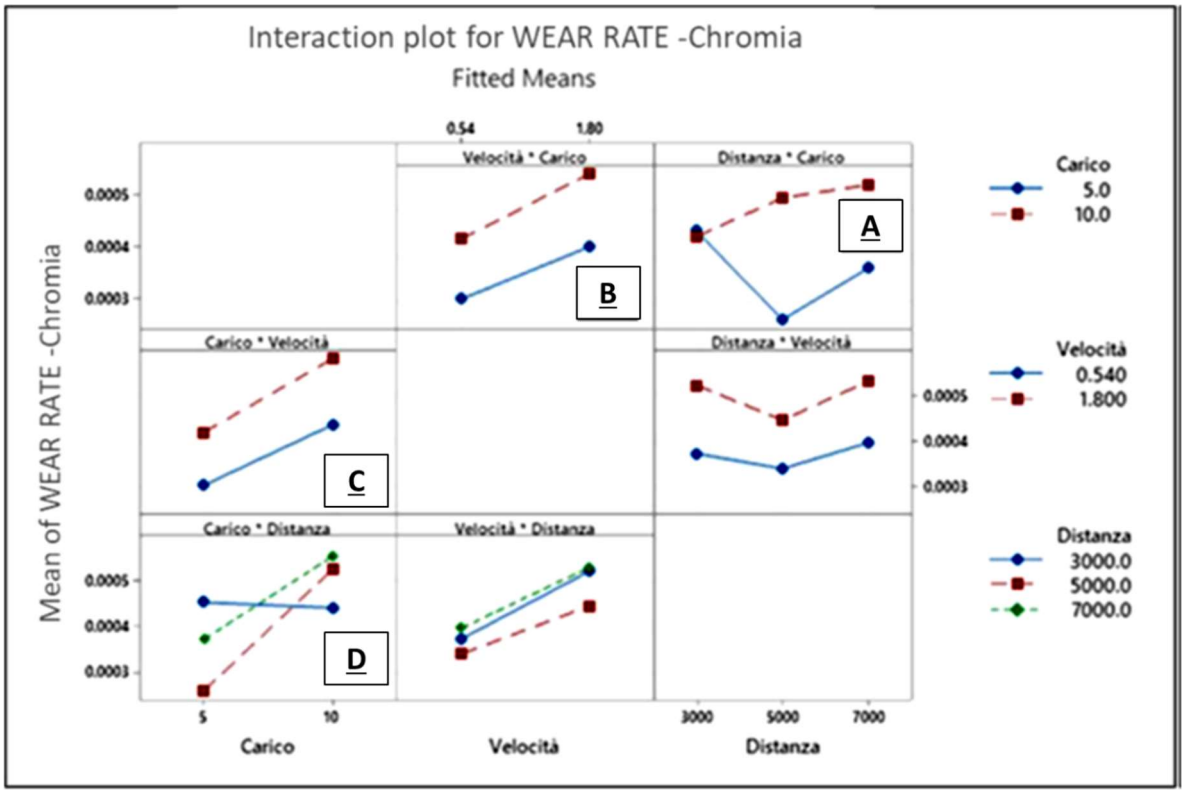

Figure 37: Interaction plot for the specific wear rate (unit: $mm^3/(N \cdot m)$) of un-reinforced PTFE sliding against Chromia coated surface.

The distance-load interaction graph shows that, in high load conditions (graph "A", 10 N), as the sliding distance increases, the wear rate tends to an asymptotic trend; this means that as the sliding distance increases, the ratio between the volume of removed material and the sliding distance becomes constant. This suggests that as the sliding distance increases, a very stable PTFE transfer-film forms, keeping the wear rate constant over time.

The speed and the load are very significant factors on the determination of wear rate. As shown in the speed-load combination graph (graphs "B" and "C") an increasing of both the speed and the load leads to an increase of the wear rate. which could be connected to an increasing of the contact temperature, which lowers the mechanical properties and wear resistance of PTFE [19] .Even if the tribofilm forms, the increase in load probably results in a more than linear increase in the volume of material removed from the PTFE pin by delamination, according to the mechanism by which sheets of material detach from the pin surface. This mechanism keeps the tribofilm "well powered" by always new debris, but does not allow to maintain low wear. The possible influence of the sliding speed on the temperature evolution has been investigated in depth through the study of the thermal conductivity (Section 3.2). This parameter has been obtained by means of

thermal conductivity measurements carried out on the polymer and on the counter-surfaces.

Figure 38 shows the Pareto chart of the statistically significant effects on the friction coefficient of unreinforced PTFE against Chromia coated surface.

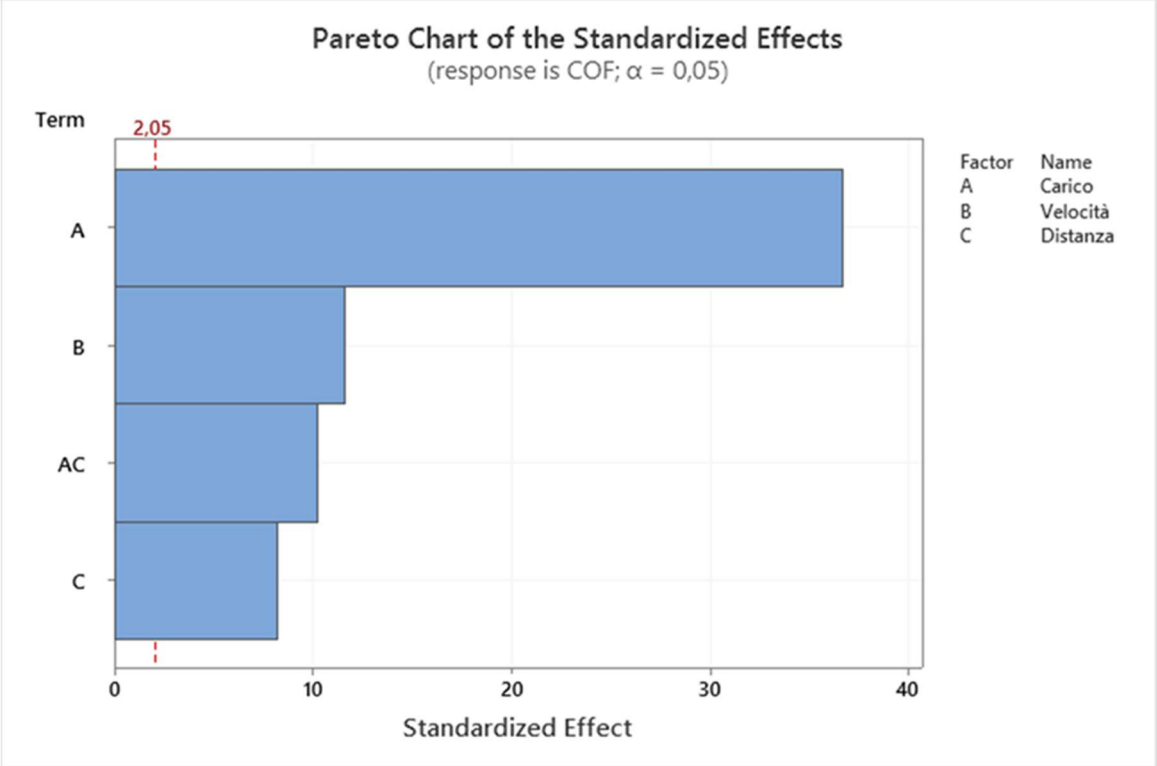

Figure 38: Pareto graph of the statistically significant effects on the friction coefficient of unreinforced PTFE against Chromia coated surface. The light blue bars are the analysed factors according to the Bonferroni crtiterion. Legend: A = load, B= speed, C = distance.

From this graph it can be deduced that the load, the speed and the distance are influential parameters on the friction coefficient. In this case the friction coefficient of unreinforced PTFE increases linearly with the sliding distance, probably due to the increasingly large volume of removed material that does not adhere firmly to the counter-surface, following the usual mechanism of formation and detachment of PTFE from the pin surface: as excess debris is accumulated in the contact region, it could hinder the sliding process somewhat. It is also possible that increasing chemical alteration of the tribofilm with increasing sliding distance slightly compromises its ability to keep low friction. In any case, distance is the least influential among the three factors investigated in this study, as confirmed by Figure 39, which shows the interaction plot for the coefficient of friction (COF) of unreinforced PTFE against a Chromia coated surface.

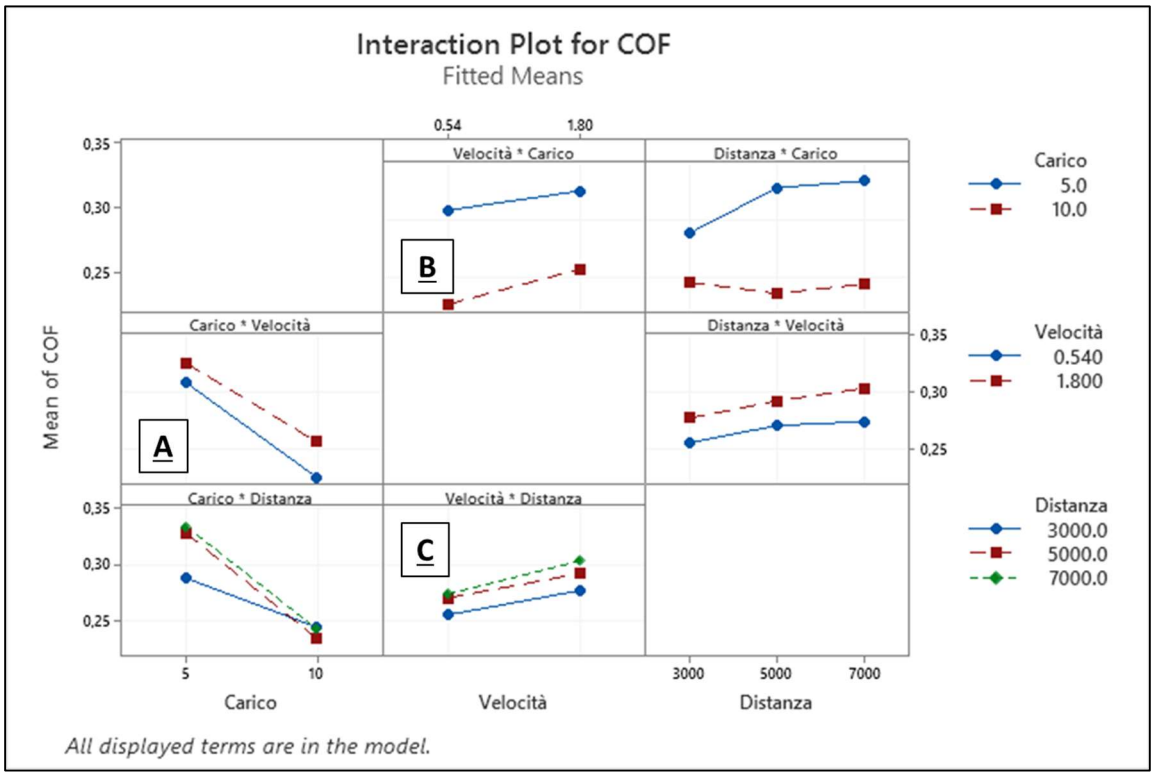

Figure 39: Interaction plot of COF of unreinforced PTFE sliding against Chromia coated surface.

The coefficient of friction decreases as the load increases, regardless of the test speed (graph "A"); the COF line has the same slope at low and high-speed conditions: this means that a transfer of polymeric material occurs, probably on the pores of the coating, which promotes a larger fraction of lubricious polymer-polymer contact though it is not effective to reduce wear as well (see previous considerations).

The coefficient of friction is in general inversely proportional to the increasing of the load and directly proportional to the speed (graph "B"), regardless of the sliding distance (graph "C"), i.e. the coefficient of friction increases with an increase of the speed and with a decrease of the load, and vice versa the coefficient of friction decreases when the speed decreases and the load increases [19].

Speed is therefore a significant factor as high speeds reduce the stability of the transfer-film and/or might induce thermo-mechanical alterations to the polymer itself.

The analyses carried out on the samples with the scanning electron microscope show that the material, especially in conditions of high load (10 N) and high speeds (1.8 m/s), tends to delaminate in contact with chromia coating surface. These lamellae, presumably made

by crystalline PTFE areas, detach and settle on the chromia counter-surface during the test, with some being back-transferred onto the pin itself (Figure 40).

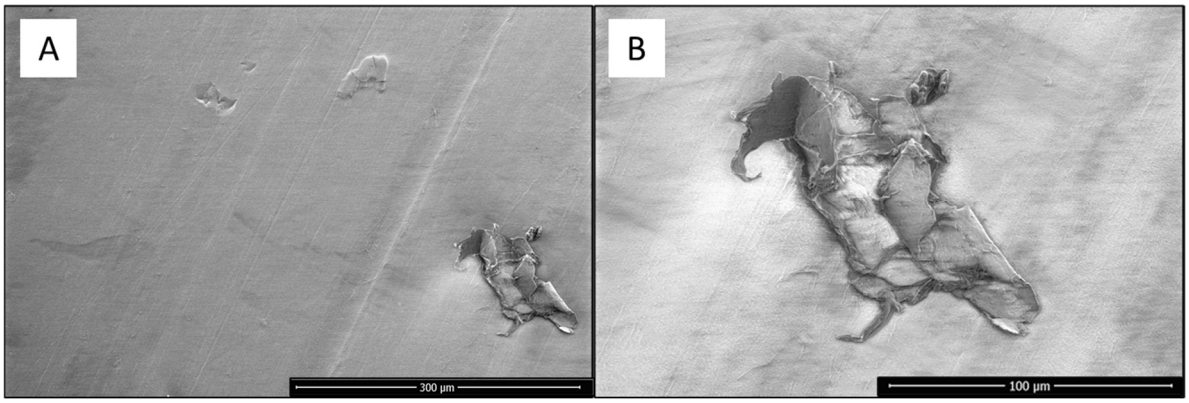

Figure 40: SEM pictures of the worn surface of the PTFE pin after sliding against the chromia coated surface at low magnification (A) and high magnification (B): creation of lamellar structures on the sample.

SEM pictures of the wear traces of Chromia coated discs confirm the DOE results. The wear rate increases with an increasing of the load and the speed, while the coefficient of friction, regardless of sliding distance, decreases as the load increases as more polymeric material is detected on the disc after the sliding test (Figure 42). The polymer debris is also confirmed to consist of large lamellae.

At the same time, the coefficient of friction assumes a high value when the speed is high: this is likely because high sliding speeds prevent the transfer-film from adhering to the counter-surface and therefore there is a continuous transition from the polymer-polymer contact to the polymer-metal contact, which involves removal of material (Figure 41)

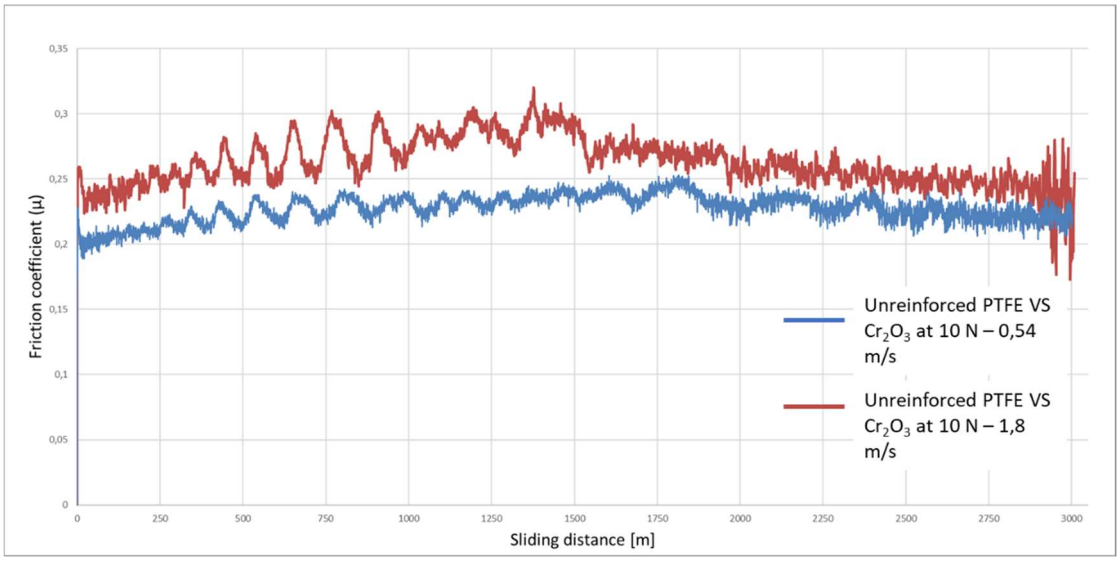

Figure 41: Friction coefficient of unreinforced PTFE against Cr2O3 at 10 N load - 0,54 m/s (blue curve) and at 10 N load - 1.8 m/s sliding speed (red curve).

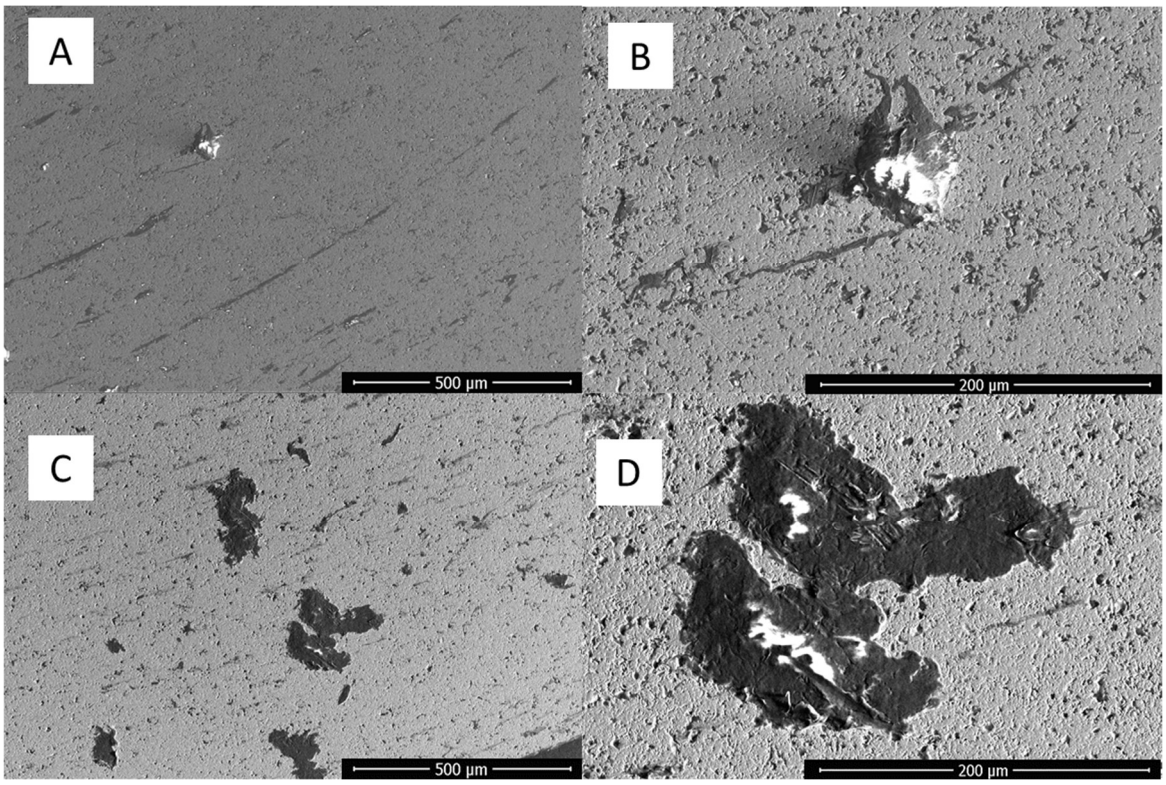

Figure 42: SEM pictures of the wear traces on the Chromia coated surfaces at low magnification (A,C) and at high magnification (B,D). Figure A and B are the wear traces after the sliding test at 5N load and 0,54 m/s speed; figure C and D are the wear traces after the sliding test at 10N load and 0,54 m/s speed. The highest quantity of removed material is detected in conditions of high load (C, D).

SEM pictures in Figure 43 and Figure 44 show that:

- the polymeric material is kept inside the characteristic pores of the coated counter-surfaces (spectrum 3 of Figure 43);
- at the same load, at high speeds (Figure 44, C-D) the transfer-film is not stable, and massive blocks (C) and/or large, curled rolls (D) of PTFE debris appear, which are more or less evenly distributed on the wear track.

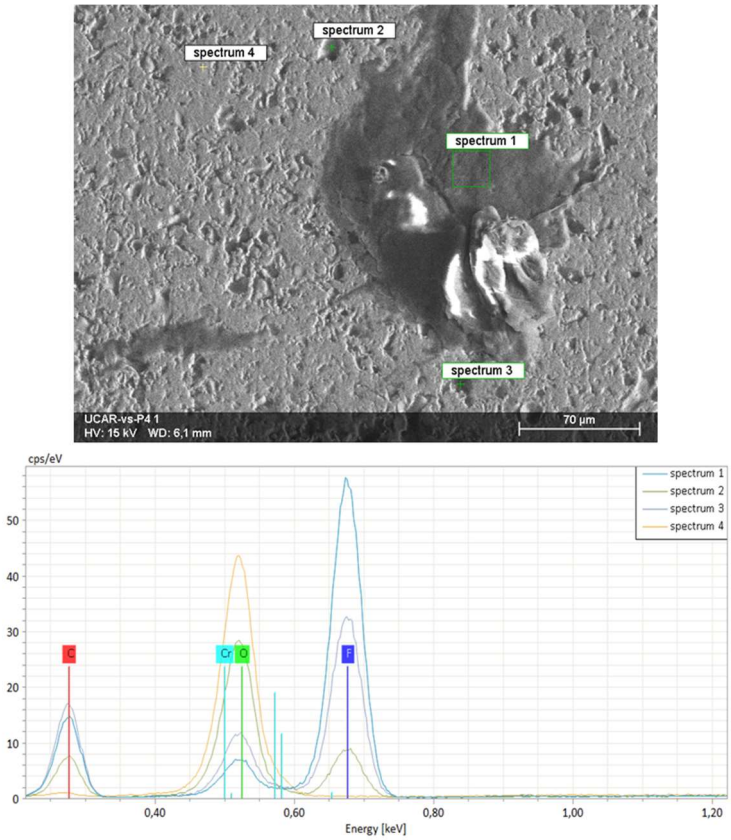

Figure 43: SEM pictures of the PTFE debris on the Chromia coated surface after the pin on disc test at 10 N load and 0.54 m/s speed: by EDX spectra, especially spectrum 3, the presence of PTFE inside the pores of the coating is detected.

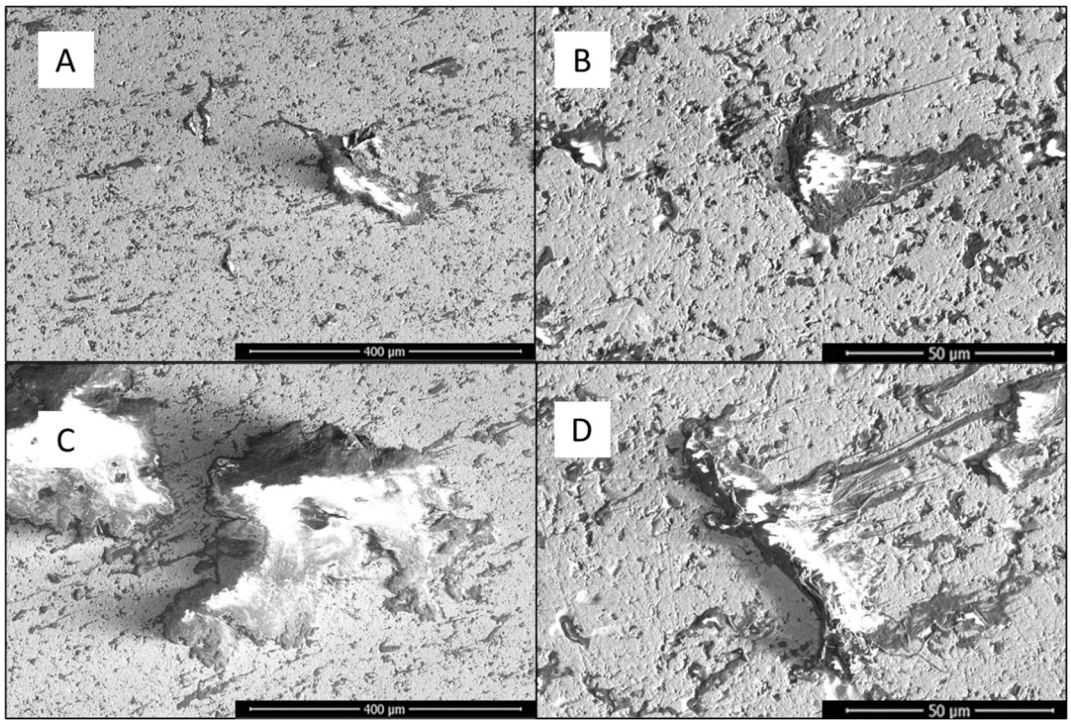

Figure 44: SEM pictures of the wear traces on the Chromia coated surfaces at low magnification (A,C) and at high magnification (B,D). Figure A and B are the wear traces after the sliding test at 10 N load and 0.54 m/s speed; figure C and D are the wear traces after the sliding test at 10 N load and 1.8 m/s speed. Massive blocks of PTFE are detected on the wear track. (C, D).

3.3.2 *Unreinforced PTFE against uncoated AISI 304 stainless steel*

The picture below (Figure 45) shows the Pareto chart for the wear tests with unreinforced PTFE against uncoated AISI 304 stainless steel surface.

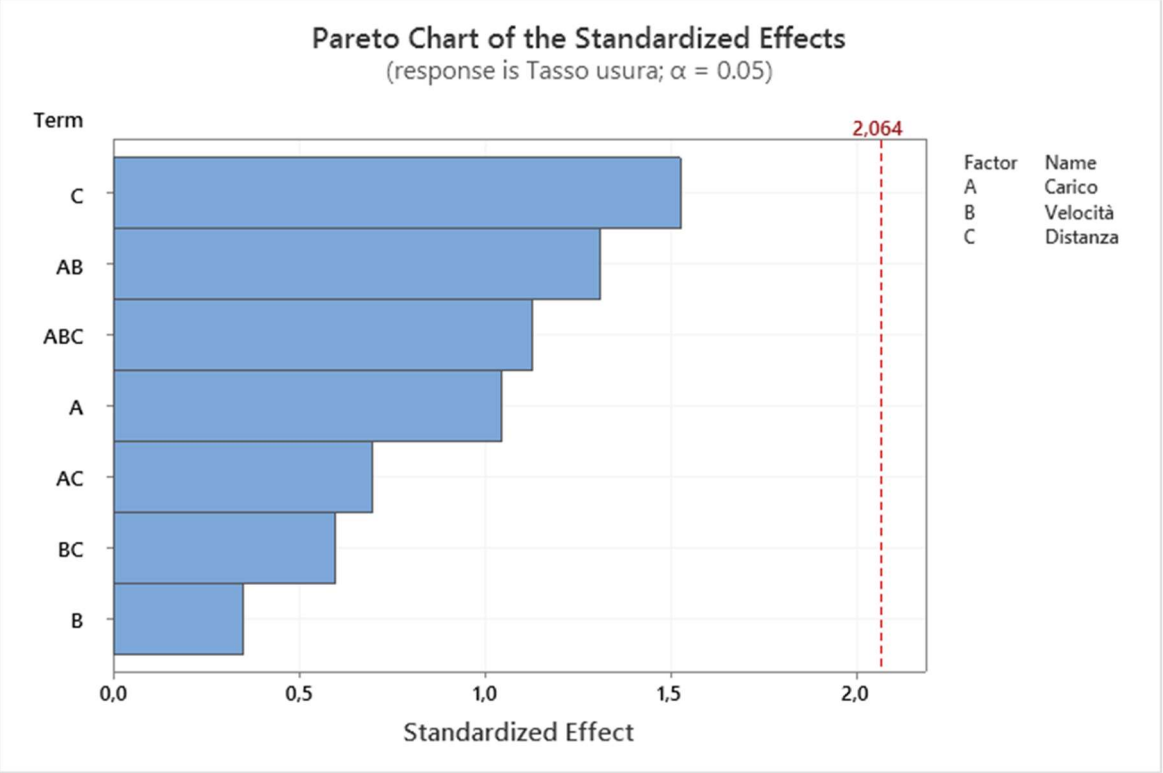

Figure 45: Pareto graph of showing the factors' and interactions' effect on the wear rate of unreinforced PTFE against uncoated AISI 304 stainless steel disc. Legend: A = load, B = speed, C = distance.

Load and speed, unlike the case of the Chromia coated surfaces, do not influence the wear rate of unreinforced PTFE in a way that can be regarded as being statistically significant. The interaction graphs of the factors selected for the analysis of the wear rate of unreinforced PTFE in contact with stainless steel AISI 304 are shown in Figure 46.

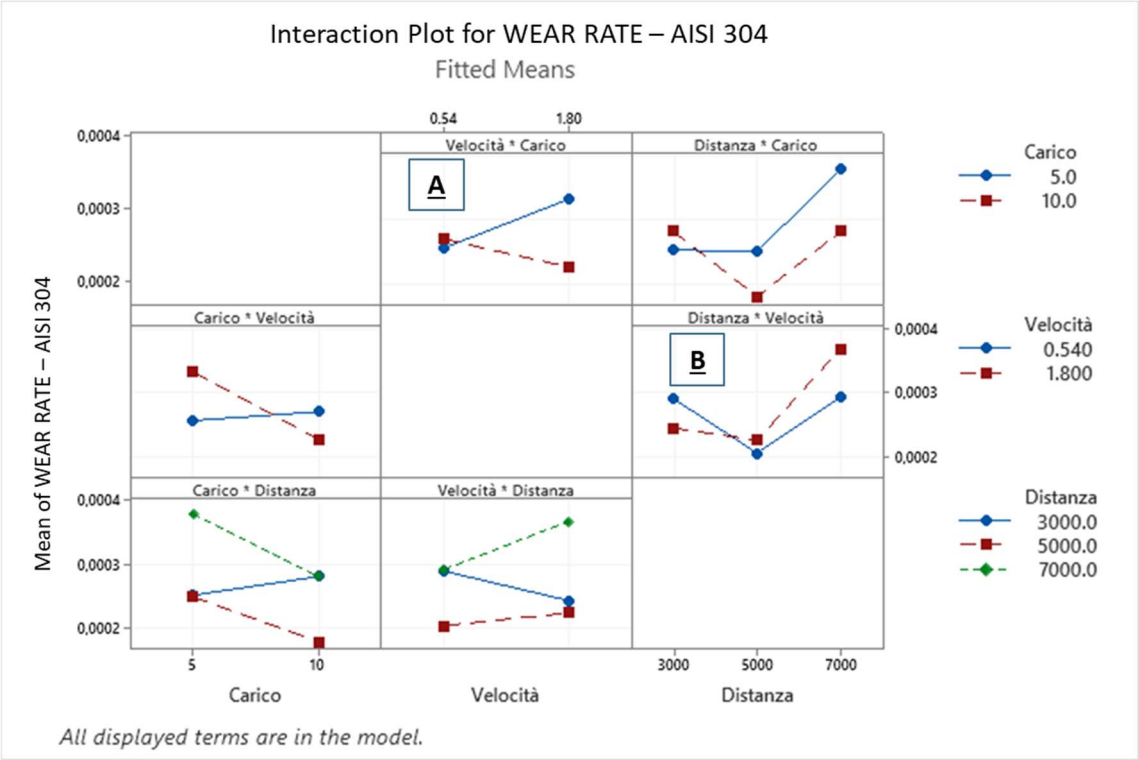

Figure 46: Interaction plot of the effects on the specific wear rate (unit: $mm^3/(N \cdot m)$) of unreinforced PTFE against uncoated stainless steel AISI 304 disc.

Although statistically no factor is particularly significant, it is possible to attempt to analyse some trends from the graphs (Figure 46). As shown in the graph "B" the sliding distance would seem to influence the wear rate as the speed changes: in fact, at low sliding distances the wear rate is high at low speeds, at high sliding distances the wear rate is high at high speeds. This may be due to the fact that the low speed, at low sliding distance, does not favour a stable tribofilm, while the combination of high sliding distances and high speeds make the tribofilm unstable, resulting in an increase of the wear rate. Analysing the effect of the load-speed interaction on the wear rate (graph "A"), the influence of the load, at low speeds, is not significant; at higher speed, the effect of the load is somewhat more significant, and in particular the wear rate decreases at high load. This phenomenon could be explained by higher coverage of the counter-surface with the transfer film (Figure 47). It would therefore seem that, unlike the tests against Cr_2O_3-coated steel, the formation of a more continuous transfer film is beneficial to both the wear rate and (as shown later in this paragraph) the friction coefficient. Section 3.3.1, to the contrary, showed that greater coverage of the Cr_2O_3-coated surface by a tribofilm was associated with lower friction but higher wear loss of the pin.

Accordingly, as shown the graph B, the difference between wear rates at high and low loads becomes greater as the sliding distance increases, probably because, at high sliding distances the transfer-film becomes more unstable with lower loads.

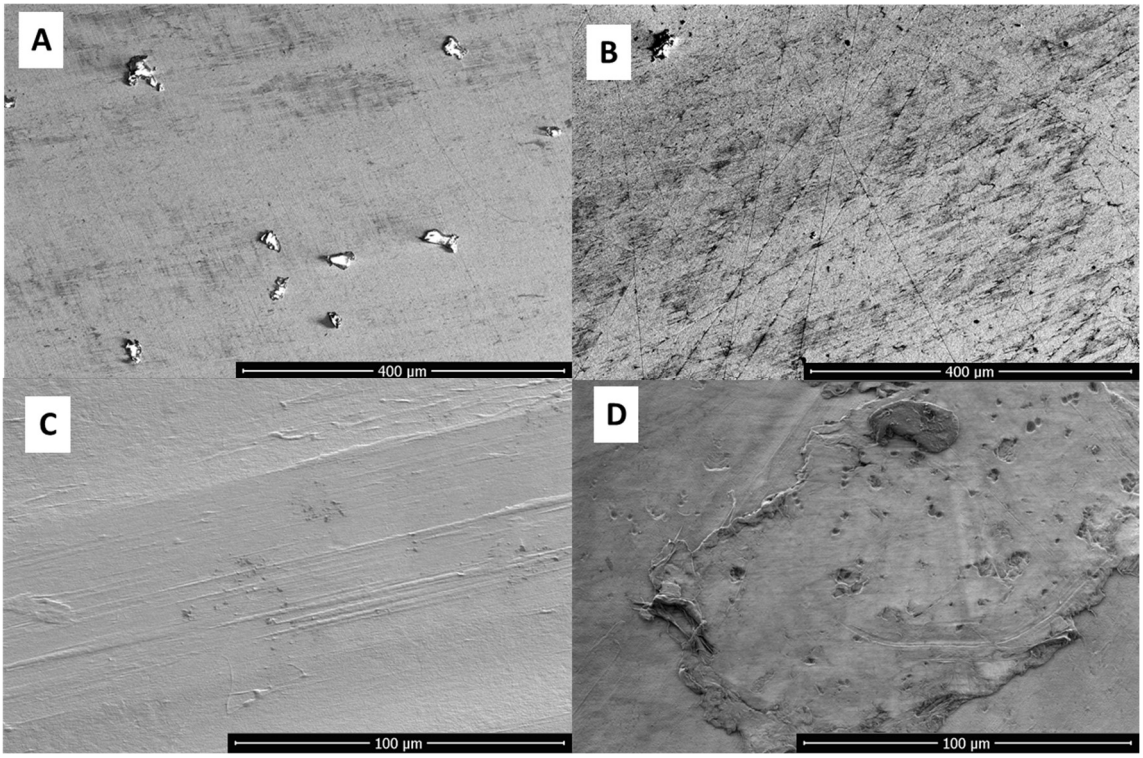

Figure 47: SEM pictures of the PTFE pin and the wear track on the stainless-steel disc at 5 N load and 1.8 m/s (A,C); at 10 N load and 1.8 m/s (B,D).

Figure 48 shows the Pareto graph of the magnitude of the effects on the friction coefficient of unreinforced PTFE against un-coated AISI 304 stainless steel surface. In this case, load is the only significant parameter: in particular an increase in the load always corresponds to a reduction in the friction coefficient, probably due to the greater amount of PTFE debris deposited on the counter-surface.

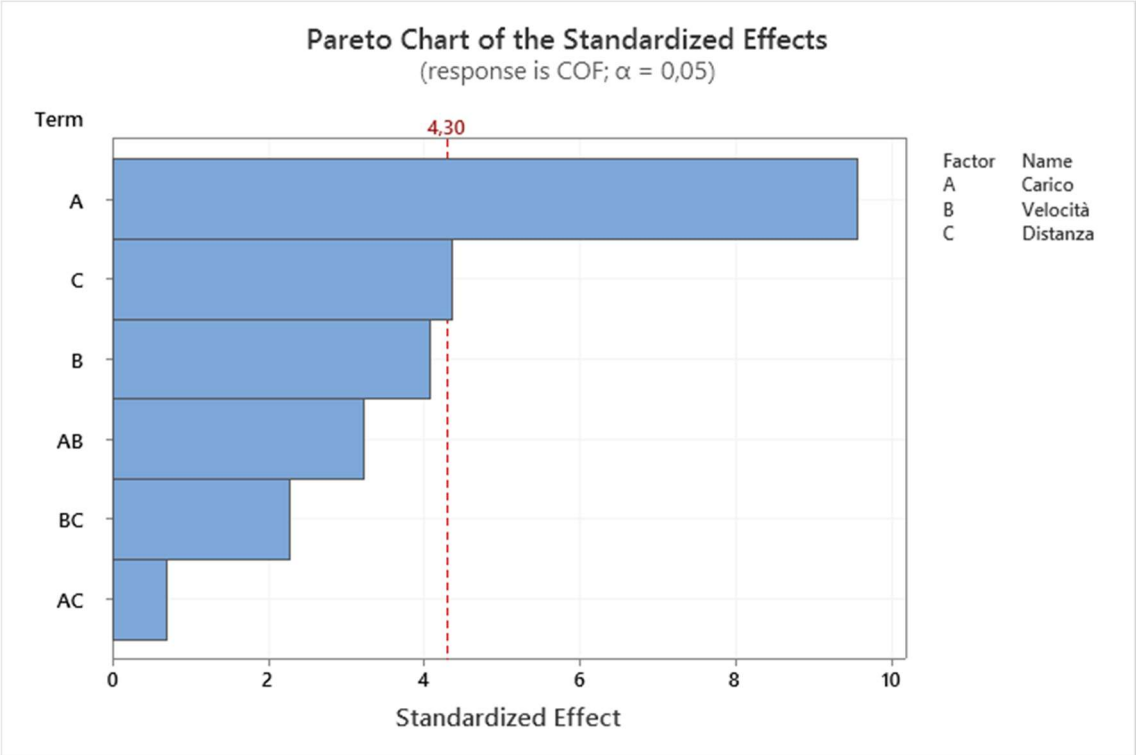

Figure 48: Pareto graph of the statistically significant effects on the friction coefficient of unreinforced PTFE against un-coated AISI 304 stainless steel surface. Legend: A = load, B= speed, C = distance.

The following graphs (Figure 49) show the interaction plot for the coefficient of friction of unreinforced PTFE against the uncoated AISI 304 stainless steel disc.

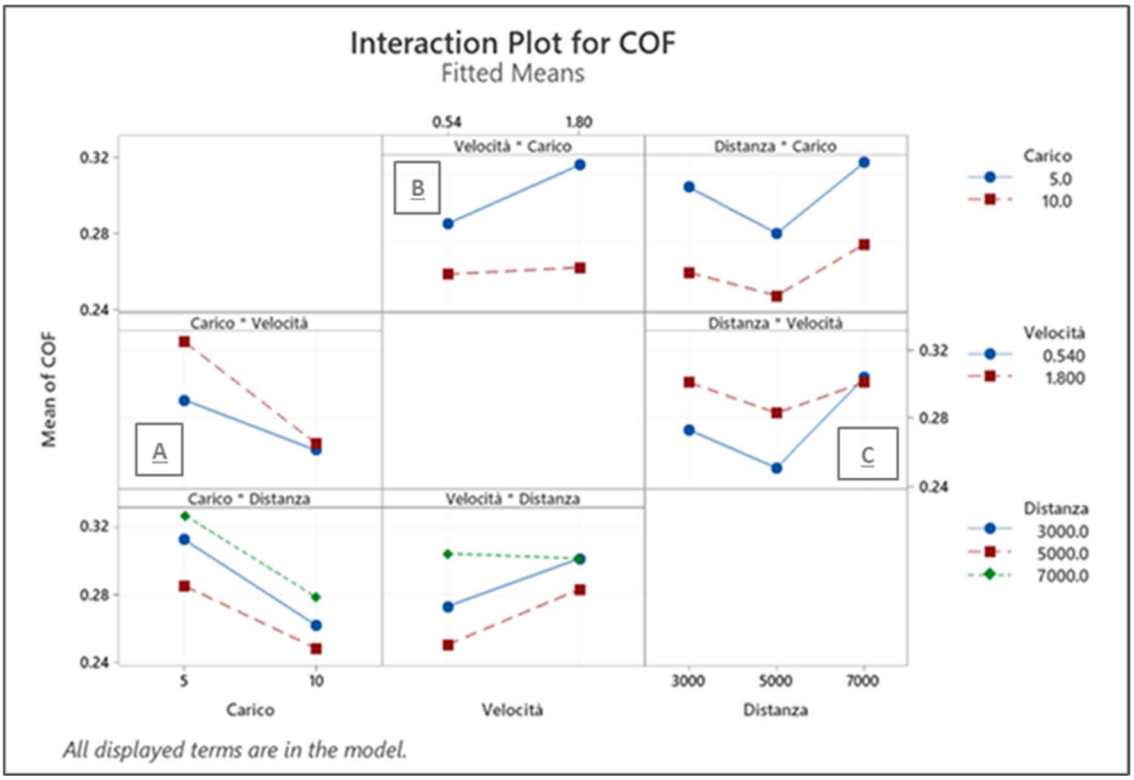

Figure 49: Interaction plot of the effect on the wear rate of unreinforced PTFE against uncoated AISI 304 stainless steel disc.

Increasing the load in any speed condition (graph A) contributes to an improved transfer of polymeric material to the mating surface, stabilizing the transfer-film and promoting polymer-polymer contact, as noted previously (Figure 47D). Then, a lower value of the coefficient of friction is reached at higher loads.

Graph B shows that, regardless of the applied load, increasing the speed leads to an increase in the coefficient of friction. The less the applied load, the greater the influence of the sliding speed on the coefficient of friction.

As shown in the graph C, the sliding distance seems to have little effect on friction. It would seem that, with increasing sliding distance, the friction coefficient first decreases somewhat, then it increases again. This might suggest that coverage by the transfer-film increases at first; then, it becomes unstable by further increasing the sliding distance.

3.4 Tribological behaviour of PTFE-based composites

3.4.1 GF-PTFE

The results of the pin-on-disc tribological tests on GF-PTFE composites are reported in this section. Further data and discussions on the wear mechanisms triggered between the pin and the counter-surface are detailed in [63].

3.4.1.1 GF-PTFE against AISI 304 surface

In pin-on-disc tests, the friction coefficient usually rises during the earliest stages (Figure 50) The temperature of the pin, monitored at the location indicated in Figure 29 (Section 2.5), also increases during the test, eventually approaching a constant condition. Indeed, the pin is subjected to steady-state heating conditions, at least as soon as the friction coefficient attains a stable value. Therefore, after a transient period, a stable temperature profile is established between the contact surface, subject to a constant heat flux, and the metallic holder, which, in a first approximation, acts as a heat sink of nearly infinite heat capacity (compared to the pin).

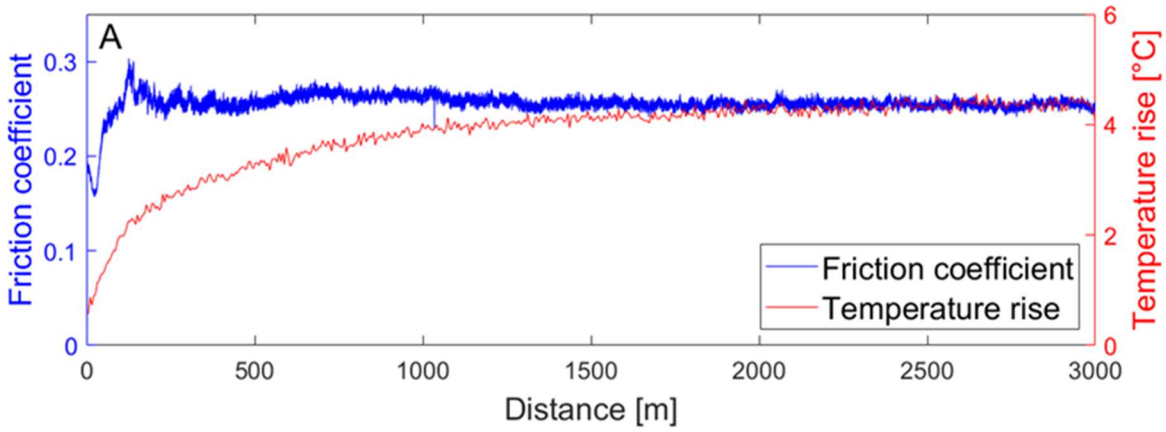

Figure 50: Examples of friction coefficient and temperature rise curves for GF-PTFE tested against AISI 304 at 0.54 m/s speed, 10 N load.

The coefficient of friction in higher-speed cases (Figure 51) tends to stabilize after approximately 400 seconds with a value between 0.23 and 0.28. The temperature increasing during the tests, in the higher load test, tends to reach around 8° C, although stabilizing after about 1000 s. In the test at 5 N load, the temperature increasing is lower, around 2°C. Such behaviour indicates that the load affects the reached temperatures during the test.

With the same coefficient of friction, in fact, the tangential force increases proportionally to the increase of the normal load. Likewise, the work dissipated by friction, at the same sliding distance, also increases.

Consequently, in the higher load test, a double heat output is dissipated. In addition, there is also a change in contact conditions (e.g.: formation of transfer films) which may alter the heat distribution between the contact bodies.

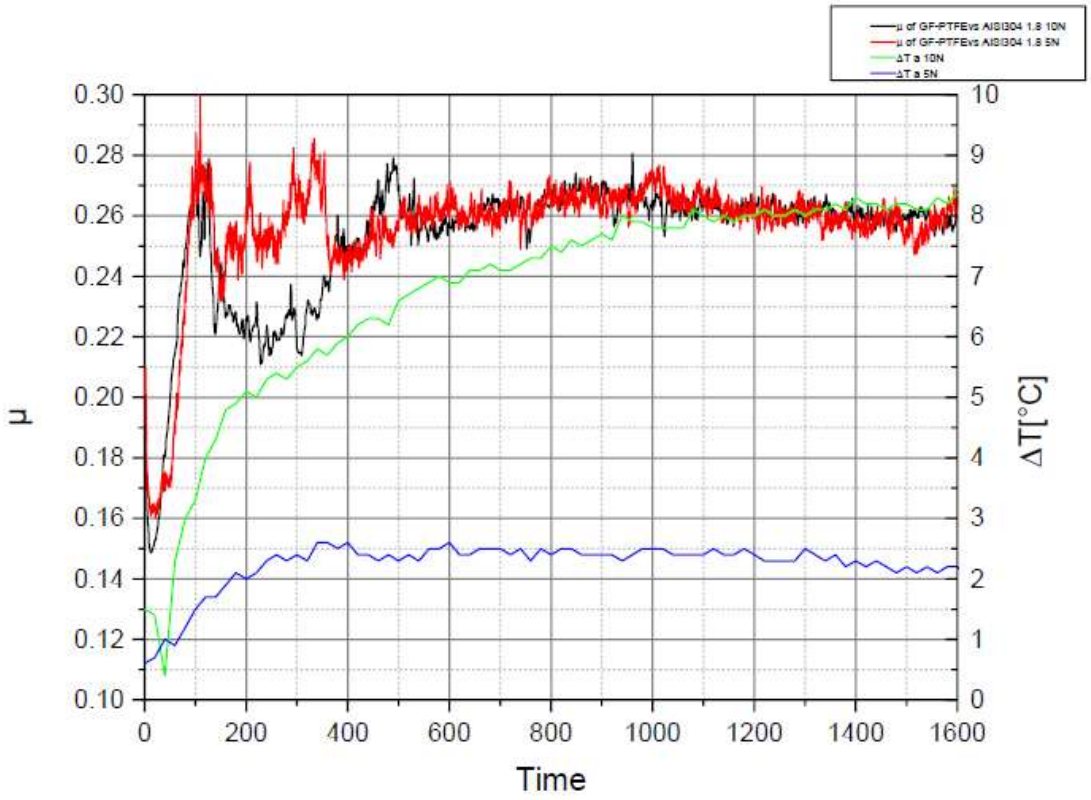

Figure 51: Friction coefficient and temperature raise curves of GF-PTFE vs AISI304 at 1,8 m/s sliding speed and both load conditions (5N-10N)

The coefficient of friction (Figure 52) in conditions of low sliding speeds, has a value between 0.24 and 0.28, but in this case tends to stabilize around 1000 s. The temperature difference tends to stabilize as the coefficient of friction but from 2000 s onwards, with a higher temperature variation in the higher load case, as happened in the higher speed tests, for the same reason as above. It could be expected that the temperature increase at lower speed because a lower amount of heat is generated by the friction dissipation. The temperature rises only 4°C, instead of 8°C, but this difference is recorded only in the case of the tests at higher loads.

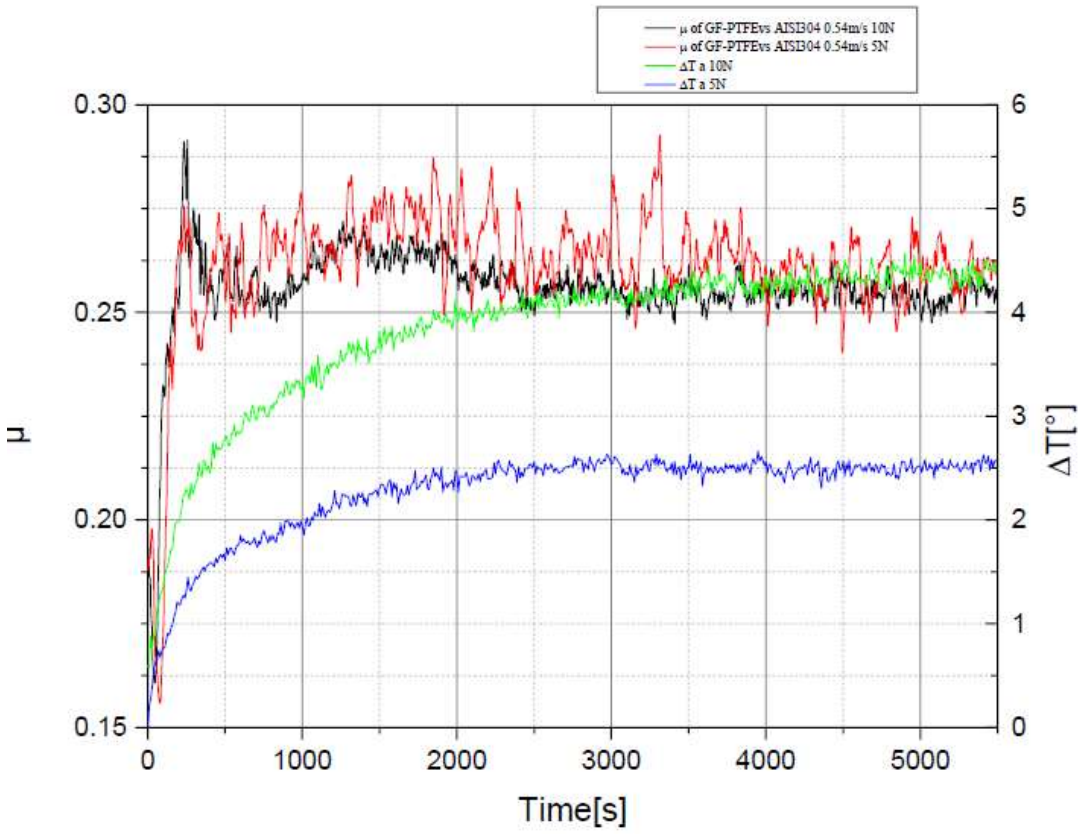

Figure 52: Friction coefficient and temperature raise curves of GF-PTFE vs AISI304 at 0,54 m/s sliding speed and both load conditions (5N-10N)

3.4.1.2 GF-PTFE against Cr_2O_3 coated surface

The coefficient of friction of GF-PTFE against Cr_2O_3 coated surface (Figure 53) is between 0.18 and 0.20, which is lower than in the previous case, although it tends to be less stable than the one observed with the counterpart in AISI304. In conditions of 10 N load, the coefficient of friction stabilizes after 800 s and the ΔT obtained is about 7°C; the temperature tends to stabilize like the coefficient of friction. At 5 N load, the coefficient of friction is not perfectly constant and tends to stabilize only in the final part of the test fluctuating between 0.21 and 0.23, then slightly higher values, accompanied by a ΔT of about 3,5°C, therefore lower than when the load is greater, for the reasons already mentioned.

It is particularly interesting that the temperature increasing in the test at 10 N load is lower than the one observed against uncoated AISI304, although the latter has a higher thermal conductivity and, consequently, a greater capacity to remove heat released by friction from the contact area.

This means that the reduction of the friction coefficient (therefore, of the total amount of the dissipated heat) with Cr_2O_3 counter-surface has a preponderant effect compared to the lower thermal conductivity of the coating itself, which would tend to increase pin temperature instead.

In conditions of 5N load, the temperature increasing against Cr_2O_3 coated surface is slightly higher than the one observed against AISI304 surface. In this case, the reduction of the friction coefficient (therefore, the dissipated thermal power) is less; in this case the effect of the lower thermal conductivity of the coating prevails, which removes less heat from the contact area, so that the most part of the developed heat is absorbed by the pin.

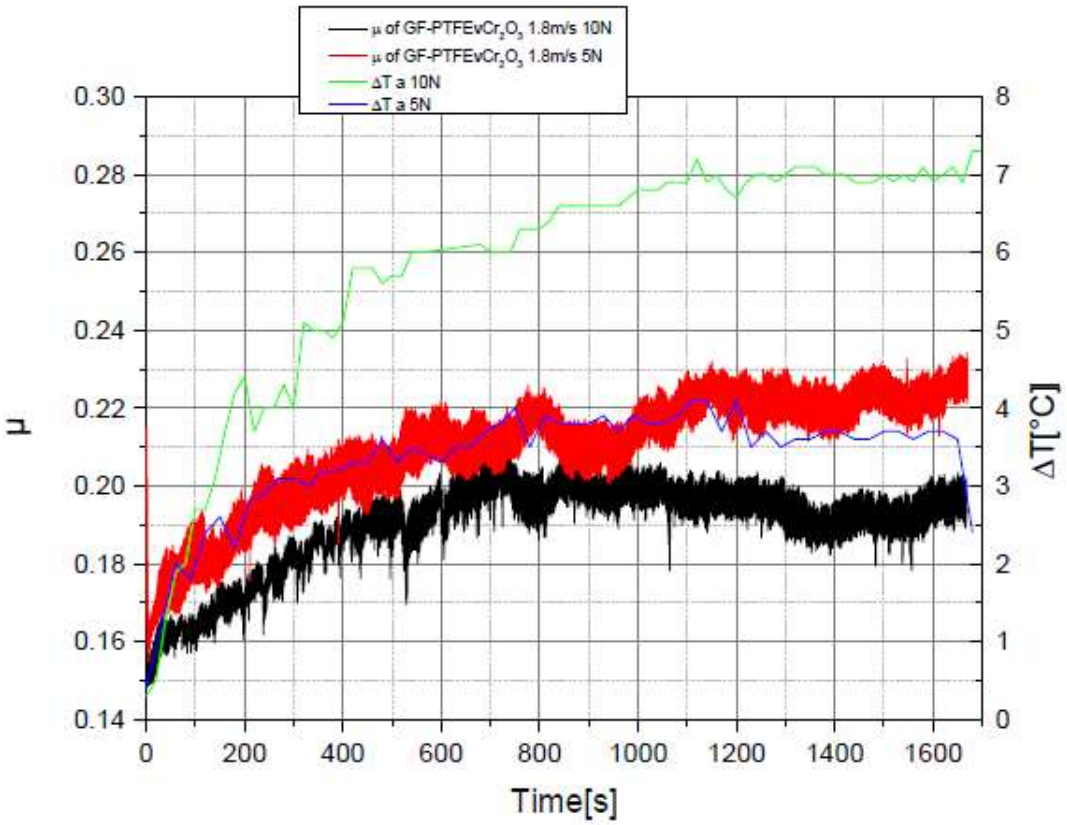

Figure 53: Friction coefficient and temperature raise curves of GF-PTFE against the Chromia coated surface at 1,8 m/s sliding speed and both load conditions (5N-10N)

The coefficient of friction of the pin tested at 10N load and 0,54 m/s sliding speed rapidly stabilizes at about 0,18 with a corresponding temperature increasing between 3°C and 4°C.

The pin tested at 5 N load, as in the previous case, has a value of the coefficient of friction fluctuating between 0.215 and 0.230; the temperature profile tends to stabilize already from 2000 s onwards.

From the comparison with the same tests against AISI304 surface it can be deduced that a strong reduction of the friction coefficient in the test with 10N load, determines a minor increasing of the temperature against Cr_2O_3 coated surface, although the latter acts as thermal insulator. At 5 N load, however, a lower reduction in the friction coefficient makes the effect of the low thermal conductivity of Cr_2O_3 coating sensitive, so that the temperature increasing of the pin is comparable.

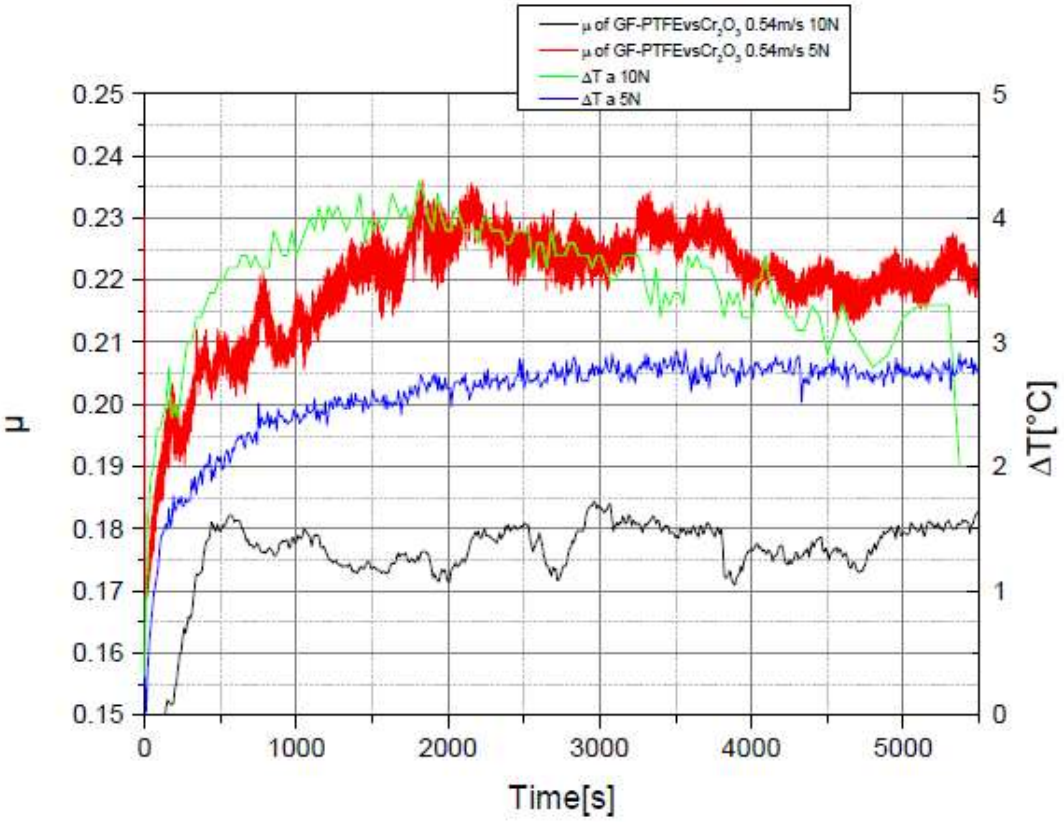

Figure 54: Friction coefficient and temperature raise curves of GF-PTFE against the Chromia coated surface at 0,54 m/s sliding speed and both load conditions (5N-10N).

Summarising, in Figure 55 are represented the average steady-state friction coefficient and maximum temperature rise in GF-PTFE pin on disc tests. Dots indicate theoretical bulk temperature rise calculated according to Ashby et al.'s model [25]

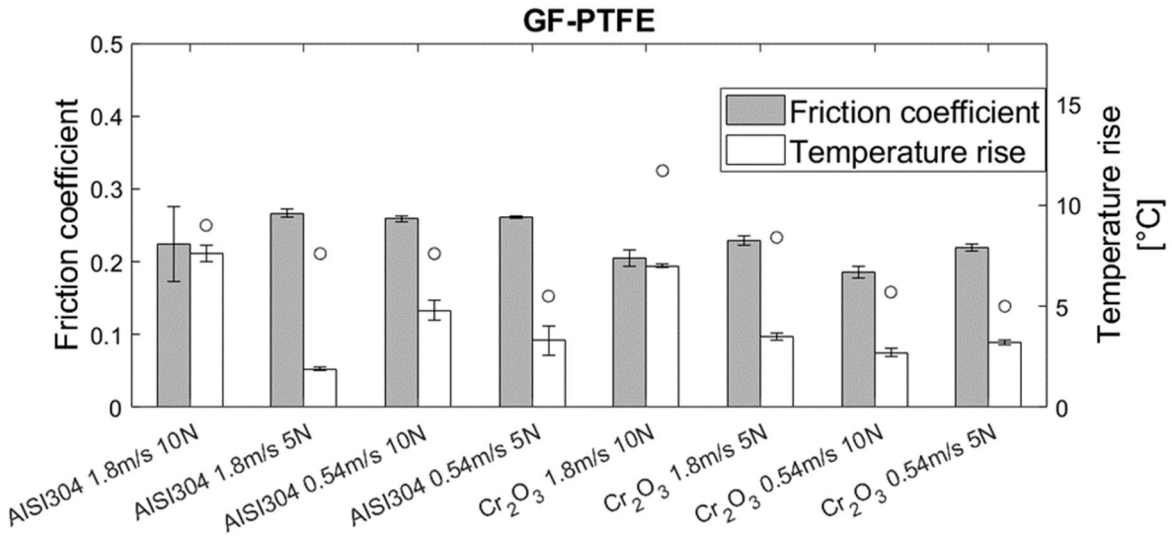

Figure 55: Average steady-state friction coefficient and maximum temperature rise in GF-PTFE pin on disc tests. Dots indicate theoretical bulk temperature rise calculated according to Ashby et al.'s model [25].

3.4.1.3 Analysis of the wear mechanism of GF-PTFE

GF-PTFE is characterized by a higher wear rate against AISI304 uncoated, compared to tests against Cr_2O_3 coated surface (Figure 56). The PTFE composite is particularly sensitive to the variation of the contact conditions (speed, load), when tested against AISI 304 uncoated surface, with specific wear rates higher as sliding speed and load increase.

The wear rate of GF-PTFE against the Cr_2O_3 coated surface is more stable and lower compared to the CF-PTFE wear rate (Section 3.4.2.3)

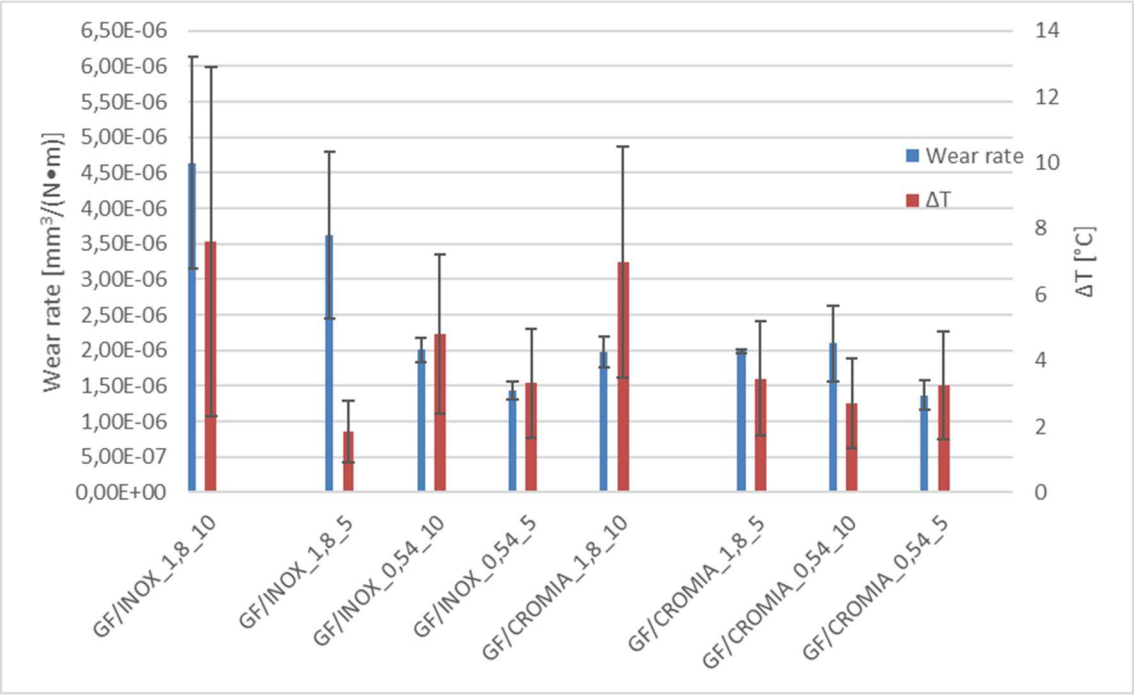

Figure 56: Wear rate and temperature rise of GF-PTFE

The GF-PTFE composites tend to develop a tribo-layer on their surface at the end of the sliding wear tests (Figure 57).

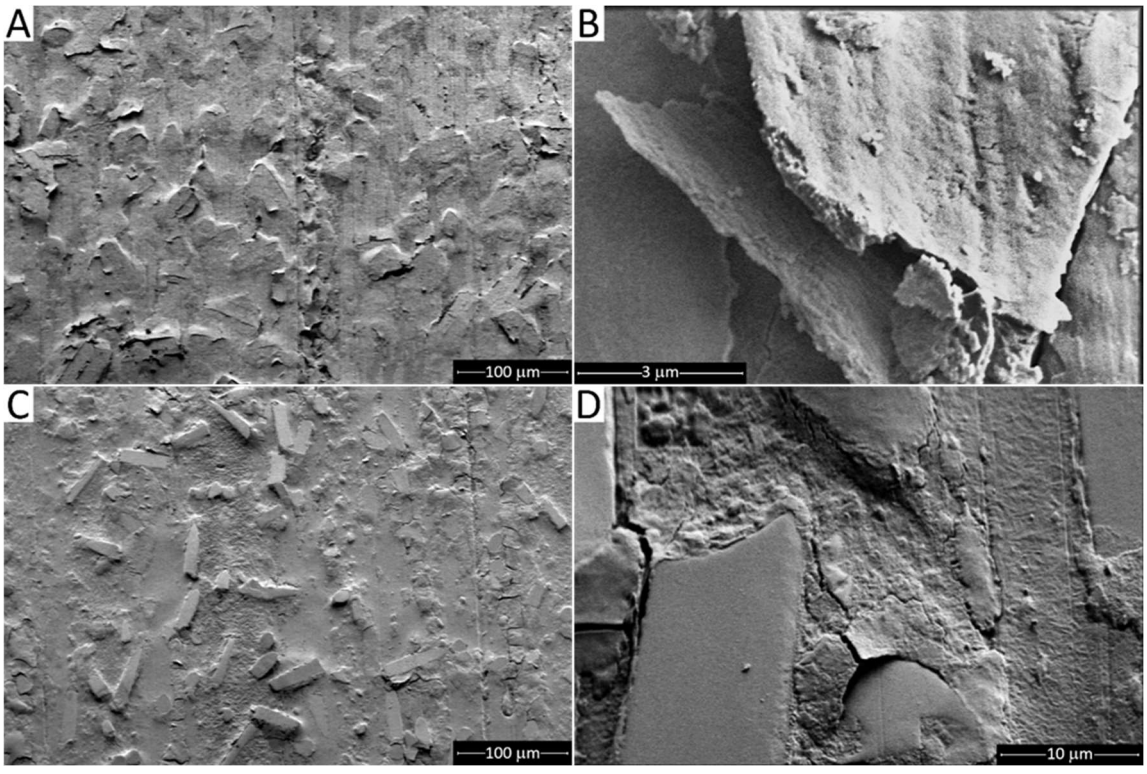

Figure 57: SEM micrographs of the worn surfaces of the GF-PTFE composite pin after ball-on-disc sliding wear tests against uncoated AISI 304 (A,B) and plasma sprayed Cr_2O_3 (C,D) at 10 N load, 1.8 m/s speed. Overviews (A,C) and details (B,D). Images are a mix of secondary and backscattered electron signals [63].

On the surface of the pins slid against uncoated AISI 304 (Figure 57A), in particular, the existence of the fibres is only inferred morphologically through the protrusions on the worn surface. By contrast, there is no meaningful difference in contrast levels between the protrusions and the surrounding matrix, despite the large difference in average atomic mass between silicate glass and PTFE. This means they are all covered by a compositionally uniform tribo-layer. When the samples are imaged at 3 kV accelerating voltage, indeed, the electron beam cannot cross through the tribo-layer that covers both fibres and matrix, although the layer sometimes looks less than 1 μm thick (Figure 57B). This is confirmed by cross-sectional views (Figure 58B), where the thickness of the tribo-layer can be seen to change from several micrometres at some locations to <1 μm at others (see the arrows on the right side).

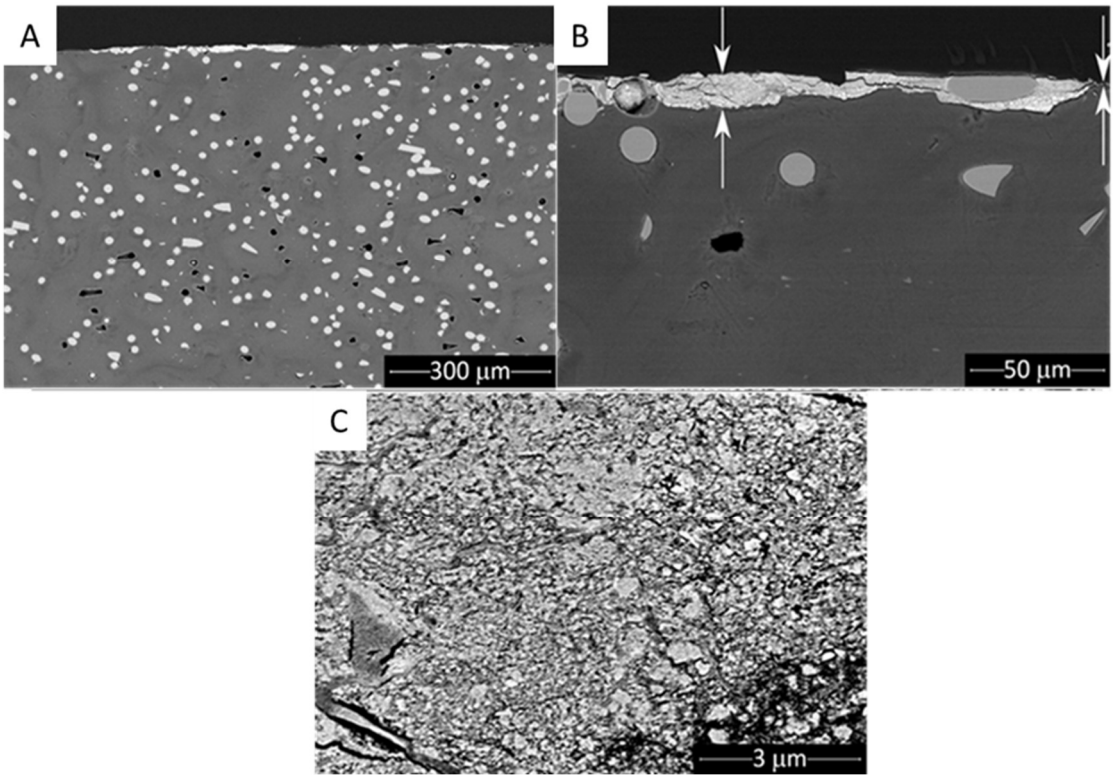

Figure 58: SEM micrographs showing the cross-sections of a GF-PTFE pin after pin-on-discs tests against uncoated AISI 304 at 10 N load, 1.8 m/s speed: overviews (A,), intermediate-magnification images showing the tribo-layer (B) and details of the same (C) when the white arrows indicate the tribo-layer [63].

The coverage of the worn surface by this tribo-layer is revealed even more distinctly by the detail of Figure 59A: there, a partially dislodged glass fibre is seen to be covered by the same tribo-layer that also appears on the surrounding matrix.

When viewed in greater detail, the tribo-layer appears to be made up by the compaction of fine, mostly sub-micrometric debris particles (Figure 58C). EDX spectra acquired at

12 kV acceleration voltage on both the surface (Figure 59C, spectra 1 and 2) and the cross-section (Figure 59D, spectra 1 and 2) of the tribo-layer show the simultaneous presence of elements originating from the matrix (C and F), the glass fibres (O, Si, Al, Ca) and, to a small but non-negligible extent, the steel counter-surface (Fe, Ni, Cr). This mean debris from all the elements of the tribo-system, including the uncoated stainless-steel disc, concur to the formation of the tribo-layer. On the surface, in particular, the same elements are present both on the protruding fibre (Figure 59C spectrum 1) and the surrounding matrix (Figure 59C, spectrum 2). The peaks of O, Si, Al and Ca grow a bit more intense when the EDX spectrum of the tribo-layer is acquired on top of a glass fibre (Figure 59C, spectrum 1), because at 12 kV voltage, the X-ray generation region does extend past the tribo-layer into the underlying fibre.

The tribo-layer tends to delaminate in the form of platelets (Figure 57 B), and cracks are accordingly seen running along its section, roughly parallel to the surface (Figure 58B, Figure 59B).

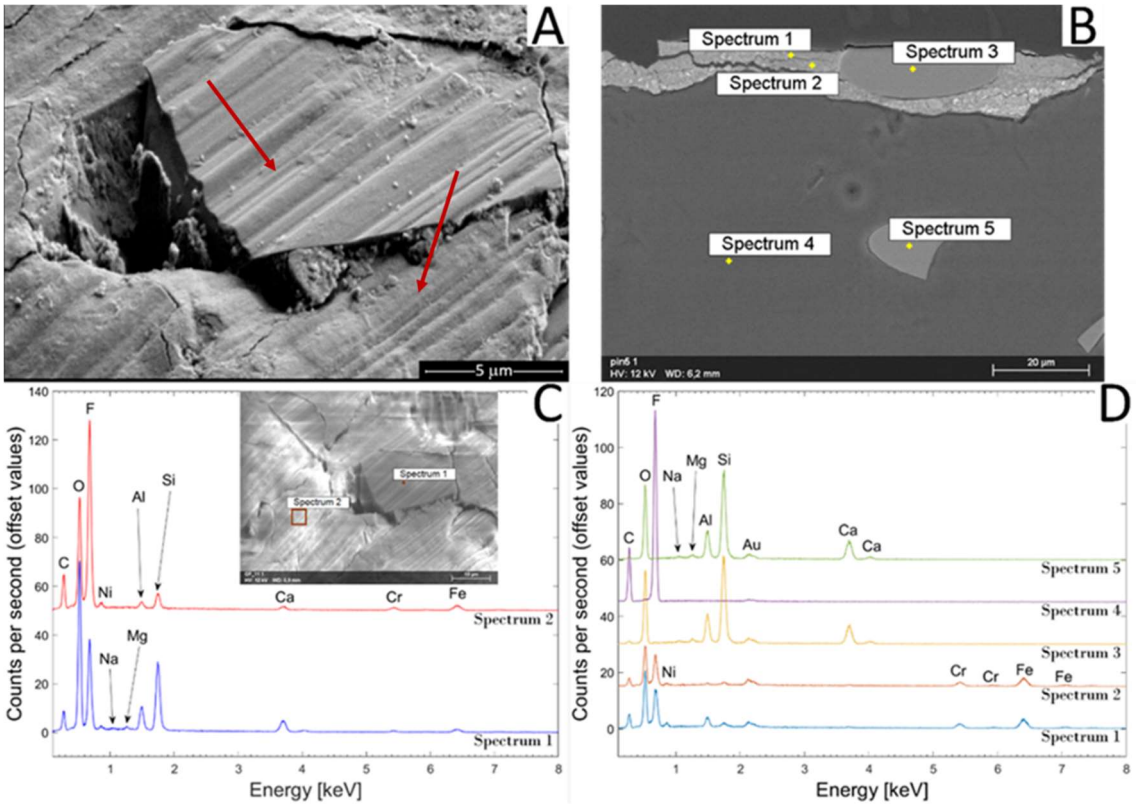

Figure 59: SEM micrographs showing a detail of the worn surface of a GF-PTFE pin after pin-on-disc sliding wear tests against uncoated AISI 304 at 10 N load, 0.54 m/s speed (A) and of the cross-section of an analogous pin after ball-on-disc sliding wear tests against uncoated AISI 304 at 10 N load, 1.8 m/s speed (B), and corresponding EDX spectra (C,D) [63].

The resulting platelet-like debris can be found among the loose debris particles (Figure 60A – label 1). A detailed view (Figure 60B) confirms that platelets consist of the same compacted, sub-micrometric particles seen in Figure 58C. Ribbons (Figure 60A– label 2) can also be identified in the debris.

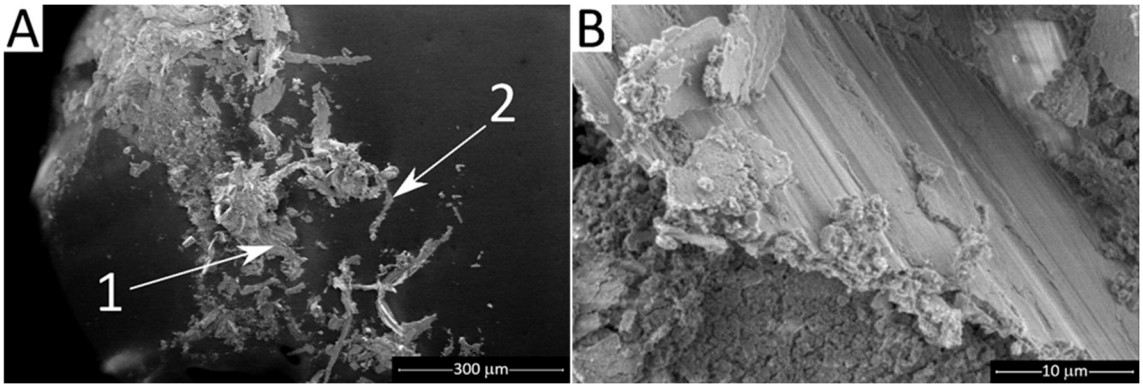

Figure 60: SEM micrograph showing loose debris collected after a pin--disc test of the GF-PTFE pin slid against uncoated AISI 304 at 10 N load, 1.8 m/s speed: overview (A) and detail (B). Labels: 1 = platelet-like debris, 2 = ribbon debris [63].

Despite its non-measurable wear loss, testified by the absence of a depression in the wear scar area (see the cross-section in Figure 61A), the uncoated AISI 304 counter-surface displays shallow grooves (Figure 61A, Figure 62A,C), consistent with the presence of (Fe,Ni,Cr)-based debris in the tribo-layer (Figure 59B).

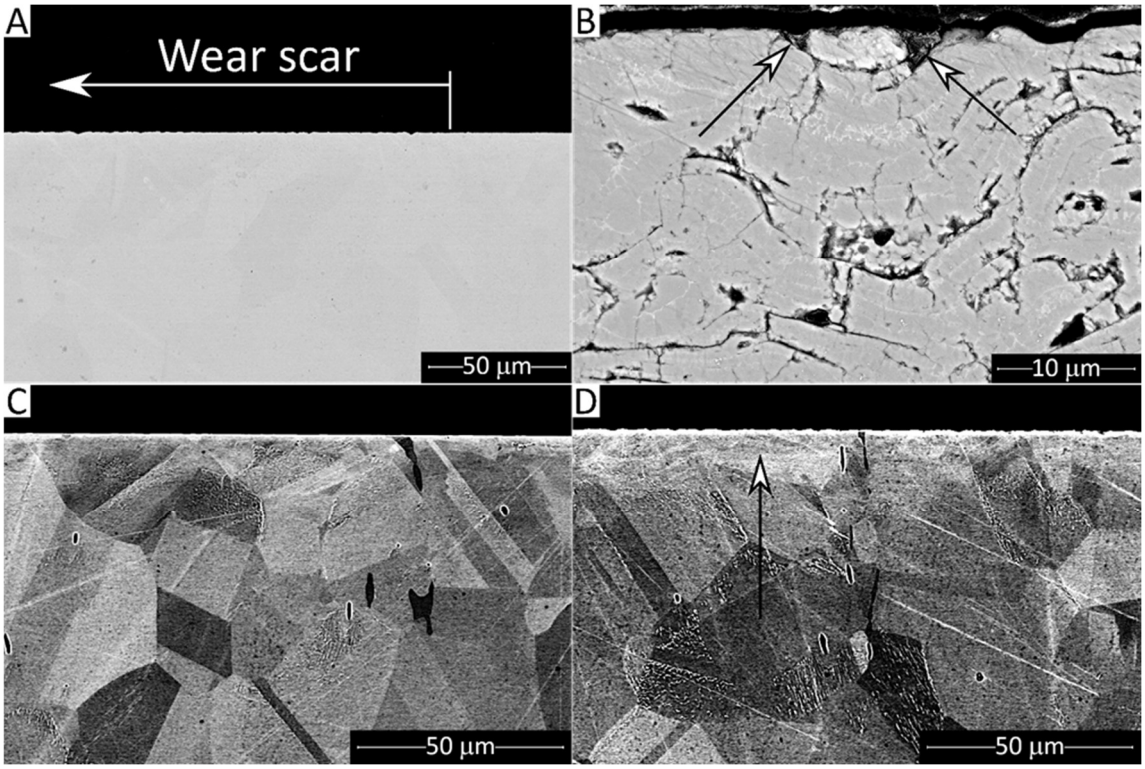

Figure 61: SEM micrographs of the cross-section of (A) the uncoated AISI 304 steel disc (test conditions: 10 N load, 0.54 m/s speed) and (B) the Cr2O3-coated disc (test conditions: 10 N load, 1.8 m/s speed), and channelling-contrast micrographs of (C) an unworn portion of the uncoated AISI 304 steel disc and (D) a worn portion of the same (test conditions: 10 N load, 1.8 m/s speed) [63].

Directly below the worn surface of the uncoated AISI 304 steel discs, channelling contrast micrographs reveal a micrometre-thin layer of plastically deformed material (comparing the unworn sample in Figure 61C and a worn sample in Figure 61D: the plastically deformed region is marked by an arrow).

When viewed in detail, the grooves on the worn disc surface retain some tribo-layer (Figure 62C).

When the GF-PTFE pins are slid against the Cr_2O_3-coated discs, the tribo-layer on the pin surface, though qualitatively similar, is less continuous (Figure 57C). The layer still consists of a compaction of sub-micrometric debris, but in some areas, uncovered fibres (Figure 57D) and uncovered PTFE matrix emerge. Moreover, EDX spectra (not shown here) reveal no Cr, i.e. there is no measurable fraction of debris coming from the disc. Indeed, the latter shows no wear at all (Figure 62B, D), except maybe for the pull-out of few splats. This is obviously consistent with its much higher hardness (Section 3.1).

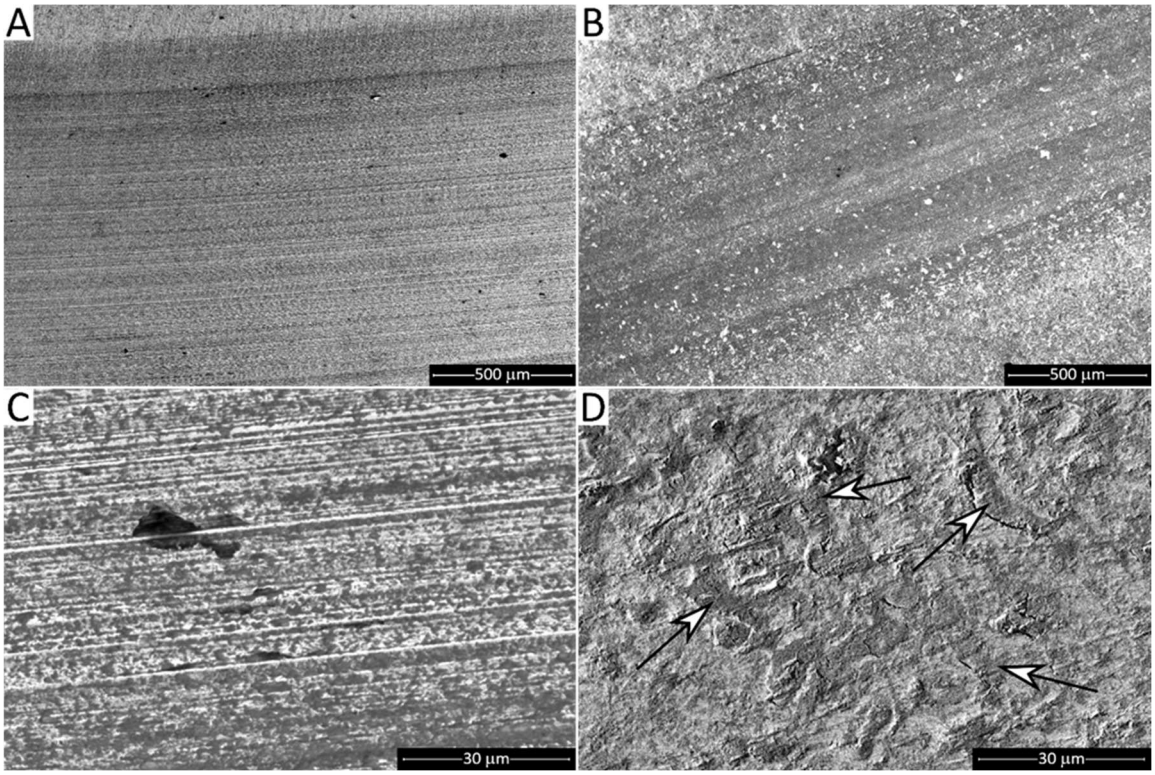

Figure 62: SEM micrographs of the worn surfaces of the uncoated AISI 304 steel disc (A: overview, C: detail) and Cr2O3-coated disc (B: overview, D: detail) after ball-on-disc sliding wear tests against GF-PTFE composite pins (10 N load, 1.8 m/s speed [63]).

By contrast, the many open pores appearing on the polished coating are almost entirely filled by transferred tribo-layer. At low magnification, indeed, the coating surface seems to be smoother inside the sliding trace than it is outside (Figure 62B). The regions with bright contrast outside the trace, which, in a secondary-electrons micrograph, reflect charge accumulation effects around the boundaries of open pores, tend to disappear where the pin was slid. Magnified views confirm that almost all the open pores and valleys are filled by transfer material having darker contrast, some of which is marked by arrows in Figure 62D. Open pores filled by transfer material can also be identified on the cross-section (Figure 61B: the arrows point to pits filled with dark-contrast debris from the pin). Its composition was verified by EDX analyses (not shown here). In even more detail, all pits and valleys existing on the polished Cr_2O_3 surface (Figure 63A), from the largest to the smallest ones, are filled with polymer-based debris after sliding against the GF-PTFE pins (Figure 63B: arrows). Accordingly, EDX signal from F is found in both large (Figure 63C,D: spectrum 1) and small (spectrum 2) valleys, whilst it is obviously not found on the smooth parts of the surface (spectrum 3). It means a large fraction of the overall contact surface on the disc consists of polymer-based transfer material.

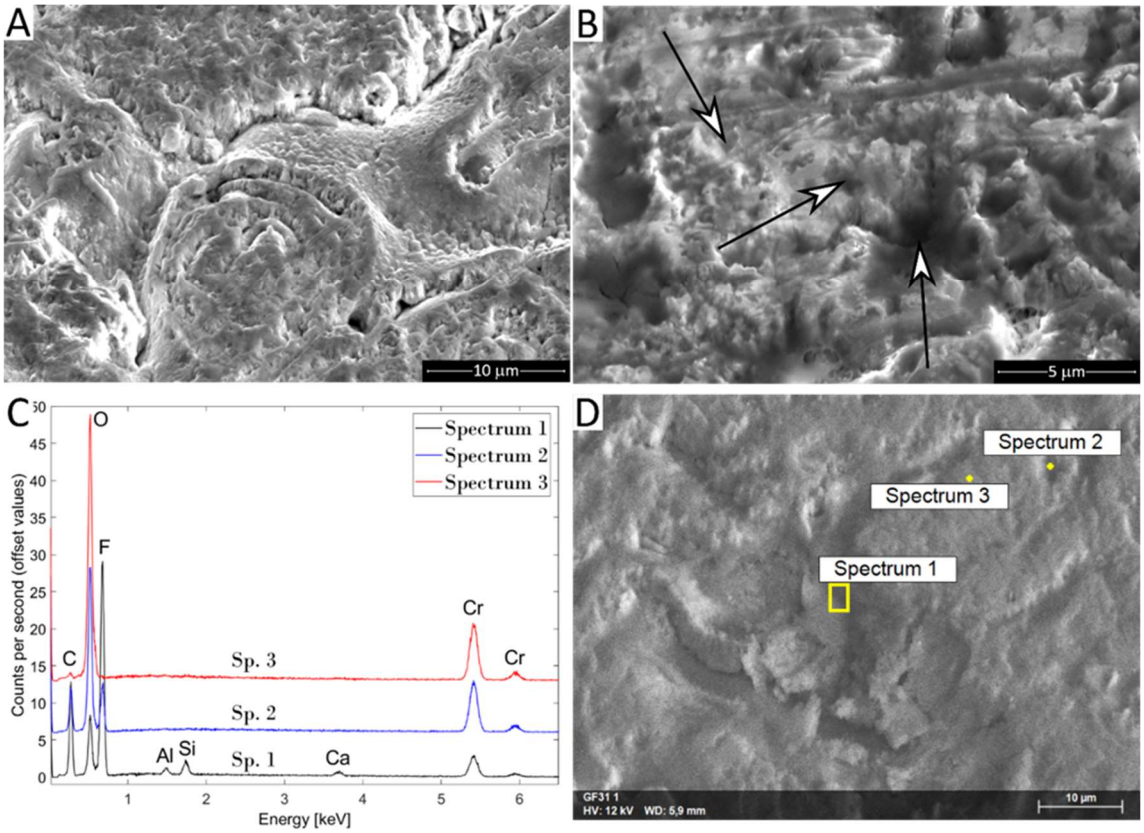

Figure 63: Magnified SEM views of the surface of Cr_2O_3 coating (A) in its pristine, polished condition and (B) after pin-om-disc sliding wear test against GF-PTFE at 10 N load, 1.8 m/s speed; EDX spectra (C) acquired on the surface of Cr_2O_3 coating after pin-on-disc sliding wear test against GF-PTFE at 5 N load, 0.54 m/s speed (D). Arrows in panel B mark debris filling the pores [63].

3.4.2 CF-PTFE

The results of pin-on-disc tribological tests on CF-PTFE composites are reported in this section. As above discussed for the GF-PTFE composites, further data and discussions on the wear mechanisms triggered between the pin and the counter-surface are detailed in [63].

3.4.2.1 CF-PTFE against AISI 304 surface

The evolution of the friction coefficient and the temperature variation of the tested material at 1,8 m/s and at both loading conditions is showed in Figure 64. In the first test the value of the friction coefficient varies between 0.28 and 0.32, thus assuming higher values than those of GF-PTFE under similar test conditions, together with an increasing of the temperature profile, up to 11 ° C, higher than the previous case.

There are two possible explanations for this difference:

- A higher value of the friction coefficient determines a more heat dissipation in the contact area.
- The increased thermal conductivity allows the CF-PTFE composite to remove the dissipated heat more effectively in the contact area; therefore, the "bulk" temperature of the pin increases more.

The coefficient of friction of the pin tested at 5N load initially stabilises at around 0,25 and then increases again towards the end of the test, until reaching a value close to 0,32.

This trend does not occur together with a linear increasing of the temperature, which stabilizes after 800 s, reaching values between 4°C and 5°C.

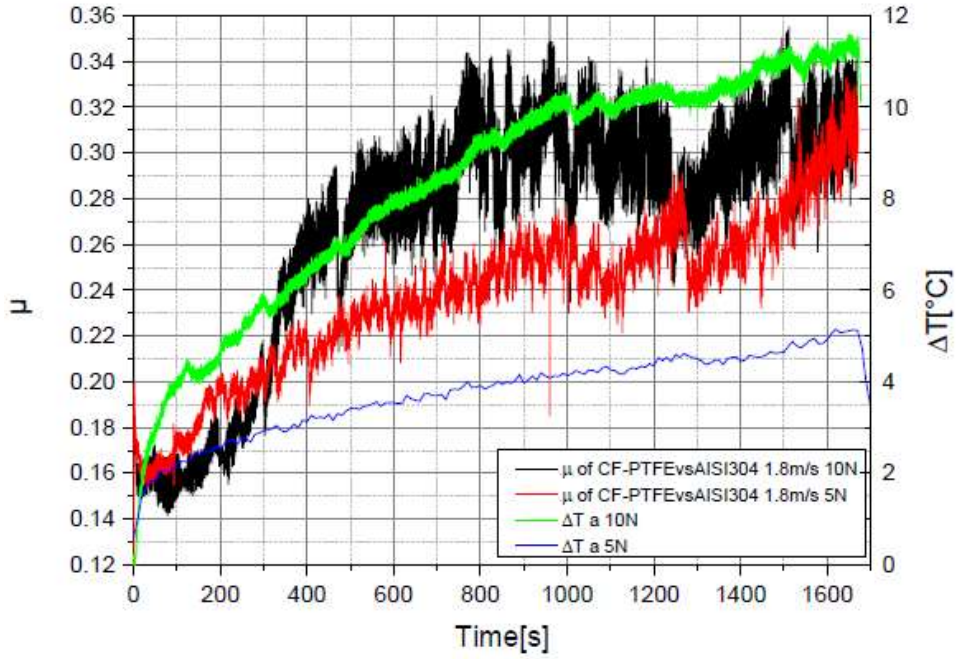

Figure 64: Friction coefficient and temperature rise curves of CF-PTFE against AISI 304 surface at 1,8 m/s sliding speed and both load conditions (5N-10N)

The trend of the friction coefficient of the pin tested at 10N and 0,54 m/s (Figure 65) is initially stable and then increases with thesliding distance; the temperature variation ΔT also shows the same trend. Differently, the pin tested at 0.54 m/s sliding speed and 5 N load, has a good stability of the coefficient of friction (with values between 0,33 and 0,36) and an increasing of the temperature, which after 2000 s stabilizes to a value of 3°C.

The temperature increases are higher than those observed for GF-PTFE pins under the same conditions, probably for reasons like those discussed above. InIn this case, too, in fact, the friction coefficients produced by CF-PTFE pins are higher than those produced by GF-PTFE pins under the same conditions.

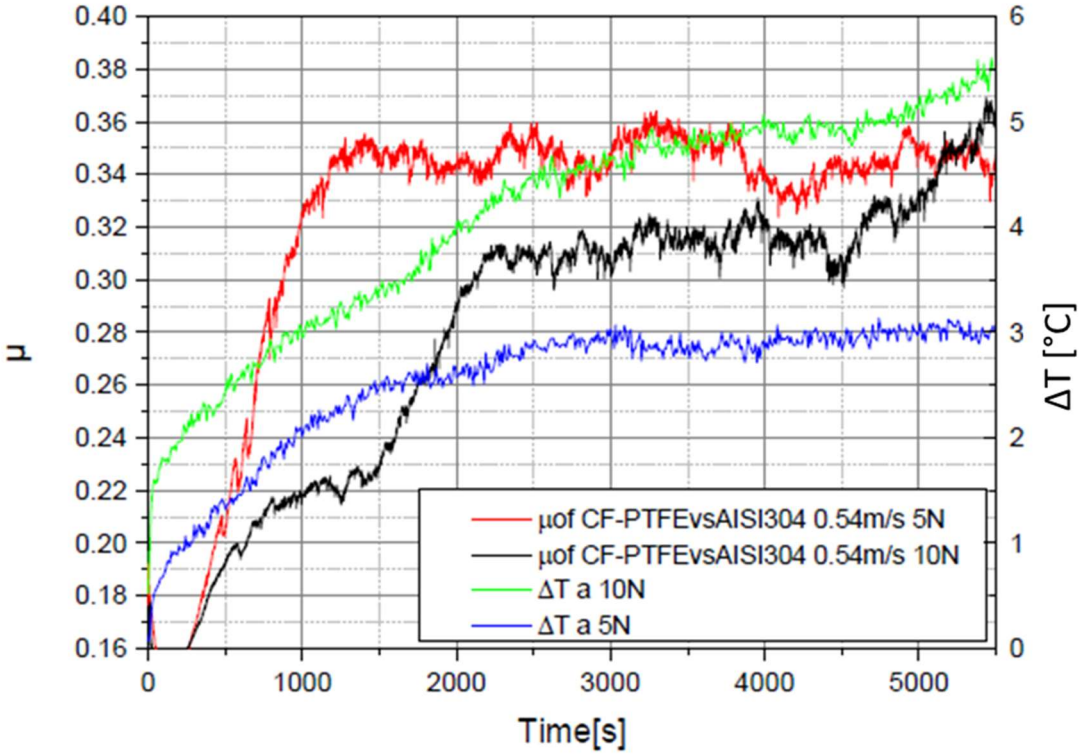

Figure 65: Friction coefficient and temperature rise curves of CF-PTFE against AISI 304 surface at 0,54 m/s sliding speed and both load conditions (5N-10N).

3.4.2.2 CF-PTFE against Cr_2O_3 Coated surface

The friction coefficient of CF-PTFE against the Cr_2O_3 coated surface (Figure 66) does not stabilize and is followed by a continuous temperature increasing. The maximum reached temperatures are higher than those produced by GF-PTFE pins under the same conditions.

CF-PTFE is a material with a higher thermal conductivity than GF-PTFE, so its most effective ability to remove heat from the contact area plays an important role in determining the overall temperature increase of the pin, which is greater than in the previous cases.

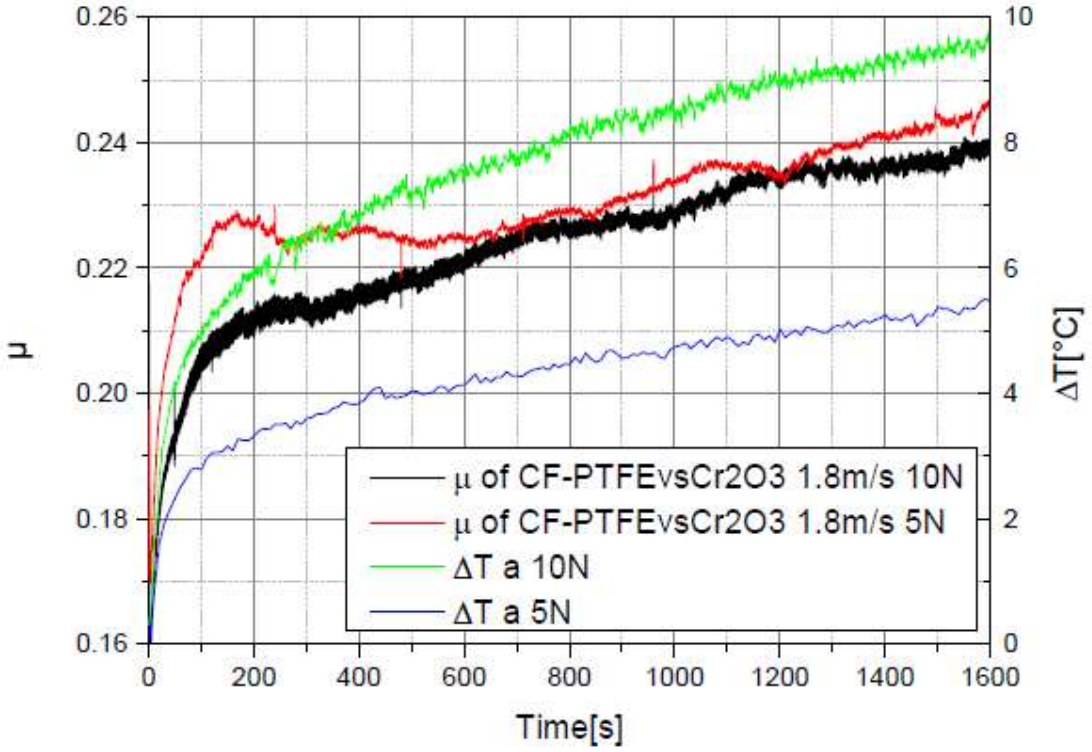

Figure 66: Friction coefficient and temperature rise curves of CF-PTFE against Cr_2O_3 coated surface at 1,8 m/s sliding speed and both load conditions (5N-10N).

The friction coefficient of the tested pin at 10 N load and 0,54 m/s of sliding speed (Figure 67) increases linearly up to a maximum value of 0,23; the temperature variation has about the same behaviour of the friction coefficient and stabilizes around 6°C from 4000 s onwards.

Differently, the trend of the friction coefficient of the pin tested at 5N load and 0,54 m/s is stable from 4000 s onwards, unlike the temperature variation ΔT that can be defined as stable already from 1000 s. The temperature increasing could be explained with the same considerations made previously regarding the behaviour of GF-PTFE under the same conditions.

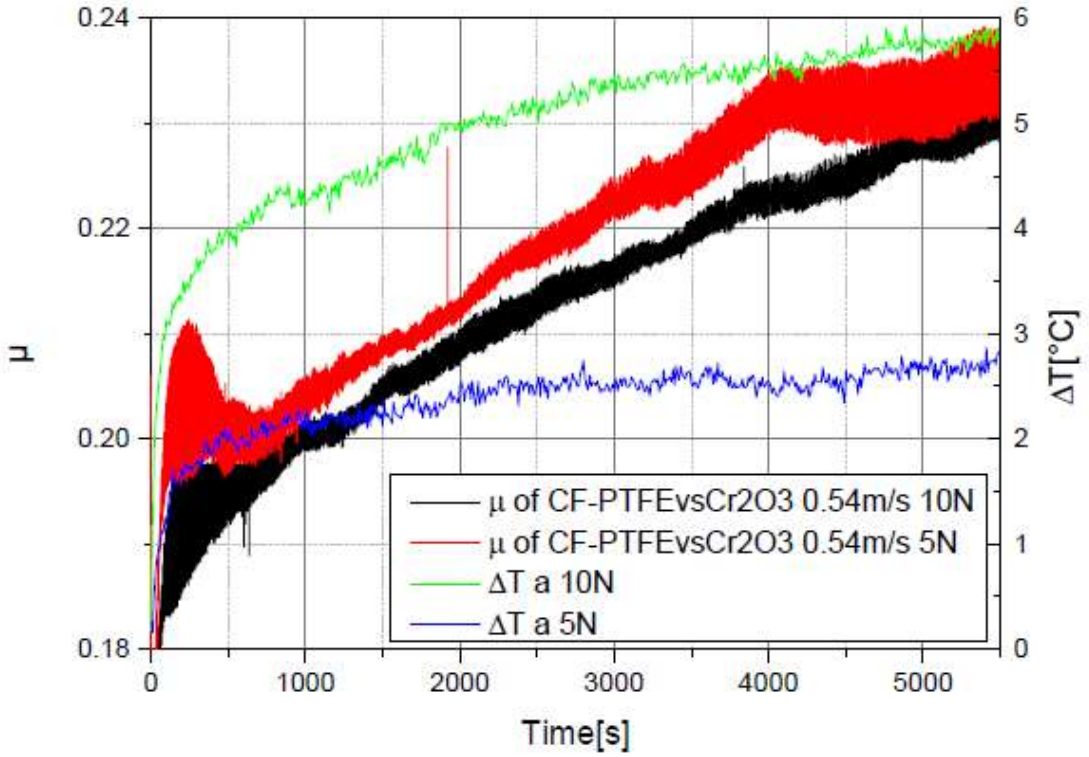

Figure 67: Friction coefficient and temperature rise curves of CF-PTFE against Cr_2O_3 coated surface at 0,54 m/s sliding speed and both load conditions (5N-10N).

Summarising in Figure 68 the average steady-state friction coefficient and maximum temperature rise in CF-PTFE pin on disc tests are represented. As in the previous case of GF-PTFE, dots indicate theoretical bulk temperature rise calculated according to Ashby et al.'s model.

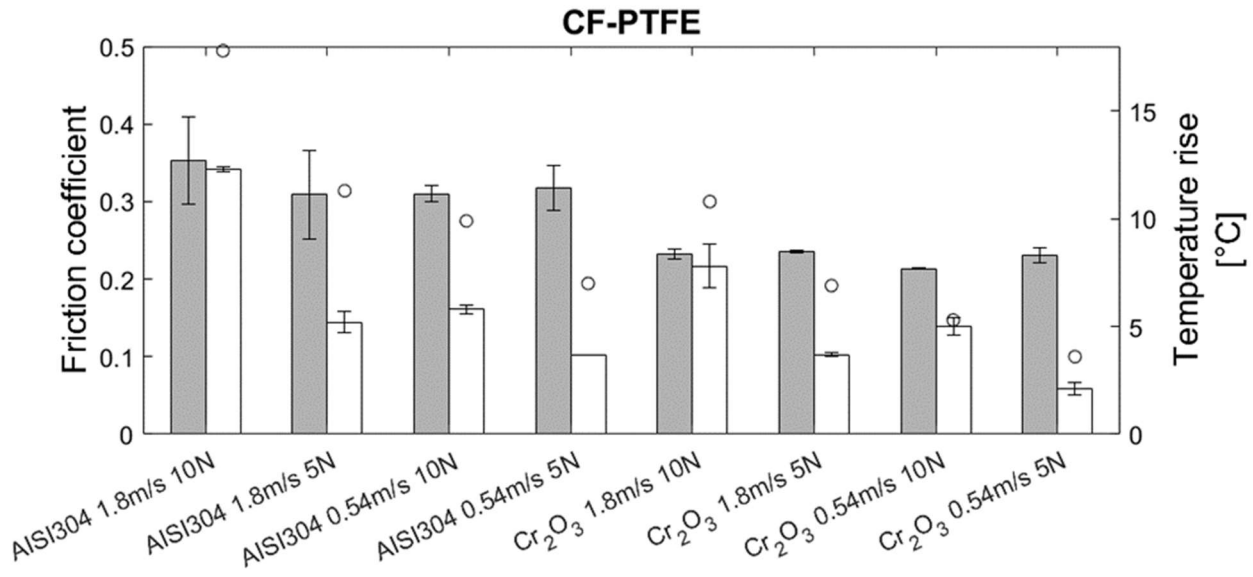

Figure 68: Average steady-state friction coefficient and maximum temperature rise in CF-PTFE pin on disc tests. Dots indicate theoretical bulk temperature rise calculated according to Ashby et al.'s model [25]

3.4.2.3 Analysis of the wear mechanism of CF-PTFE

The wear loss of the CF-PTFE composites (Figure 69) is lower than that of the GF-PTFE composites against uncoated AISI 304, whereas it is higher against Cr_2O_3-coated counterparts.

CF-PTFE composites, in fact, wear more when paired to Cr_2O_3-coated surfaces than they do against uncoated AISI 304, whereas GF-PTFE composites wear more when in contact with uncoated AISI 304 stainless steel surface, except under the mildest test conditions (0.54 m/s speed, 5 N load). The wear loss of CF-PTFE against uncoated steel is consistent with the literature, which reports [64, 65, 66, 67] specific wear rates roughly between 1×10^{-6} and 2×10^{-6} $mm^3/(N\cdot m)$ for CF-PTFE composites with 15 vol.% carbon fibres slid against metal surfaces.

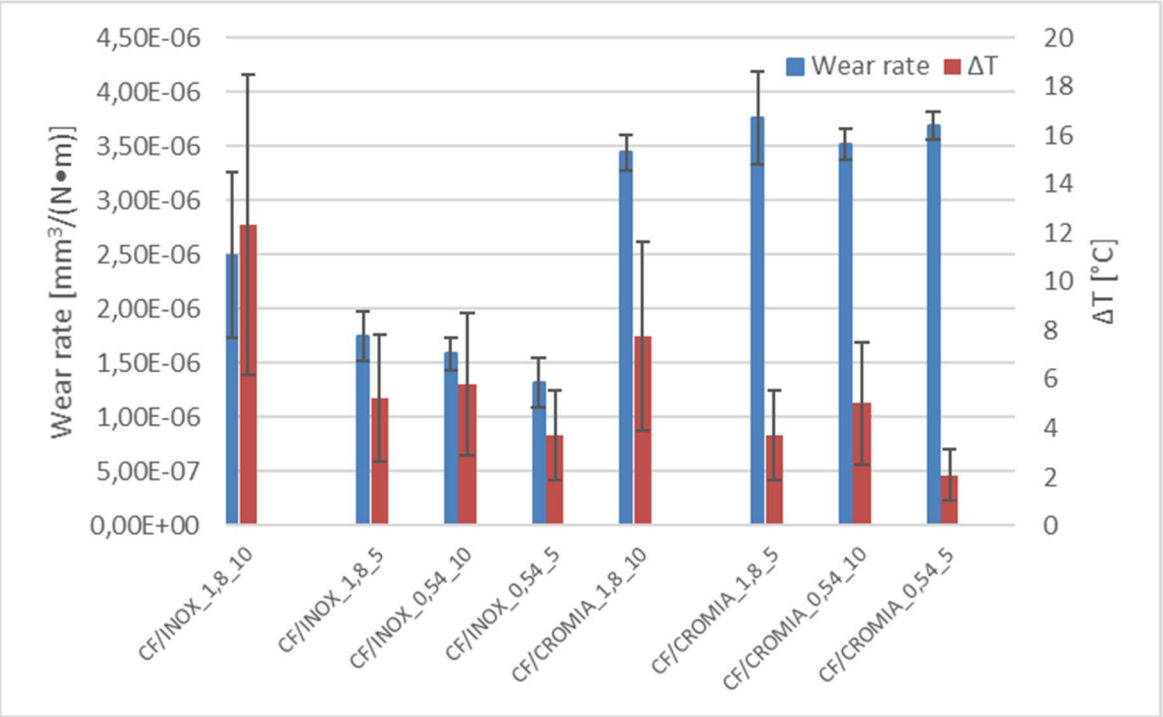

Figure 69: Wear rate and temperature rise of CF-PTFE.

The worn surfaces of CF-PTFE pins exhibit much fewer traces of a tribo-layer, if any. When slid against uncoated AISI 304 stainless steel (Figure 70A,B), some debris is built-up around the protruding fibres, whereas most of the surface is uncovered.

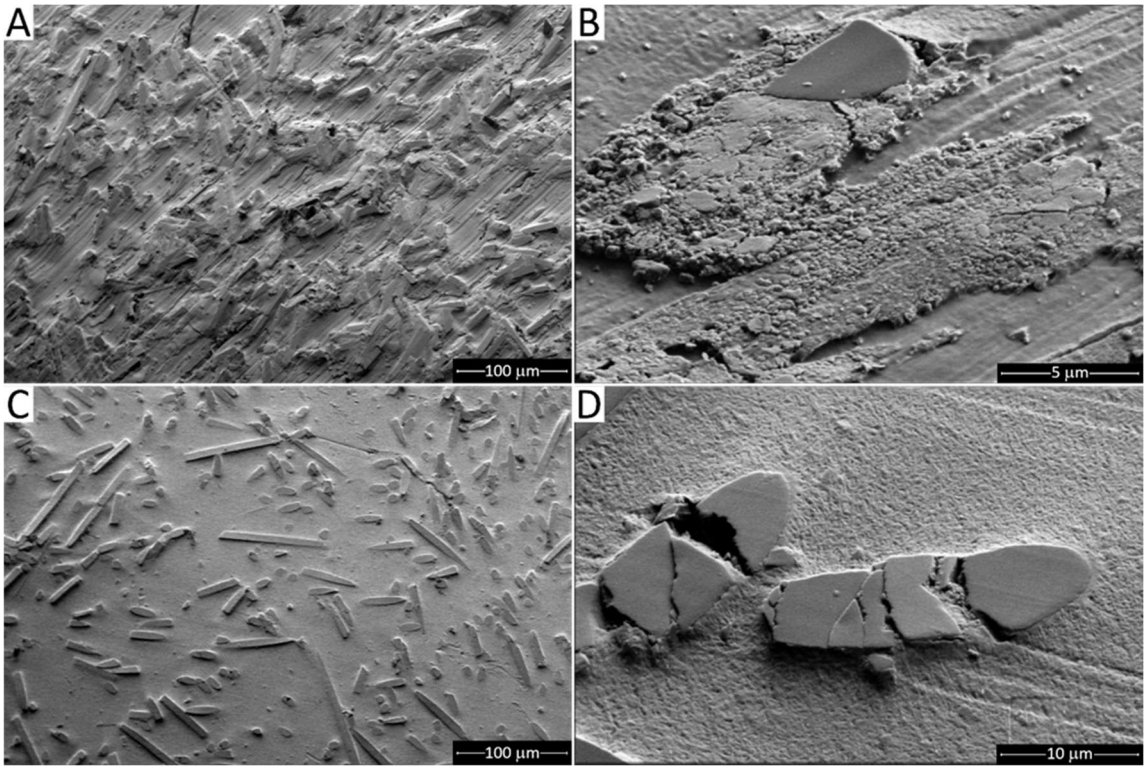

Figure 70: SEM micrographs of the worn surfaces of the CF-PTFE composite pin after pin-on-disc sliding wear tests against uncoated AISI 304 (A,B) at 5 N load, 1.8 m/s speed, and against plasma sprayed Cr2O3 (C,D) at 10 N load, 1.8 m/s speed. Overviews (A,C) and details (B,D). Images are a mix of secondary and backscattered electron signals [63].

This thin, irregular layer of debris retained between protruding fibres can also be seen on the polished section (Figure 71B, C: circle and arrow). Its bright contrast in backscattered electrons imaging mode indicates the presence of some debris from the stainless-steel counter-surface, which is also confirmed by EDX spectra (not shown here). These build-ups tend to be not as densely compacted as those seen previously in Figure 57 and Figure 59A: individual fine particles can still be identified (Figure 70B)and they are larger, blockier than the extremely fine ones making up the tribo-layer on GF-PTFE pins in Figure 57. When slid against the Cr_2O_3-coated surface, the tribo-layer is completely absent (Figure 70C, D).

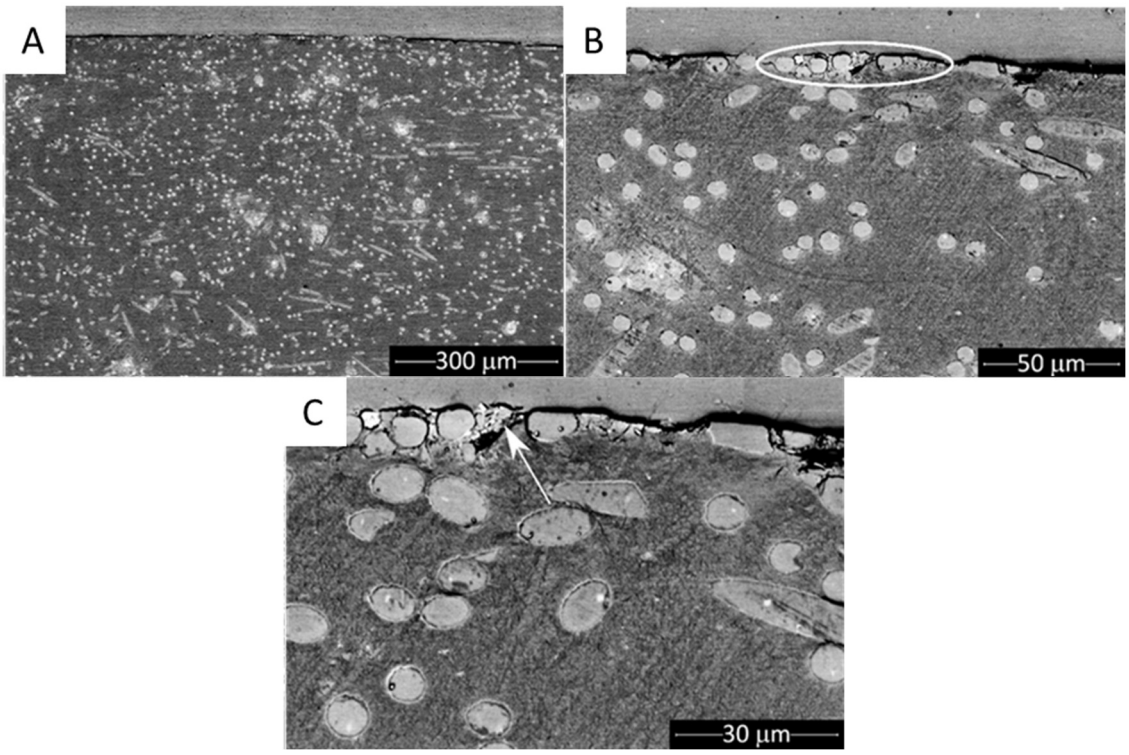

Figure 71: SEM micrographs showing the cross-sections of a CF-PTFE pin after pin-on-disc tests against uncoated AISI 304 at 10 N load, 1.8 m/s speed: overviews (A), intermediate-magnification images showing the tribo-layer (B) and details of the same (C). Arrows and circles in panels B and C indicate the tribo-layer [63].

The counter-surfaces also exhibit less transfer material, compared to the tests against the GF-PTFE composites. This is true both for uncoated AISI 304 (compare Figure 72B to Figure 62B) and for the Cr_2O_3-coated disc. In the latter case, the overview shows some empty pores in the wear trace, recognisable through their bright boundaries (Figure 72C). Detailed views confirm that some pores, including some of the large ones, are mostly empty (Figure 72D), though others are partly or entirely filled.

The loose debris does not contain platelet-like particles, but chunks of carbon fibres (Figure 73A), micrometric fragments broken from the same (Figure 73B), and fine particles probably coming from the PTFE matrix. All these constituents do not seem to be particularly well compacted.

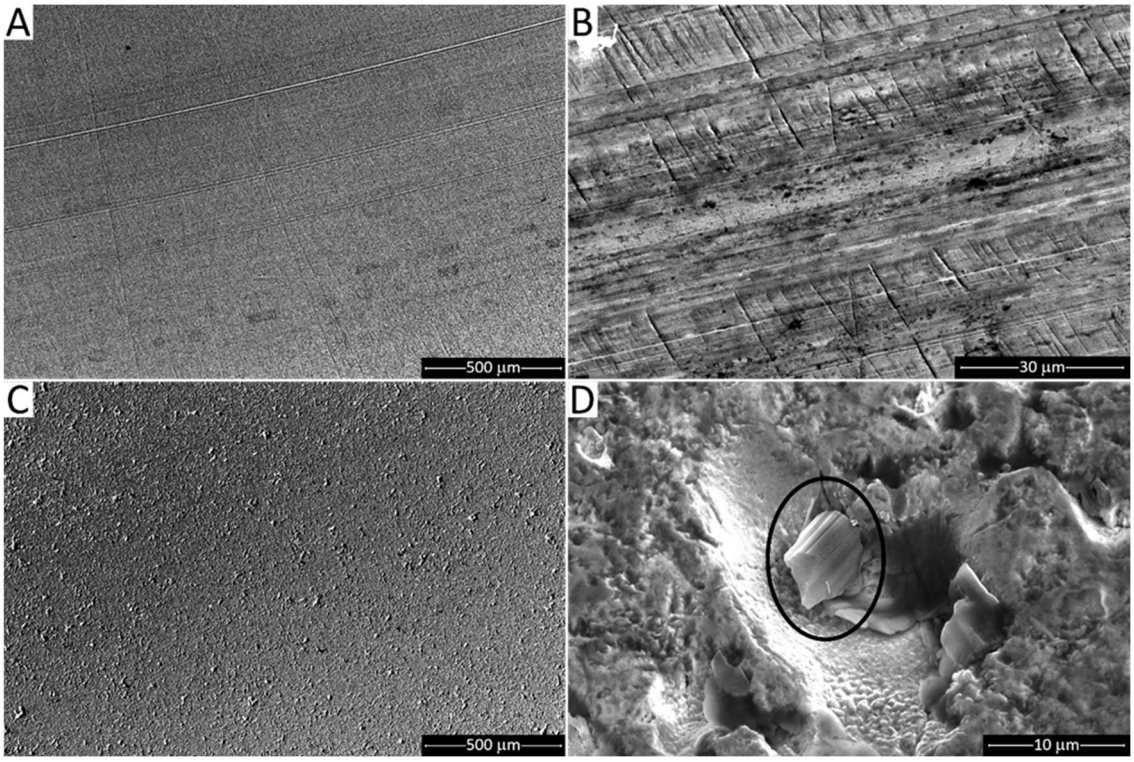

Figure 72: SEM micrographs of the worn surfaces of the uncoated AISI 304 steel disc (A,B) and Cr_2O_3-coated disc (C,D) after pin-on-disc sliding wear tests against CF-PTFE composite pins at 10 N load, 1.8 m/s speed. Overviews (A,C) and details (B,D). The circle indicates a broken fragment of a carbon fibre [63].

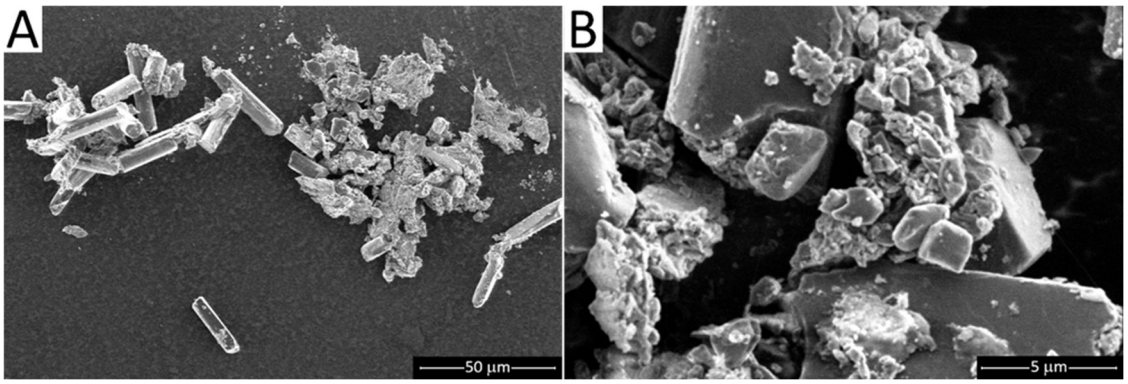

Figure 73: SEM micrograph showing loose debris collected after a pin-on-disc test of the CF-PTFE pin slid against a Cr_2O_3-coated disc at 10 N load, 1.8 m/s speed: overview (A) and detail (B) [63].

3.4.3 Sintek BRL

3.4.3.1 Sintek BRL against AISI 304

The evolution of the friction coefficient and the temperature variation of the tested material at 1.8 m/s and at both loading conditions is shown in Figure 74. In tests both at 5 N and 10 N load, the value of the friction coefficient has a maximum of 0.32, which is maintained longer at higher load, then it starts decreasing to 0.2, a steady-state value which is maintained to the end of the test in both cases. The maximum temperature increase with a load of 5 N is 4 °C, whilst a temperature rise of 11°C is measured at 10 N load. The last section of the temperature curve at 5 N load shows a decreasing trend because the thermographic camera continued to measure the temperature even after the test was finished.

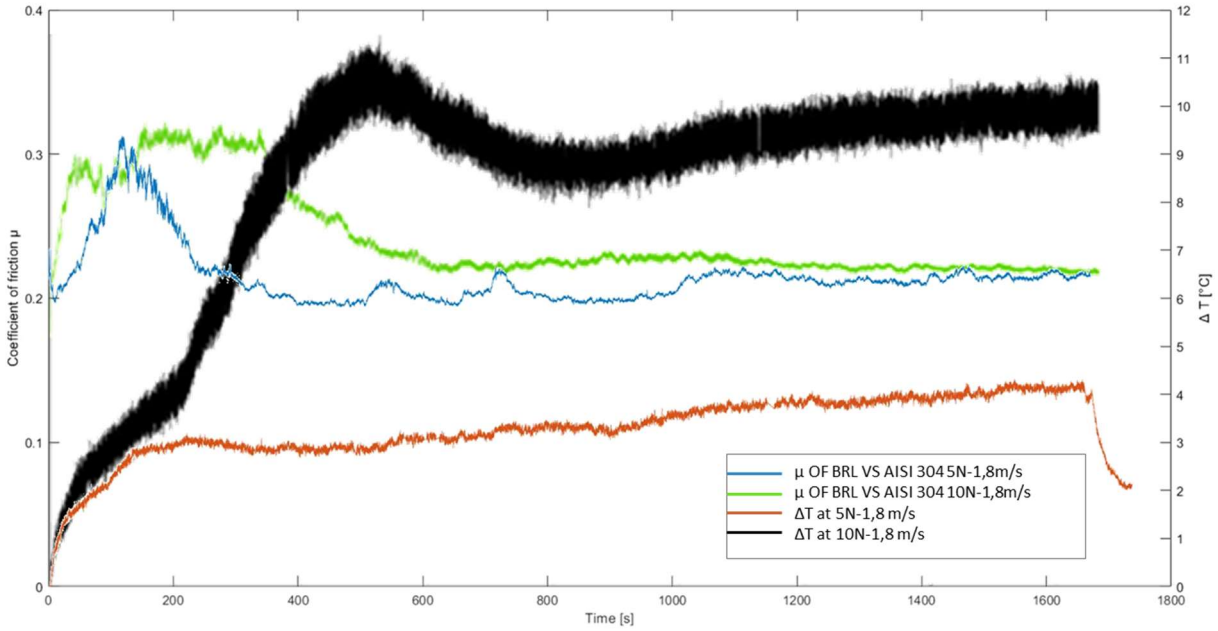

Figure 74: Friction coefficient and temperature rise curves of Sintek BRL against AISI 304 surface at 1.8 m/s sliding speed and both load conditions (5 N-10 N).

At 0.54 m/s sliding speed (Figure 75) the value of the friction coefficient always varies between 0.2 and 0.32, and the maximum temperature rise is 3.5 °C.

The decreasing temperature rise with decreasing load and speed is an expected outcome, since the power dissipated through friction is a linear function of both speed and normal load. Hence, with nearly constant friction coefficient values (as seen from the largely identical steady-state values of approximately 0.2), the temperature rise should change linearly with both parameters. According to Asbhy et al.'s model [25], for example, the

bulk temperature rise on the contact surface can be estimated as $\Delta T = \frac{\mu F_N v}{A_n} \cdot \left(\frac{1}{R_1} + \frac{1}{R_2}\right)^{-1}$, where R_1 and R_2 are the thermal resistances associated to the pin and the disc (dependent on their thermal conductivity and characteristic dimensions) and A_n is the nominal contact area (coinciding with the area of the worn surface of the pin). The only potential source of non-linearity in the dependence of ΔT on F_N and v is the varying value of A_n as a function of the wear loss. In fact, even assuming that Archard's wear equation is applicable (i.e. volume loss is proportional to applied load), the worn surface area (i.e. the area of the base of a spherical cap) does not vary linearly with the wear volume (i.e. the volume of a spherical cap) because of the spherical geometry of the pin.

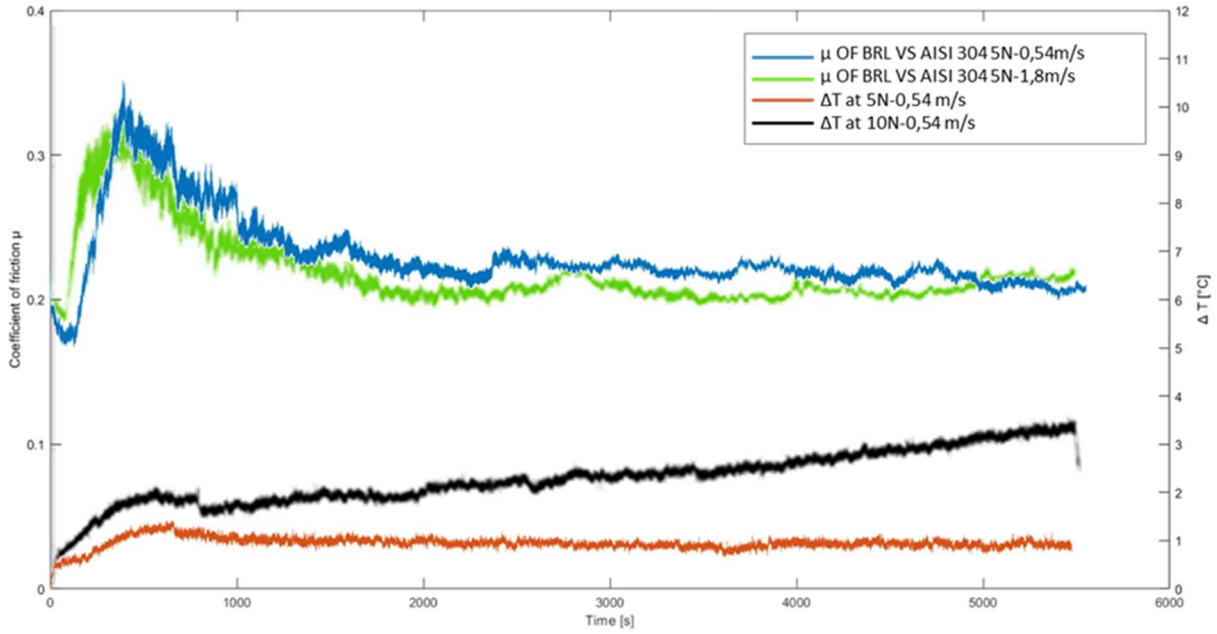

Figure 75: Friction coefficient and temperature rise curves of Sintek BRL against AISI 304 surface at 1.8 m/s sliding speed and both load conditions (5 N-10 N).

3.4.3.2 Sintek BRL against Chromia

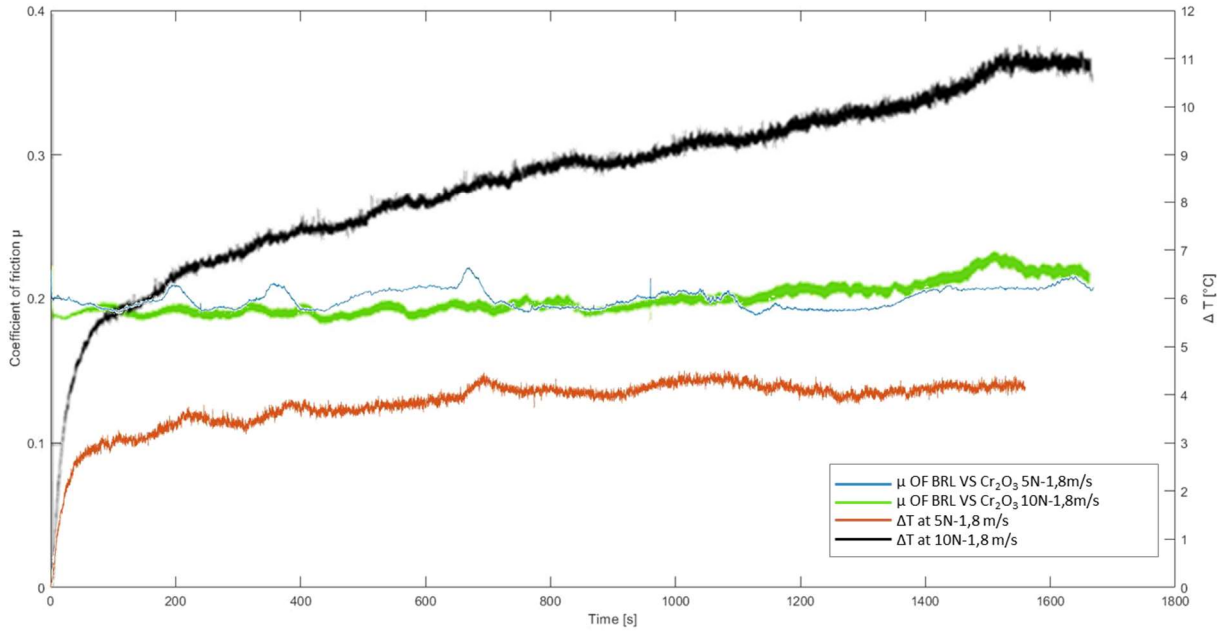

Figure 76: Friction coefficient and temperature rise curves of Sintek BRL against Chromia coated surface at 1.8 m/s sliding speed and both load conditions (5 N-10 N).

The trend of friction coefficient of Sintek BRL against the Chromia coated surface at 1.8 m/s (Figure 77is more stable than against the uncoated surface; its value is about 0.2 in both load conditions, and it is attained almost from the very beginning of the test, without an initial peak value. At 10 N load, the temperature increases linearly with the sliding distance until it stabilises almost at the end of the test around 11°C. Instead at 5 N load, the temperature has an increasing trend up to 400 s and then it is kept stable to little more than 4 °C. Because the steady-state friction coefficient against Chromia is approximately the same as it is against steel, it is reasonable to find fully comparable levels of temperature rise. This also means that the lower thermal conductivity of chromia compared to stainless steel has little influence on the bulk temperature rise. Perhaps, the difference between the thermal properties of the surface of both discs is lessened as a rather thick transfer layer, which is probably a thermal insulator, is built up especially on stainless steel, as will be shown later in Section 3.4.3.3.

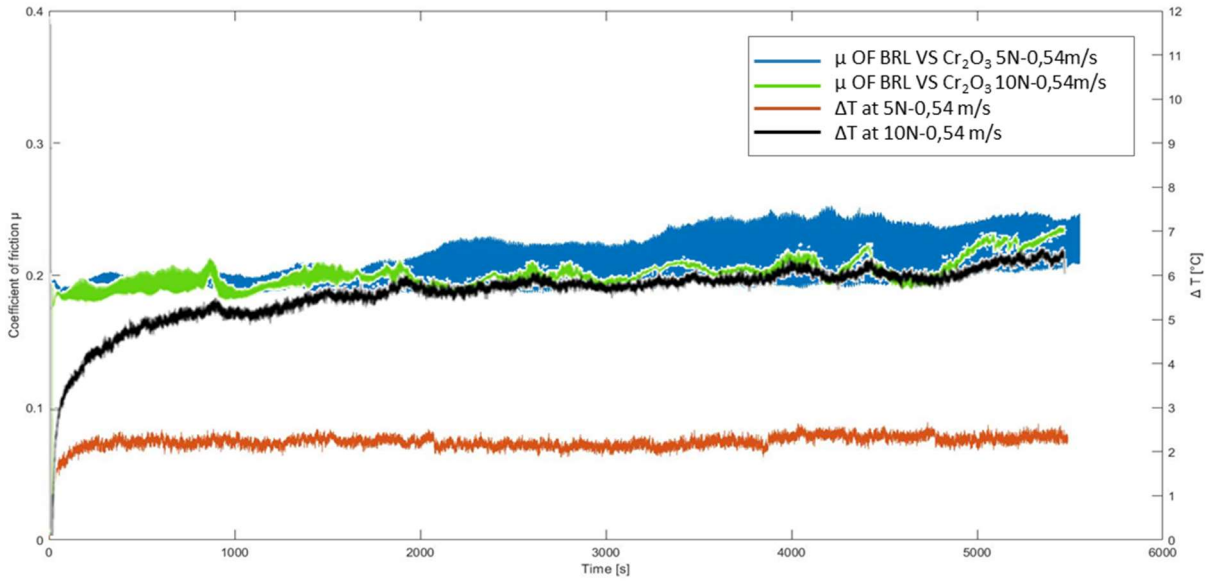

Figure 77: Friction coefficient and temperature rise curves of Sintek BRL against Chromia coated surface at 0.54 m/s sliding speed and both load conditions (5 N-10 N).

Figure 77 shows that at 10 N load, the temperature increases linearly with the sliding distance until it stabilises at 2000 s around 11°C. Instead at 5 N load, the temperature stabilizes from the first moments of the test around 2.5 ºC.

Again, these results are consistent with the approximately linear relation expected between bulk temperature rise, applied load and speed, given that the friction coefficient value never changes much.

Figure 78 summarises the average steady-state friction coefficient and maximum temperature rise recorded in the pin on disc tests with Sintek BRL. The figure confirms that the eventual steady-state friction coefficient is substantially independent of test conditions and counterpart material, as it settles at 0.21 – 0.22 in all cases. As in the previous cases ,dots indicate theoretical bulk temperature rise calculated according to Ashby et al.'s model [25]. In general, the model agrees quite well with the measured values, the differences being of 2 °C – 3 °C at the most. In particular, the model corroborates captures the decreasing trend of temperature with decreasing load and speed.

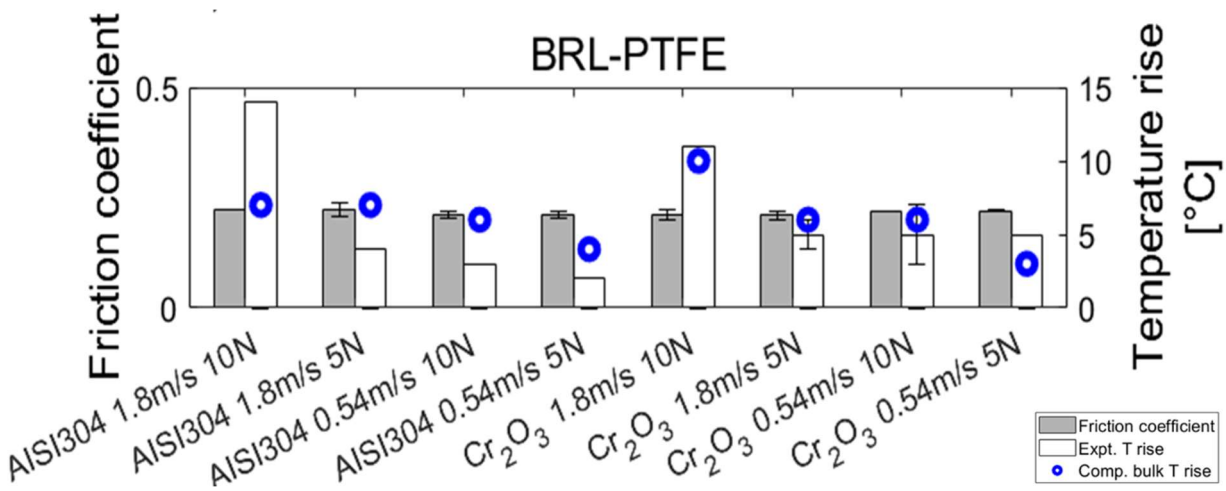

Figure 78: Average steady-state friction coefficient and maximum temperature rise in Sintek BRL pin on disc tests.

3.4.3.3 Wear mechanism of Sintek BRL

The maximum value of the specific wear rate of Sintek BRL against unclated stainless steel occurs in conditions of 10 N load and 1.8 m/s sliding speed: high-speed tests show that the wear rate against uncoated stainless steel depends strongly on the applied load; in fact, by varying the load from 5 N to 10 N the wear rate increases by a factor of 3 (Figure 79).

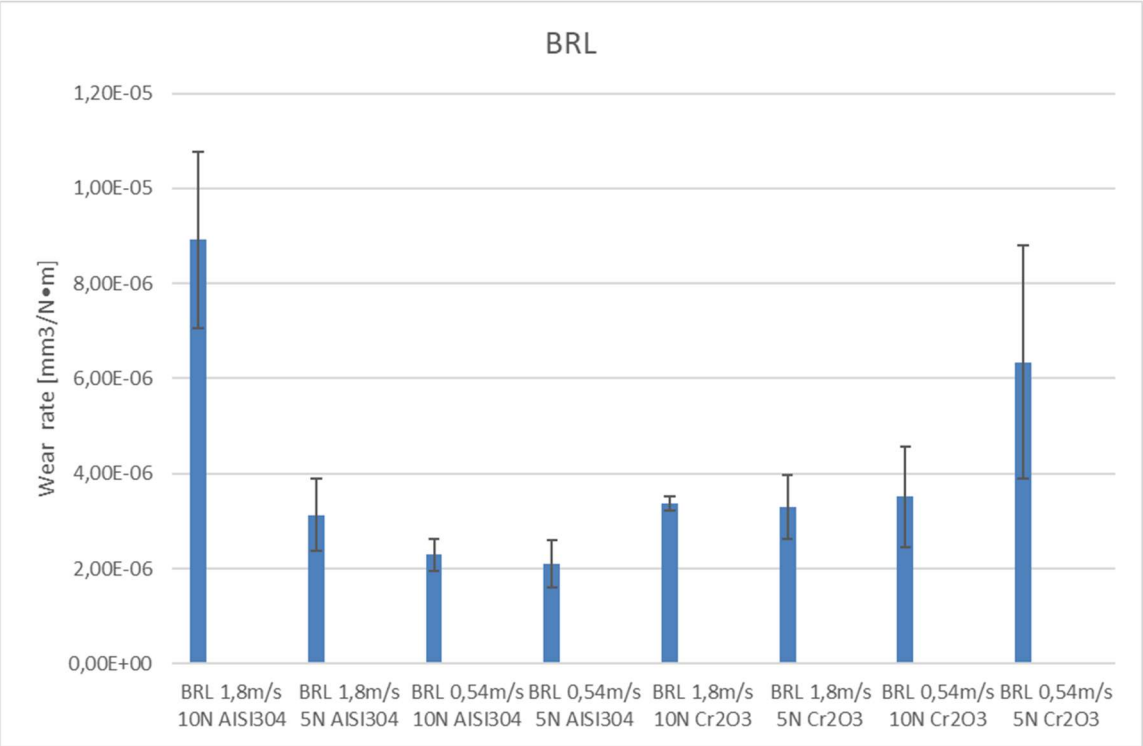

Figure 79: Wear rate of Sintek BRL against AISI 304 and Chromia coated surfaces in different operating conditions.

The load dependence is lower in the case of tests performed against uncoated stainless steel at 5 N load, a sign that the synergic effect of the load and speed leads, under extreme conditions, to the passing of a critical threshold.

By contrast, the wear rate of Sintek BRL against the Chromia coated surface is less dependent on test conditions and it is even higher in conditions of 5 N load and 0.54 m/s sliding speed. In general, the wear loss is greater when the material is in dynamic contact with the Chromia coated surface, except for the condition of highest load and speed.

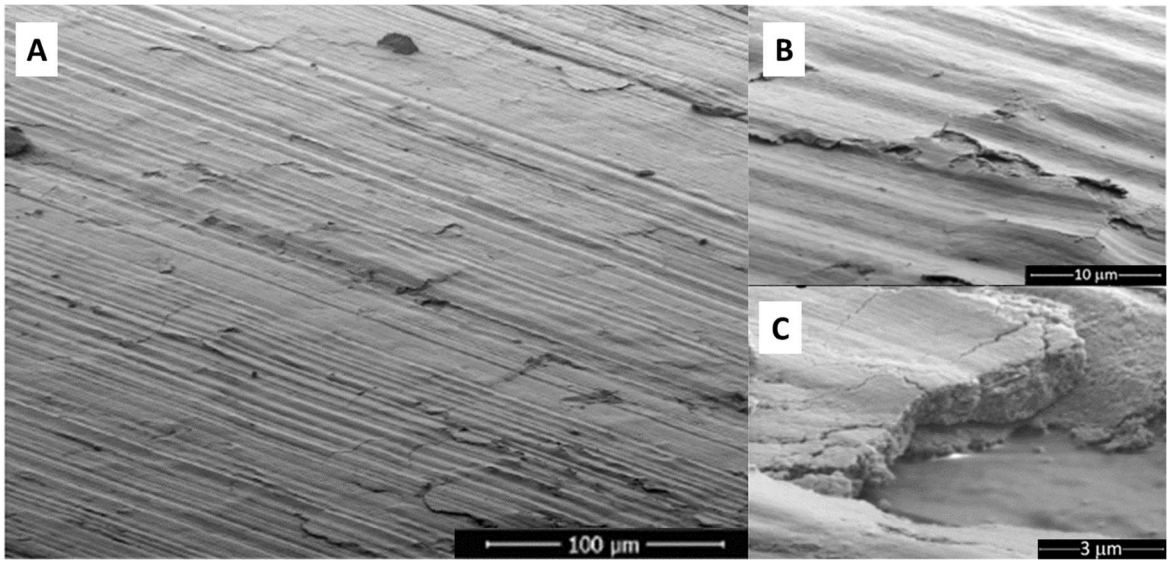

Figure 80: SEM micrographs of the Sintek BRL pin after sliding against the AISI 304 surface at 10 N load and 1.8 m/s sliding speed at low magnification (A), high magnification (B-C).

The worn surface of the pin aftter sliding against the stainless steel counterpart is macroscopically quite planar and uniform (Figure 80A) but, in detail, it has several microcracks and signs of delamination (Figure 80B). At even higher magnification (Figure 80C) the worn surface appears to be a continuous layer of fine compacted wear debris. Longitudinal grooves in the sliding direction appear on this compacted layer.

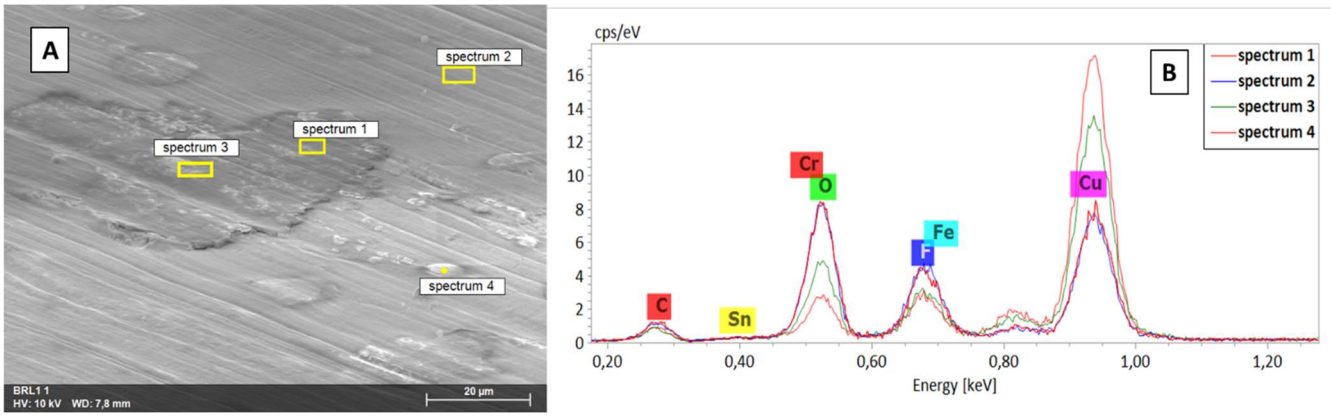

Figure 81: SEM micrographs of Sintek BRL pin after sliding against the AISI 304 surface at 10 N load and 1.8 m/s sliding speed (A) and EDX spectra acquired on the pin surface (B).

EDX spectra acquired at 10 kV on the worn pin surface (Figure 81, points 1 and 2) revealed the formation of the transfer-film, as there are both elements deriving from the pin (such as Cu, Sn, F) and from the disc (as evidenced by the peaks of Fe and Cr).

EDX spectra acquired in the lighter areas (Figure 81, points 3 and 4) show a more intense Cu peak, indicating that those areas are probably the bronze lamellae. In particular, since these brighter areas were not visible in the images acquired at 3 kV (Figure 80) but appeared in the micrographs acquired at 12 kV (Figure 81), it is clear that even the particles are covered by the transfer-film layer, which can be partly penetrated by the electron beam when it is accelerated at 12 kV but not at 3 kV.

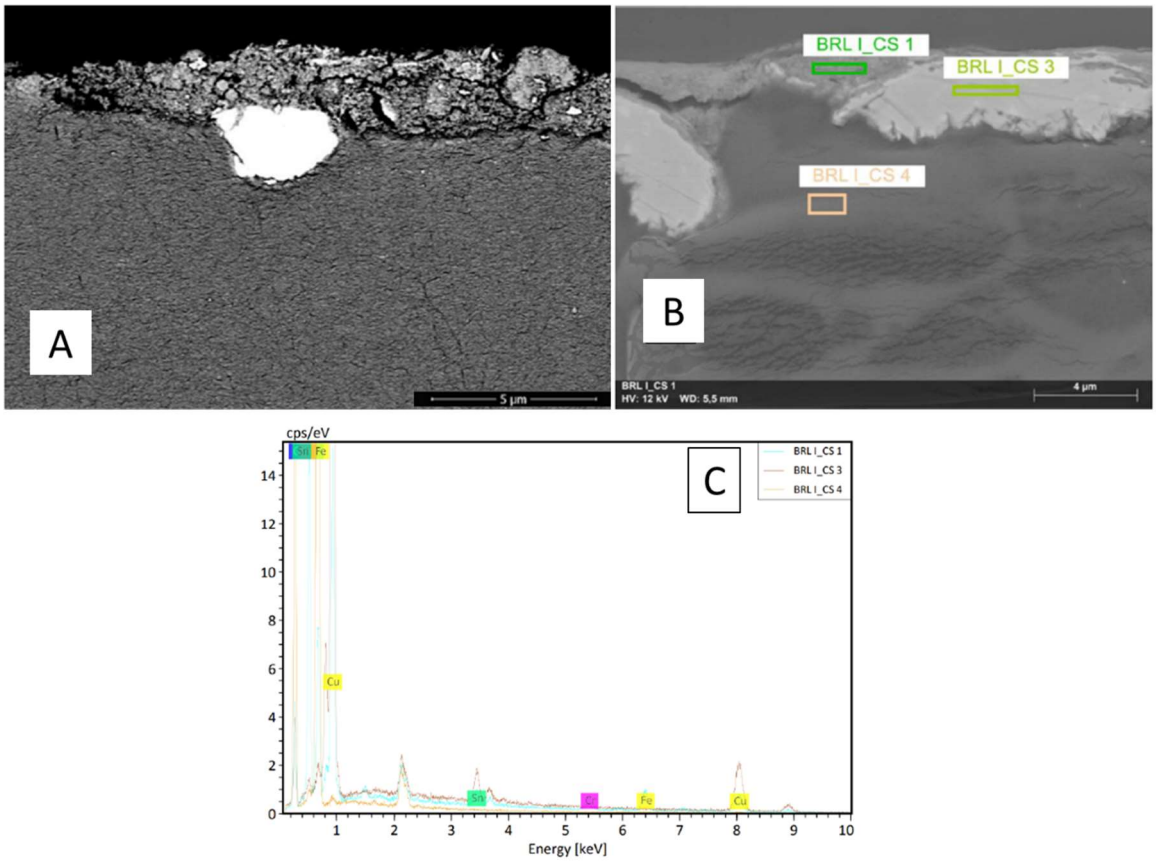

Figure 82: SEM images of the section of the Sintek BRL pin against AISI 304 tested at 10N load and 1.8 m/s siding speed acquired at 3 kV (A) and 12 kV (B) and the acquired EDX spectra (C).

From the section of the pin (Figure 82) it is possible to identify the surface layer, whose thickness is not uniform but ranges from <1 µm to several micrometres at some locations. The pin base consists mainly of PTFE (Figure 82C, BRL_I_CS4) with dispersed bronze particles (Figure 82C, BRL_I_CS3). The transfer-film layer developed against the uncoated AISI 304 surface is particularly thick near bronze particles (Figure 82C, BRL_I_CS1) that protrude from the worn surface of the pin.

The corresponding wear trace on the disc surface (Figure 83A) is also uniformly covered by the transfer-film previously observed on the pin surface (Figure 80), as confirmed by the EDS analysis where the presence of F, Cu and Sn is highlighted. The transfer-film

layer on the disc surface also shows signs of longitudinal abrasion, which suggests that the hard constituents on the two surfaces and/or in the loose debris cause slight, mutual abrasion.

A local layer delamination (Figure 83C, spectrum 1) shows the surface of the underlying disk, as is also evident from the presence of transverse marks of lapping the disk itself. The presence of these processing lines is an indication of how minimal the depth of the grooves, left by the pin during the sliding contact, is: the volume of material removed from the disc is extremely reduced and, at some places, the original machined surface was preserved. At other locations, however, some abrasion of the disc occurred, as is inferable by the roughened profile of the steel surface under the tribofilm in Figure 83B. This is consistent with the detection of elements from the disc (e.g. Fe, Cr) in the tribofilm even on the pin surface.

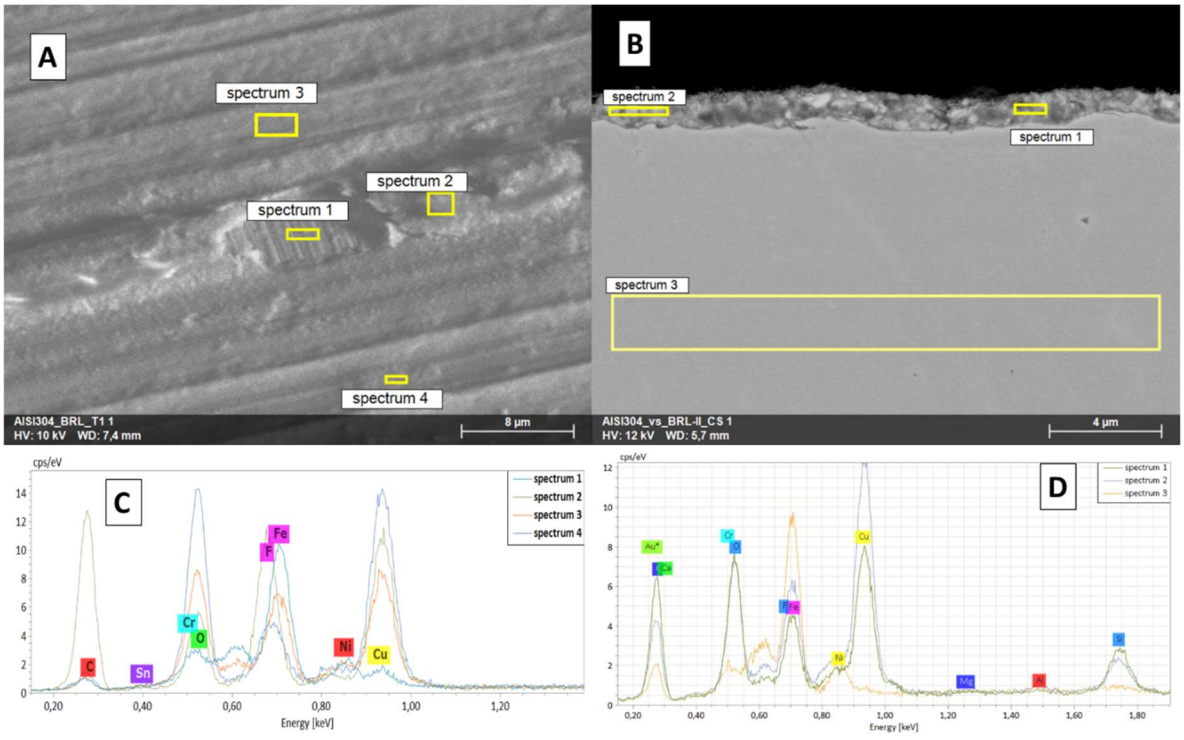

Figure 83: SEM micrograph of the AISI 304 stainless steel disc surface after sliding wear testing against the Sintek BRL pin at 10 N load, 1.8 m/s speed (A), and a section of the disc after sliding wear testing against the Sintek BRL pin at 5 N load, 0.54 m/s speed (B), and corresponding EDX spectra (C-D).

Analysing the section of the disc it is deduced that the formation of a continuous and homogeneous transfer-film is strongly facilitated by the roughening of the counter-surface that is able to accumulate particles and form a compact layer (Figure 83B). EDX

spectra 2 and 3 of Figure 83D show an intense peak of oxygen, which suggests the tribo-oxidation of the metal debris in the transfer-film.

The wear debris (Figure 84) contains two deeply different types of particles: large, “lumpy” particles, typical of adhesive wear, containing entire bronze lamellae, and (Figure 84**Errore. L'origine riferimento non è stata trovata.**C) very fine fragments similar to those seen in the transfer-film in (Figure 82A, Figure 83B). It can be assumed that the larger lumps were formed during an initial phase of severe adhesive wear induced by high contact pressures, corresponding to the initial section of the friction curves characterized by higher (up to 0.32) and more unstable COF. Under these conditions, the bronze particles could not prevent the formation and propagation of sub-surface cracks in the pin, so that large blocks of material including multiple particles were detached. When the contact pressure decreases enough, a transition occurred to moderate tribochemical wear, with the formation of a tribofilm also promoted by the roughening of the disc surface, and abrasive wear as a secondary mechanism (testified by the groove on the surface of the pin). Namely, the debris produced by both the PTFE matrix and the bronze particles, the latter partially tribo-oxidized, mixed with the equally tribo-oxidized debris released from the disc and led to the formation of a transfer-film on both surfaces in contact, allowing to stabilise contact conditions and resulting in more moderate wear and lower, stable friction. Bronze particles, protruding from the composite wear surface, helped to sustain much of the contact, limiting the removal of material from the PTFE matrix.

The much lower wear loss recorded at lower speed and lower load is probably associated to the shorter duration of the initial high-wear stage, as is testified by the shorter duration of the associated high-friction regime in the friction curves seen in 3.4.3.1.

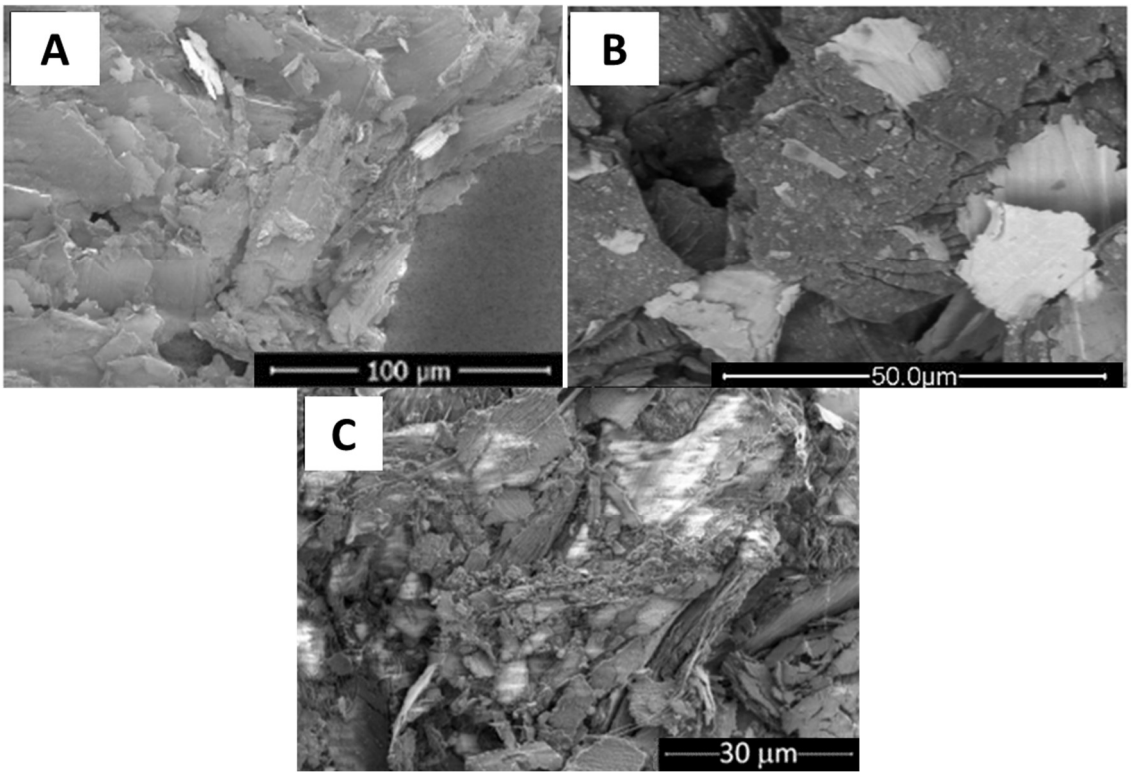

Figure 84: SEM micrographs showing loose debris collected after a pin-on-disc test of the Sintek BRL pin slid against uncoated AISI 304 at 10 N load, 1.8 m/s speed.

The rapid degradation of the pin probably slows down when there is enough debris on the surface to create a separation layer between the pin and the disk. After that, the mechanism is stable: the rubbing will proceed in conditions of minimum wear and friction until the end of the test.

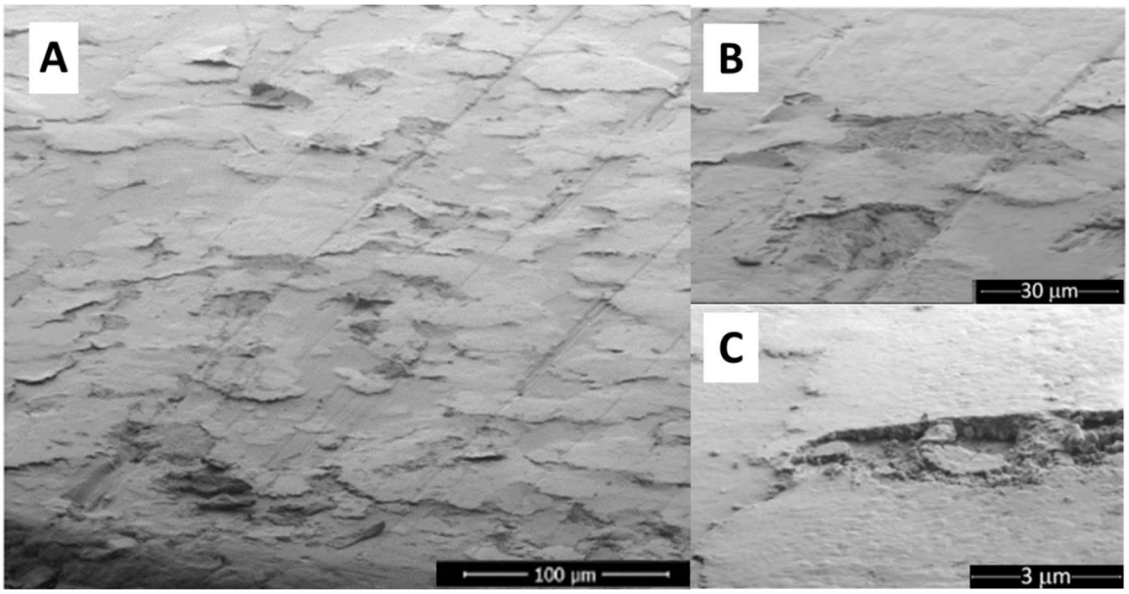

Figure 85: SEM micrographs of the worn surface of the Sintek BRL pin tested at 10 N load and 1.8 m/s sliding speed against the Chromia coated surface: low magnification (A), high magnification (B,C).

The pin surface becomes more uneven when in contact with the Chromia-coated disc. There are protrusions covered by a layer consisting of finely compacted debris that undergoes a periodic delamination due to accumulation of fatigue (Figure 85C).

The distribution of the areas covered by transfer-film suggests that the latter selectively covers the bronze particles and the immediately adjacent areas, since in the areas not covered by transfer-film the bronze particles are not visible, but only the PTFE matrix.

Figure 86 shows the EDS analyses carried out on the worn surface of the pin. Compared to the tests carried out on AISI 304, there are areas covered by a substantial layer of transfer-film (Figure 86B, spectra 2 and 3) that cover the lamellae of bronze, while in the deeper valleys (Figure 86B,spectrum 1) there is only PTFE, not covered by transfer-film, to confirm what discussed above.

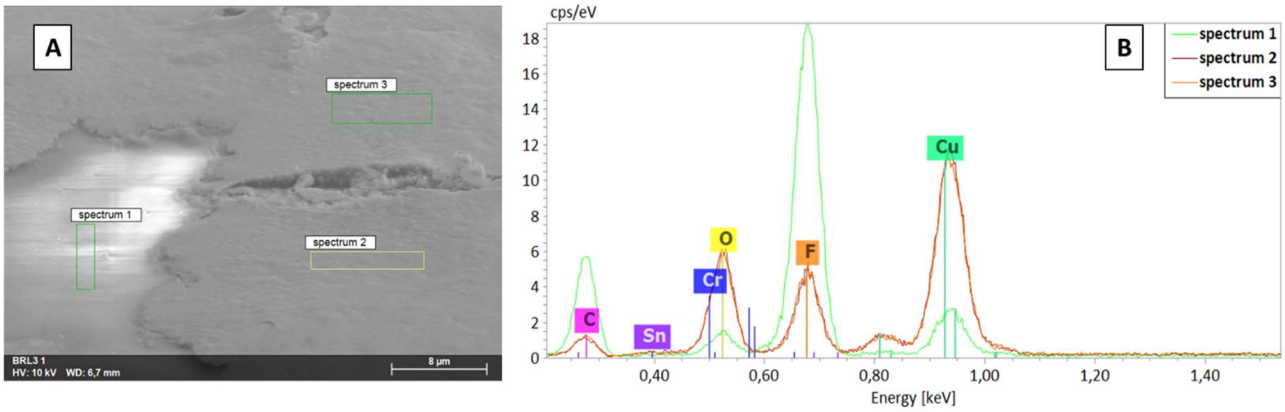

Figure 86: SEM micrographs of Sintek BRL pin against Cr_2O_3 coated surface, tested at 10N load and 1,8 m/s sliding speed (A) and EDX spectra acquired on the pin surface (B).

In addition, different from the tests performed against uncoated AISI 304, the transfer-film does not contain elements from the counter-surfaces (Cr is not present in Figure 86B, spectra 2 and 3), but only from the pin itself.

The worn trace on the Chromia surface is shown in Figure 87A. The pores of the coating are filled with debris and, in addition, an irregular layer of debris is also detectable on the outer surface of the disc. The wear of the counter-surface is, even more in this case, almost undetectable.

The debris released after the pin-on-disc test against the coated counter-surface contains some particles of lamellar shape and others with elongated, ribbon-like shape (Figure 88). This debris probably has a different origin from the one seen against stainless steel: in this case the shape is characteristic of abrasive wear. The edges of the deep pores on the surface of the Chromia coated disc (as confirmed by the profilometric study of the disc, *Table 9*) acted as cutting edges against the pin, removing chips from the pin. The absence of adhesive wear justifies the absence of the highest and most unstable initial phase of friction, as observed in the tests against steel; this is probably due to the different chemical nature of the counter-surface. The abrasive wear phenomenon tends to fade over time, with the pores of the counter-surface that tend to fill with the debris released, again determining the transition to a more moderate abrasive wear regime and prevalent tribo-oxidative wear, probably responsible for the formation of lamellar debris resulting from the delamination of the transfer-film accumulated in the pores of the disc and on the bronze particles on the pin.

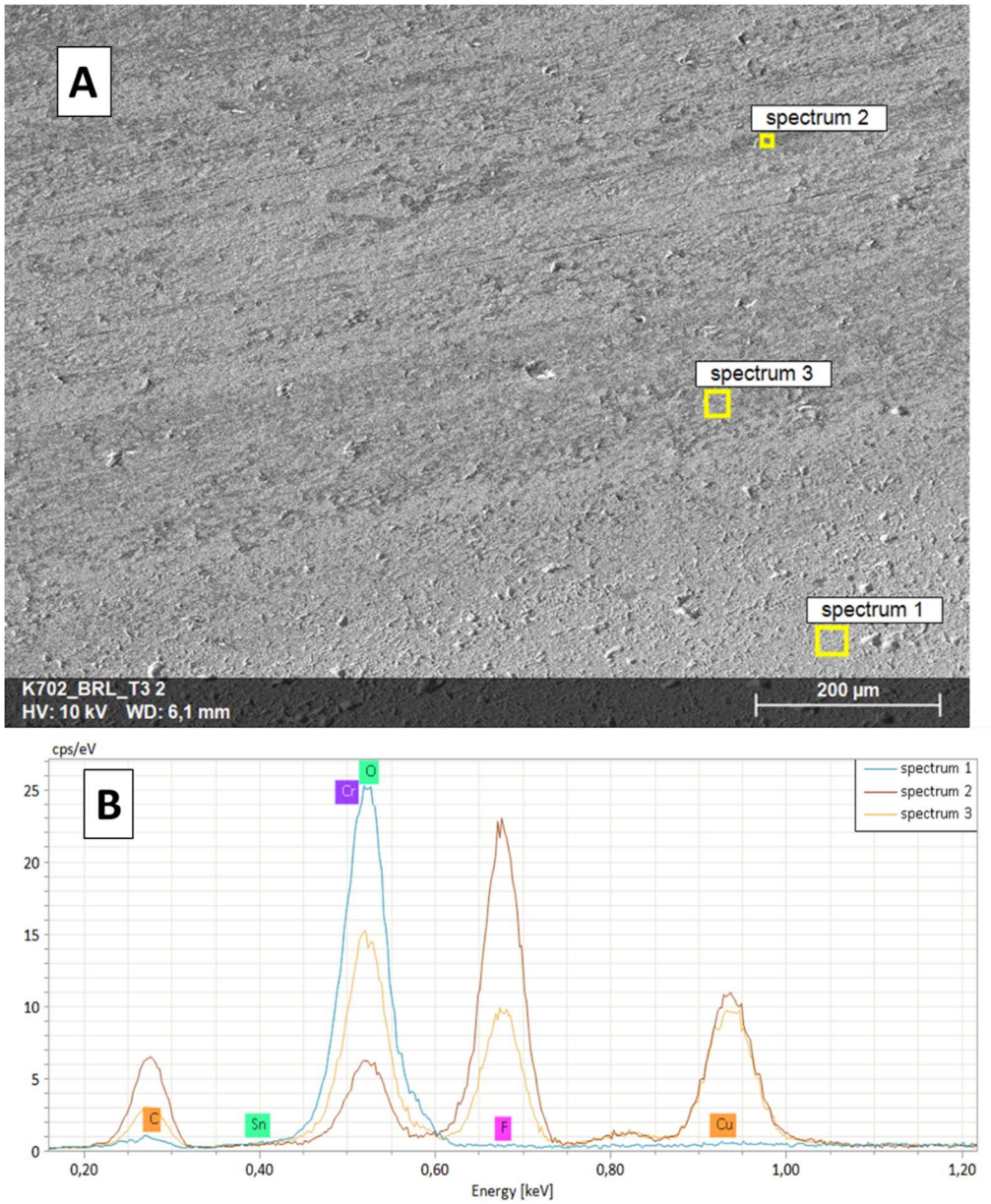

Figure 87: SEM micrographs of the wear trace on the surface of the Chromia coated disc after a pin-on-disc test carried out at 10N load and 1,8 m/s sliding speed

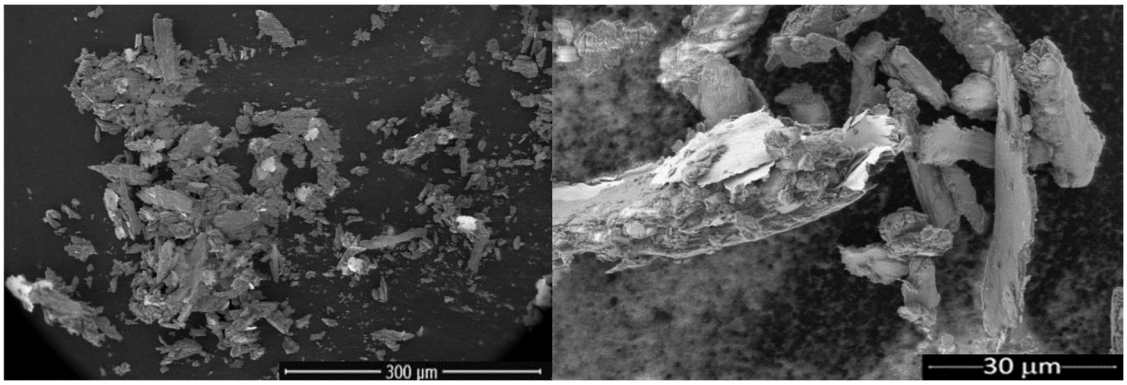

Figure 88:SEM micrograph showing loose debris collected after a pin-on-disc test of the Sintek BRL pin slid against Chromia coated surface at 10 N load, 1.8 m/s speed.

3.4.4 Sintek BRS

3.4.4.1 Sintek BRS against AISI 304

The results in Figure 89 show a coefficient of friction that reaches high peak values, slightly above 0.3, against the stainless steel disc. The value decreases and the trends tend to settle in the second part of the test, reaching a steady-state regime. The behaviour is therefore analogous to the one seen with Sintek BRL. Temperature rise values are also similar: at 10 N load and 1.8 m/s sliding speed the rise temperature reaches a value of 12

°C when the friction peaks above 0.3, stabilizing after that around 10 °C. At 5 N load the rise temperature reaches lower values, around 4 °C.

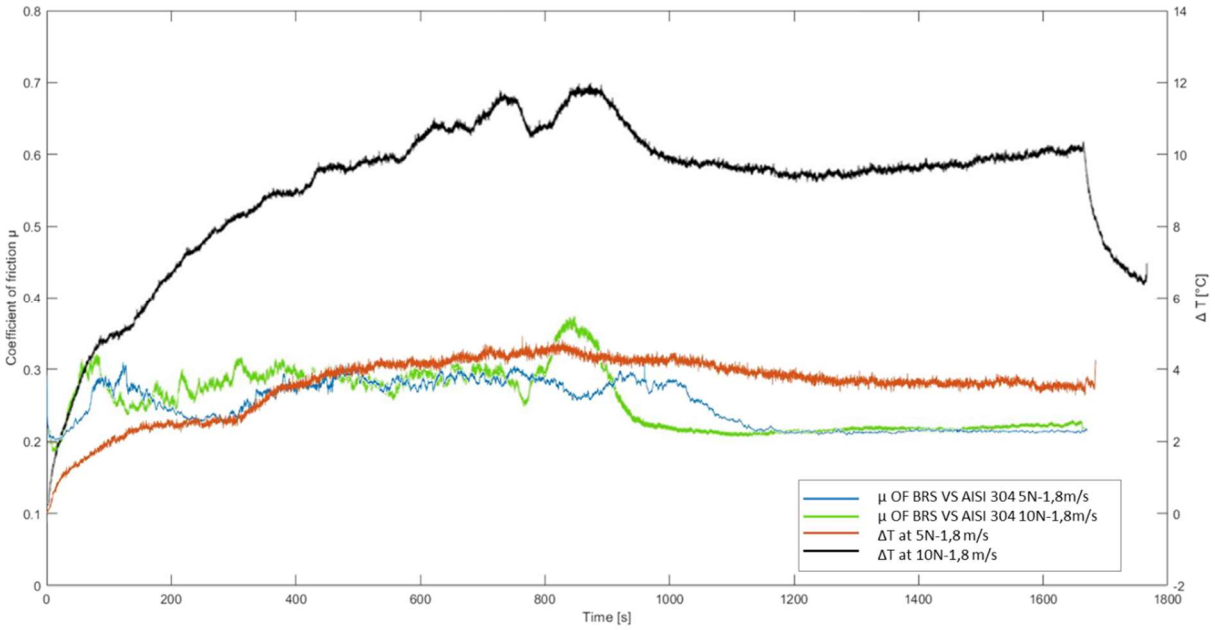

Figure 89: Friction coefficient and temperature rise curves of Sintek BRS against AISI 304 surface at 1.8 m/s sliding speed and both load conditions (5 N-10 N).

Also at 0.54 m/s (Figure 90), the behaviour under both load conditions is analogous to that seen with Sintek BRL: the friction coefficient reaches high peak values after 1000 s (maxima are close to 0.4 and therefore slightly higher than in the case of Sintek BRL), after which it begins decreasing and stabilizes at about 0,23 until the end of the test. The temperature correspondingly rises by about 2 °C at 5 N and 3.5 °C at 10 N, consistent with the expected dependence on both load and speed.

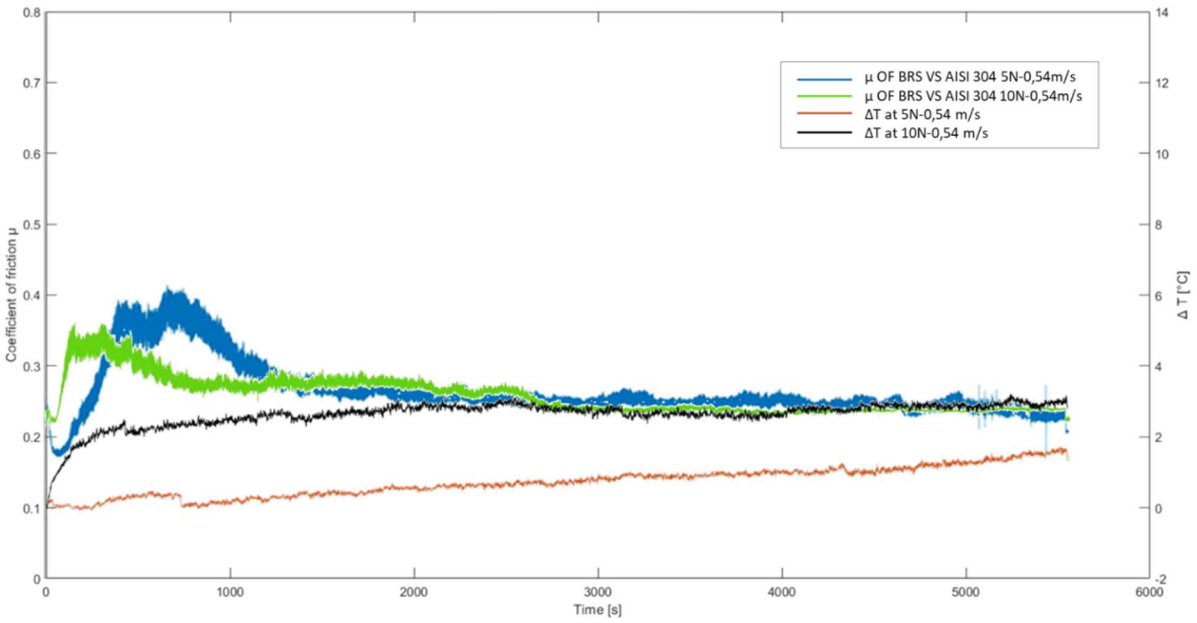

Figure 90: Friction coefficient and temperature rise curves of Sintek BRS against AISI 304 surface at 0,54 m/s sliding speed and both load conditions (5N-10N).

3.4.4.2 Sintek BRS against Chromia

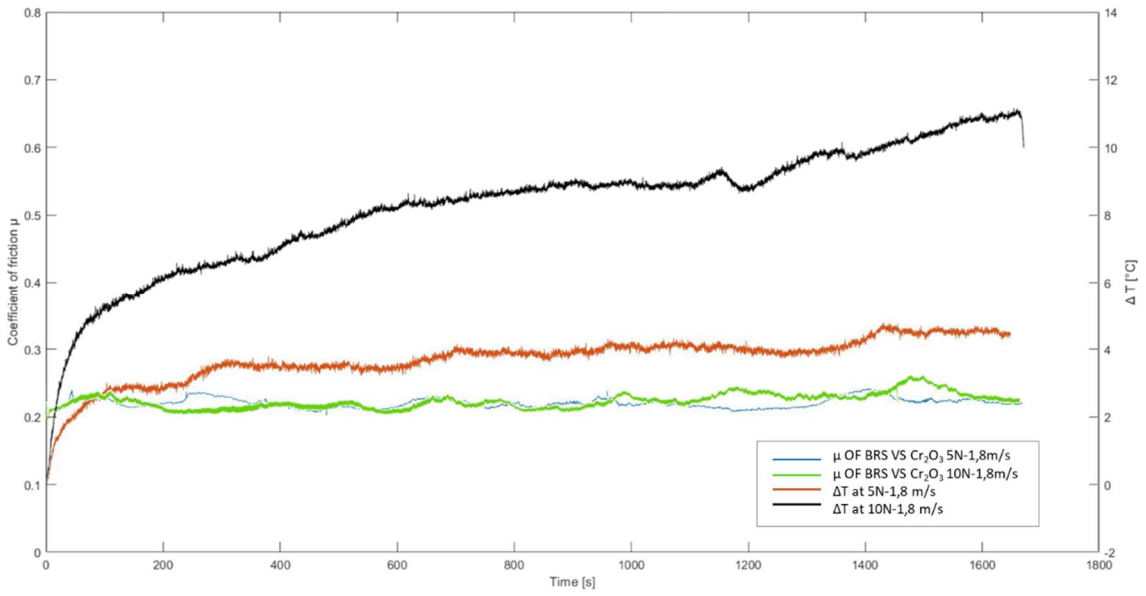

Figure 91: Friction coefficient and temperature rise curves of Sintek BRL against Chromia coated surface at 1.8 m/s sliding speed and both load conditions (5 N-10 N).

As in the previous cases the friction coefficient against the Chromia coated surface, at 1.8 m/s and in both load conditions, is more stable than against the uncoated surface, with a value slightly above 0.2 and no peak in the early stages (Figure 91).

The temperature at 10 N load increases linearly with the sliding distance, reaching a final value of 11 °C. At 5 N load the temperature tends to stabilize after 700 s, reaching a value of 5 °C.

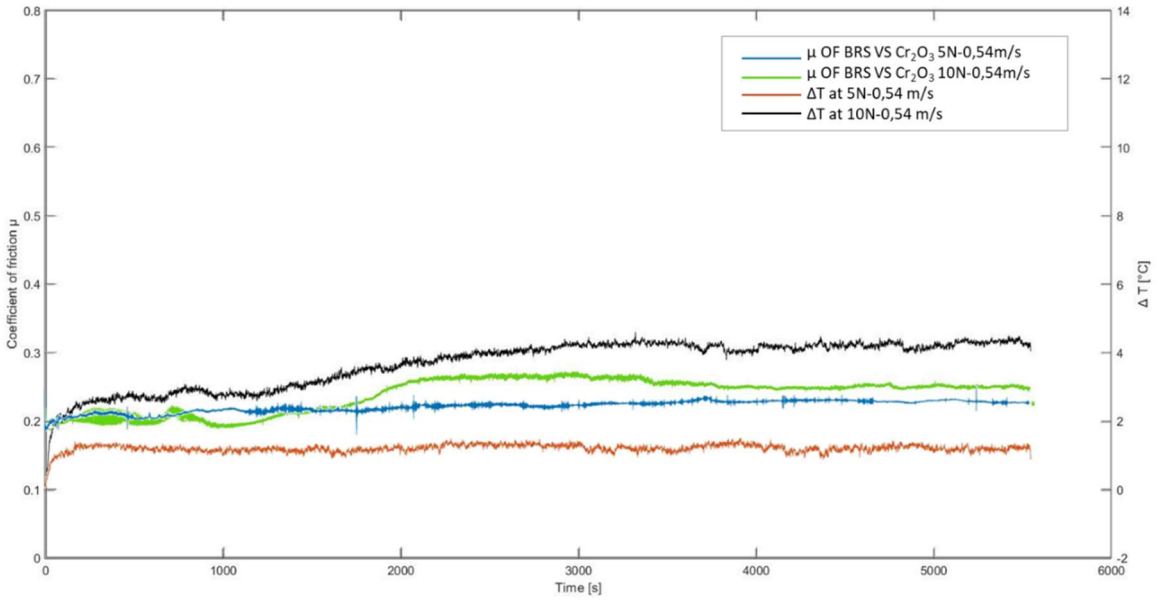

Figure 92: Friction coefficient and temperature rise curves of Sintek BRL against Chromia coated surface at 0.54 m/s sliding speed and both load conditions (5 N-10 N).

At 0.54 m/s (Figure 92) the friction coefficient shows a more stable trend at 5 N load: the rise temperature does not exceed 2 °C until the end of the test, while at 10 N load it reaches around 5 °C. In general, the friction coefficient has lower values than against uncoated steel: at low values of friction coefficient correspond also low values of wear rate (Figure 94 - Section 3.4.4.3).

Figure 93 summarises the average steady-state friction coefficient and maximum temperature rise in the pin on disc tests with Sintek BRS pins. As in the previous cases the white dots indicate theoretical bulk temperature rise calculated according to Ashby et al.'s model. These are, again, within 2 °C of the experimental value except for the tests at the highest load and speed, where some notable deviations occur especially for the test against uncoated stainless steel. The actual temperature rise is much higher than the numerically predicted value, maybe because the latter does not account for the temperature rise occurring during the high-friction stage at the beginning of the test. Because that friction peak was higher and more prolonged than with Sintek-BRL, its effect on temperature was probably quite significant.

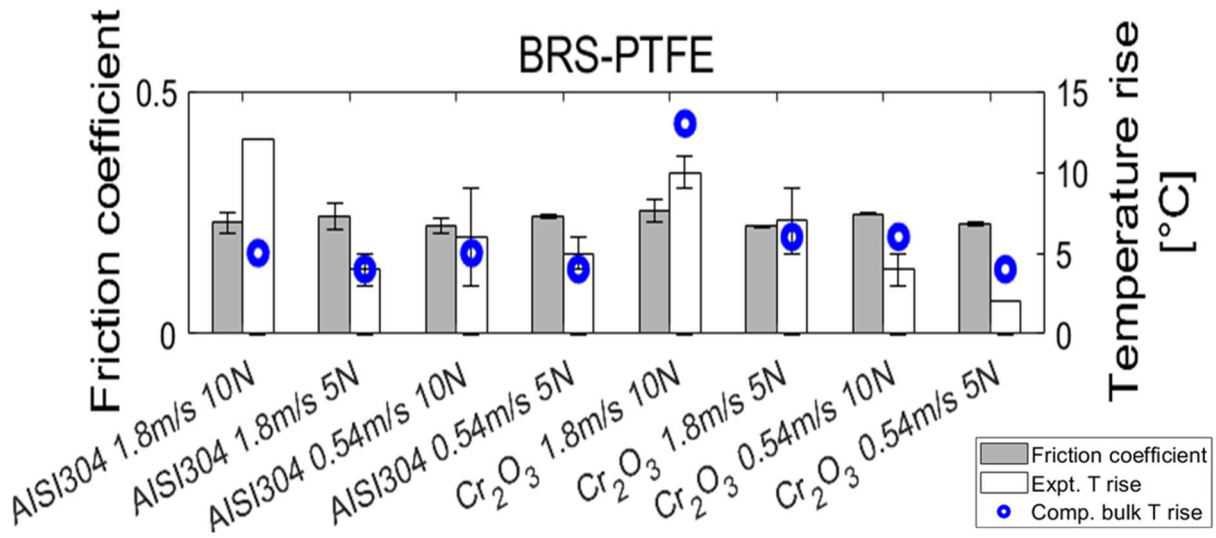

Figure 93: Average steady-state friction coefficient and maximum temperature rise in pin on disc tests with the Sintek BRS material.

3.4.4.3 Wear Mechanism of Sintek BRS

The maximum value of the wear rate of Sintek BRS occurs in conditions of 1.8 m/s sliding speed against AISI 304 disc. The differences between high and low speed are even more pronounced than they were for Sintek BRL, with values respectively 5 and 4 times higher in conditions of 1.8 m/s sliding speed at 10 N and 5 N load, compared to the values at 0.54 m/s. Wear rates against the Chromia coated surface are much less dependent on test conditions and, therefore, at high speed they are much lower than against uncoated steel. In general, the values of the wear rate recorded in the case of the spheroidal bronze filler are higher than those measured with lamellar filler.

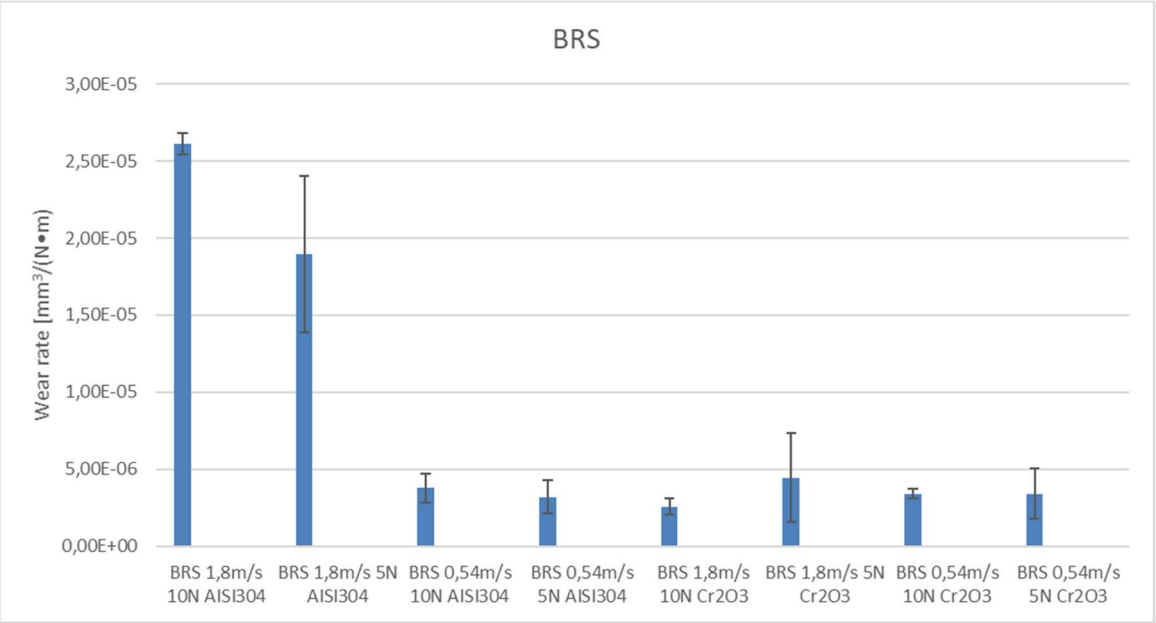

Figure 94: Wear rate of Sintek BRS against uncoated AISI 304 and Chromia coated surfaces under different test conditions.

The worn surface of the pin against uncoated AISI 304 is analogous to that already seen for Sintek BRL (Figure 95). In fact, the pin surface is completely covered by a transfer-film consisting of very fine compacted wear debris, well visible in the detail of Figure 95C, with some cracked and delaminated areas and longitudinal grooves.

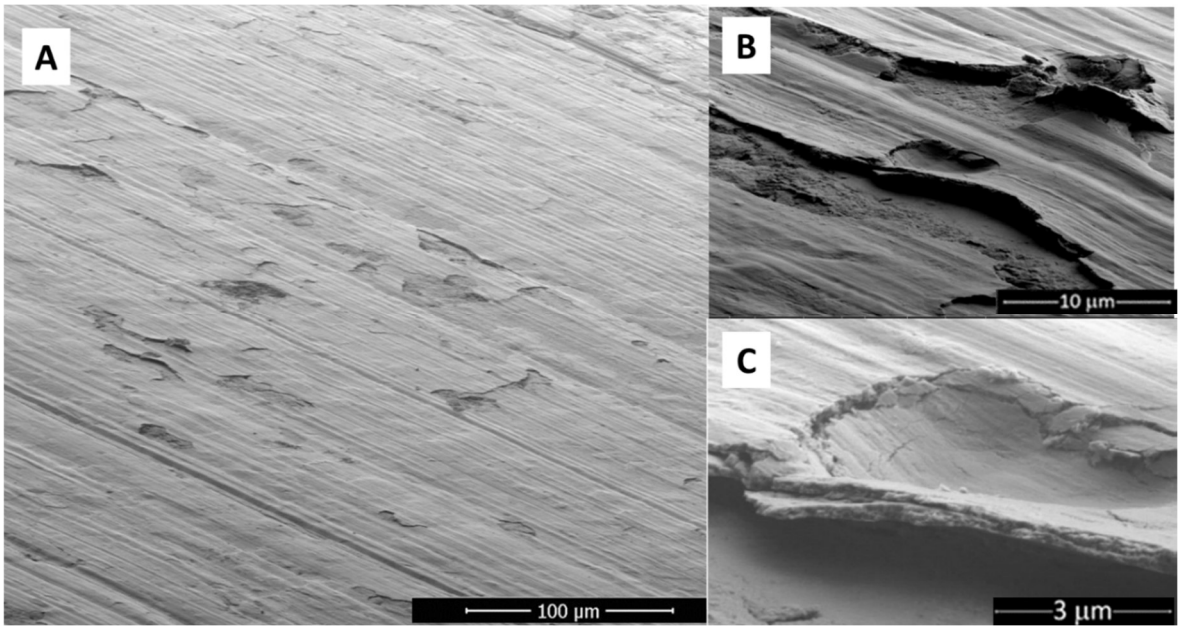

Figure 95: SEM micrographs of the Sintek BRS pin against AISI 304 surface at 10 N load and 1.8 m/s sliding speed at low magnification (A) and high magnification (B-C).

There are irregular cracks due to the delamination of the film following an accumulation of residual stresses in the layer, linked to the addition of material during the tribological

process and the continuous shear deformation to which it is subjected. As in the previous case of Sintek BRL, images acquired at 3 kV do not allow to distinguish the bronze particles from the surrounding matrix, as both are covered by a layer of transfer-film thick enough to prevent the generation of signal from the underlying material.

EDS analyses carried out on the surface of the worn pin confirm the presence of an evenly distributed transfer-film formed through the compaction of wear debris (Figure 96, spectra 2 and 4), where some debris from the stainless-steel disc (Fe, Cr) is mixed with debris from the pin (F, Cu).

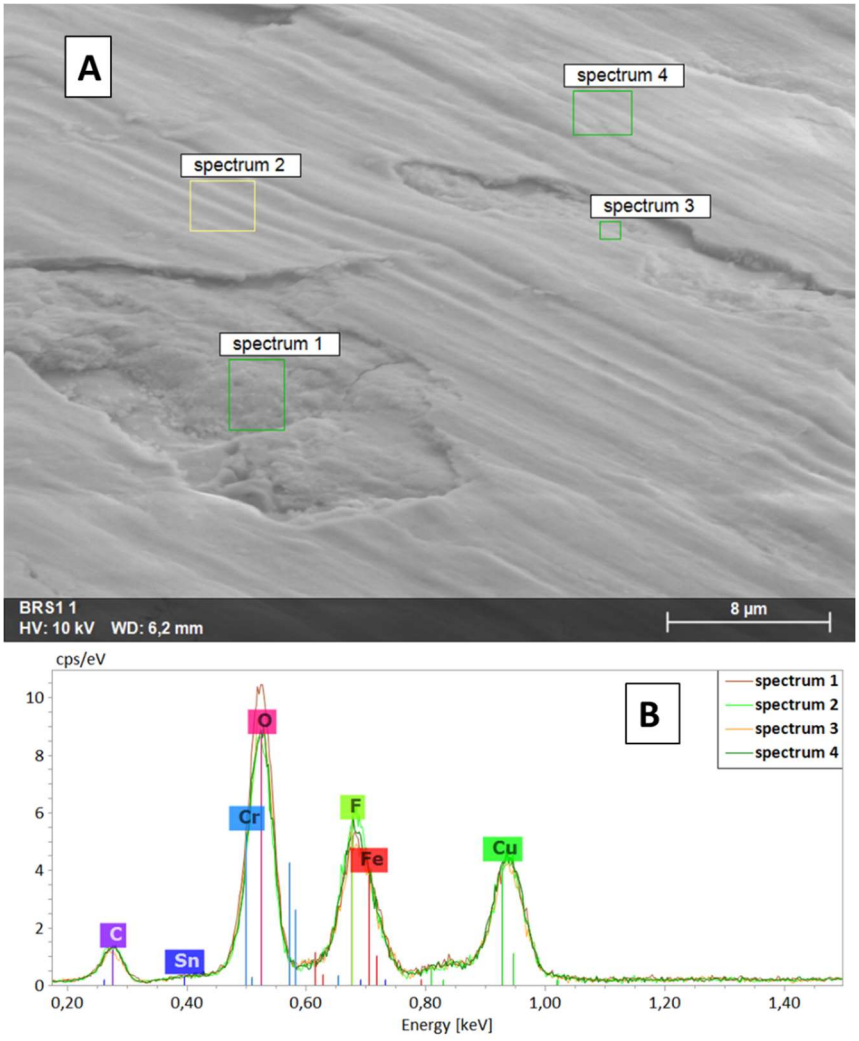

Figure 96: SEM micrographs of the worn surface of the Sintek BRS pin tested against the AISI 304 surface at 10 N load and 1.8 m/s sliding speed (A) and EDX spectra acquired on the pin surface (B).

The stainless steel disc is analogously covered with a thin layer of transfer-film along the wear track, such that the marks of lapping and polishing below are not visible (Figure

97). The film shows abrasive grooves, due to debris trapped between the two surfaces and/or to the bronze particles protruding from the pin surface.

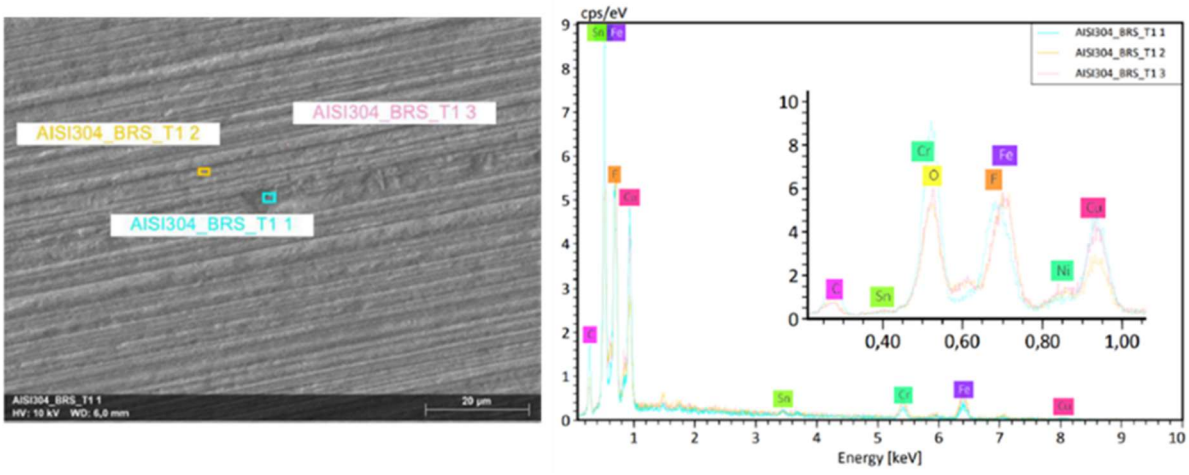

Figure 97: SEM micrographs of the stainless steel AISI 304disc surface and corresponding EDX spectra (with zoomed-in view in the inset).

SEM micrographs (Figure 98) of the debris collected after wear testing against uncoatd stainless steel reveal the presence of some compact blocks of material: the bronze, initially spheroidal, suffered a strong plastic deformation that caused the flattening, while PTFE has a "fibrous" morphology as it undergoes severe plastic deformation due to the high nominal contact pressure and the high friction coefficient in the early stages of the test. These debris blocks, with evident signs of yield and plastic deformation, were indeed probably produced in the early stages of contact, due to adhesive wear of the pin against the steel disc, just as it happened for the Sintek BRL pins.

At high magnifications (Figure 98C) the presence of very fine dusty debris is evident, probably produced at a later stage of the test, when the initial adhesive wear mechanism transitioned to prevailing tribo-chemical wear. In this case a transfer-film of oxidized and compacted debris is formed, which, protecting both the pin and the disc surfaces, have prevented further adhesive wear and mitigated friction.

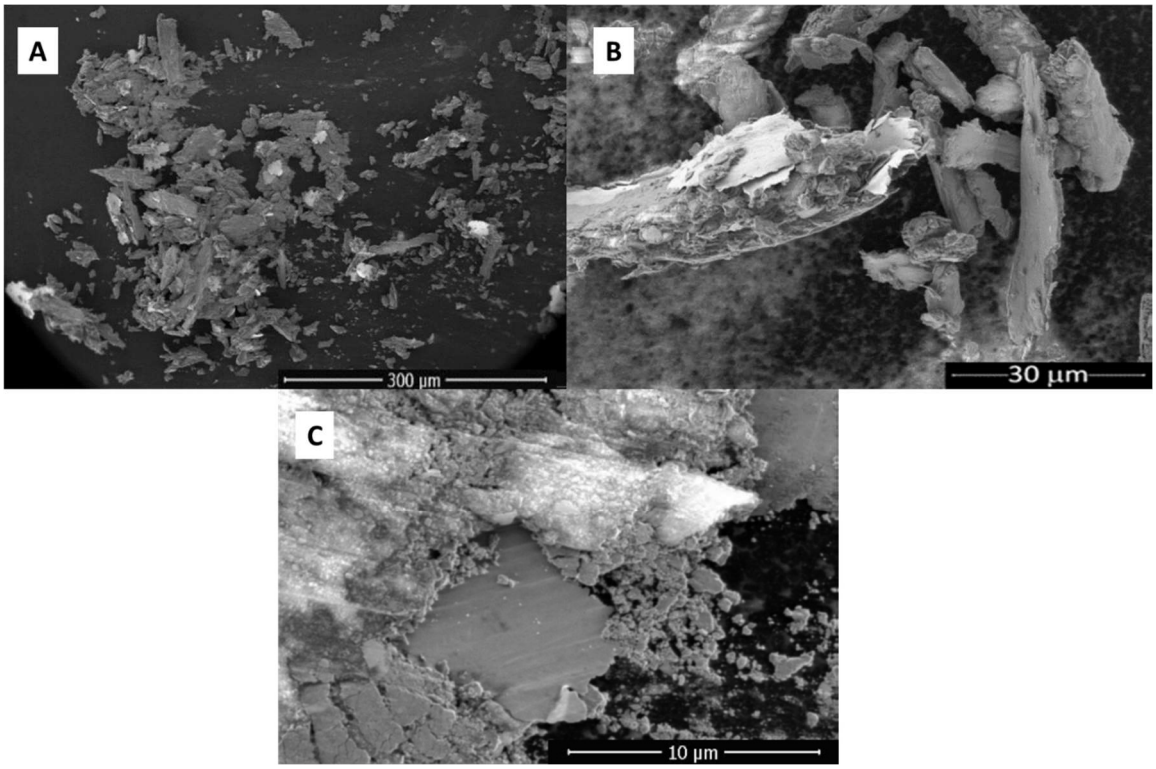

Figure 98: SEM micrographs showing loose debris collected after a pin-on-disc test of the Sintek BRS pin slid against AISI 304 disc at 10 N load, 1.8 m/s speed.

Once again, the worn surface of the pin after sliding against the Chromia coated surface is more irregular, with the transfer-film not evenly distributed, probably because the latter is formed preferentially in contact with bronze particles, leaving uncovered the PTFE matrix. It is therefore inferred that, just as it happened with the GF-PTFE and CF-PTFE composites, the contribution of the debris from the stainless-steel disc is important to improve the adhesion and homogeneity of the tribofilm.

The images (Figure 99) suggest that wear does not uniformly involve the pin: the abrasive grooves move preferably in the PTFE matrix (Figure 99B), finding less resistance from the material, bypassing the bronze particles.

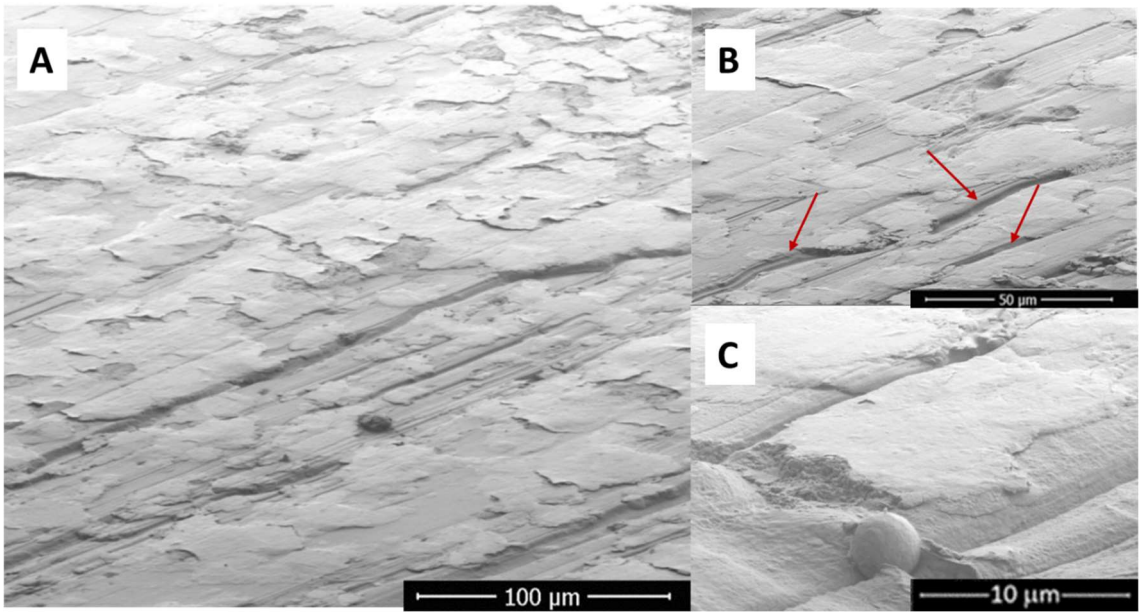

Figure 99: SEM micrographs of the Sintek BRS pin against Chromia coated surface at 10N load and 1,8 m/s sliding speed at low magnification (A), high magnification (B-C). The red arrows (B) indicate the abrasive grooves on the PTFE matrix.

Some bronze particles better linked to the surrounding PTFE matrix have suffered a slight abrasion, exposing a flat and slightly raised surface from the matrix, around which the debris particles were collected.

In other cases, on the other hand, semi-spherical cavities are observed, probably a consequence of the expulsion of bronze particles poorly attached to the surrounding matrix. In Figure 99C in particular, there is a clearly visible bronze particle which, displaced from its original location, has crept along the PTFE surface.

The filler in this case does not effectively reinforce the PTFE due to the poor adhesion of spherical bronze particles. This was not observed with lamellar bronze particles, as the irregular shape allowed better bond with the matrix through mechanical interlocking.

The EDX spectra acquired from the pin surface confirm the previous considerations (Figure 100): bronze particles protruding from the surface are seen at the locations labelled as spectrum 1 and spectrum 2, and the direction of the abrasion grooves through the PTFE matrix is deviated from these well-adhering particles. Spectrum 4 in Figure 100 shows the composition of a compact tribofilm layer with the presence of Cu and Sn as well as F. The transfer-film layer, however, does not cover the whole surface (spectrum 6 corresponds to uncoated PTFE matrix).

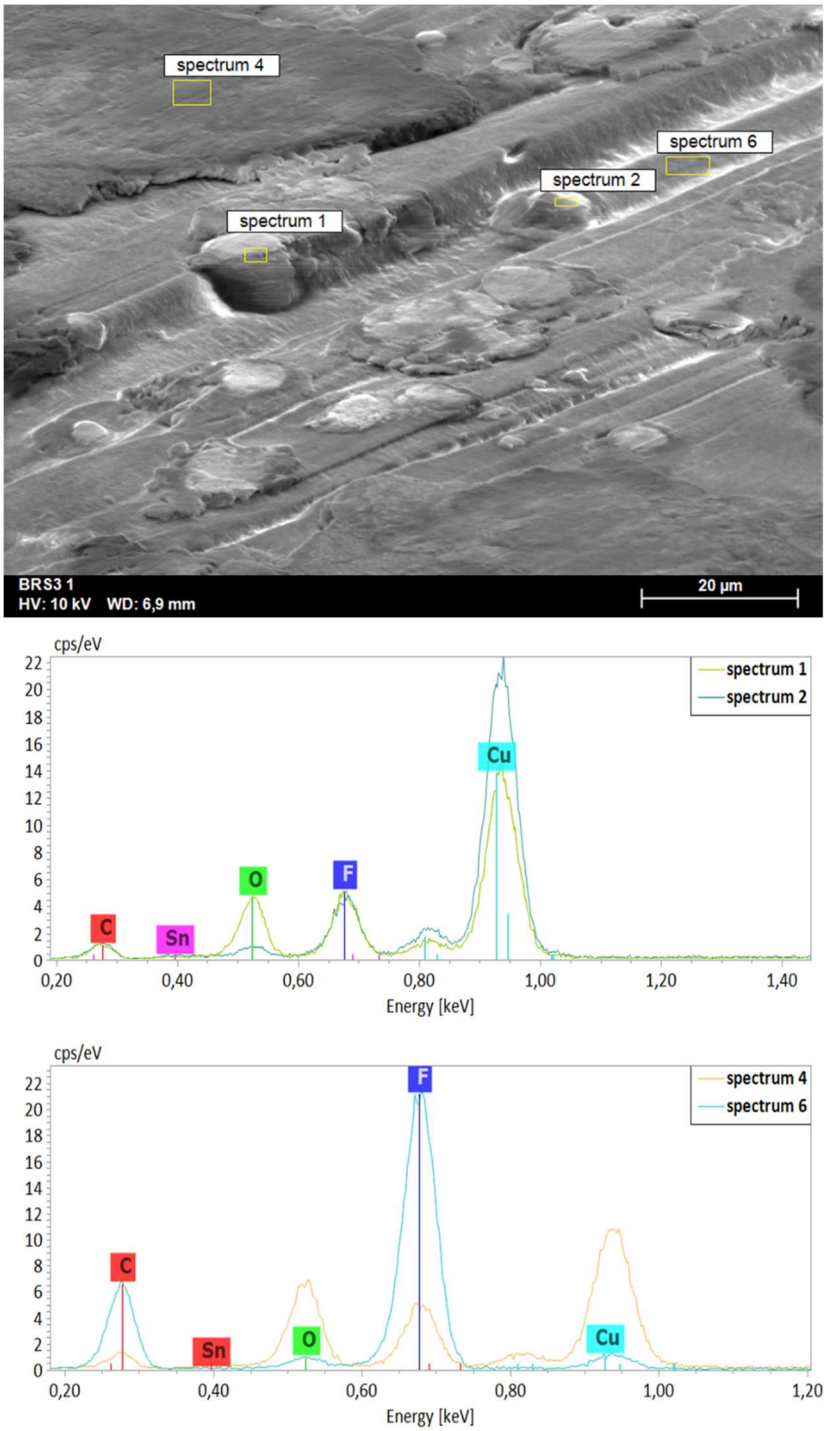

Figure 100: SEM micrograph of Sintek BRS pin against Chromia coated surface, tested at 10N load and 1,8 m/s sliding speed and EDX spectra acquired on the pin surface.

SEM images of the debris collected at the end of the tests against the Chromia coated surfaces (Figure 101) mostly show lamellar fragments consisting of compacted debris, due to the periodic delamination of the transfer-film: in this case, therefore, all the debris

found was representative of the stationary conditions, when tribo-chemical wear was already the dominant mechanism.

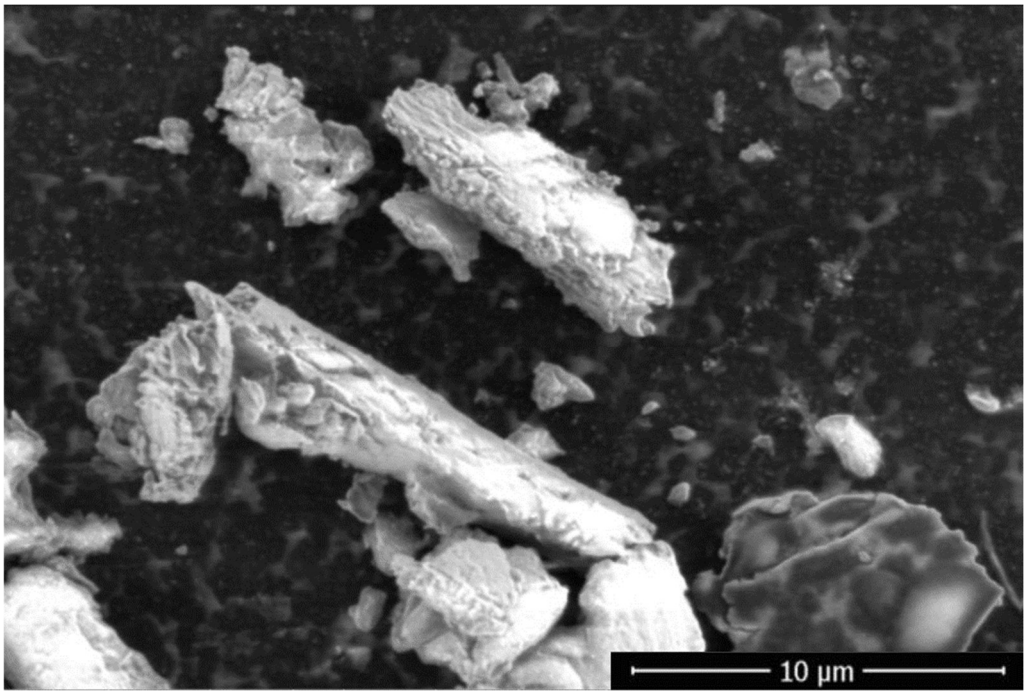

Figure 101: SEM micrographs showing loose debris collected after a pin-on-disc test of the Sintek BRS pin slid against Chromia coated disc at 10 N load, 1.8 m/s speed.

3.4.5 Sintek PK10

3.4.5.1 Sintek PK10 against AISI 304

The average friction coefficient produced by Sintek PK10 against the uncoated steel surface (Figure 102) is higher than it is for the bronze-PTFE composites in both load conditions, although the initial high-friction stage is not detectable: the friction coefficient increases slightly during the early stages of the test and tends to settle at a steady.state value. The temperature rise reaches around 9 °C at 10 N load conditions and around 4 °C

at 5 N load, i.e. values are similar to those measured with the bronze-filled materials, despite the lower thermal conductivity.

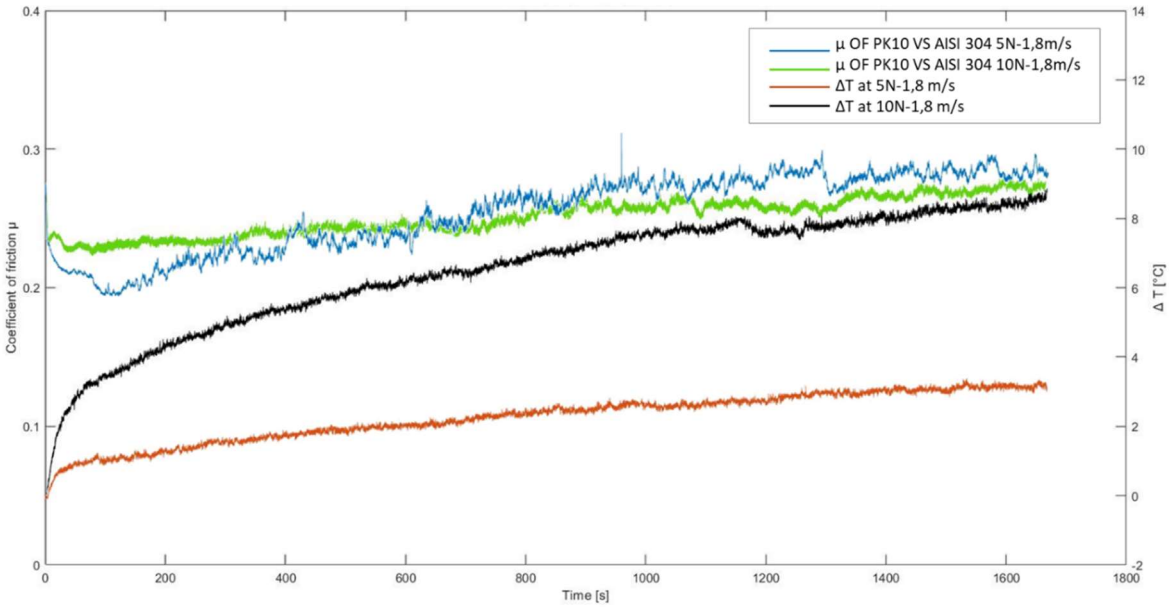

Figure 102: Friction coefficient and temperature rise curves for Sintek PK10 against uncoated AISI 304 at 1.8 m/s sliding speed under both load conditions (5 N-10 N).

At 0.54 m/s sliding speed (Figure 103) the friction coefficient increases under both load conditions until 900 s: after that, at 10 N load it starts decreasing reaching an average value of 0.22 until the end of the test. The temperature rise is rather limited, less than 4 °C at 10 N and around 1 °C at 5 N.

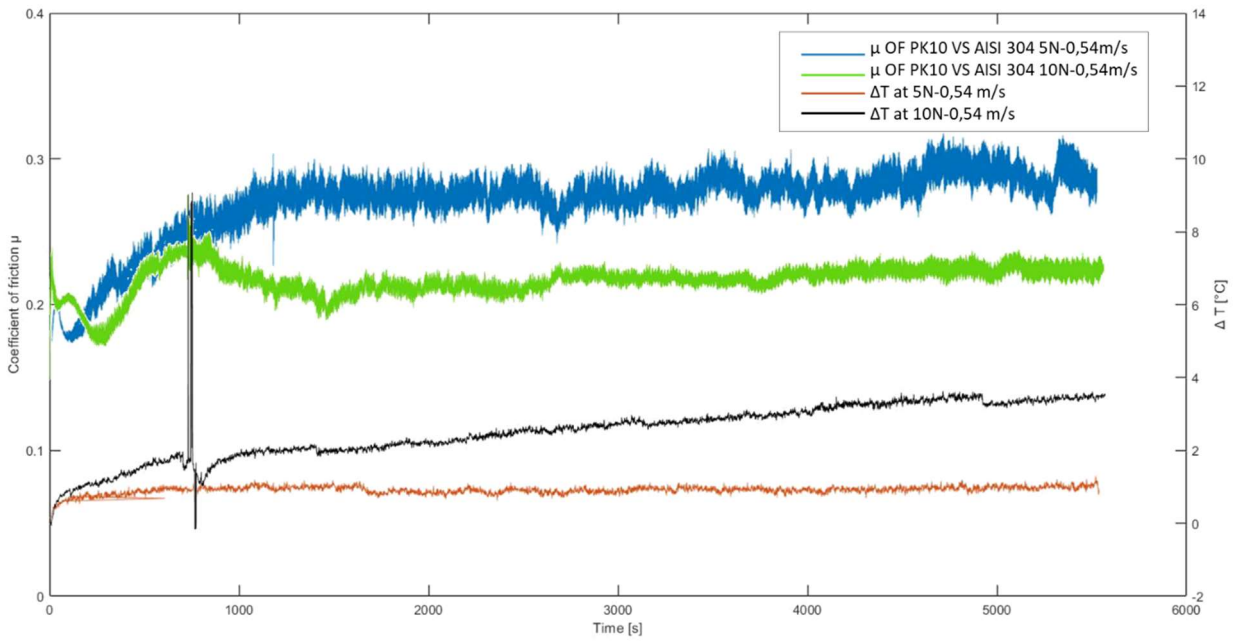

Figure 103: Friction coefficient and temperature rise curves for Sintek PK10 against uncoated AISI 304 at 0.54 m/s sliding speed and both load conditions (5 N-10 N).

3.4.5.2 Sintek PK10 against Chromia

The friction coefficient of Sintek PK10 against the Chromia coated surface at 1.8 m/s is even more stable than against the uncoated surface, and it has a value (in both load conditions) below 0.3.

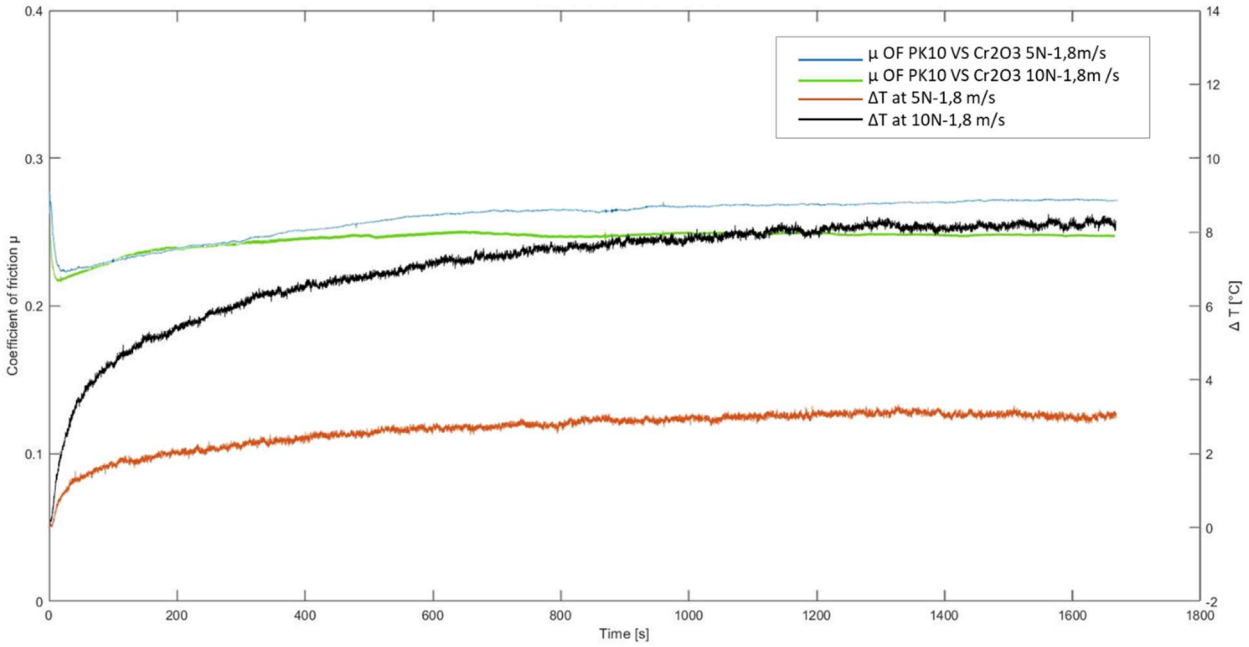

Figure 104: Friction coefficient and temperature rise curves for Sintek PK10 against the Chromia coated surface at 1.8 m/s sliding speed and under both load conditions (5 N-10 N).

At 0.54 m/s (Figure 105) the friction coefficient is even lower, with values around (5 N load) or below (10 N load) 0,2 until the end of the test and, like it happened with the uncoated counter-surface, the temperature rise does not exceed 1 °C at 5 N load and 4 °C at 10 N load. In general, the bulk temperature rise for the Sintek PK10 is comparable to or even lower than for the bronze-PTFE composites.

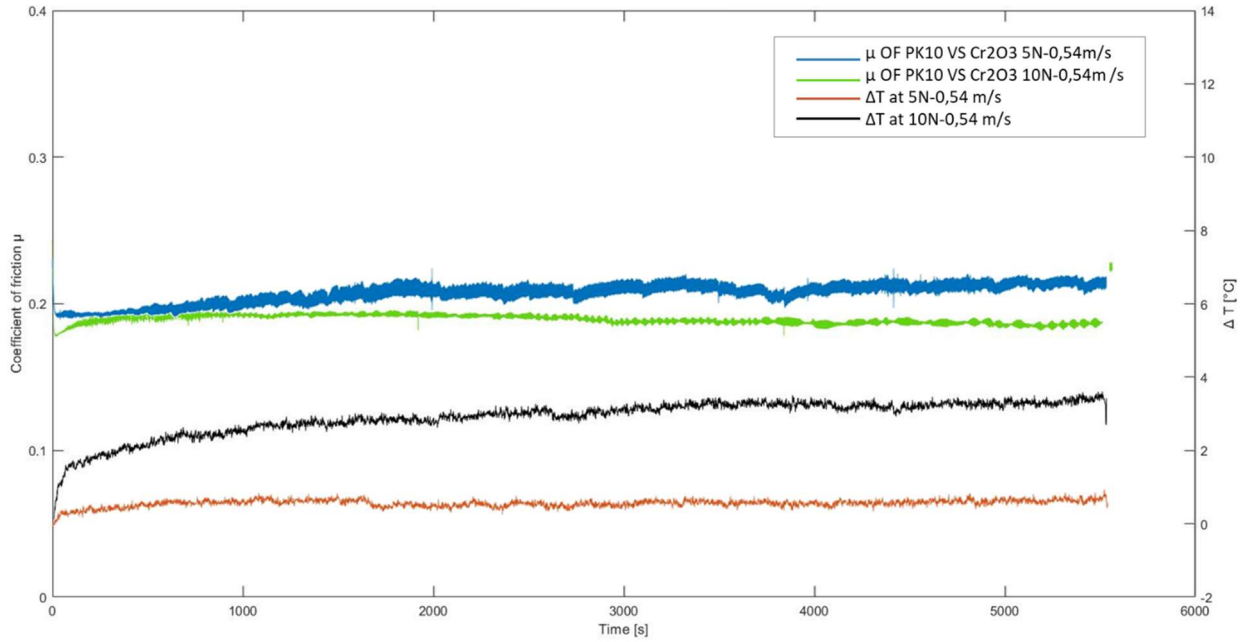

Figure 105: Friction coefficient and temperature rise curves for Sintek PK10 against the Chromia coated surface at 0.54 m/s sliding speed and under both load conditions (5 N-10 N).

Figure 106 summarises the average steady-state friction coefficient and maximum temperature rise in the pin on disc tests with Sintek PK10. As in the previous cases the white dots indicate theoretical bulk temperature rise calculated according to Ashby et al.'s model. Notably, the experimental values are, in this case, systematically lower than the calculated ones, which is understandable because the temperature was not measured exactly at the contact surface, but slightly behind it, and because the outer surface of the pin was cooled by convection. The fact that this systematic difference did not occur with the bronze-filled pins, where, by contrast, the measured temperature rise was often higher than the calculated one (though by few °C at most), corroborates the previous considerations on the role of the initial high-friction regime in promoting faster heating of the pin than is predicted using a model where only the final, steady-state friction coefficient value is employed.

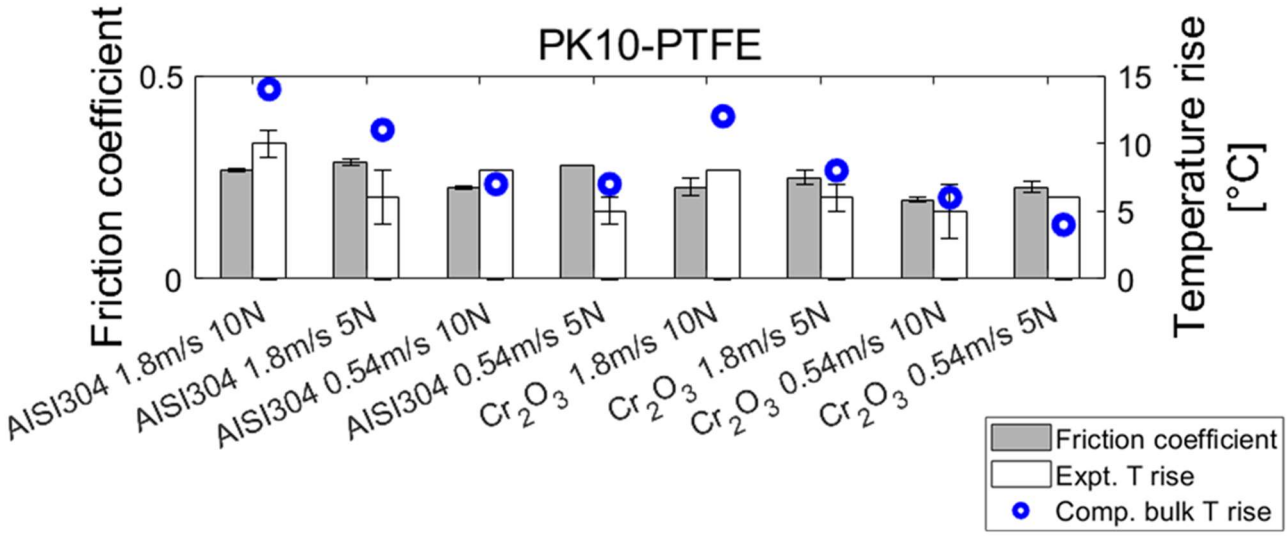

Figure 106: Average steady-state friction coefficient and maximum temperature rise measured in pin on disc tests with Sintek PK10.

3.4.5.3 Wear mechanism of Sintek PK10

The wear rate of Sintek PK10 against AISI 304 disc decreases with decreasing speed and load and it is generally lower than it is against the chromia-coated disc. Whilst this trend matches that observed for the bronze-filled pins against the same uncoated stainless steel counter-surface, the dependence is less marked, and specific wear rates values are always notably lower. Specific wear rates for Sintek PK10 pins against uncoated stainless steel are indeed between 1×10^{-6} and 2×10^{-6} $mm^3/(N\cdot m)$, whilst values $>2\times10^{-6}$ $mm^3/(N\cdot m)$, and sometimes even $>10^{-5}$ $mm^3/(N\cdot m)$, were reported for bonze-filled Sintek BRL and Sintek BRS composites. Against the Chromia coated surface, wear rates are higher, though they are still comparable to or mostly lower than the wear rates measured for bronze-filled pins against the same counter-surface.

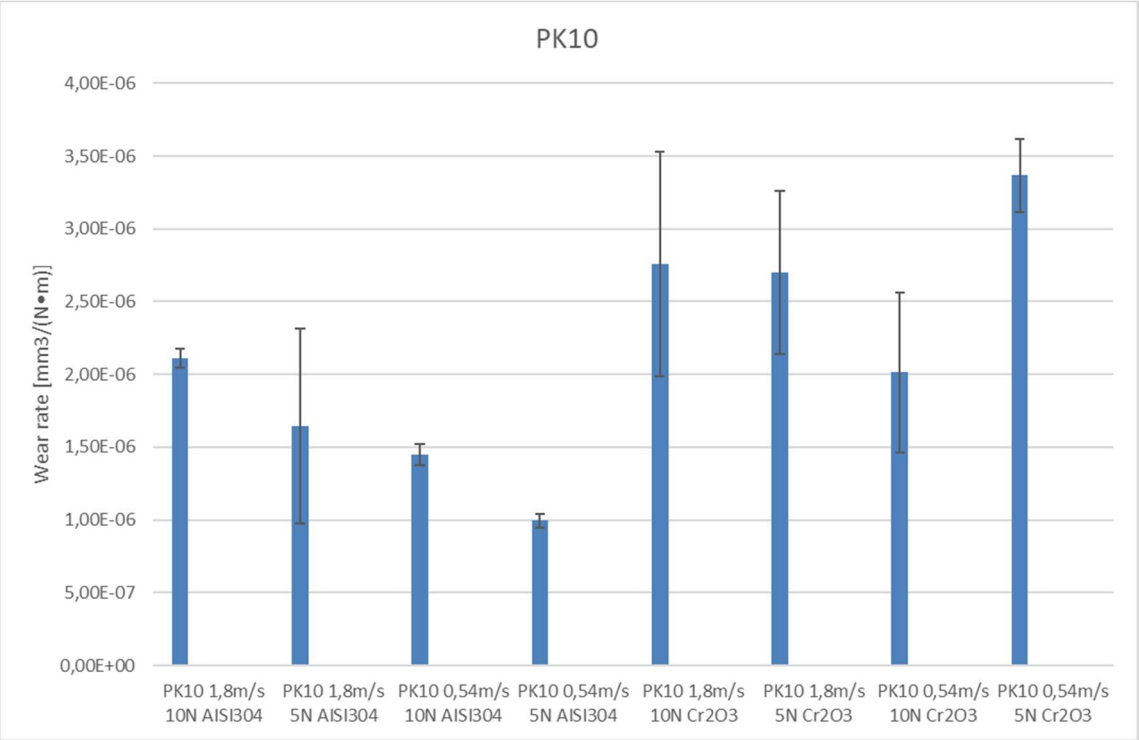

Figure 107: Wear rate and friction coefficient of Sintek PK10 against AISI 304 and Chromia coated surfaces under different test conditions.

SEM micrographs of the pin surface show ridges made mainly by protruding filler particles, alternating with valleys where the softer PTFE matrix has been worn more severely. All these areas are covered by a thin transfer-film layer, especially visible from Figure 108C.

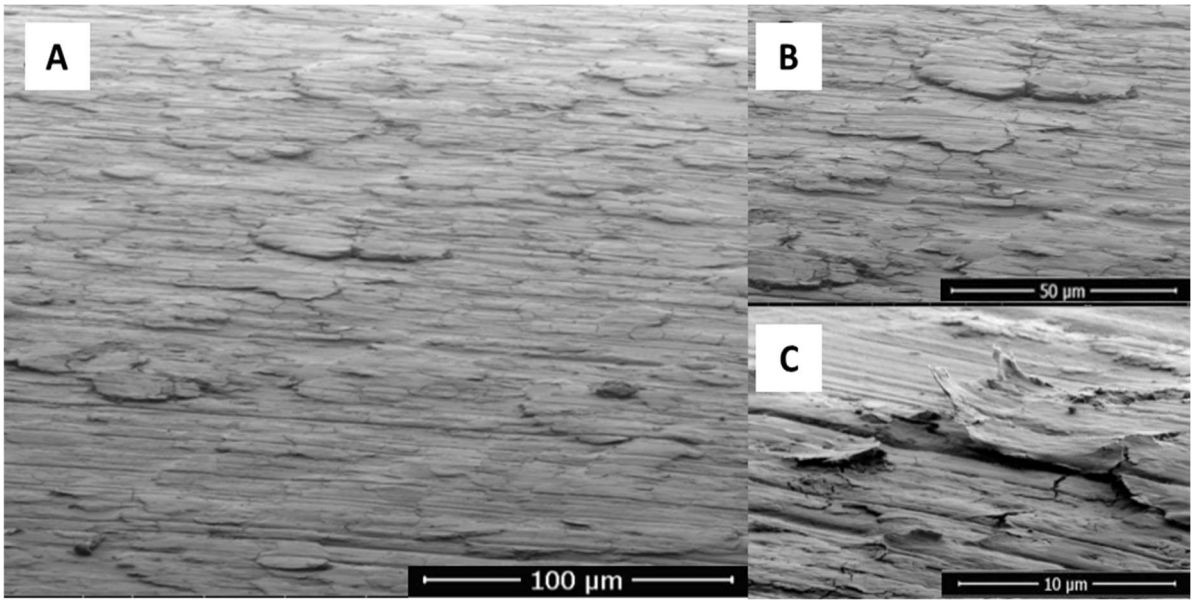

Figure 108: SEM micrographs of the Sintek PK10 pin tested against the uncoated AISI304 surface at 10 N load and 1.8 m/s sliding speed: low magnification (A), high magnification (B-C).

The pin has areas where the transfer-film is not perfectly adhered and tends to delaminate because the accumulation of plastic strain during continuous sliding.

EDS analysis suggests that, during the wear process, debris were released from the counter-surface, which is made evident by the Fe and Cr peaks on the sample (Figure 109).

The debris released by the counterpart is distributed over the entire pin surface and it particularly accumulates close to the PEEK particles, protruding from the PTFE matrix (Figure 109, spectra PK10_1 13 and PK10_1 15).

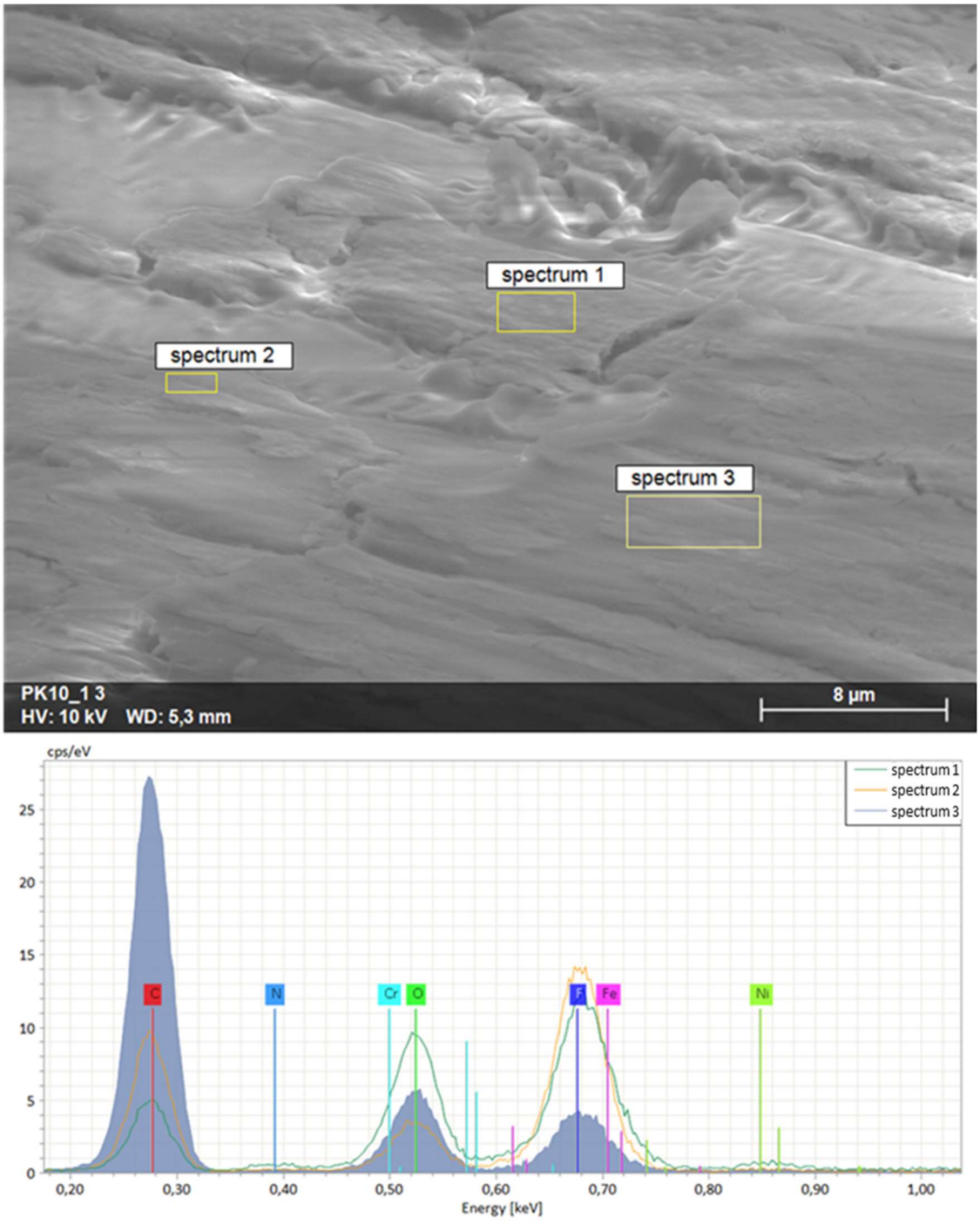

Figure 109 SEM micrograph of Sintek PK10 pin against AISI 304 surface, tested at 10N load and 1,8 m/s sliding speed and EDX spectra acquired on the pin surface.

Protruding PEEK particles are also seen on the surface of Sintek PK10 tested against the Chromia-coated disc. In this case the difference between PTFE and PEEK is sharper as the surface is not entirely covered by a transfer-film. To the contrary, most of the surface

is free of transfer material; the only traces of a tribofilm is visible next to the PEEK particles (Figure 110C)

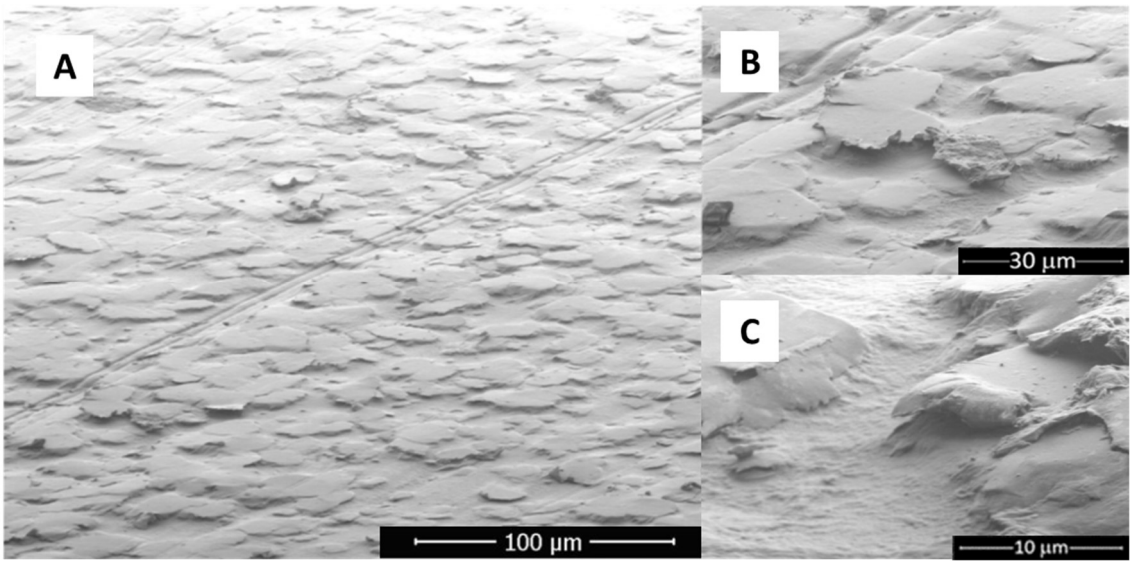

Figure 110: SEM micrographs of the Sintek PK10 pin against Chromia coated surface at 10N load and 1,8 m/s sliding speed at low magnification (A), high magnification (B-C).

The EDS analyses on pin surface showed that a very low amount of debris was released from the disc, as the peak of Cr is poorly visible and present only in the spectrum 1 in Figure 111.

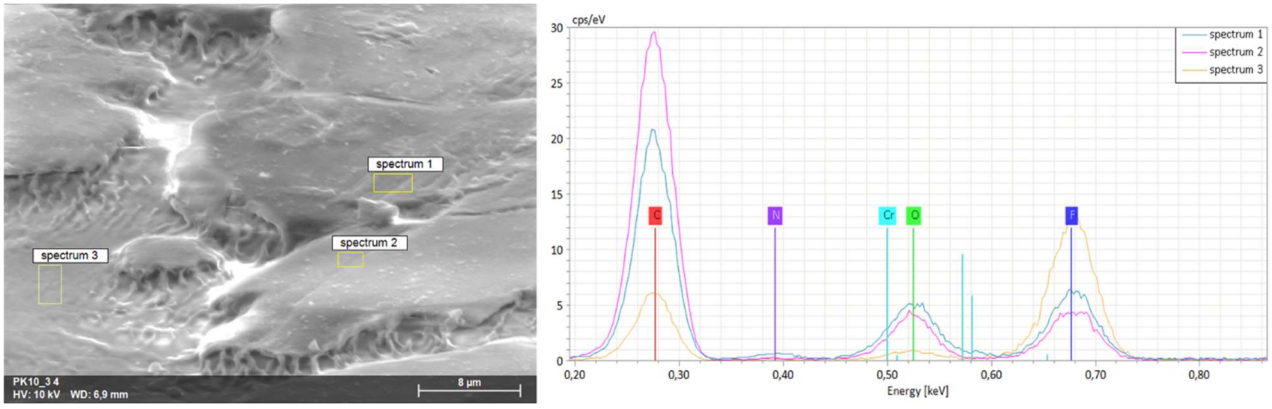

Figure 111: SEM micrograph of Sintek PK10 pin against Chromia coated surface, tested at 10N load and 1,8 m/s sliding speed and EDX spectra acquired on the pin surface.

The results of these analyses, compared with those of the PTFE composites reinforced with bronze, highlight the importance of metal debris (at least partially oxidized) released from the counter-surface and/or the filler for the formation of transfer-film. PTFE composites reinforced with bronze formed a discontinuous transfer-film containing oxidized particles of bronze as well as PTFE debris even in the tests against the Chromia

coated surface, where there is no substantial contribution of wear debris from the counterpart. PTFE composites reinforced with PEEK do not form the transfer-film due to the absence of any source of metal debris particles, whereas a film, albeit rather thin, was formed when these composites were tested against the stainless-steel surface.

This is confirmed by the EDS analyses carried out on the discs (Figure 112).

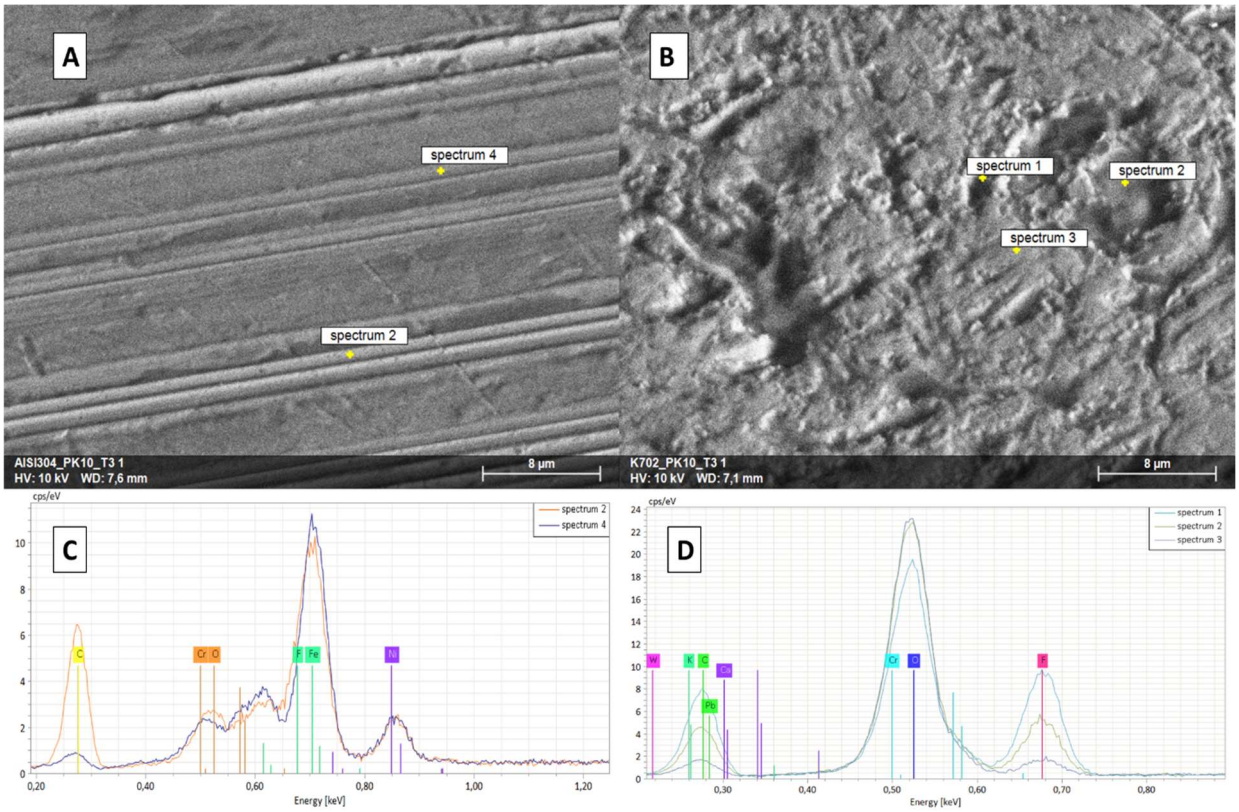

Figure 112: SEM micrographs of the stainless steel AISI 304disc surface (A) and relative EDX spectra (C), of the Chromia coated surface (B) and relative EDX spectra (D). Both surfaces were studied against Sintek PK10.

The AISI 304 disc (Figure 112A) is covered by a very thin transfer-film layer, evenly distributed on the entire surface. A compact transfer-film forms when the operating speed is low (0.54 m/s), and its formation is promoted by the particles, which are not ejected during sliding.

The Chromia coated surface (Figure 112B) shows the presence of debris within the open pores, characteristics of the disc, while a compact layer was not formed on the outer surface. This may again be due to a lower affinity of PTFE and/or PEEK debris with the Chromia coating and could explain the higher specific wear rates of this composite against the coated disc, compared to the uncoated one.

Another possible explanation of the high wear rate of the PTFE composite against the Chromia is related to the bad thermal conductivity of the tribological system. Both polymer and disc are made of two thermally insulating materials. During the sliding the polymer chains, failing to dissipate the heat in the contact area, might degrade, this might result in a release of debris from the sample. However, temperature measurements would not support this hypothesis.

The debris released during the contact with the stainless-steel disc (Figure 113A) contains some blocky particles and very fine debris. The former might have been formed due to adhesive wear in the early stages; however, the much smaller size of this debris is consistent with the lower wear rate and the absence of an initial friction peak. Adhesive wear is therefore much less severe, and the wear mechanism readily transitions to dominant tribo-oxidation. Against the Chromia coated surface (Figure 113B), the characteristic elongated shape of a polymer chip. Like the bronze-filled samples, the PTFE+PEEK composites were subjected to abrasive cutting by the sharp-edged pore boundaries of the chromia coating, producing the observed chips. Whilst the effect tends to fade as the test proceeds, as the released PTFE debris will gradually fill the pores, it explains why the wear loss, in this case, is more similar to the bronze-filled sample and higher than it is against uncoated steel.

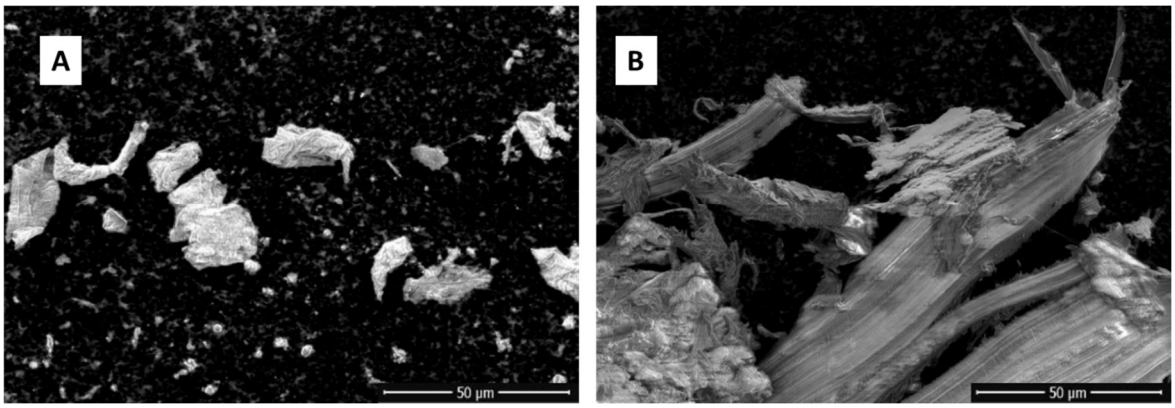

Figure 113: SEM micrographs showing loose debris collected after a pin-on-disc test of the Sintek PK10 pin slid against AISI 304 disc (A) and Chromia coated surface (B) at 10 N load, 1.8 m/s speed.

Therefore, the morphology of the particles is strictly dependent on the type of counterpart.

3.4.6 Sintek PK20

3.4.6.1 Sintek PK20 against AISI 304

The friction coefficient of Sintek PK20 against uncoated steel (Figure 114) at 1.8 m/s sliding speed maintains a stable value throughout the test, reaching the steady state already after a few cycles and a maximum value of 0.3. The trend is therefore the same as for Sintek PK10, albeit with higher friction values.

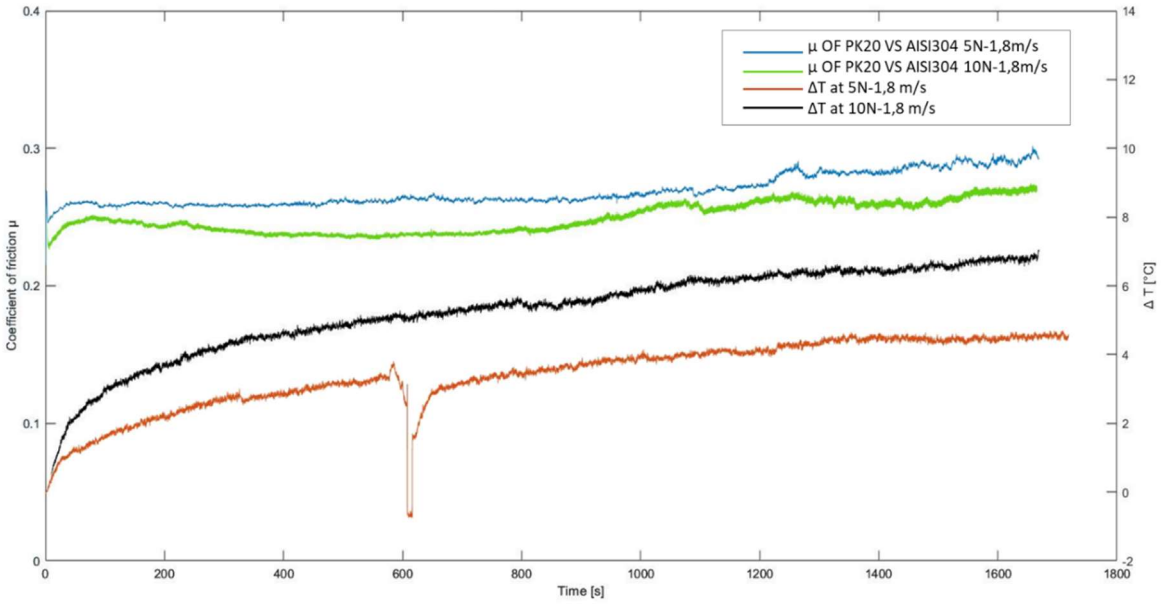

Figure 114: Friction coefficient and temperature rise curves for Sintek PK20 tested against uncoated AISI 304 at 1.8 m/s sliding speed and under both load conditions (5 N-10 N).

At 0.54 m/s the friction coefficient also keeps rather stable, like it happens at 1.8 m/s sliding speed, but values are significantly lower, around 0.22 (Figure 115).

Once again, temperatures do not increase by more than a few °C, with the highest rise being less than 8 °C at 10 N, 1.8 m/s.

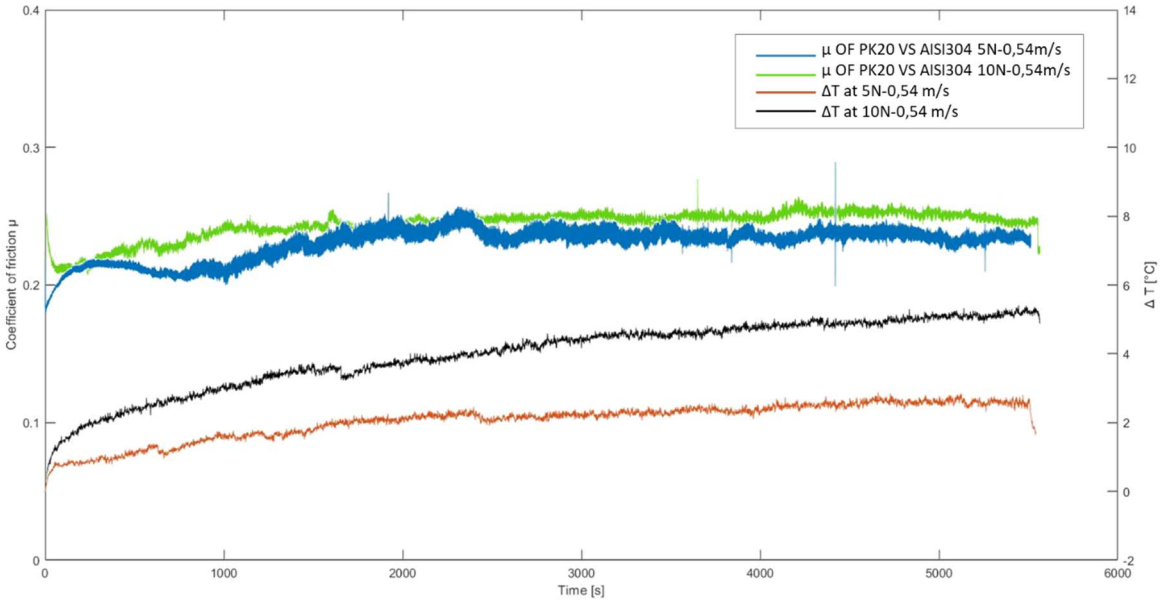

Figure 115: Friction coefficient and temperature rise curves for Sintek PK20 tested against uncoated AISI 304 at 0.54 m/s sliding speed and under both load conditions (5 N-10 N).

3.4.6.2 Sintek PK20 against Chromia

The friction coefficient of Sintek PK20 against the Chromia coated surface at 1.8 m/s sliding speed (Figure 116) is a little bit higher than at 0.54 m/s (Figure 117), showing a "flatter" curve.

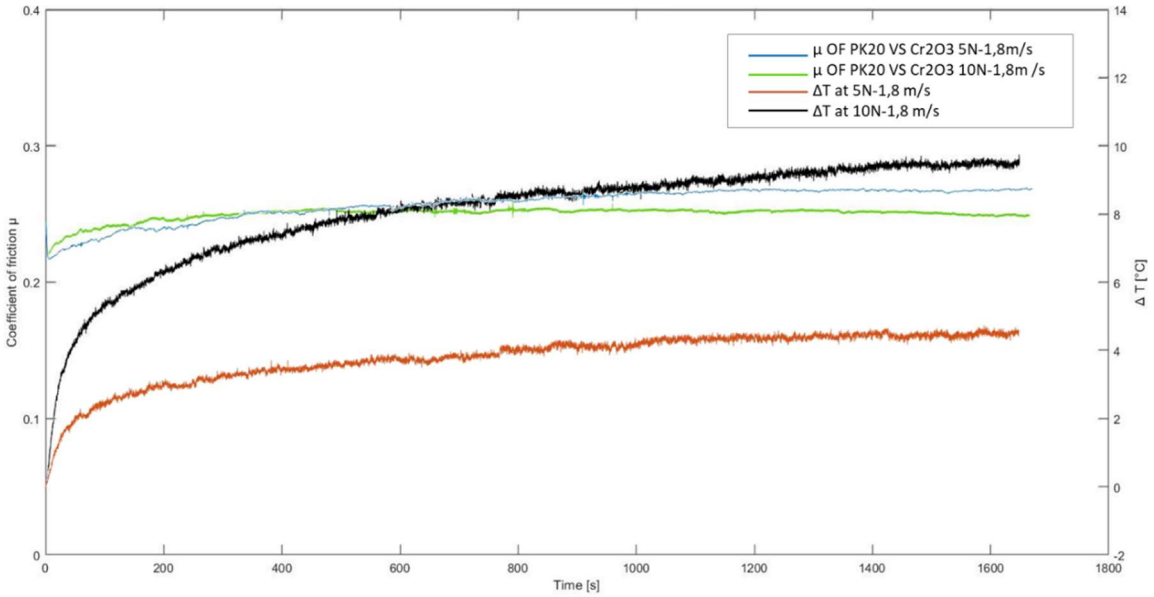

Figure 116: Friction coefficient and temperature rise curves of Sintek PK20 against Chromia coated surface at 1,8 m/s sliding speed and both load conditions (5N-10N).

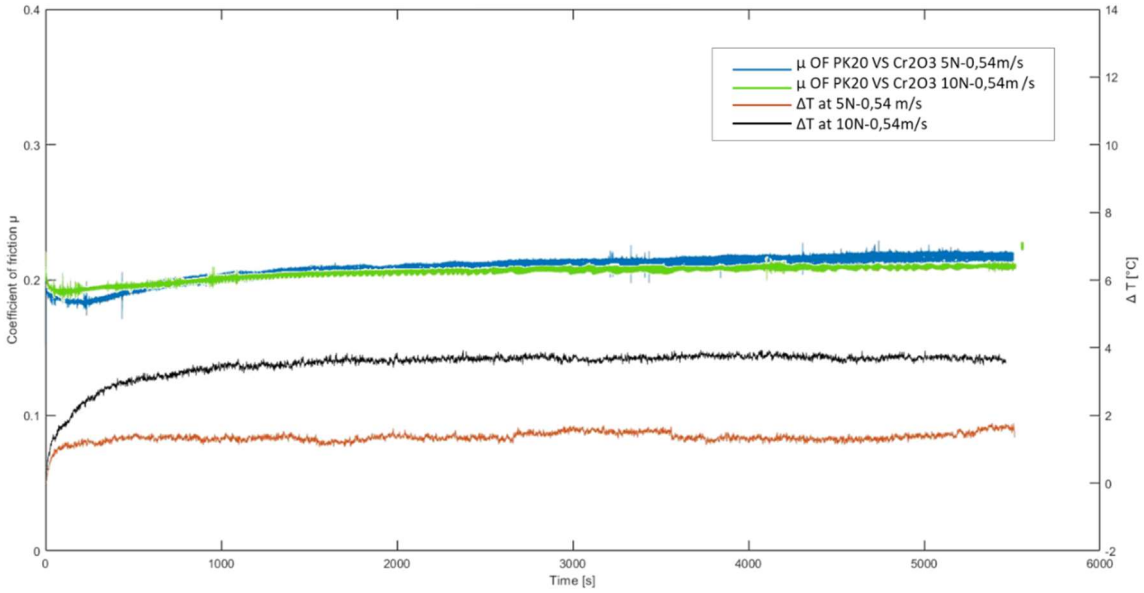

Figure 117: Friction coefficient and temperature rise curves of Sintek PK20 against Chromia coated surface at 0,54 m/s sliding speed and both load conditions (5N-10N).

Figure 118 confirms that measured rises follow the same trend that is predicted by theoretical bulk temperature rises (empty dots) calculated according to Ashby et al.'s model, although the experimental values are lower by a few °C because the measurement was not made exactly on the contact surface, and because of convective cooling of the outer surface. Thus, all considerations put forward in Section 3.4.5.2 concerning the relevant role of the high-friction stage at the beginning of the tests with bronze-filled composites in raising the contact temperature even above the theoretical prediction (a phenomenon that does not occur with PEEK-filled composites where such peak is systematically absent) are confirmed.

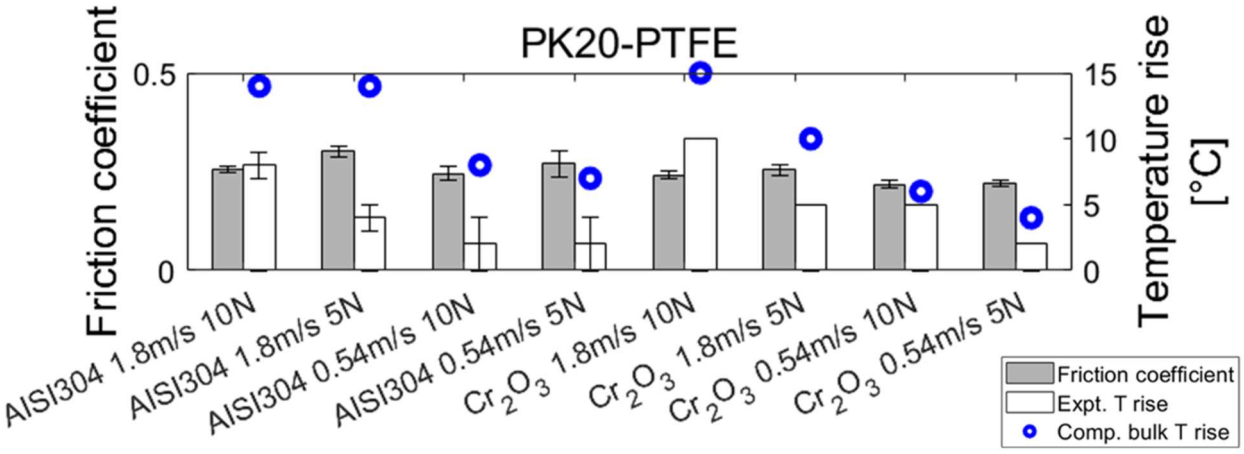

Figure 118: Average steady-state friction coefficient and maximum temperature rise in Sintek PK20 pin on disc tests.

3.4.6.3 Wear mechanism of Sintek PK20

The wear rates of Sintek PK20 against the AISI 304 disc are generally slightly lower than the corresponding values for Sintek PK10, indicating a favourable effect of increasing filler content. Values are systematically lower at 5 N load, regardless of the sliding speed, which means that, with 20 wt.% PEEK, the dependence of wear rate against steel on velocity is mostly suppressed, different from all other particle-reinforced samples examined previously. Wear rates against the chromia-coated disc are also largely independent of test conditions, and slightly lower than they were for the Sintek PK10 samples.

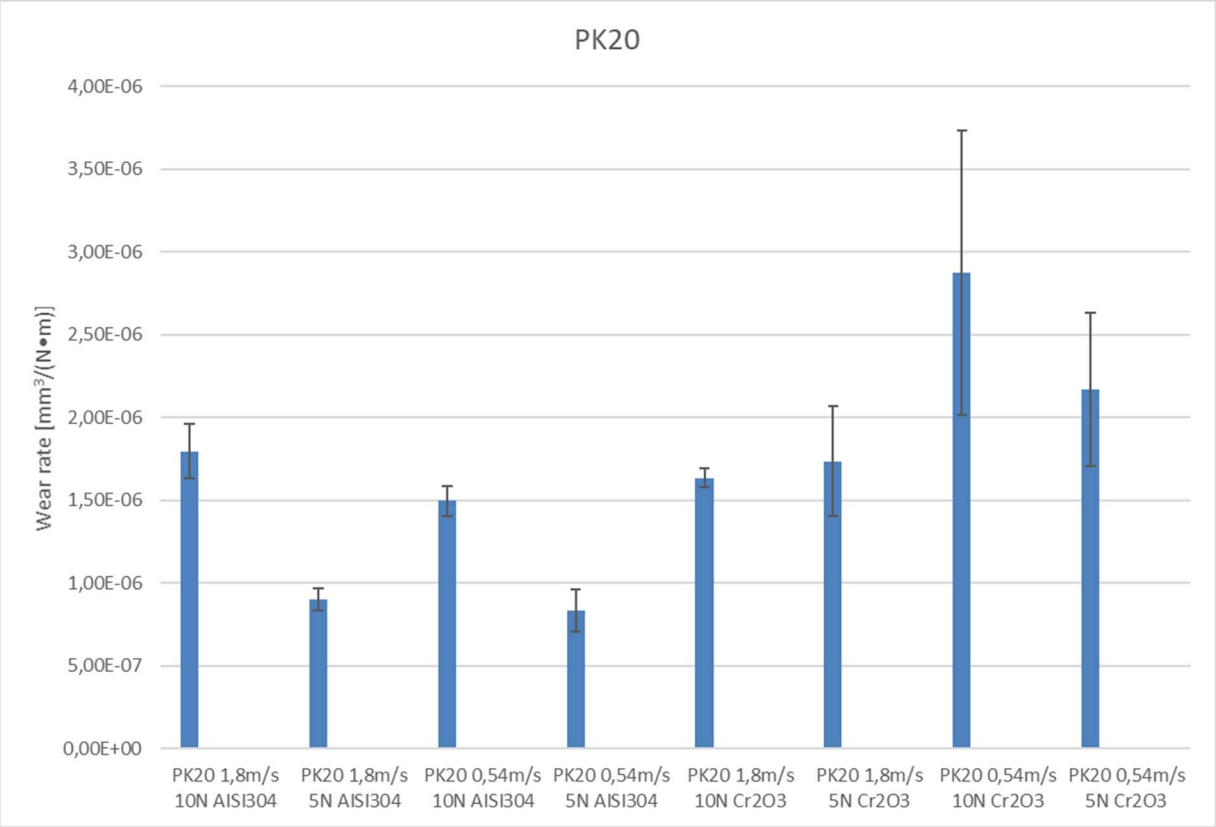

Figure 119: Wear rate and friction coefficient of Sintek PK20 against AISI 304 and Chromia coated surfaces under different test conditions.

The pin surface after testing against the AISI304 disc shows more frequent ridges than were found on the Sintek PK10 sample, due to the higher amount of filler inside the composite. A transfer-film still covers the entire surface but undergoes a periodic cracking and delamination (Figure 120C), again reflecting a dominant tribochemical wear mechanism under steady-state conditions.

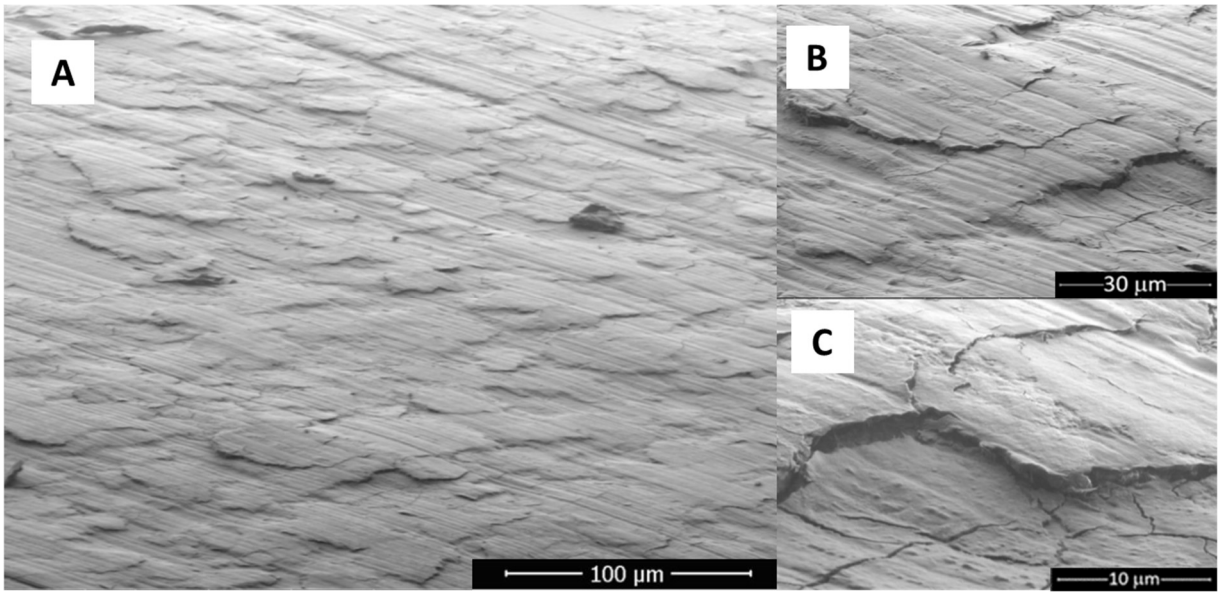

Figure 120: SEM micrographs of the Sintek PK20 pin against AISI304 surface at 10N load and 1,8 m/s sliding speed at low magnification (A), high magnification (B-C).

EDS analysis on the pin surface against AISI 304 disc has shown, in correspondence of the ridges, a mixed composition of well compacted debris released by the pin and the counter-surface: in fact, the peaks of Cr, Fe and Ni are visible (Figure 121, spectra 1 and 2). Spectrum 3, corresponding to a valley on the surface, is mainly characterized by PTFE (highlighted by the Fluorine peak), with smaller detectable amounts of Fe and Cr.

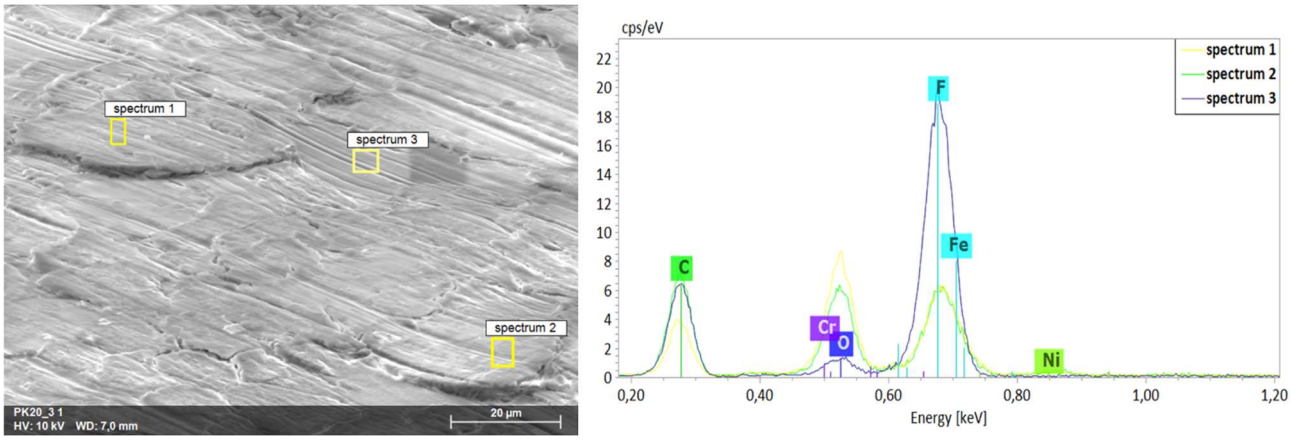

Figure 121: SEM micrograph of Sintek PK20 pin against AISI 304 surface, tested at 10N load and 1,8 m/s sliding speed and EDX spectra acquired on the pin surface.

The analysis of the cross-section of the pin against AISI 304 confirm the formation of a transfer film, albeit not continuous, which can reach a maximum thickness of 2 µm (Figure 122A). There are also areas along the wear surface where PEEK particles are increasingly protruding as the surrounding PTFE matrix is worn (Figure 122B). The transfer-film is formed close to these protrusions, as previously noted.

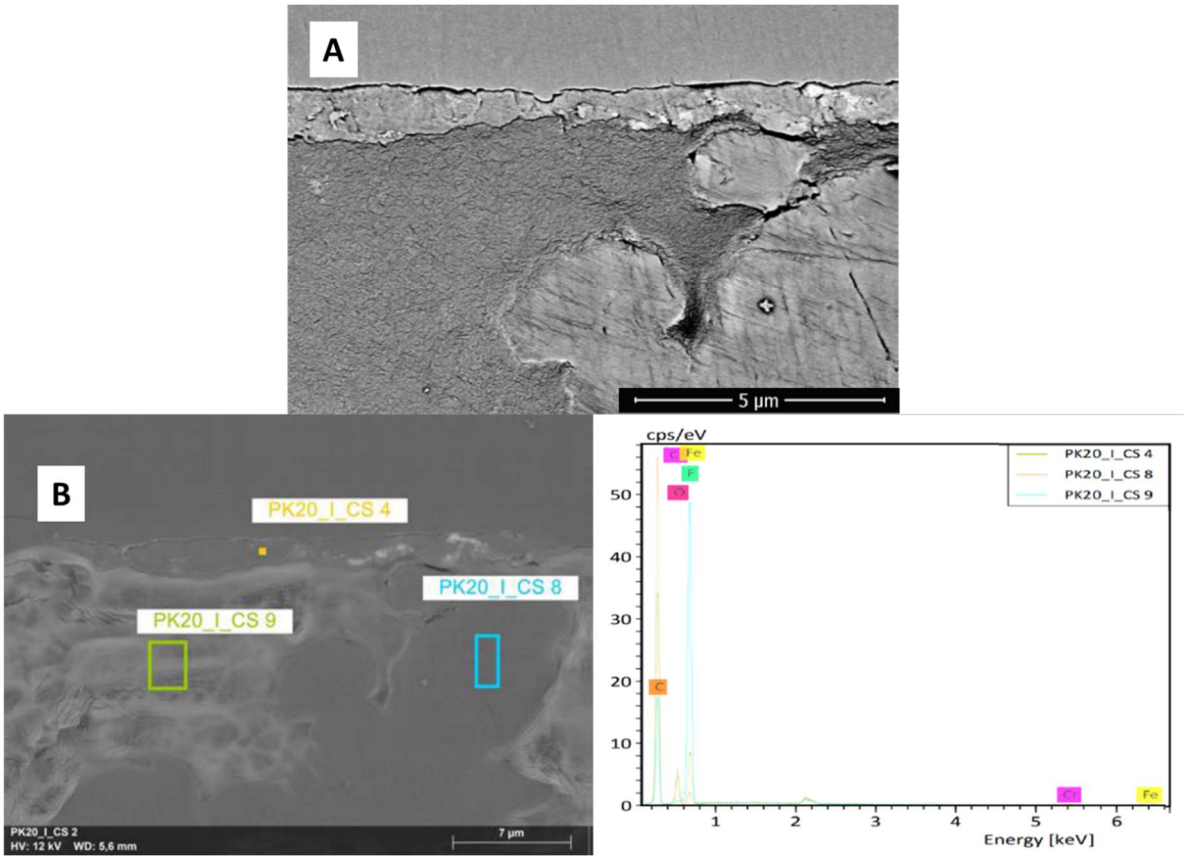

Figure 122: SEM micrographs of the cross-section of the Sintek PK20 pin tested at 10 N load and 0.54 m/s against AISI 304, acquired at 3 kV (A) and 12 kV (B).

As previously observed for Sintek PK10, the worn surface of the pin against the Chromia coated surface is not covered by a transfer-film layer, thus making the difference between the protruding PEEK particles and the PTFE matrix even more visible. Emerging PEEK particles are the areas around which small accumulations of debris are created, but they do not form a compact transfer-film (Figure 123C).

EDS analyses on the pin surface confirm that the ridges, with a more intense Oxygen signal and a weak Fluorine signal (Figure 124, spectra 1 and 2), consist of PEEK, only partially covered by PTFE- debris, which instead have accumulated more in correspondence to the valleys (Figure 124,spectrum 3). Finally, in this case the transfer-film is not evenly distributed on the pin surface and Chromium signals, related to debris released from the counter-surface, are only sporadically present.

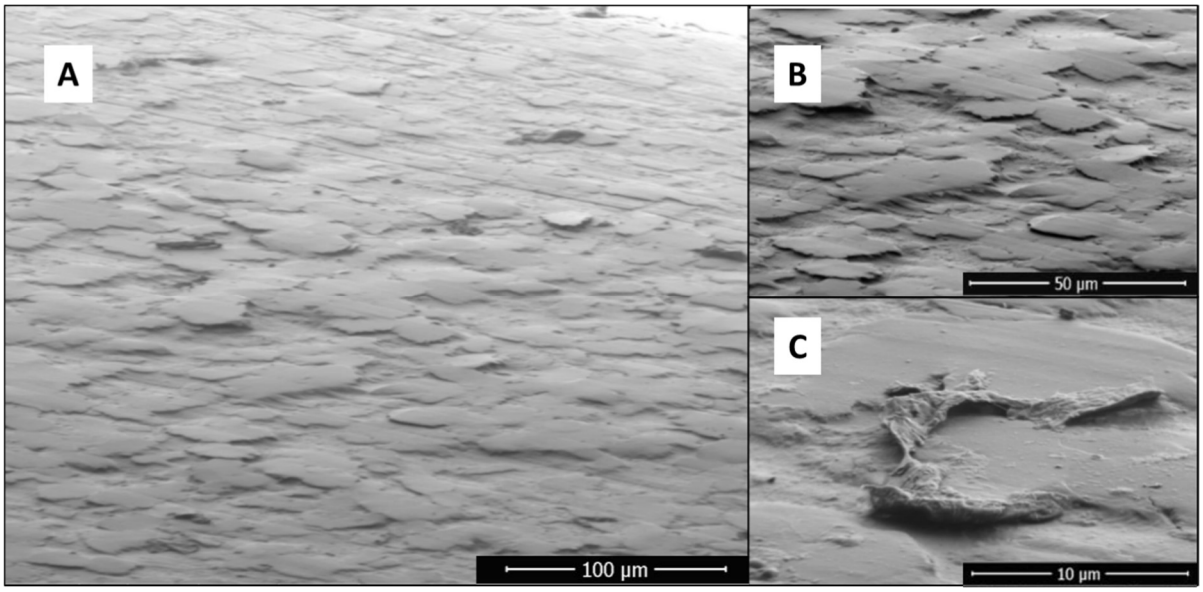

Figure 123: SEM micrographs of the Sintek PK20 pin against Chromia coated surface at 10N load and 1,8 m/s sliding speed at low magnification (A), high magnification (B-C).

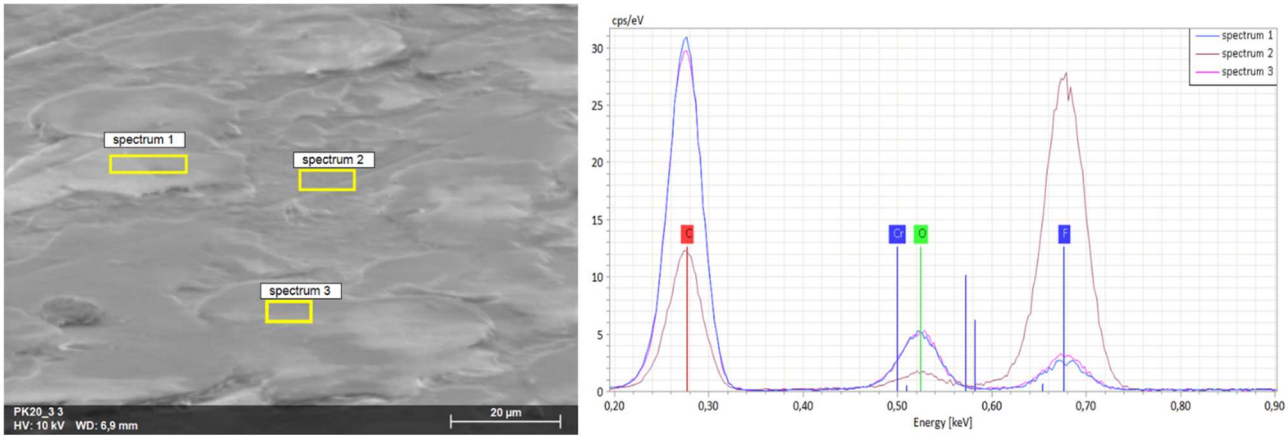

Figure 124: SEM micrograph of Sintek PK20 pin against Chromia coated surface, tested at 10N load and 1,8 m/s sliding speed and EDX spectra acquired on the pin surface.

EDS analyses on both coated and uncoated surfaces demonstrated no clear wear and tear signs and showed irregularly distributed debris: probably because of the higher relative fraction of PEEK on the worn surface of the pin, a continuous layer of transfer-film has not been formed in either case (Figure 125A,B). PEEK is indeed known not to have the same ability as PTFE to form tribofilms on mating surfaces. Particle agglomerations with random size did not consolidate in a compact layer and showed a non-perfect adhesion to the substrate, partially detaching from it.

On the Chromia coated surface, in particular, debris clusters tends to be retained in the open porosities (Figure 125B): this is also confirmed by the cross-section analysis of the disc (Figure 126, spectrum 1 corresponds to a debris-filled pore where an intense F peak is identifiable).

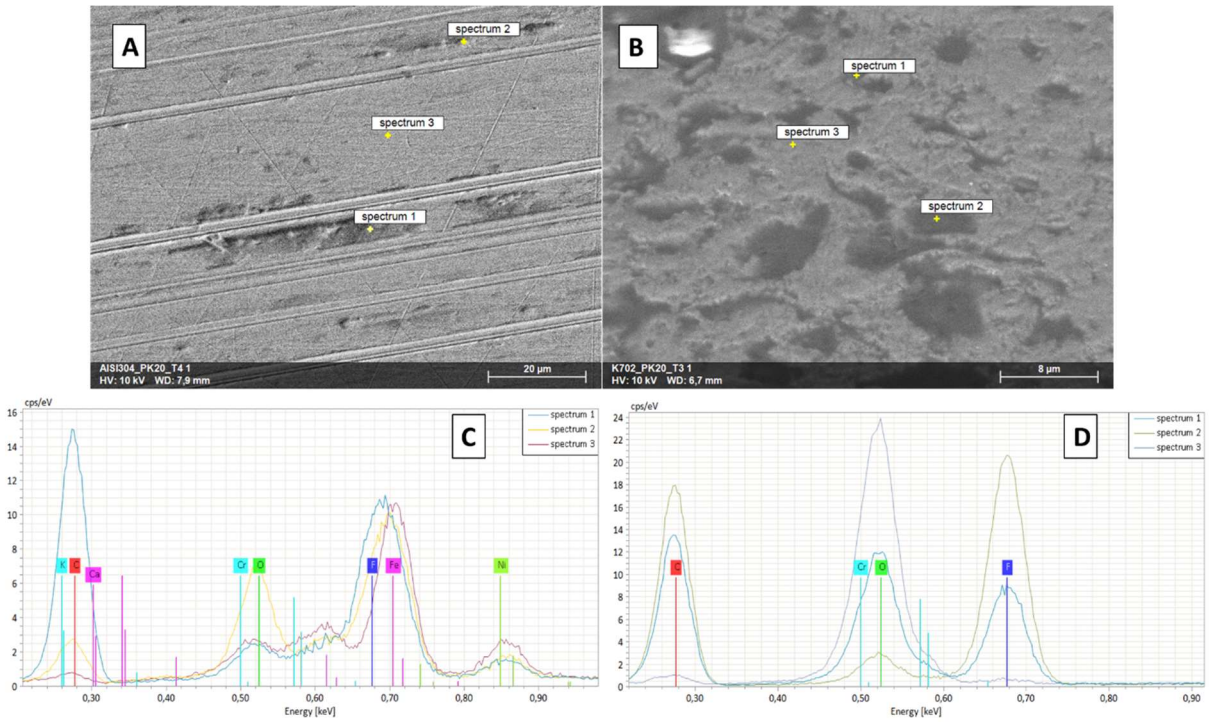

Figure 125: SEM micrographs of the AISI 304 stainless steel disc surface (A) and corresponding EDX spectra (C), of the Chromia coated surface (B) and corresponding EDX spectra (D). Both surfaces were studied after the tribological tests against Sintek PK20 at 10 N load, 1.8 m/s speed.

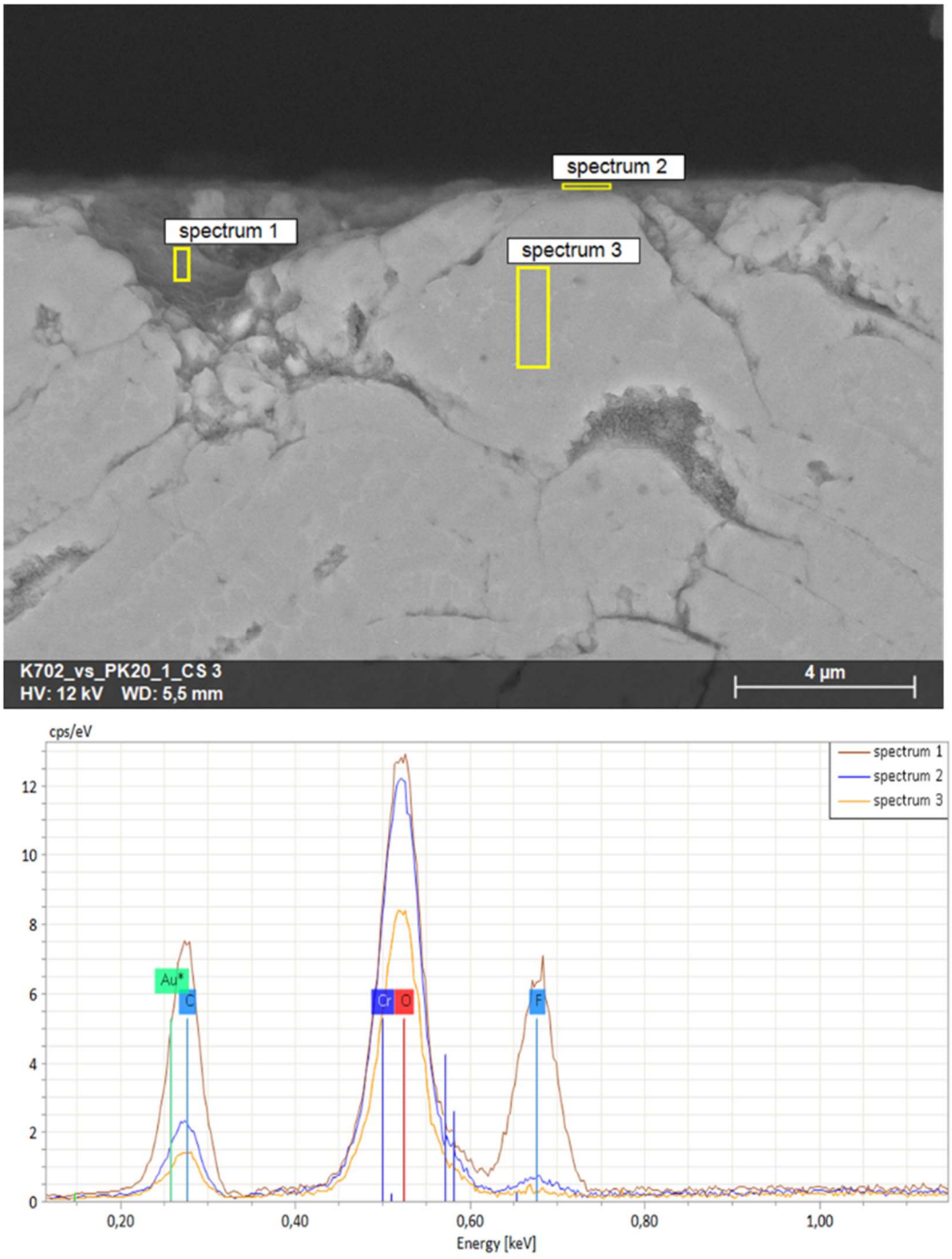

Figure 126: SEM micrograph and corresponding EDX spectra of the cross-section of the Chromia coated disc after test against Sintek PK20 at 10 N load, 0.54 m/s speed.

The morphological difference found on the worn disc surfaces against PTFE composites reinforced with PEEK, compared to tests against PTFE composites reinforced with bronze, is due to the different chemical nature of the filler and to the debris released by the latter: bronze particles release oxidized debris which are chemically similar to both uncoated and coated counter-surfaces. This phenomenon favours the formation of a continuous and compact transfer-film on the surface of the PTFE composites reinforced

with bronze. With samples containing PEEK, on the other hand, the transfer-film forms only when oxidized metal debris is released by the wear of the uncoated counter-surface. Figure 127 show the SEM pictures of debris released during the pin-on-disc test with both counter-surfaces. The debris generated from the contact with AISI 304 (Figure 127A) consists of fine particles, characteristic of the tribochemical, together with a few lamellar particles, probably corresponding to pulled-out PEEK particles. This again testifies to the limited occurrence of adhesive wear even in the early stages of the test. In particular, in this case, blocky debris indicative of adhesive wear cound not be found, consistent with the further decrease in wear rates compared to Sintek PK10. Against the Chromia coated surface (Figure 127B) the debris are jagged and elongated; probably the open porosity of the latter surface is still causing abrasive wear even with the Sintek PK20 pin, explaining why its volume loss is higher than against stainless steel disc.

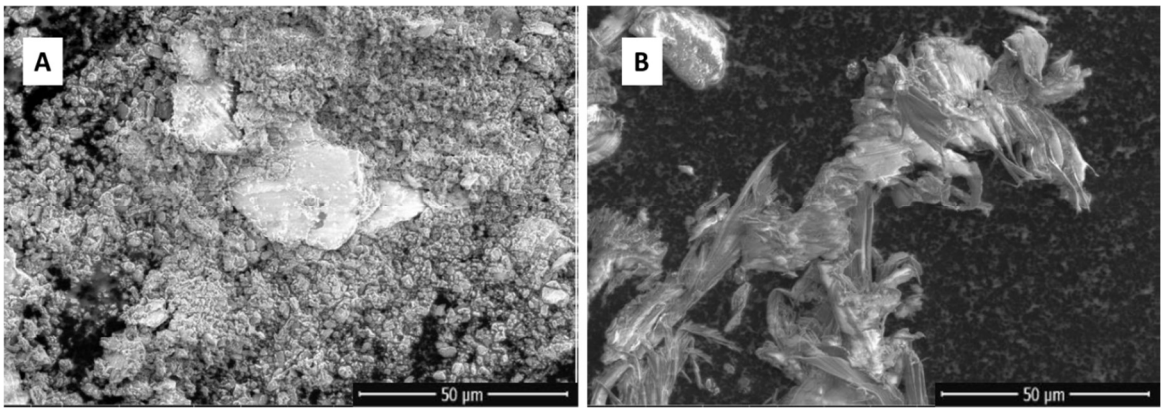

Figure 127: SEM micrographs showing loose debris collected after pin-on-disc tests of Sintek PK20 slid against the uncoated AISI 304 disc (A) and the Chromia coated surface (B) at 10 N load, 1.8 m/s speed.

3.5 FT-IR and Raman Analyses

To characterize the tribo-layer more comprehensively and to identify the functional groups on the worn pin surface, FT-IR analysis and micro-Raman spectroscopy were carried out, comparing the worn samples with untested (pristine) ones.

Whilst the FT-IR spectra of glass-fibre reinforced PTFE in pristine conditions only exhibit signal due to the PTFE matrix, with no contribution from the filler, the spectra acquired on worn surfaces under all the conditions examined (Figure 128, Figure 129, Figure 130, Figure 131) have additional peaks at 600 cm^{-1} and 970 cm^{-1}, assigned to O-Si-O and Si-O-Si vibrations [68], as well as an increasingly high background signal at low wavenumbers, typical of inorganic compounds and probably due to the debris

containing comminuted glass fibre fragments as well as oxidized stainless steel debris. A broad band at 3000 – 3600 cm^{-1} belongs to adsorbed water molecules [68]. The broad peak around 1660 cm^{-1} can be assigned to -OH groups adsorbed on the surface of the glass debris [68] and/or to carboxylate groups, because of partial oxidation of the PTFE molecules [69].

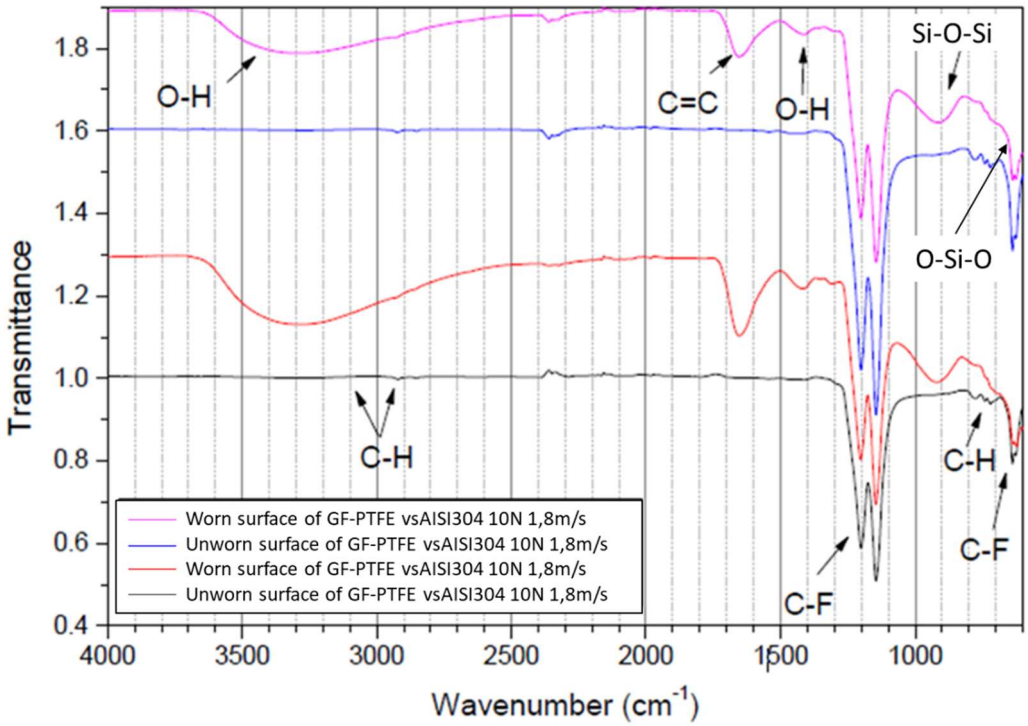

Figure 128: Comparison of FT-IR spectra of GF-PTFE before and after pin-on-disc tests against the uncoated AISI 304 surface, at 10 N load and 1.8 m/s sliding speed.

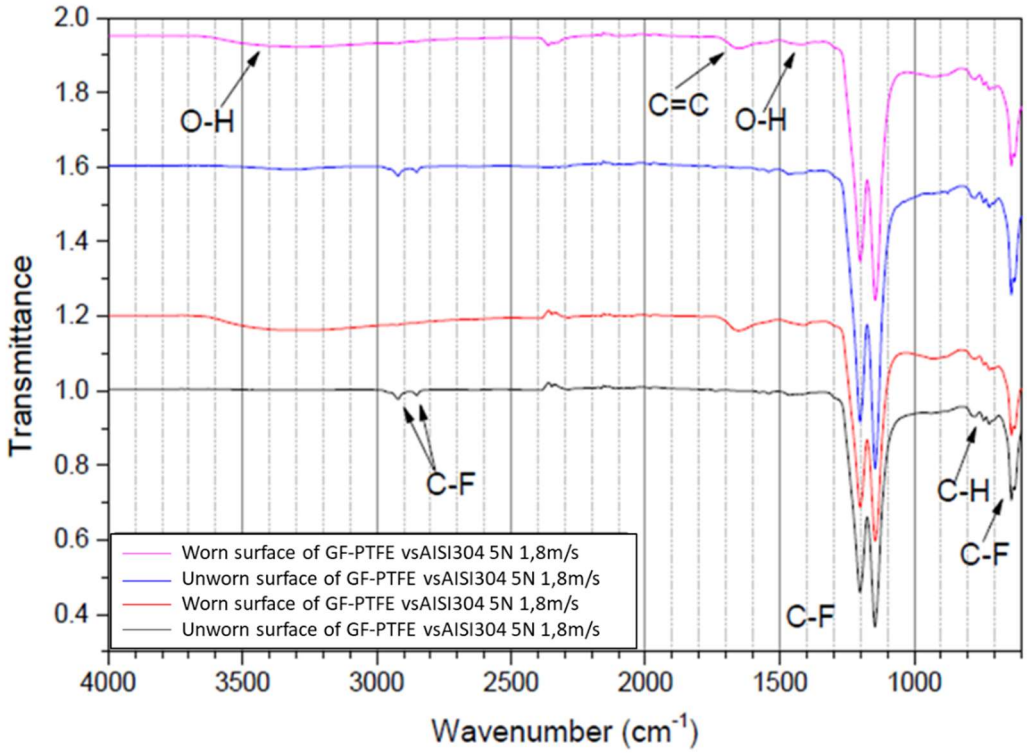

Figure 129: Comparison of FT-IR spectra of GF-PTFE before and after pin-on-disc tests against the uncoated AISI 304 surface, at 5 N load and 1.8 m/s sliding speed.

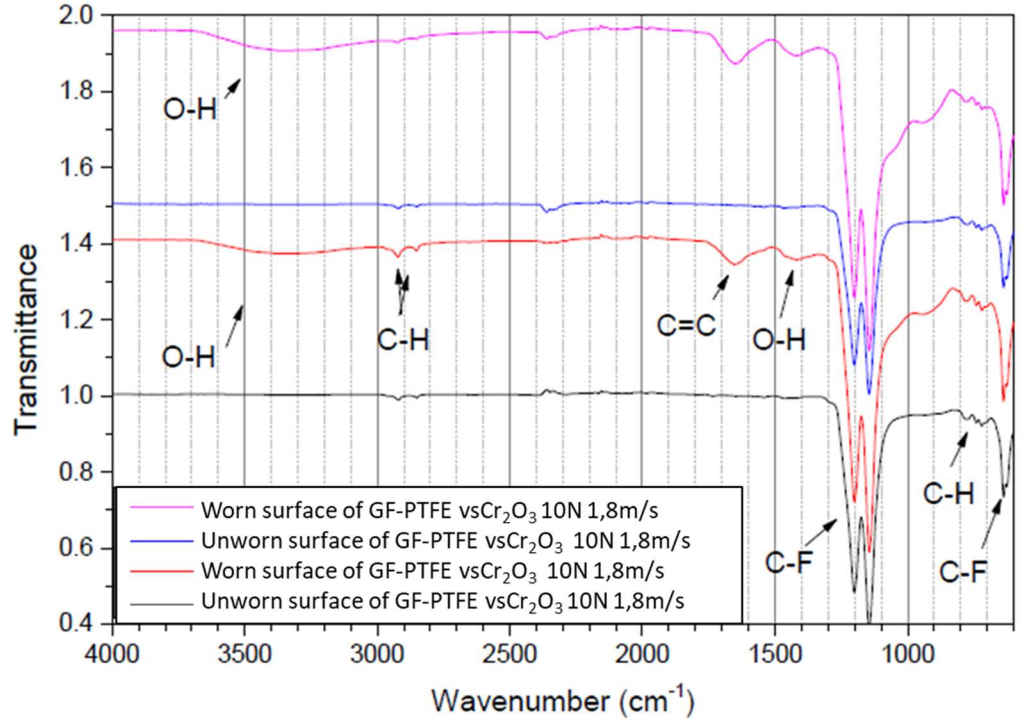

Figure 130: Comparison of FT-IR spectra of GF-PTFE before and after pin-on-disc tests against the Chromia coated surface at 10 N load and 1.8 m/s sliding speed.

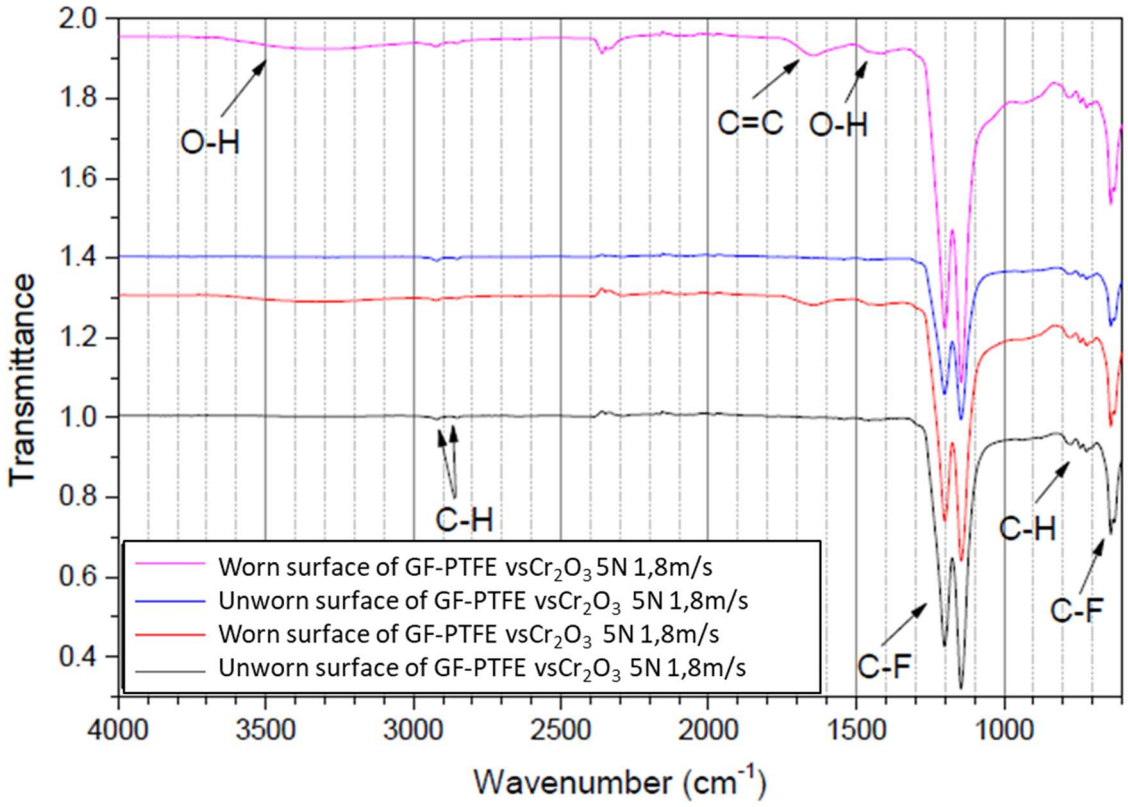

Figure 131: Comparison of FT-IR spectra of GF-PTFE before and after pin-on-disc tests against the Chromia coated surface at 5 N load and 1.8 m/s sliding speed.

The FTIR spectra of worn CF-PTFE samples do not show any of the additional signals previously discussed for worn GF-PTFE, which is consistent with the reduced or absent coverage by a tribo-layer.

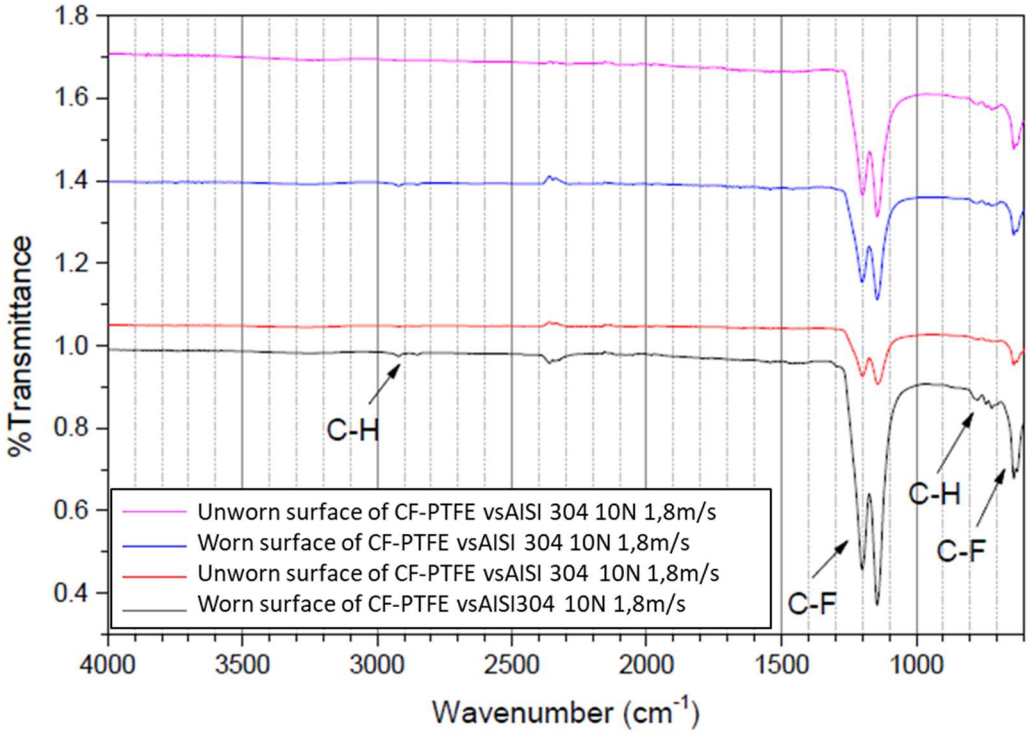

Figure 132: Comparison of FT-IR spectra of CF-PTFE before and after pin-on-disc tests against the uncoated AISI 304 surface, at 10 N load and 1.8 m/s sliding speed.

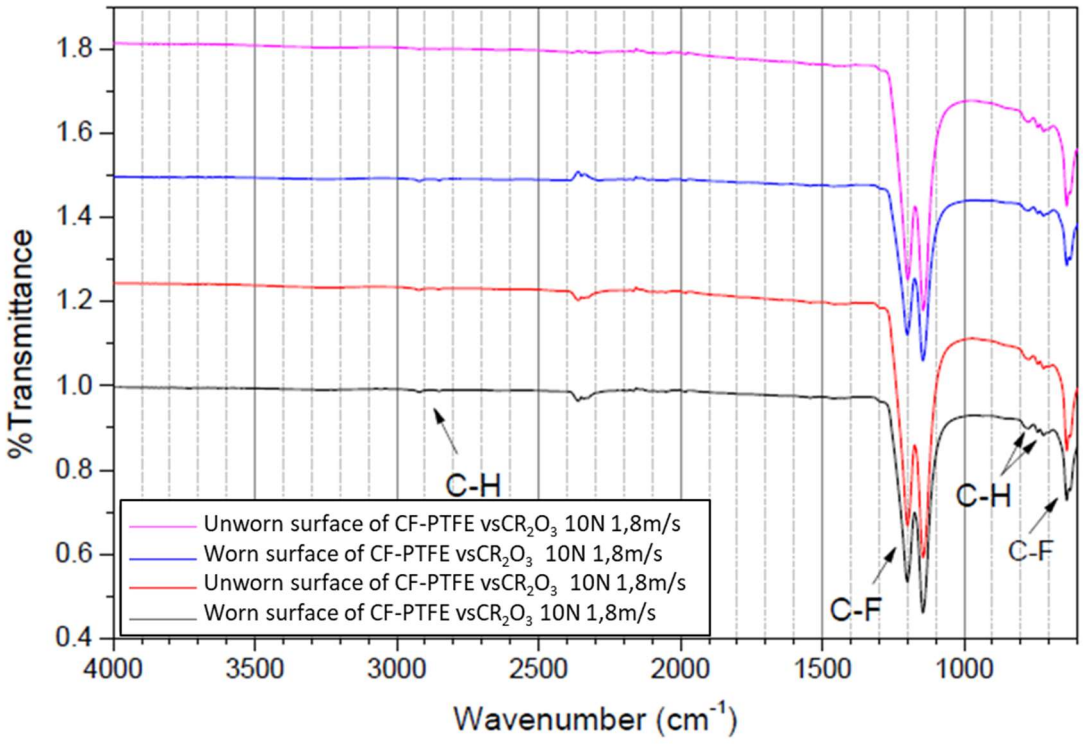

Figure 133: Comparison of FT-IR spectra of CF-PTFE before and after pin-on-disc tests against Chromia coated surface, at 10 N load and 1.8 m/s sliding speed.

PTFE composites reinforced with bronze and PEEK also exhibit a band at 3000-3600 cm^{-1} and a peak around 1660 cm^{-1}, both of which grow more intense when the sample is more uniformly covered by a tribofilm, as it is the case especially for pins tested against the stainless-steel counterpart, and for bronze-filled pins in comparison to PEEK-filled pins. As mentioned above, the 3000-3600 cm^{-1} band is representative of the -OH groups related to the moisture. It is therefore deduced that the adsorption of moisture from the environment occurs whenever the debris contains fine oxide-based particles, coming either from tribo-oxidation of metallic debris from the counterpart, or from the filler itself (glass fragments or tribo-oxidized bronze debris), and this adsorption plays a key role in favouring the bond between the particles, ensuring a more compact and homogeneous transfer-film. This is systematically associated with lower friction, though not always with lower wear.

In spectra acquired on worn composites reinforced with bronze (Figure 134, Figure 135), moreover, there is the same background signal previously seen with woth GF-PTFE composites: the transmittance tends to decrease towards the lowest wavenumbers because of the oxides produced by tribo-oxidation of debris from both bronze particles and the stainless-steel disc.

In the composites reinforced with PEEK (Figure 136, Figure 137), additional bands appear due to PEEK. Specifically, the absorption related to the bonds of the aromatic chains is visible at 1600-1585 cm^{-1} and 1500 - 1400 cm^{-1}: these grow more intense in the worn samples than the untested ones, reflecting the protrusion of PEEK particles out of the worn PTFE matrix as noted repeatedly in Sections 3.4.5 and 3.4.6.

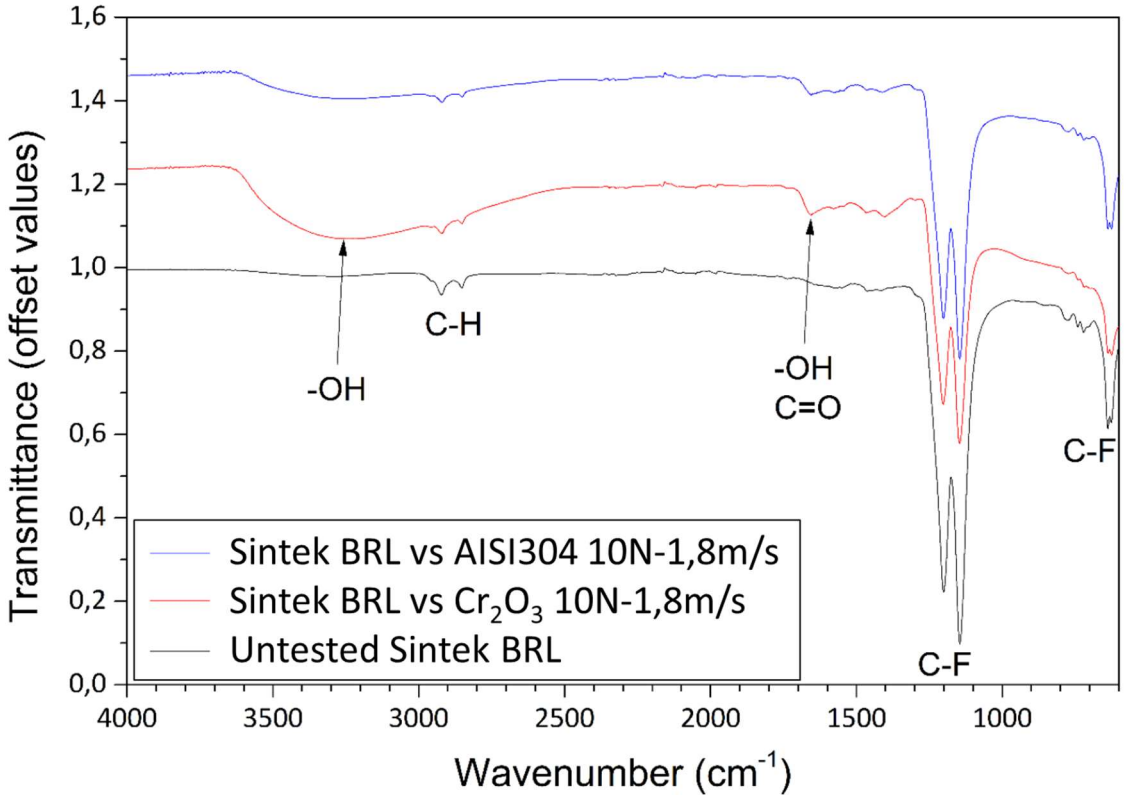

Figure 134: FT-IR spectra of Sintek BRL before and after pin-on-disc testing.

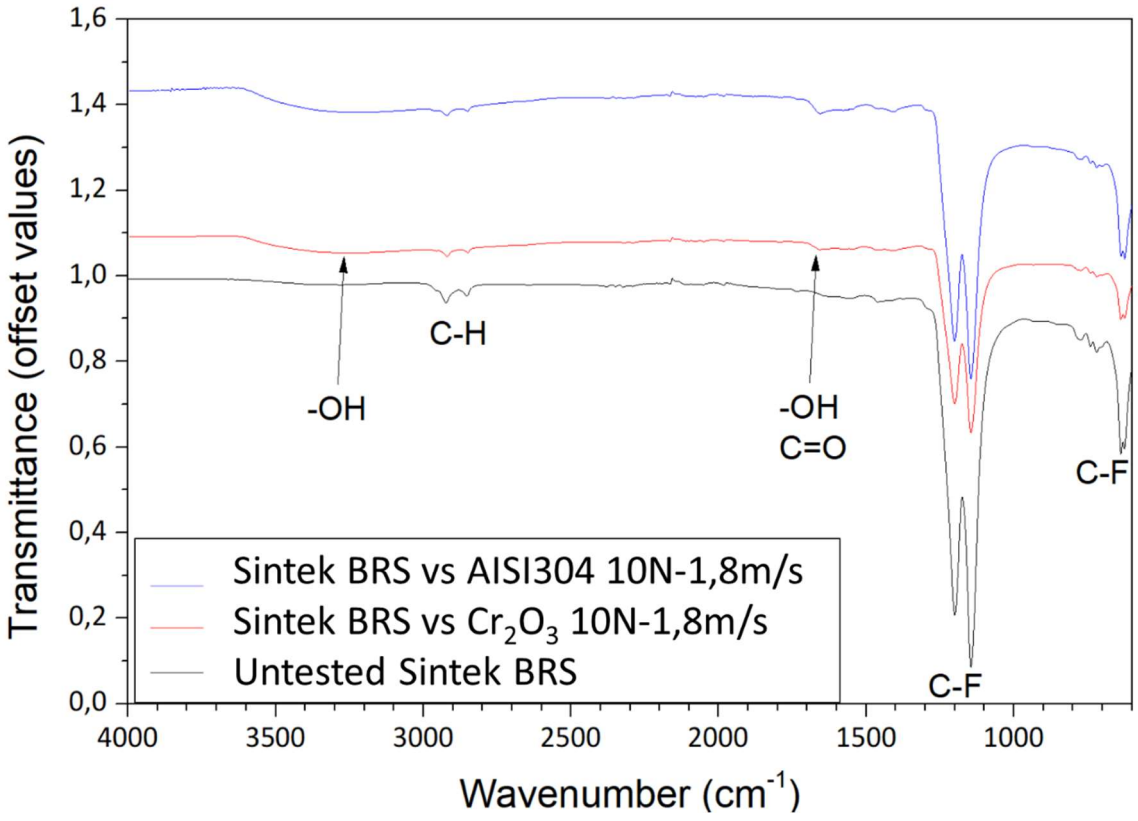

Figure 135: FT-IR spectra of Sintek BRS before and after pin-on-disc testing.

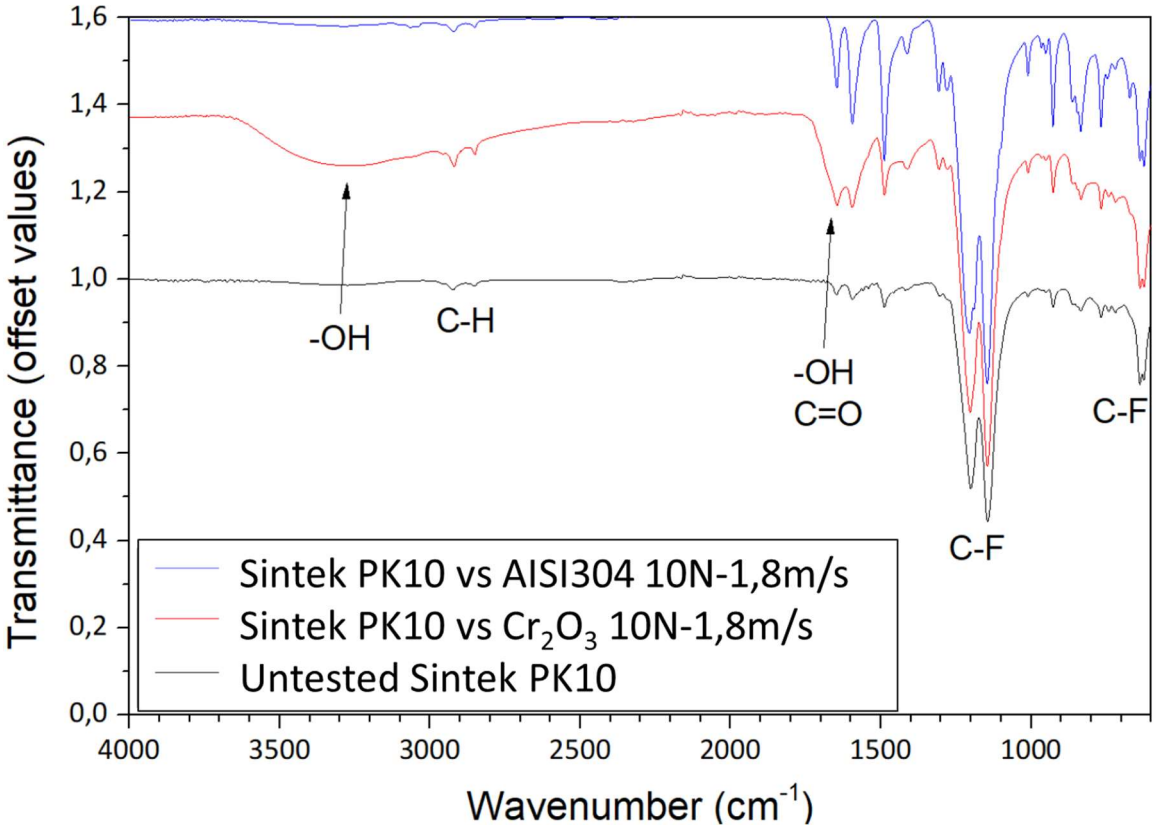

Figure 136: FT-IR spectra of Sintek PK10 before and after pin-on-disc testing.

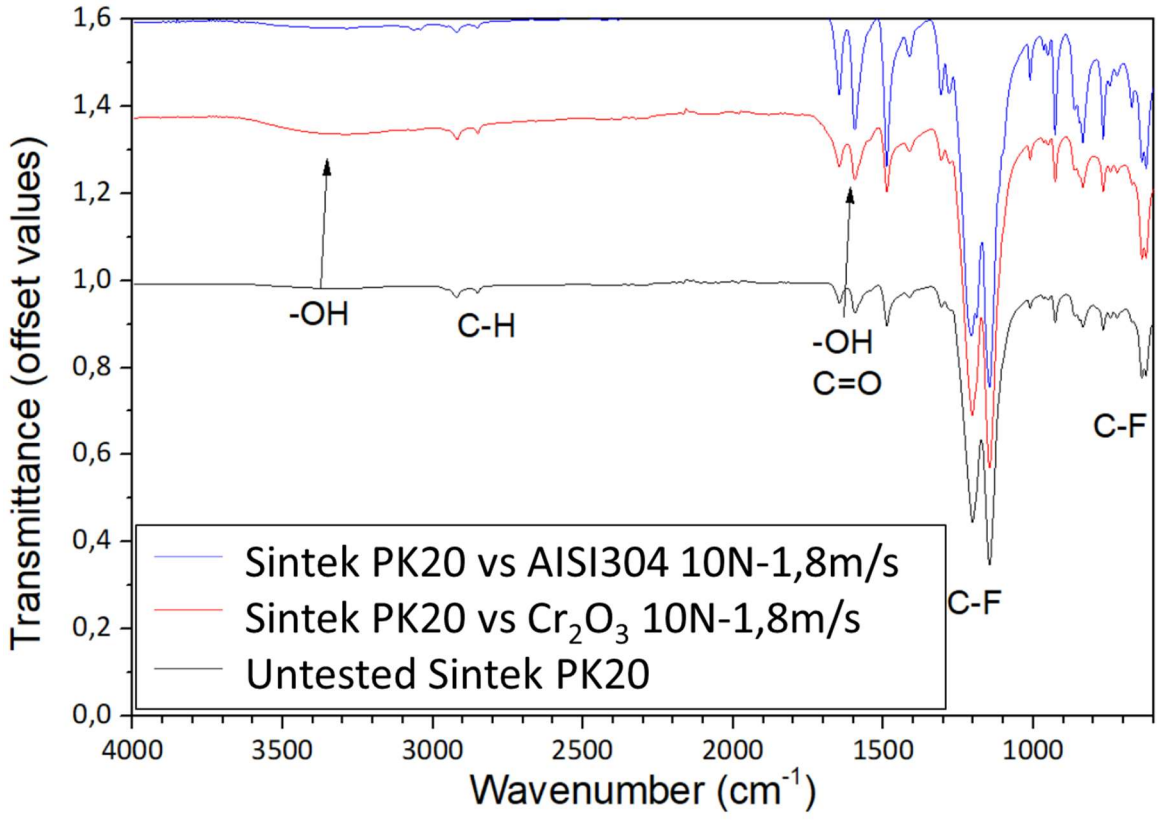

Figure 137: FT-IR spectra of Sintek PK20 before and after pin-on-disc testing.

In order to clarify the nature of the tribofilms developed on the GF-PTFE pins, micro-Raman spectra were acquired of the tribo-layer differ from the signal of pure PTFE, obtained from the unworn matrix, because they exhibit additional, weak and broad bands roughly located around 500 cm^{-1} and 1050 cm^{-1} (Figure 138). These are better highlighted by plotting the difference between the two spectra (see asterisks). Based on the literature [70], they can be assigned to the silicate glass debris, confirming its existence in the tribo-layer.

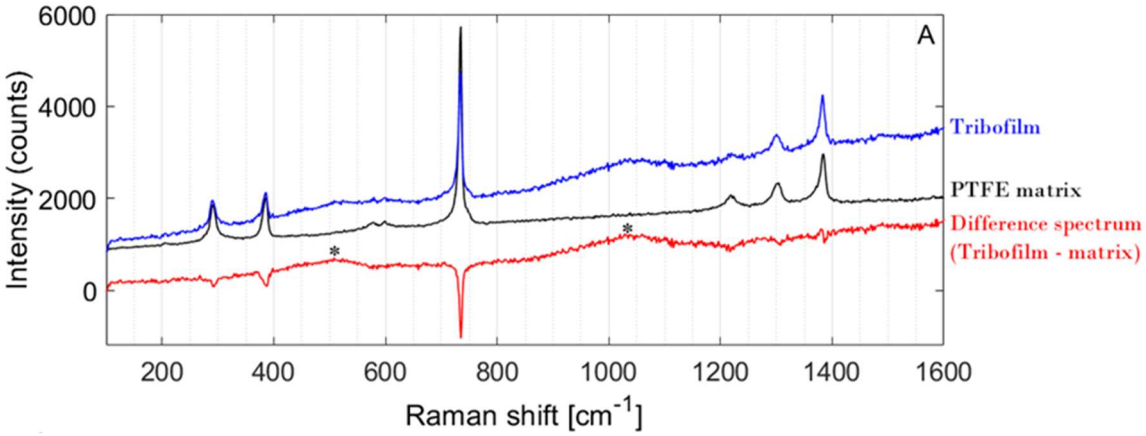

Figure 138: Micro-Raman spectra acquired on the unworn PTFE matrix and the tribo-layer on the GF-PTFE pin tested against uncoated AISI 304 at 10 N load, 1.8 m/s speed

In the case of bronze-filled composites, it is especially interesting to note that spectra acquired on the pin and on the stainless-steel counter-surface are clearly different (Figure 139). Spectra acquired on the disc are dominated by a band between 500 - 750 cm^{-1} related to the presence of mixed amorphous oxides [71], involving both bronze reinforcement elements and the counter-surface. Raman signal from PTFE is not detectable: whilst PTFE debris is certainly present, as testified by the presence of F signal in EDX spectra, its amount is probably insufficient to produce a discernible signal above the background caused by the amorphous oxides. To the contrary, the spectra acquired on the pin show a central peak at 734 cm^{-1} and secondary peaks at 1350/1400 cm^{-1} and at 300/400 cm^{-1} characteristic of PTFE and, therefore, indicative of the larger amount of PTFE in the tribofilm attached to the pin [72].

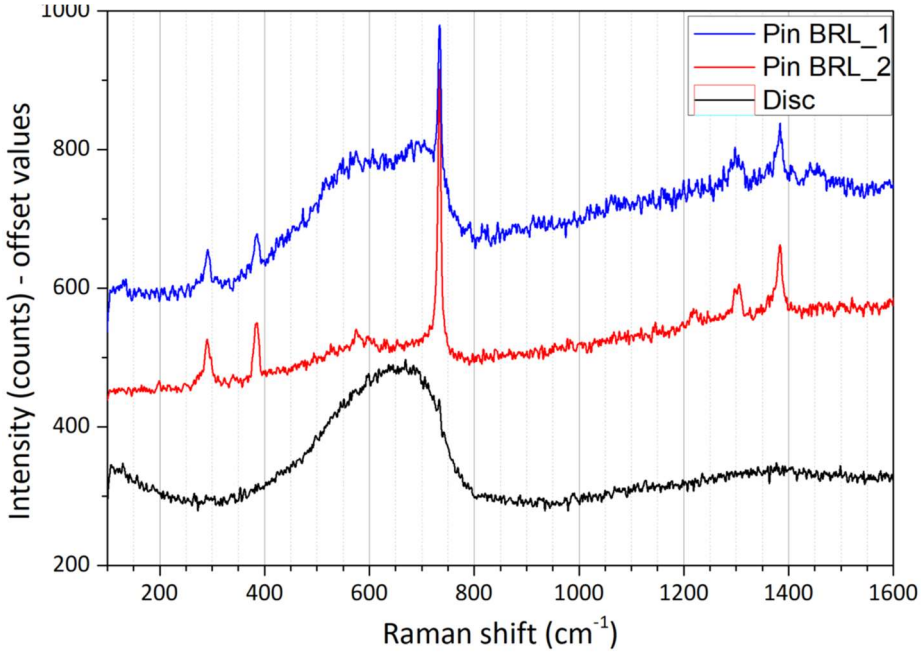

Figure 139: Micro-Raman spectra acquired on the Sintek BRL pin tested against uncoated AISI 304 surface at 10 N load, 1.8 m/s speed and on the stainless-steel disc.

While the spectrum "Pin BRL_2" shows the only PTFE signal, the spectrum "Pin BRL_1" also shows the mentioned band between 500 - 750 cm^{-1}, related to the presence of mixed amorphous oxides [71]. In conclusion, the composition of the transfer-film is different on the two mating bodies: it is rich in mixed oxides on the metallic counter-surface, whilst it contains a higher amount of PTFE on the pin surface, probably due to the higher mutual chemical affinity between the PTFE matrix of the pin and the PTFE debris, and between the oxidized debris and the metal counter-surface, respectively.

Raman analyses were also performed on the Chromia coated disc and on the bronze-filled pins tested against it (Figure 140,Figure 141).

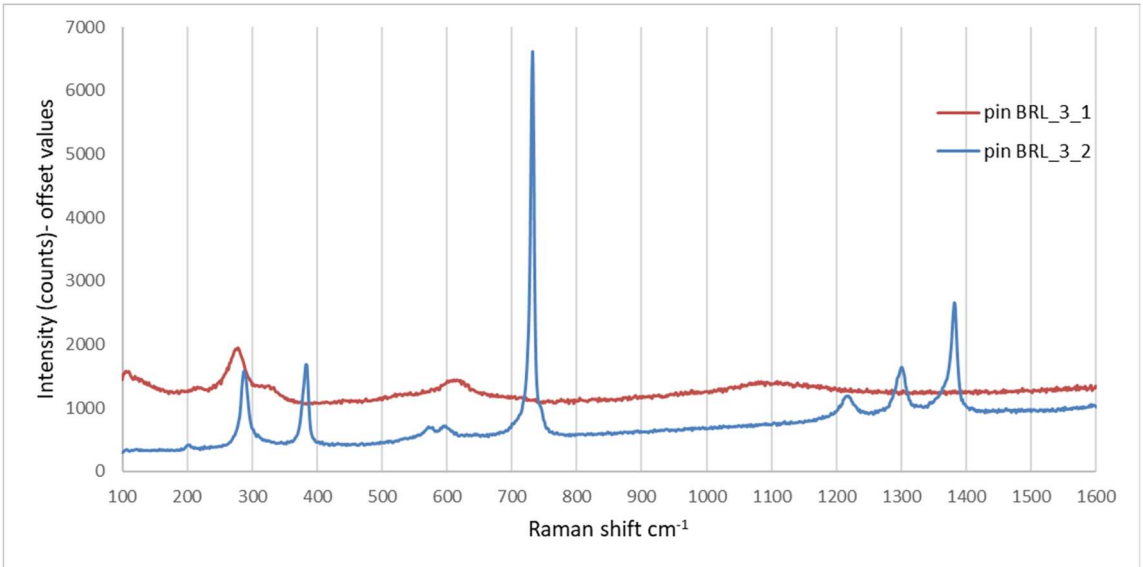

Figure 140: Micro-Raman spectra acquired on the Sintek BRL pin tested against Chromia coated surface at 10 N load, 0.54 m/s speed and on the disc.

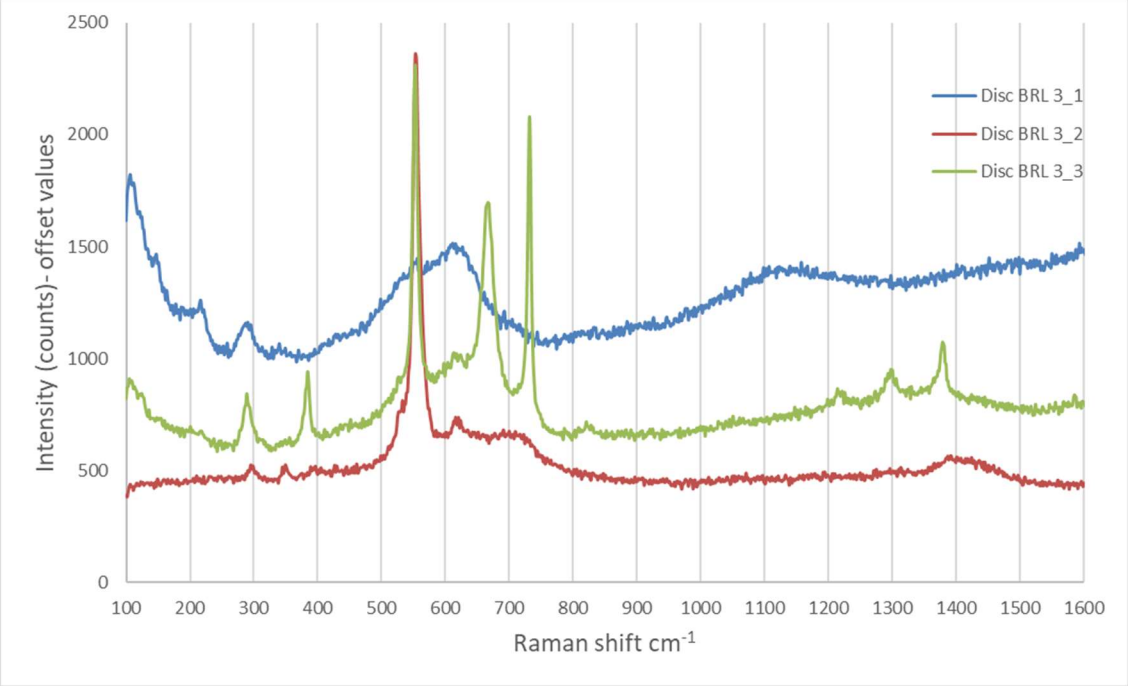

Figure 141: Micro-Raman spectra acquired on the wear tracks of the Chromia coated disc after testing against Sintek BRL at 10 N load, 0.54 m/s speed.

In some areas of the pin the PTFE is fully exposed (Figure 140, BRL3_2), in other areas the acquired signal is attributable to a metallic oxide (Figure 140, BRL 3_1). On the disk surface, spectrum BRL 3_3, acquired within the pores (Figure 141), suggests the presence of PTFE (peak at 734 cm^{-1}), confirming that the open porosity of the disc holds the wear debris. Figure 142 indicates the point where the BRL 3_3 spectrum of Figure 140 was

acquired. Other spectra correspond to Cr_2O_3 itself (BRL 3_2) or to metal oxides, in this case clearly deriving from tribo-oxidation of bronze debris (BRL 3_1).

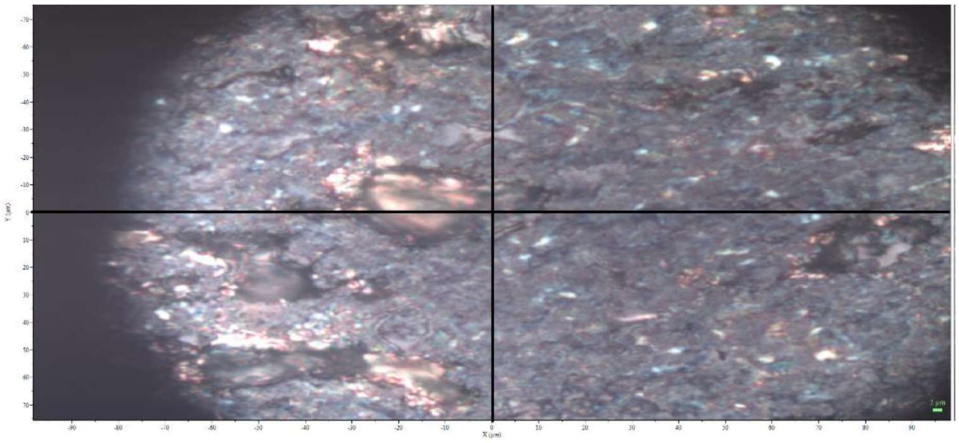

Figure 142: Optical micrograph of the wear track on the Chromia coated disc after pin-on-disc testing against Sintek BRL at 10 N load, 0.54 m/s speed. The central point, evidenced by the crossed axes, is the porosity investigated by Raman spectroscopy (spectrum BRL 3_3).

4 Creation and validation of the regression model

The study of the wear mechanisms of PTFE composites was carried out with the aim to identify the most influential parameters on the wear rate of the polymer. From the results obtained with the tests showed in this work it was concluded that neither the temperature developed in the contact area, nor the sliding distance have a significant influence on the tribological behaviour of the polymer.

As previously discussed, the other aim of this work was the design and development of a model able to provide predictive data on the useful life of PTFE based material components, because the prediction of the useful life of fluorinated polymers and polymer matrix composites in tribological applications would be a significant improvement compared to the simple “trial and error” approach. This model is based on an equation that identifies the relationship between the independent variables of the process and the desired result (dependent variable).

In order for the model to possess practical usefulness, its predictions must be validated not only against pin-on-disc tests themselves, but it is also essential to verify that they match reasonably well with actual wear rates encountered in practical applications. Therefore, a test bench was built to mimic an important application of PTFE-based composites in sealing systems, as detailed later in this work, and the wear rates predicted through a regression model built on the pin-on-disc results were validated against results obtained with the test bench.

At this stage, bench tests were only run on a limited set of tribological couples; therefore, the model was also built only for those systems. The materials were chosen based on the availability of the semi-finished products. In future developments, the regression model will then be developed for all PTFE composites studied in this thesis. Furthermore, the regression model was generated by considering only the Chromia coated surface in the tribological coupling, since the test bench, where the gaskets were tested, is not made of uncoated steel components.

Specifically, the wear rate results obtained from the tribological tests carried out on PTFE composites reinforced with spherical bronze particles (Sintek BRS) and on both PEEK-reinforced PTFE composites (Sintek PK10 and Sintek PK20) against the Chromia coated surface were selected as these materials were further employed in imported into the Minitab software to generate a regression model corresponding.

The experimental plan performed on these samples (as well as on all other composites) indeed corresponded to a 2-factor, 2-level factorial plan (Table 10) using load and sliding speed as variable factors. The sliding distance, as previously discussed, was not included in the factorial plan, as the first tests carried out on unreinforced PTFE concluded that this is the least influential parameter, compared to load and sliding speed, for determining the material wear rate.

Load (N)	5	10
Sliding speed (m/s)	0.54	1.8

Table 10: Factorial plan for pin-on-disc testing of all PTFE composites against each disc counter-surface.

The regression models for the chosen PTFE composites are listed in table below: the resulting value of wear rate must be multiplied by 10^{-6} $mm^3/(N•m)$.

Wear rate regression model	
Sintek BRS vs. Cr_2O_3	wear rate = 2.02 + (0.174 • Load) + (2.54 • Speed) – (0.320 Load • Speed)
Sintek PK10 vs. Cr_2O_3	wear rate = 5.62 – (0.392•Load) – (1.65 • Speed) + (0.224 • Load • Speed)
Sintek PK20 vs. Cr_2O_3	wear rate= 1.32 + (0.209 •Load) + (0.29 •Speed) – (0.127 Load • Speed)

Table 11: regression models for the specific wear rates of the chosen tribosystems.

To validate this model, as mentioned above, it was considered essential to obtain a correlation between the results of tests carried out on a small scale ("pin on disk" tests) and the results obtained on a test rig, so that this equation can also be used on real components.

The test bench is a rotary manifold (Figure 143, Figure 144) that has been designed to test mainly the sealing of gaskets subjected to operating conditions typical of the Food & Beverage field. The operating principle of the rotary manifold is based on the rotation of the outer sleeve, while the internal shaft, on which the seals exercise their sealing function, is fixed (Figure 145).

The slewing ring (highlighted in blue in Figure 144), on which the PTFE samples are mounted, is integral with the outer sleeve and replaces the ball bearings, which cannot be used as the body is in contact with sanitizing agents: for this reason, a highly wear resistant material, with a low friction coefficient and high chemical compatibility is required.

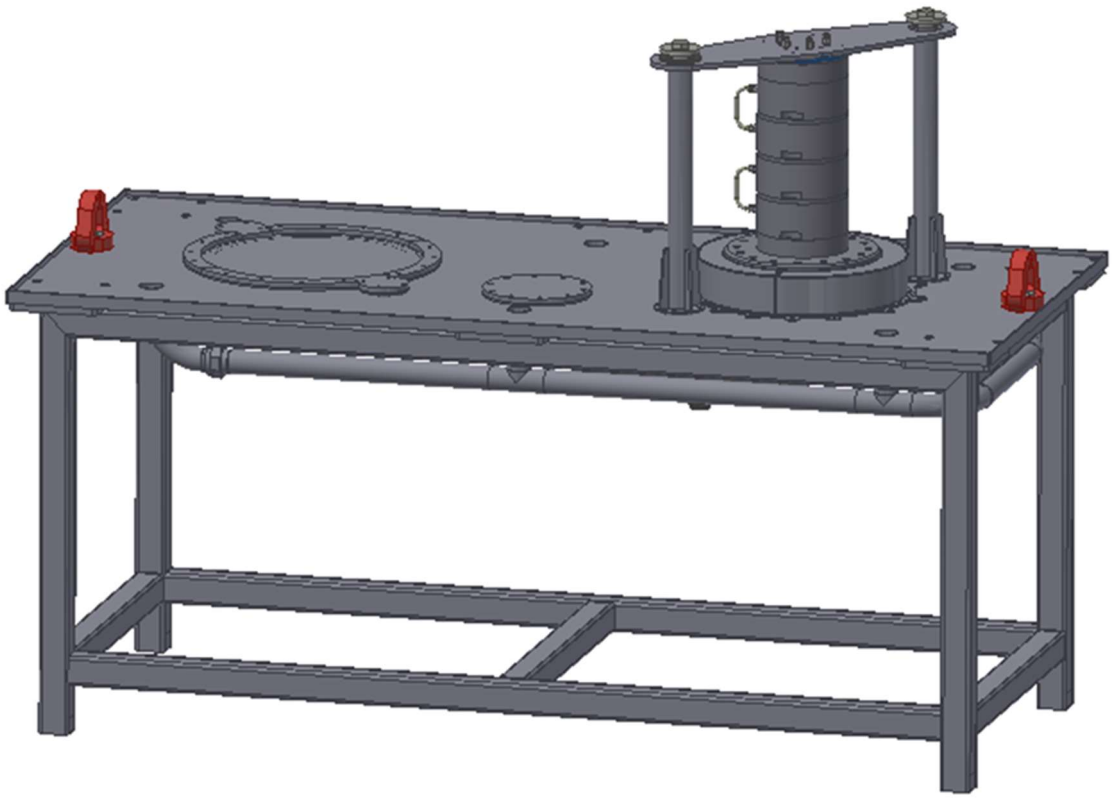

Figure 143: general diagram of the rotary manifold.

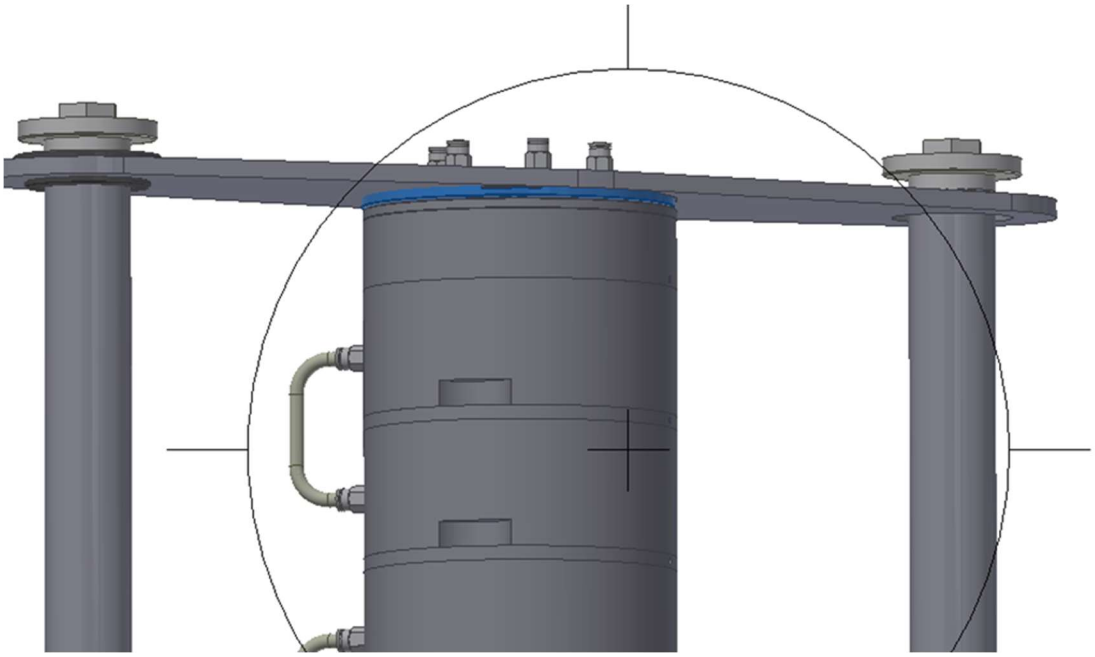

Figure 144: detail of the slewing ring (highlighted in blue) where the samples are mounted.

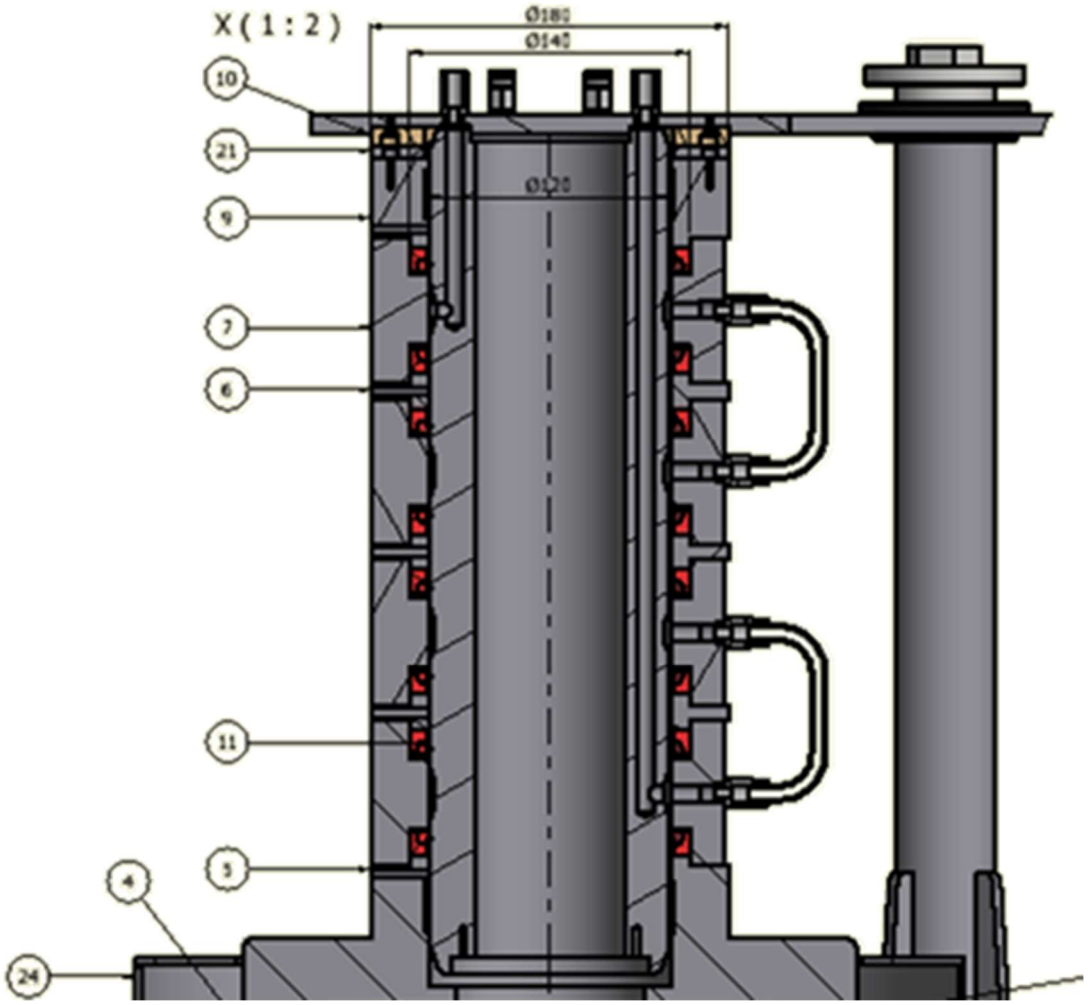

Figure 145: cross section of the rotary manifold. The red elements are representative of the seals.

In order to measure the wear loss of the slewing ring, three polymer pins were inserted into cavities of matching geometry machined into the ring itself, so that they could be subsequently removed from the ring for measurement.

Figure 146 shows the cross section of the tested samples mounted into the slewing ring.

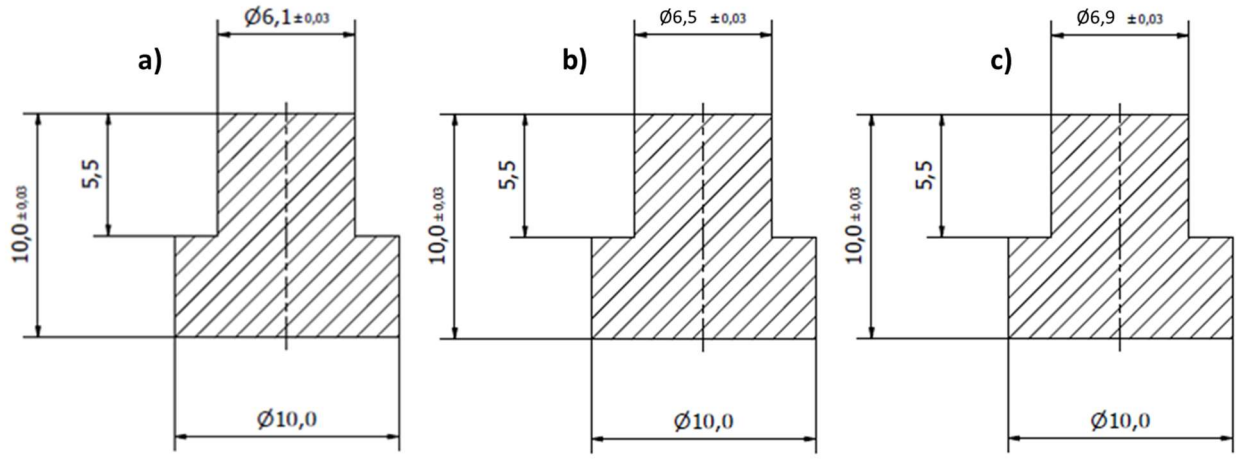

Figure 146: Cross section of the tested samples on the slewing ring: a) cross section of Sintek PK20 sample; b) cross section of Sintek BRS pin; c) cross section of Sintek PK10 sample.

The operating conditions of the rotary manifold are fixed: the total load acting on the three samples mounted into the slewing ring, at 120° from each other, is 300 N (which must be distributed on the samples), and the sliding speed is 0.16 m/s.

Table 12: operating conditions of the test rigTable 12 shows the operating conditions of the test rig:

Load (N)	Sliding speed (m/s)	Test duration (s)	Counter-surface
100	0.16	13284 (24 h)	Cr_2O_3

Table 12: operating conditions of the test rig

At the end of the test the volume of removed material, whose average value is shown in Table 13, was calculated by measuring the height of the remaining cylindrical part of the sample, and it was converted to the specific wear rate (Table 13).

	Average value of volume of removed material (mm^3)	Average value of wear rate [$mm^3/(N \cdot m)$]
Sintek BRS	11.61±1.33	$8.74 \cdot 10^{-6} \pm 9.95 \cdot 10^{-7}$
Sintek PK10	5.61 ±1.12	$4.22 \cdot 10^{-6} \pm 8.45 \cdot 10^{-7}$
Sintek PK20	2.62±0.58	$1.97 \cdot 10^{-6} \pm 4.45 \cdot 10^{-7}$

Table 13: Volume loss and specific wear rate - average values measured through the test rig.

To verify the correspondence between the results of the test rig and the analytical model, the value of the normal load acting on the pin, in the pin-on-disc test, must be calculated. In this case, the value of the normal load was calculated by FEM analysis using the contact pressure of each PTFE composite sample resulting from the test rig. FEM analysis was carried out to calculate the contact load acting on the nodes that build up the flattened surface of the pin (of the pin-on-disc test). This value was then used for the pin on disc test, whose results in terms of wear rate were imported into the DoE to generate the regression model and compare them with the test rig results. Replacing the load values calculated with FEM analysis in the material regression model (Table 14), a predicted value of the wear rate is obtained.

Table 14 shows the load values resulting from FEM analysis and compares the wear rate value obtained from the regression model with the wear rate resulting from the test rig.

	Load (N)	Wear rate (regression model from DoE)	Wear rate (Test rig)
Sintek BRS	2.2	$2.67 \cdot 10^{-6}$	$8.74 \cdot 10^{-6}$
Sintek PK10	1.33	$4.91 \cdot 10^{-6}$	$4.22 \cdot 10^{-6}$
Sintek PK20	2.0	$1.74 \cdot 10^{-6}$	$1.97 \cdot 10^{-6}$

Table 14: Comparison between the specific wear rate (unit: $mm^3/(N \cdot m)$) calculated with the regression model and that resulting from the test rig.

The obtained results from the regression model and the test rig are very similar (especially for the Sintek PK10 and Sintek PK20 pins), and the wear rate values are of the same order of magnitude.

A further verification was made carrying out pin on disc tests (up to now, just on Sintek PK20: verification tests on other materials have been planned and will be carried out in

future developments of the work) at 2 N load, 0.16 m/s sliding speed and 13284 m sliding distance: the measured wear rate value was $6.79 \bullet 10^{-7}$ $mm^3/(N \bullet m)$, which is somewhat lower than the test rig result and the prediction from the regression model.

The possible explanation of this difference in the wear rate values between regression model, test rig and pin on disc may concern the type of contact, which in the case of pin on disc testing is of "non-conformal" type. The top of the pin, in contact with the counter-surface, has a spherical shape: in the first moments of the test the contact pressure is higher because it acts on a much smaller area, and it decreases as wear gradually distributes the normal force on an increasingly large surface (flattening of the pin).

Further developments have already been planned for the consolidation of the analytical model by DoE, adding other parameters such as service temperature or the presence of contact liquids.

5 Conclusions

In accordance with the literature, the load and the speed are significant parameters on the wear rate of unreinforced PTFE, as evaluated with the Design of Experiment method. The tribological tests were carried out at different sliding distances, from which it was deduced that the sliding distance itself was not a particularly influential parameter, as the volume of removed material increased mostly linearly with it, either using the Cr_2O_3 coated surface (thermally insulating and harder; ceramic) or uncoated AISI 304 surface (thermally conductive and softer; metallic) as counterparts. For this reason, all the subsequent tribological tests on reinforced PTFE composites were carried out at the minimum sliding distance value of 3000 m.

Another significant parameter in the tribological pair could be the contact temperature at the interface between the mating bodies, as it could affect the tribological behaviour of the polymeric material and the stability of the transfer-film. This parameter was studied by conducting pin-on-disc tests with two distinct counter-surfaces and with pin having different families of thermally conductive or insulating fillers added to the PTFE matrix.

The thermal insulation effect of the ceramic coating did play a significant role on flash heating, which is a more localized phenomenon, though it would not raise the temperature to levels that would seriously degrade the PTFE matrix. In the most extreme case, the overall bulk + flash temperature rise is of about 76.5 °C (Table 15,Table 16).

			GF-PTFE		PK10		PK20	
Counter-surface material	Speed (m/s)	Load (N)	Bulk temperature rise (°C)	Flash temperature rise (°C)	Bulk temperature rise (°C)	Flash temperature rise (°C)	Bulk temperature rise (°C)	Flash temperature rise (°C)
Uncoated AISI 304	1.80	10	9.0	31.1	9	35	11.4	33.9
	1.80	5	7.6	29.4	4	30.9	5.4	31.7
	0.54	10	7.6	18.8	9	17	5.7	18.1
	0.54	5	5.5	15.8	4	16.6	3.1	16.2
Cr_2O_3-coated AISI 304	1.80	10	11.7	56.1	9	60.4	13.3	63.2
	1.80	5	8.4	51.1	5	54.3	4.8	55
	0.54	10	5.7	28.5	7	29.5	3	32.2
	0.54	5	5.0	27.1	6	27.7	1.3	27.2

Table 15: bulk and flash temperature rises of "thermally insulant" PTFE composites calculated using Ashby et al.'s model [73] modified by Wang and Rodkiewicz [26].

			CF-PTFE pin		BRL-PTFE pin		BRS-PTFE pin	
Counter-surface material	Speed (m/s)	Load (N)	Bulk temperature rise (°C)	Flash temperature rise (°C)	Bulk temperature rise (°C)	Flash temperature rise (°C)	Bulk temperature rise (°C)	Flash temperature rise (°C)
Uncoated AISI 304	1.80	10	17.8	41.4	13.5	30.8	14	31.5
	1.80	5	11.3	32.2	4.4	25.9	5	27.5
	0.54	10	9.9	21.0	3.8	16.2	7	16.9
	0.54	5	7.0	17.9	2.2	13.6	6	15
Cr_2O_3-coated AISI 304	1.80	10	10.8	61.4	11.4	57.3	4	65.4
	1.80	5	6.9	52.1	6.1	48	9	49.9
	0.54	10	5.3	31.5	6.8	31.9	5	35
	0.54	5	3.6	27.9	4.9	27	5	27.6

Table 16: bulk and flash temperature rises of "conductive" PTFE composites calculated using Ashby et al.'s model [25] modified by Wang and Rodkiewicz ([26]).

Nonetheless, the changes in friction coefficients produced by the various tribo-systems were very significant and could not be clearly explained considering only the thermal properties of the mating bodies. Therefore, the investigation included a careful study of wear mechanisms, including the tribofilm formation, its distribution on the mating surfaces and its influence on the friction behaviour and the wear mechanisms. The tribofilm properties do depend on load, speed and temperature, but the nature of the fillers used to reinforce the PTFE matrix played a crucial role on the tribological behaviour.
The experimental findings, in fact, led to the following conclusions:

- The tribo-systems' responses (specific wear rate, friction coefficient, and wear mechanisms) depend critically on the combination between reinforcement type and counter-surface material.
- Lower friction coefficients in the range of 0.19 – 0.25 were usually observed when tribo-systems develop uniform tribofilms covering one or both surfaces. In this work, this occurred most remarkably with glass fibre- and bronze particles-filled PTFE composites. This is related to a tribochemical wear mechanism whereby tribo-layers are developed on both the composite itself and the counter-surface. As the glass fibres or the bronze particles wear down, they release hygroscopic, oxide-based debris particles (glass debris or tribo-oxidized bronze debris) that adsorb hydroxyl groups and molecular water from environmental humidity. Cohesive interactions (hydrogen bonding) between particles with adsorbed humidity lend compactness to the tribo-layer, which also entrains PTFE debris.
  Carbon fibre-reinforced composites cannot establish analogous tribo-layers due to the different chemical nature and fracture behaviour of the carbon fibres. The

same can be said of PEEK-reinforced composites. PEEK is indeed known not to possess the same tribofilm formation ability of PTFE, nor can it elicit the same tribo-oxidation and humidity adsorption mechanisms as do finely comminuted metal oxides.

With stainless steel as counterpart, the release of tribo-oxidized steel debris due to abrasion also plays a significant role in the formation of the tribofilm. Indeed, regardless of the composition of the pin, greater tribofilm coverage has was always observed on the pin after testing against stainless steel than against chromia, which has no wear loss. On the other hand, the open porosity of chromia helps retaining the tribofilm on the counter-surface, as pores are filled with transfer material.

Therefore, the friction coefficient produced by the glass fibre- and carbon fibre-reinforced PTFE composites was lower against chromia (0.19-0.23 and 0.21-0.23 respectively) than against stainless steel (0.21-0.26 and 0.31-0.33 respectively), because in the former case the pin was less covered by the tribofilm, but on the other hand the counter-surface was more covered. Bronze-filled PTFE, on the other hand, has such ability to produce continuous and thick tribofilms on every surface (including the pin and the counter-surface, regardless of whether it is uncoated stainless steel or chromia), that no difference could be seen in the steady-state friction coefficients (0.21-0.22, especially with lamellar bronze particles which are more firmly attached to the matrix and, therefore, more effective).

– Whilst tribofilm coverage is usually conducive to low friction, it is not always a guarantee of low wear. To the contrary, tribofilm formation is often associated with higher pin wear. Indeed, glass fibre- and bronze particles-reinforced composites usually suffer greater wear loss against uncoated stainless steel (in most cases $>2\times10^{-6}$ $mm^3/(N\cdot m)$, usually $>3\times10^{-6}$ $mm^3/(N\cdot m)$), than do carbon fibre- and PEEK particles-reinforced ones (usually $<2\times10^{-6}$ $mm^3/(N\cdot m)$), although the latter develop much less tribofilm coverage, as mentioned previously. Indeed, the tribo-layer is repeatedly delaminated by abrasion and surface fatigue and reformed by compaction of newly released debris. A surface where wear-resistant fillers, such as carbon fibres or PEEK particles, directly bear the contact load is often better at preventing wear against steel, though it causes higher friction because the solid-lubricating action of PTFE is largely lost.

- Between the two types of bronze particle morphologies studied in this work, the lamellar one achieves the best performances: the particles adhere more firmly to the matrix and, gradually becoming worn, release tribo-oxidized bronze powders that contribute to the transfer-film formation along with PTFE debris released from the pin. The spheroidal morphology, while ensuring a good distribution of the filler during mixing, is not strongly adhered to the matrix as in the case of lamellar morphology. Therefore, entire particles can be ejected from the matrix during the sliding, releasing less dust.
- In addition, bronze particles-filled PTFE composites suffer adhesive wear in the initial stages of contact with stainless steel, which also causes initially high friction (>0.3) and results in slightly higher contact temperatures than would be expected theoretically based on the low, steady-state friction only. When the contact pressure decreases, the reduced wear severity allows the formation of the transfer-film both on the surface of the composite and on the counter-surface, with a different morphology and different debris released.
- When comparing uncoated and chromia-coated stainless steel counter-surfaces, the pores on the chromia surface are particularly effective at retaining the transfer material and at reducing friction, except for PEEK-reinforced composites as mentioned above. However, they are potentially damaging in terms of wear. Most materials indeed exhibit greater wear loss against chromia (e.g. wear rates against chromia are $>3\times10^{-6}$ $mm^3/(N\cdot m)$ for bronze particles- and carbon fibre-reinforced composites, around or above 2×10^{-6} $mm^3/(N\cdot m)$ or PEEK-reinforced composites) than against uncoated stainless steel. The sharp edges of the open pores, indeed, were seen to break the carbon fibres and cause abrasive wear of bronze particles- and PEEK particles-filled PTFE. The only exceptions to this trend are bronze-filled composites at high load/speed because adhesive wear against the steel surface before the tribofilm is established is even more severe than abrasion by the chromia surface, and glass fibre-reinforced composites, probably because the debris released by the composite is especially effective at filling in the pores, thus hindering their abrasive effects.
- The bulk temperature of the composites never increases by more than 10 – 15 °C even under the most severe conditions tested in this work. The flash temperature rise on contacting asperities was also estimated to be <50 °C under all conditions.

As a result, even the most extreme temperature peaks attained during flash heating do not exceed 100 °C. The magnitude of the friction coefficient developed by a specific tribo-couple seems to affect bulk surface temperatures more than do the thermal conductivity and diffusivity of the mated materials.

– The regression model of Sintek BRS, Sintek PK10 and Sintek PK20 generated with the DoE, considering load, and sliding speed as input variables, shows that there is a good match between small scale tests (pin-on-disc tests) and large-scale tests on sealing components (test rig). Thanks to this model it is possible to perform simple pin-on-disc tests and obtain a reasonable agreement (order of magnitude) with the test-rig experiment: this significantly reduces the response time to ATP customers, regarding the service life of polymer gaskets.

6 References

[1] A. Abdelbary, Wear of Polymer and composites, Elsevier, 2014.

[2] G. Straffelini, “Friction and Wear - Methodologies for Design and Control.,” p. p. 21–60, 2015.

[3] Elsevier, Introduction to Fluoropolymers 17-35, 2013.

[4] S. Ebnesajjad, Fluoroplastics Volume 1: Non-Melt Processible Fluoropolymers- The Definitive User's Guide and Data Book, Oxford, UK: (William Andrew), 2015.

[5] S. Ebnesajjad, Fluoroplastics. Plastic Design Library Series, Elsevier.

[6] S. Ebnesajjad, Introduction to Fluoropolymers- Materials, Technology and Applications, Elsevier.

[7] J. B. H. T. v. d. G. G. W. W. E.-U. D. E. O. K. R. David Parker, Polymers, High-Temperature. Ullmann's Encyclopedia of Industrial Chemistry., Wiley-VCH Verlag GmbH & Co. KGaA, Weinheim, 2012.

[8] “https://www.pslc.ws/italian/ptfe.htm,” [Online].

[9] Q. J. W. a. Y.-W. C. (Eds.), Encyclopedia of Tribology, 2013.

[10] M. Alessandro, *Tesi di Dottorato: Comportamento tribologico di materiali per componenti di interesse industriale.,* 2014.

[11] A. J.F., “The temperature of rubbing surfaces,” Vols. 2(6): 438-55, 1959.

[12] A. A., Effect of vertical cracks at the surface of polyamide 66 on the wear characteristics during sliding under variable loading conditions, Alexandria, Egypt : University of Alexandria, 2011.

[13] P. G. J., “A relationship between abrasive wear and the cohesive energy of materials,” 1970.

[14] L. J.K., “Abrasive wear of polymers,” Vols. Wear ,14 (4): 223–9, 1969.

[15] F. I. R. O. a. L. E. Ratner S.B., “Connection between the wear resistance of plastics and other mechanical properties,” Vols. 12 (7): 37-9.

[16] M. A.F., “Effect of molecular weight on properties of HDPE,” Vols. 27: 44-8, 1971.

[17] H. U. B. f. e. K. Hertz, “Journal fur die reineund angewandte Mathematik,” Vols. 92, pp. 156-171, 1881.

[18] D. Vincenzo, Fondamenti di tribologia ,vol. 1, Napoli,: ed. CUEN.

[19] Y. U. a. S. T. K. Tanaka, Wear, 1973.

[20] M. K. W. D. R. A. K. S. Hooke C.J., “Meausurement and prediction of the surface temperature in polymers gears and its relationship to gear wear.,” Vols. 115 (1): 119-24, 1993.

[21] e. a. D.M. Price, “Thermal conductivity of PTFE and PTFE composites in: Proceedings of the 28th Conference of the North American Thermal Analysis Society,” October 4–6, 2000.

[22] B. P. A. I. Marcello Conte, “Role of crystallinity on wear behavior of PTFE composites,” *Wear,* Vols. Volume 307, Issues 1–2, 30 September 2013, Pages 81-86.

[23] S. Bahadur, “The development of transfer layers and their role in polymer tribology,” *Wear,* Vols. 245 (2000), pp. 92-99.

[24] G. W. &. B. A. W. Stachowiak, “Engineering tribology,” 2014.

[25] A. J. K. H. Ashby MF, “Temperature Maps for Frictional Heating in Dry Sliding.,” in *Tribology Transactions*, vol. 34, 1991, p. 577–587.

[26] C. R. Y. Wang, “Temperature maps for pin-on-disk configuration in dry sliding, Tribology International,” vol. 27 (1994) 259–266.

[27] S. K. Biswas and K. Vijayan, “Friction and Wear of PTFE - a Review,” *Wear,* 1992.

[28] J. K. H. S. a. B. D. L. Ye, “Transfer Film Evolution and Its Role in Promoting Ultra-Low Wear of a PTFE Nanocomposite,” *Wear,* vol. 297(1–2), p. pp. 1095–1102., 2013.

[29] K. Z. Z. a. S. A. K. Friedrich, “Effects of Various Fillers on the Sliding Wear of Polymer Composites,” *Composites Science and Technology,* Vols. 65(15-16 SPEC. ISS.), p. pp. 2329–2343, 2005.

[30] B.J. Briscoe, in K.L. Mittal (Ed.), Physicochemical Aspects of Polymer Surfaces, Plenum Press, New York, 1983, pp. 387-412..

[31] K. H. M. S. Gabriele Gottschalk-Gaudig, “S-PTFE Processing Handbook,” Carl-Schurz-Straße 1,41453 Neuss, Germany, 2018 Dyneon GmbH.

[32] G. H. I. Ö. W. W. B. a. J. B. Zhang, “Formation and Function Mechanisms of Nanostructured Tribofilms of Epoxy-Based Hybrid Nanocomposites,” *Wear,* vol. 342–343, p. pp. 181–188., 2015.

[33] Y. Şahin, “Dry Wear and Metallographic Study of PTFE Polymer Composites,” in *Mechanics of Composite Materials*, (2018) , p. 403–414..

[34] K. F. H. Voss, “Sliding and abrasive wear of short glass-fibre reinforced PTFE-composites,” *Journal of Materials Science Letters.,* vol. 5, p. 1111–1114, 1986.

[35] P. M. M. B. Y. S. P. Johansson, “Effect of humidity and counterface material on the friction and wear of carbon fiber reinforced PTFE composites,” *Tribology International,* vol. 157 , 2021.

[36] M. Y. Y. W. C.. Wang, “The influence of metal surface composition on the tribological properties of filled PTFE/steel couples,,” *Tribology International,* vol. 37, p. 645–650, 2004.

[37] K. Tanaka, “Friction and Wear of Glass and Carbon Fiber-Filled Thermoplastic Polymers,” *Journal of Lubrication Technology,* vol. 99, pp. 408-414, 1977.

[38] G. Nikas, “Friction and Wear of Seals, in: G.E. Totten (Ed.), Friction, Lubrication, and Wear Technology,” *ASM International, Materials Park, OH, USA,* p. 957–968, 2017.

[39] A. P. E. B. C.H. Suhrberg, “Einfluss der Kontaktoberfläche auf den PTFE-Transfer glasfaserverstärkter PTFE-Verbundwerkstoffe,” *Tribologie & Schmierungstechnik,* vol. 54, p. 18–23, 2007.

[40] D. C. E. A. Fontaine J, “Fundamentals of the Tribology of DLC Coatings.,” p. p. 139–54., 2008.

[41] 2. Ceramic Seal Surface Rebuild and Protection.

[42] L. D., “Wear-Resistant Coatings.,” in *ASM Handbook - Volume 5A: Thermal Spray Technology, Materials Park, OH, USA: ASM International*, In: Tucker Jr. RC, editor, 2013, p. p. 253–6..

[43] Z. Y. H. a. G. B. Lin, “Enhancing Tribological Characteristics of PEEK by Using PTFE Composite as a Sacrificial Tribofilm-Generating Part in a Novel Dual-Pins-on-Disk Tribometer,” *Wear,* p. 460–461, 2020.

[44] T. N. J. K. K. A. K. K. K. a. K. M. 2. “. Onodera, “Structure and Function of Transfer Film Formed from PTFE/PEEK Polymer Blend,” *Journal of Physical Chemistry C,* vol. 121, p. 14589–14596.

[45] Wang Y., Yan F., “A study on tribological behaviour of transfer films of PTFE/bronze.,” *Wear,* vol. 262, p. 876–882., 2007.

[46] B. D. B. S. e. a. Pasha BAM, “Studies on wear resistance of PTFE filled with glass and bronze particles based on Taguchi technique Nizamuddin.,” *J Thermoplasc Compos Mater,* no. 26(2), p. 243–259., 2012.

[47] B. D. B, *Contribution a`l’e´tude du comportement tribologique et des pro prie´te´s me´caniques de polyme`res thermoplastiques charge´s de lubrifiants solides en poudre.,* Franche-Comte´ University, France., 2014.

[48] A. N. S. K. M. a. D. M. Charfi, “Tribological Behaviors of PTFE-Based Composites Filled with Bronze Microparticles,” *Journal of Thermoplastic Composite Materials,* 2019.

[49] H. P. A. P. S. Amin, “A Review on Thermal Spray Coating Processes, International Journal of Current Trends in Engineering & Research Scientific Journal Impact Factor, pp. 556–563,,” vol. 2, 2016.

[50] P. Vuoristo, ““Thermal Spray Coating Processes,” pp. 229–276 in S. Hashmi, C. J. Van Tyne, G. F. Batalha, B. Ylbas, Eds. Comprehensive Materials Processing, ISBN:978-0-08-096532-1.,” 2013.

[51] R. M. K.N. Strafford, “Plasma Sprayed Ceramic Coatings,” Surface Engineering, http://doi.org/ 10.1201/9780203737798-1.,” Vols. 40, pp. 3–20, 2019,.

[52] R. S. I. S. a. C. S. K.N Strafford, “Surface engineering, Processes and applications, Technomic Publishing,” 1995.

[53] “Chromium (III) Oxide, Cr2O3 (Eskolaite).,” (accessed February 22, 2021). [Online].

[54] Y. W. R. T. M. M.-L. R. G. a. A. R. J.E. Fernandez, “Friction and wear behaviour of plasma-sprayed Cr2O3 coating against steel in a wide range of sliding velocities and normal loads,” 1996.

[55] “304 Stainless Steel.,” (accessed February 22, 2021).. [Online].

[56] D. S. J. K. T. V. L. L. P. V. G. Bolelli, “Tribological properties of plasma sprayed Cr2O3, Cr2O3–TiO2, Cr2O3–Al2O3 and Cr2O3–ZrO2 coatings.,” Vols. 203931, doi:10.1016/j.wear.2021.203931, 2021.

[57] G. D. J.-R. F. J. H. L. R. B. Hay, “Simultanous Measurements of Thermal Diffusivity and Thermnal Conductivity of Ceramic Coatings at High Temperature by Laser Flash Method”.

[58] D. D. E.N. Brown, “The role of crystalline phase on fracture and microstructure evolution of polytetrafluoroethylene (PTFE),” Vols. 46 -3056–3068. doi:10.1016/j.polymer.2005.01.061., 2005.

[59] E. Clark, “The molecular conformations of polytetrafluoroethylene: forms II and IV„” Vols. 40 - 4659–4665. doi:10.1016/S0032-3861(99)00109-3., 1999.

[60] L. A. R. C. W. P. S.E. Ziemniak, “Thermodynamics of Cr2O3, FeCr2O4, ZnCr2O4, and CoCr2O4,” vol. 39 1474–1492. doi:10.1016/j.jct.2007.03.001., 2007.

[61] O. o. m. f. P. (PTFE), “ http://www.matweb.com/search/DataSheet.aspx?MatGUID=4d14eac958e5401a8fd152e1261b6843,” (accessed February 22, 2021).. [Online].

[62] “E-Glass Fiber Generic,” [Online]. Available: http://www.matweb.com/search/DataSheet.aspx?MatGUID=d9c18047c49147a2a7c0b0bb1743e812.

[63] F. Amenta, G. Bolelli, S. Pedrazzi, G. Allesina, F. Santeramo, A. Bertarini, P. Sassatelli and L. Lusvarghi, “Sliding wear behaviour of fibre-reinforced PTFE composites against coated and uncoated steel.,” *Wear,* vol. 204097, 2021, 486–487.

[64] G. L. Y. G. L. Z. Y. X. F. Z. G. Z. X. Fan, “Role of reinforcement types and silica nanoparticles on tribofilm growth at PTFE-Steel interface.,” vol. 143 (2020) 106035.

[65] Q. W. T. W. F. Song, “Effects of glass fiber and molybdenum disulfide on tribological behaviors and PV limit of chopped carbon fiber reinforced Polytetrafluoroethylene composites,” vol. 104 (2016) 392–401.

[66] L. W. J. L. F. K. A. L. T. W. Q. W. M. Lv, “Surface energy, hardness, and tribological properties of carbon-fiber/polytetrafluoroethylene composites modified by proton irradiation,” vol. 132 (2019) 237–243.

[67] X. F. H. W. X. L. Y. Shi, “Tribological properties of PTFE composites filled with surface-treated carbon fiber,” Vols. 42-8465–8469. doi:10.1007/s10853-007-1767-7., 2007.

[68] J. C. M. L. F. H. M. Wang, “Structure and properties of soda lime silicate glass doped with rare earth,” *Physica B: Condensed Matter,* vol. 406 (2011) 187–191.

[69] A. O. T. S. P. G. A. B. A.P. Vasilev, “Investigation of the Influence of Complex Fillers on the Properties and Structure of Polytetrafluoroethylene,” *Journal of Friction and Wear,* vol. 39 (2018) 427–432.

[70] D. V. C. S. B.O. Mysen, “Relations between the anionic structure and viscosity of silicate melts - a Raman spectroscopic study,” vol. 65 (1980) 690–710..

[71] A. B. S. M. S. Ramathan, “Surface coating of ceria nanostructures for high-temperature oxidation protection,” 2018.

[72] J. L. a. B. F. J. “. Koenig, “Raman Scattering and Band Assignments in Polytetrafluoroethylene,” 1969.

[73] J. A. H. K. M.F. Ashby, “Temperature Maps for Frictional Heating in Dry Sliding,” vol. 34 (1991) 577–587.

[74] S. M. L. C. J. a. Z. M. Beckford, “The Influence of Cu Nanoparticles on the Tribological Properties of Polydopamine/PTFE + Cu Films,” *Tribology Letters,* vol. 59(1), 2015.

[76] H. C. a. K. Habig, Tribologie Handbuch, Reibung und Verlschleiss,Vieweg., 1992.

[77] S. G. F. G. S. Golchin A., “Break-away friction of PTFE materials in lubricated conditions, in “Tribology International”,” Vols. volume 48, pagg. 54-62, 2012.

[78] D. E. a. L. J.K., The wear of Polymers in Treatise on Materials Science and Technology, Academic Press., 1979.